STEAM FLOW DISTRIBUTION IN AIR-COOLED CONDENSERS

by:

Toni Zipfel

Thesis presented in partial fulfilment of the requirements for the degree Master of Mechanical Engineering at Stellenbosch University

Thesis Supervisor: Prof. D.G. Kröger

Department of Mechanical Engineering
University of Stellenbosch
March 1996

DECLARATION

I, Toni Zipfel, the undersigned hereby declare that the work contained in this thesis is my own original work and has not previously, in its entirety or in part, been submitted at any university for a degree.

28 day of May 1996

SYNOPSIS

In this thesis the parameters affecting the steam flow distribution through an air-cooled steam condenser, as found in power generating plants is investigated. The investigated condenser configuration consists of bundles with single rows of tubes. It is required to design the air-cooled condenser in such a way that the flow through each individual finned tube is sufficient to allow the entering steam to condense partially or fully along the full length of the tube. Thereby the accumulation of non-condensible gases is prevented, that may otherwise form so-called dead zones which reduce the thermal efficiency of the condenser.

A thorough experimental study was performed to determine the inlet loss coefficients of the finned tubes. These were found to vary as a function of the position of the finned tube, the steam velocity in the header and the geometrical configuration of the inlets themselves.

Subsequently the flow pattern on the steam-side of air-cooled condensers, consisting of bundles with single rows of finned tubes, was analyzed. It is shown that by following this approach, a condenser can be designed in which the formation of any dead zones can be avoided. The flow distribution through an air-cooled condenser section was also determined numerically with the aid of a finite difference computer code. The results of this numerical analysis confirm the validity of the proposed design method.

Keywords:

Condenser, air-cooled, maldistribution, steam flow, manifold, inlet losses.

SAMEVATTING

In hierdie tesis word die parameters ondersoek wat die stoomvloeiverdeling deur 'n lugverkoelde kondenser, soos gevind in kragsentrales, beïnvloed. Die kondenser konfigurasie bestaan uit bundels met enkelrye vinbuise. Die kondenser moet sodoende ontwerp word dat die stoomvloei by elke afsonderlike vinbuis inlaat groot genoeg is, om gedeeltelik of volkome oor die buis se volle lengte sal kondenseer. Daarmee word die opeenhoping van onkondenseerbare gasse wat sogenaamde dooie zones kan vorm wat die termiese benuttingsgraad van die kondenser verlaag, voorkom.

'n Deeglike eksperimentele studie is deurgevoer om die inlaatverlieskoëffisiënte van die vinbuise te bepaal. Daar is gevind dat hierdie inlaatverlieskoëffisiënte as 'n funksie van die posisie van die vinbuis, die snelheid in die verdeelpyp en die geometriese uitleg van die inlate varieer.

'n Stoomkantontwerpsbenadering van 'n lugverkoelde stoomkondenser, wat uit bundels met 'n enkelry vinbuise bestaan, is in hierdie werk ondersoek. Met hierdie benadering word die kondenser ontwerp om die formasie van dooie sones te vermy. Verder is die vloeiverdeling deur 'n lugverkoelde kondenserseksie bereken, deur gebruik te maak van 'n numeriese eindige-verskille-rekenaarprogram. Die resultate van hierdie numeriese analise bevestig die geldigheid van die voorgestelde ontwerpsmetode.

Sleutelwoorde:

Kondenser, lugverkoel, wanverdeling, stoomvloei, spruitstuk, inlaatverliese.

ACKNOWLEDGEMENTS

I thank Jesus Christ, my saviour, for giving me the opportunity to complete this work.

I would like to thank my supervisor, Prof. D.G. Kröger for his advice and guidance. He has always been approachable and interested to aid at any time.

На Стоиян Димитров Поибренки

CONTENTS

Chapter 1 Introduction

Chapter 2 Fluid flow in ducts

Chapter 3 Manifold systems

Chapter 4 Experimental investigation of inlet loss coefficients

Appendix A Equations for thermo-physical properties

Appendix B Numerical solution of different flow situations with the aid of the *PHOENICS* computer code

Appendix C Calibration of aluminium pipes

Appendix D Sample calculation and tabulation of experimental data

Appendix E Discussion of the design equation for air-cooled condenser proposed by Schrey [95SC1]

Appendix F Numerical solution of air-cooled condenser flow distribution

NOMENCLATURE

A	-	Area	[m^2]
A	-	Factor	
a	-	Constant	
a	-	Dimension	[m]
B	-	Factor	
b	-	Constant	
b	-	Dimension	[m]
C	-	Factor	
C	-	Constant	
c	-	Constant	
d	-	Diameter	[m]
E	-	Approach velocity factor	
f	-	Friction factor	
g	-	Gravitational acceleration	[m/s^2]
h	-	Height	[m]
i	-	Index	
K	-	Loss coefficient	
K_0	-	Normal inlet loss coefficient with zero flow area contraction	
L	-	Length	[m]
M	-	Momentum coefficient	
m	-	Mass flow	[kg/s]
m	-	Coefficient	
N	-	Number of laterals	
P	-	Perimeter	[m]
p	-	Pressure	[N/m^2]
Q	-	Flow parameter	
r	-	Radius	[m]
S	-	Source rate	
T	-	Temperature	[K]

v	-	Velocity	[m/s]
w	-	Width	[m]
x	-	Steam quality	
z	-	Axial distance	[m]
z	-	Coordinate	
z	-	Compressibility	

GREEK SYMBOLS

α_e	-	Energy correction factor	
α_m	-	Momentum correction factor	
Γ	-	Condensation ratio	
Γ	-	Exchange coefficient	
Δ	-	Differential	
ε	-	Wall roughness	[m]
Θ	-	Angle	[radians]
θ	-	Angle	[°]
θ	-	Overall header momentum correction factor	
μ	-	Dynamic viscosity	[Ns/m^2]
ρ	-	Density	[kg/m^3]
σ	-	Area ratio	
τ	-	Wall shear stress	[N/m^2]
ϕ	-	Conserved property	

DIMENSIONLESS GROUPS

Re	-	Reynolds number	$\frac{\rho\, v\, d_e}{\mu}$

SUBSCRIPTS

c - Combining
c - Contraction
c - Condensation
corr - Correction
D - D'Arcy
d - Duct
d - Dividing
e - Equivalent
e - Expansion
fr - Friction
h - Header
i - Index
i - Inlet
l - Lateral
loc - Local
o - Outlet
r - Round
t - Tube
tot - Total
tr - Transition
v - Vapour
vr - Velocity ratio
w - Wall

CHAPTER 1

INTRODUCTION

Air-cooled steam condensers find application in power generating plants. The low pressure saturated steam leaving the turbine is led to the condenser. A typical air-cooled condenser configuration is shown in figure 1.1:

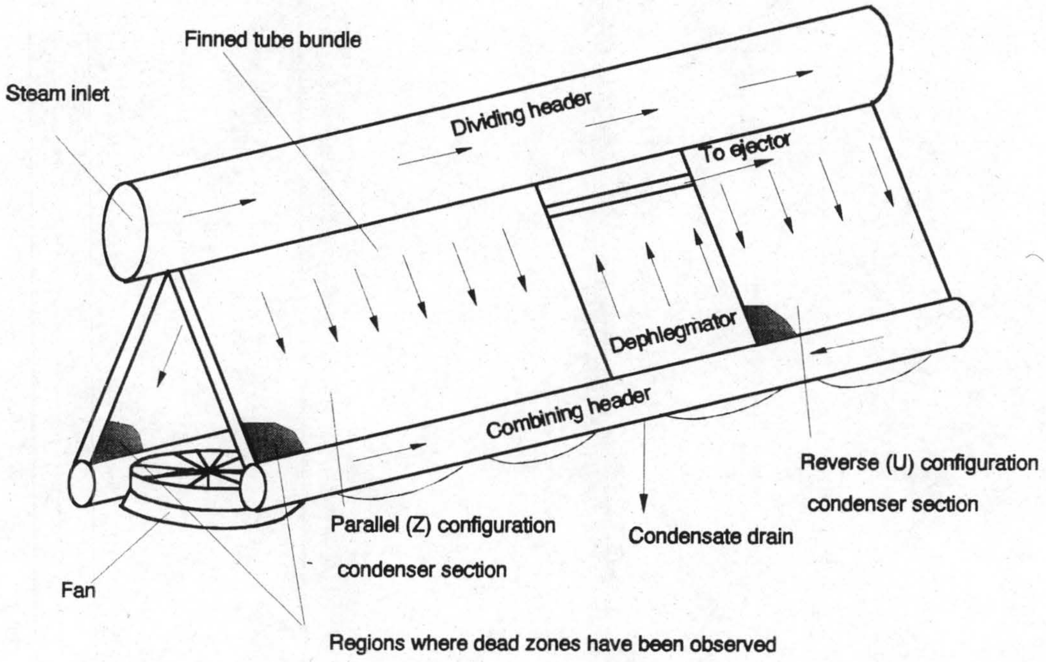

Figure 1.1: Schematic diagram of an air-cooled condenser.

The condenser consists of a dividing header from which the steam is distributed into numerous finned tubes which are configured in bundles. Two rows of bundles are arranged in the form of an A-frame as shown in the figure above. The bundles may consist of one or several rows of finned tubes. Condensation of the steam takes place inside these tubes. The latent heat of the condensing steam is removed by the air which is forced over the fins by axial flow fans. The condensate, under the action of gravity, runs downwards into the combining headers, where it accumulates. From there the condensate is pumped back to the boiler.

Because of the low absolute pressure of the steam and the large dimensions of the condenser, air and other non-condensible gases may leak into the system. This problem has been solved by allowing a part of the steam to flow uncondensed through the main condenser section to be condensed at a later stage in the dephlegmator. The non-condensible gases flow along with the excess steam to this dephlegmator, which has a similar configuration as the main condenser section, with the difference that the steam flows upwards while the formed condensate runs downward; it is therefore a reflux condenser. The non-condensible gases are removed at the top of the finned tubes of the dephlegmator by an ejector pump.

It has been found in most applications that at the lower part of some finned tubes, where they are connected to the combining header, sometimes so-called dead zones can be observed, which are regions at which no condensation occurs. The dead zones are identified by the low temperature at which the air leaves the bundle. Fahlsing [95FA1] refers to such dead zones observed at the Wyodak Power Plant occurring at the finned tubes situated at the condenser inlet and just downstream of the dephlegmator as indicated in figure 1.1. The formation of dead zones can be explained by either one or all of the following conditions being valid:

1) Due to a possible unevenly distributed air flow through the bundles, the air flow over some finned tubes might be greater than required to condense the steam along the full length of the finned tube so that it is condensed before it reaches the finned tube outlet. Thus non-condensible gases are trapped in the lower part of the finned tube, as no steam flow is present. The trapped non-condensible gases lower the efficiency of the finned tube because it is not used fully for condensation and corrosion can occur in the dead zone region.

2) Due to a possible nonuniform steam flow distribution through the finned tubes, the steam flow entering some finned tubes might be lower than the potential condensation rate of the finned tube. Again the steam will condense fully before it reaches the outlet

of the finned tube.

3) If the bundles consist of more than one row of finned tubes, different heat transfer characteristics may be experienced by the rows. Therefore, due to similar reasons as in the first two conditions, dead zones can form.

In order to avoid the formation of dead zones in air-cooled steam condensers consisting of bundles with single rows of finned tubes, the excess steam flow to the dephlegmator is designed to be of such a magnitude that the flow entering every individual finned tube of the main condenser is large enough to allow for only partial or just complete condensation in every finned tube. In order to accomplish this, it might be required that, in the case of an extremely unfavourable condenser configuration, the fraction of the steam flowing uncondensed through the condenser has to be increased to a such an extent that the thermal efficiciency of the condenser is reduced considerably as many of the finned tubes are not used to their full potential.

It is the objective of this work to analyze the flow through an air-cooled condenser consisting of bundles with single rows of finned tubes, to determine the parameters which influence the flow distribution. To simplify the investigation, a uniformly distributed air flow over the finned tubes will be assumed, to give identical condensation rates in the individual finned tubes. The emphasis will be placed on two aspects. One is the fact that, according to Van Heerden [91VA1], the inlet loss coefficients of the finned tubes vary. The inlet loss coefficients make up a part of the flow resistance of the finned tubes and thereby can contribute to a nonuniform steam flow distribution through the condenser. Therefore a thorough experimental investigation of these inlet loss coefficients will be performed and the implication of these different loss coefficients on the steam flow pattern through the air-cooled condenser will be studied. The second aspect is found in the fluid mechanics of the air-cooled condenser configuration. The static pressure difference over every individual finned tube, together with the flow resistance of the tube, determines the tube's flow rate. The static pressure difference is a function of the static pressure in the dividing and the combining header. These static header pressures may either decrease or increase along the headers, depending on the header flow direction. Thereby the pressure difference over the finned tube varies and nonuniform steam flow distribution cannot be avoided.

CHAPTER 2

FLUID FLOW IN DUCTS

2.1 INTRODUCTION

Frictional forces act against flow in a duct. Furthermore we find that if the flow situation changes, e.g. the cross-sectional duct area changes or part of the flow branches off, the flow experiences a loss in mechanical energy. The frictional effects are quantified by a dimensionless friction factor, while losses in mechanical energy due to other appurtenances are usually expressed by means of a dimensionless flow loss coefficient. Friction factors and flow loss coefficients that are encountered in air-cooled condensers will be discussed in this chapter.

2.2 DUCT FRICTION FACTOR EQUATIONS

Frictional forces act on any surface that is exposed parallel to a fluid as a result of the friction encountered between the surface and the fluid. A boundary layer is developed from the leading edge of that surface in which the net parallel velocity component changes from nil (at the surface) to the free stream velocity (at a distance δ, which is the local boundary layer thickness, perpendicular to the surface). In duct flow we encounter a pressure gradient due to frictional effects which is quantified by means of a dimensionless friction factor. In the literature two friction factor definitions are found: the Fanning and the D'Arcy friction factor (f and f_D respectively) which are defined in terms of the shear stress between the duct wall and the fluid, τ, and the fluid's mean velocity, v:

$$f_D = 4\,f = \frac{4\,\tau}{\frac{1}{2}\rho\,v^2} \tag{2.1}$$

The D'Arcy friction factor will be used in this work.

The equivalent (or hydraulic) diameter of a duct is defined as follows:

$$d_e = \frac{4\,A}{P_d} \tag{2.2}$$

where A is the cross sectional flow area and P_d the perimeter of the duct. For ducts with a circular cross-section the equivalent diameter is equal to the duct diameter while for flow between infinite parallel plates the equivalent diameter is the limit

$$d_e = \lim_{h \to \infty} \frac{4 \times w \times h}{2\,(\,w + h\,)} = 2\,w \tag{2.3}$$

where w is the distance between the plates and h the width.

The frictional pressure gradient of a fluid flowing through a duct is quantified by the following equation:

$$\frac{dp_{fr}}{dz} = f_D \frac{1}{d_e} \frac{1}{2} \rho\, v^2 \tag{2.4}$$

where v is the local mean fluid velocity at the increment. It can by shown by dimensional analysis that

$$f_D = f\left(\frac{\rho\, v\, d_e}{\mu}, \frac{\varepsilon}{d_e}\right) \tag{2.5}$$

where the first term in the bracket is known as the Reynolds number

$$Re = \frac{\rho\, v\, d_e}{\mu} \tag{2.6}$$

which characterizes the ratio of the inertia forces to the frictional forces in the fluid. The second term is the relative roughness of the duct wall, which in our applications will be set equal to nil as we assume smooth duct walls.

Laminar flow:

According to White [89WH1], the friction factor for laminar flow (Re<2300) in circular ducts is derived by making use of the Newtonian laminar shear stresses and velocity profiles

$$f_D = \frac{64}{Re} \tag{2.7}$$

while for laminar flow between infinite parallel plates the friction factor is derived in similar fashion as

$$f_D = \frac{96}{Re} \tag{2.8}$$

Turbulent flow:

For turbulent flow (Re>2300) in smooth round tubes Blasius [11BL1] presents the following approximate correlation for a Reynolds number up to 10^5

$$f_D = \frac{0.3164}{Re^{0.25}} \tag{2.9}$$

Haaland [83HA1] proposes

$$f_D = 2.7778\left(\log_{10}\left(\left(\frac{7.7}{Re}\right)^3 + \left(\frac{\varepsilon/d_e}{3.75}\right)^{3.33}\right)\right)^{-2} \tag{2.10}$$

for small values of ε/d_e.

For turbulent flow between infinite parallel plates, White [89WH1] proposes a semi-empirical equation which was derived by Prandtl by making use of experimental boundary layer data:

$$f_D = \left(2.0\log_{10}\left(Re\, f_D^{0.5}\right) - 1.19\right)^{-2} \tag{2.11}$$

This implicit equation can be approximated by an equation similar to equation (2.9) with

$$f_D = \frac{0.351072}{Re^{0.25083}} \tag{2.12}$$

The above equations are compared graphically in figure 2.1 for smooth duct flow:

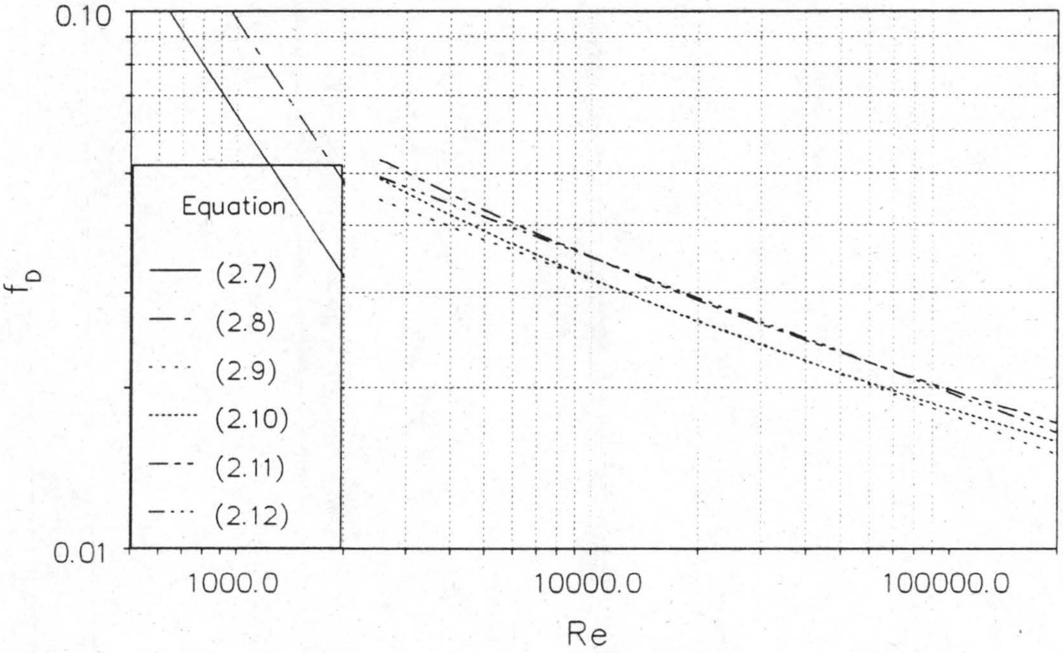

Figure 2.1: Friction factor equations for smooth duct flow.

2.3 DEFINITION OF A FLOW LOSS COEFFICIENT

Losses of mechanical energy may occur during duct flow at inlets, outlets, changes in duct cross-sectional area, branchings and other appurtenances. If body forces acting on the fluid can be ignored, the energy equation for incompressible adiabatic flow between two sections can be written as

$$\frac{p_1}{\rho} + \frac{1}{2}\alpha_{e1} v_1^2 = \frac{p_2}{\rho} + \frac{1}{2}\alpha_{e2} v_2^2 + E_{Mloss} \tag{2.13}$$

where the energy correction factor, α_e, takes into account the form of the velocity profile at the respective section and is defined as

$$\alpha_e = \frac{1}{A v^3} \int_A v_{loc}^3 \, dA \tag{2.14}$$

with v_{loc} designating the local velocity vector normal to the incremental flow area (dA) and v the mean velocity over the cross-sectional flow area (A). The loss in mechanical energy (E_{Mloss}) is expressed in terms of a dimensionless loss coefficient (K):

$$E_{Mloss} = \frac{1}{2} K v^2 \tag{2.15}$$

where v usually corresponds to v_1 or v_2, or some mean value thereof. Substitute equation (2.15) into equation (2.13) and solve for K

$$K = \frac{p_1 - p_2 + \frac{1}{2}\alpha_{e1} \rho v_1^2 - \frac{1}{2}\alpha_{e2} \rho v_2^2}{\frac{1}{2}\rho v^2} \tag{2.16}$$

It must be emphasized that the value of K is depends on the mean velocity used and therefore it must always be stated clearly on which value of v it is based.

2.4 FLOW LOSS COEFFICIENT OF A FLATTENED TUBE IN WHICH PART OF THE FLOW CHANGES FROM THE VAPOUR TO THE LIQUID PHASE

In condensation flow, the fluid changes its phase from a vapour to a liquid. The total pressure change will consist of the frictional pressure loss and the pressure gain due to the increase of the fluid's momentum. Condensation flow in a typical flattened finned tube in which the condensate flows downwards due to gravity is considered. It will be assumed that the condensation occurs at a uniform rate along the entire length of the flattened tube and that the vapour is incompressible and has constant thermo-physical properties. In our case the volume of the liquid phase that is formed during the condensation is neglected because it occupies a small part of the total flow area and it flows co-current with the steam flow. This implies that the velocities and Reynolds numbers are those of the vapour phase with reference to the full cross-sectional area and equivalent diameter.

In order to quantify the loss in total pressure over the flattened tube length two approaches will be presented: In the first approach a modified friction factor which takes into account the wall suction due to the condensation will be used. This friction factor was introduced by Groenewald [93GR1] as he found analytically and experimentally that during condensation flow the local friction factor is greater than that described by the Blasius equation (equation (2.9)) with the application of the equivalent diameter concept to provide for the flattened tube. Groenewald interpreted this higher friction factor as an effect of the wall suction due to condensation which would tend to make the local velocity profile more uniform, giving a higher wall shear stress. It can however be seen in figure 2.1 that the friction factor for flow between parallel plates (equation (2.11)) is higher than that for flow in round tubes with the same Reynolds number. Therefore we will compare the approach of Groenewald to a solution obtained by using the parallel plate friction factor correlation given in equation (2.12) ignoring the wall suction.

Consider the control volume encountered in a flattened finned tube of length L_t, width w and height h, in which condensation takes place shown in figure 2.2.

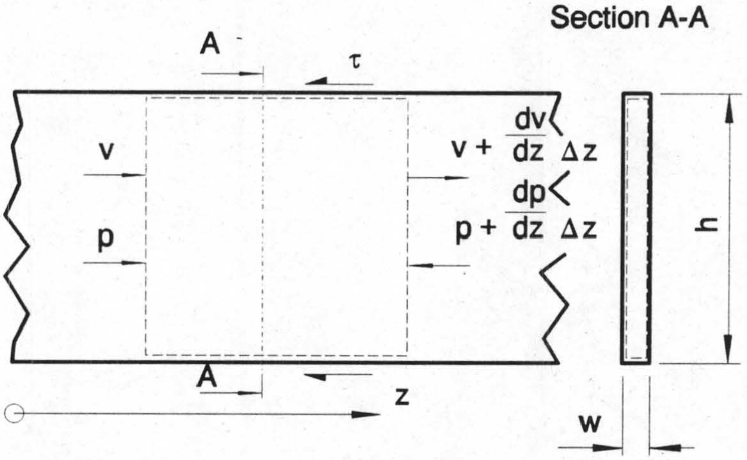

Figure 2.2: Control volume in a flattened tube with uniform axial condensation rate.

Assuming a nearly uniform velocity profile throughout the flattened tube, the following equation can be obtained by applying a local momentum balance over the control volume, after neglecting higher order terms of the differential increment, Δz:

$$-\frac{dp}{dz} - \tau \frac{P}{A_t} = 2 \rho v \frac{dv}{dz} \tag{2.17}$$

where τ is the wall shear stress, P the perimeter and A_t the cross-sectional area of the flattened tube. The wall shear stress can be expressed in terms of the D'Arcy friction factor

$$\tau = f_{Dc} \frac{1}{8} \rho v^2 \tag{2.18}$$

where the subscript c provides for the condensation effects.

Assuming a steam quality of unity at the tube inlet and a uniform condensation rate along the length of the flattened finned tube, the mean steam velocity can be written as a function of the longitudinal distance, z:

$$v = v_i \left(1 - \frac{1 - x_o}{L_t} z \right) \tag{2.19}$$

where v_i is the mean steam velocity at the inlet and x_o is the outlet steam quality. The steam quality at any point in the flattened tube is given by:

$$x = \frac{v}{v_i} = \frac{Re}{Re_i} \tag{2.20}$$

The velocities in equation (2.20) can be replaced by the respective Reynolds numbers because of the assumed constant thermo-physical properties of the vapour.

Substitute equations (2.18) and (2.2) into equation (2.17) to give:

$$\frac{dp}{dz} = -\frac{1}{2} f_{Dc} \frac{1}{d_e} \rho v^2 - 2 \rho v \frac{dv}{dz} \tag{2.21}$$

Equation (2.21) can be solved by integrating over the length of the flattened tube, L_t:

$$p_o - p_i = -\frac{1}{2}\frac{\rho}{d_e}\int_0^{L_t} f_{Dc}\, v^2\, dz - \rho\, v_i^2\left(x_o^2 - 1\right) \tag{2.22}$$

We now define the frictional static pressure drop as

$$\Delta p_{fr} = \frac{1}{2}\frac{\rho}{d_e}\int_0^{L_t} f_{Dc}\, v^2\, dz \tag{2.23}$$

In order to integrate equation (2.23) analytically we will express the condensation friction factor, the velocity and the distance variable in terms of the steam quality.

Substituting equation (2.19) into equation (2.20) and rearranging yields an expression for z in terms of the steam quality:

$$z = L_t\,\frac{1 - x}{1 - x_o} \tag{2.24}$$

By making use of equation (2.24) and a friction factor equation in terms of the Reynolds number which together with the velocity can be expressed by equation (2.20), equation (2.23) can be rewritten in terms of the steam quality as sole variable. Two of these friction factor equations will be presented in sections 2.4.1 and 2.4.2.

If the steam flow changes from turbulent to laminar, we define the transitional steam quality:

$$x_{tr} = \frac{Re_{tr}}{Re_i} \tag{2.25}$$

and take the transitional Reynolds number, Re_{tr}, as 2300. Now the flattened tube length to the transition, L_{ttr} can be derived from equation (2.24) by substituting equation (2.25) for x_{tr}:

$$L_{ttr} = \frac{L_t}{1 - x_o}\left(1 - \frac{Re_{tr}}{Re_i}\right) \tag{2.26}$$

2.4.1 FRICTION FACTOR WITH CONDENSATION WALL SUCTION EFFECT

Groenewald [93GR1] proposes a condensation friction factor that provides for the condensation effects for the flow between parallel plates. His analysis takes into account the effect of the condensation wall suction on the velocity profile in the tube for laminar and turbulent flow. The proposed friction factor correlation for the wall suction influenced friction factor for laminar flow is

$$f_{Dc} = C\, f_D \tag{2.27a}$$

and for turbulent flow

$$f_{Dc} = \left(A + \frac{B}{Re} \right) f_D \tag{2.27b}$$

A wall Reynolds number, Re_w, based on the average suction velocity component normal to the parallel walls of the flattened tube is introduced by Groenewald. For condensation flow between parallel plates this wall Reynolds number is expressed as

$$Re_w = \frac{2\, w\, m_c}{\mu\, A_w} = \frac{d_e\, m_c}{\mu\, A_w} \tag{2.28}$$

where m_c is the condensation rate of the flattened tube, w the distance between the walls and A_w the surface area of the parallel walls. From the continuity equation the above equation can be expressed in terms of the tube inlet Reynolds number

$$Re_w = Re_i \left(1 - x_o \right) \frac{w}{2\, L_t} \tag{2.29}$$

For $Re_w \leq 40$ the factors in equation (2.27a) and (2.27b) are given by the following empirical regressions

$$A = 1.041 \times 10^{-3}\, Re_w - 2.011 \times 10^{-7}\, Re_w^3 + 1.0649$$

$$B = 59.3153\, Re_w + 1.5995 \times 10^{-2}\, Re_w^3 + 290.1479$$

$$C = 1 + 6.56 \times 10^{-4}\, Re_w^2$$

In order to integrate equation (2.23) three cases have to be considered:

Case 1: $\quad$ Re_i and Re_o laminar (<2300)

Case 2: $\quad$ Re_i turbulent (>2300) and Re_o laminar (<2300)

Case 3: $\quad$ Re_i and Re_o in turbulent range (>2300)

Substitute equation (2.24) together with equations (2.27a) for laminar flow and (2.27b) for turbulent flow into equation (2.23) and make use of equation (2.20) for the Reynolds number to integrate equation (2.23) for the laminar flow region

$$\Delta p_{fr} = \frac{1}{2} \rho v_i^2 \frac{L_t}{d_e} \frac{96}{Re_i} \frac{C}{x_o - 1} \int_{x_{lam}} x \, dx \tag{2.30a}$$

and for the turbulent flow region

$$\Delta p_{fr} = \frac{1}{2} \rho v_i^2 \frac{L_t}{d_e} \frac{0.3164}{Re_i^{0.25}} \frac{1}{x_o - 1} \int_{x_{turb}} \left(A\, x^{1.75} + \frac{B}{Re_i} x^{0.75} \right) dx \tag{2.30b}$$

Using the appropriate integration boundaries the respective dimensionless frictional pressure losses over the full length of the flattened tube for the three cases are:

Case 1:

$$\frac{\Delta p_{fr}}{\frac{1}{2} \rho v_i^2} = \frac{L_t}{d_e} \frac{48\, C}{Re_i} \left(x_o + 1 \right) \tag{2.31a}$$

Case 2:

$$\frac{\Delta p_{fr}}{\frac{1}{2} \rho v_i^2} = \frac{L_t}{d_e} \frac{1}{x_o - 1}$$

$$\times \left(\frac{0.3164}{Re_i^{0.25}} \left(\frac{A}{2.75} \left(x_{tr}^{2.75} - 1 \right) + \frac{B}{1.75\, Re_i} \left(x_{tr}^{1.75} - 1 \right) \right) + \frac{48\, C}{Re_i} \left(x_o^2 - x_{tr}^2 \right) \right) \tag{2.31b}$$

Case 3:

$$\frac{\Delta p_{fr}}{\frac{1}{2}\rho v_i^2} = \frac{L_t}{d_e}\frac{1}{x_o - 1}$$

$$\times \frac{0.3164}{Re_i^{0.25}}\left(\frac{A}{2.75}\left(x_o^{2.75} - 1\right) + \frac{B}{1.75\,Re_i}\left(x_o^{1.75} - 1\right)\right) \qquad (2.31c)$$

2.4.2 PARALLEL PLATE FRICTION FACTOR USED FOR CONDENSATION FLOW IN FLATTENED TUBE WITHOUT WALL SUCTION EFFECTS

As the friction factor for flow between parallel plates is higher than that of flow in round tubes we will solve equation (2.23) for a flattened tube by using equations (2.8) and (2.12) for laminar and turbulent flow respectively to describe the parallel plate friction factor, and neglect the effect of the condensation wall suction. The condensation friction factor for the laminar and the turbulent range can be expressed in the form of

$$f_{Dc} = f_D = a\,Re^{\,b} \qquad (2.32)$$

where $a = 96$ and $b = -1$ for laminar flow and $a = 0.351072$ and $b = -0.25083$ for turbulent flow, as taken from equations (2.8) and (2.12).

Integrate equation (2.23) analytically by expressing all the variables in terms of the z:

$$\Delta p_{fr} = \frac{1}{2}\frac{\rho}{d_e}\int_0^{L_t} v_i^2\, a\, Re_i\left(1 - \frac{1 - x_o}{L_t} z\right)^{2+b} dz$$

$$= \frac{1}{2}\rho v_i^2 \frac{L_t}{d_e}\, a\, Re_i \frac{1}{x_o - 1}\left[\frac{x_o^{(3+b)} - 1}{3+b}\right] \qquad (2.33)$$

For the three case stated in the previous section the dimensionless frictional pressure loss can be determined by choosing the constants a and b appropriately and integrating equation (2.33)

Case 1:

$$\frac{\Delta p_{fr}}{\frac{1}{2}\rho v_i^2} = \frac{L_t}{d_e}\frac{48}{Re_i}\left(x_o + 1\right) \tag{2.34a}$$

Case 2:

$$\frac{\Delta p_{fr}}{\frac{1}{2}\rho v_i^2} = \frac{L_t}{d_e}\frac{1}{x_o - 1}\left(\frac{0.127701}{Re_i^{0.25083}}\left(x_{tr}^{2.74917} - 1\right) + \frac{48}{Re_i}\left(x_o^2 - x_{tr}^2\right)\right) \tag{2.34b}$$

Case 3:

$$\frac{\Delta p_{fr}}{\frac{1}{2}\rho v_i^2} = \frac{L_t}{d_e}\frac{1}{x_o - 1}\frac{0.127701}{Re_i^{0.25083}}\left(x_o^{2.74917} - 1\right) \tag{2.34c}$$

2.4.3 CONDENSATION FLOW LOSS COEFFICIENT

Assume that the energy correction factors are approximately equal to 1, the flow loss coefficient for condensation flow in a flattened tube from its inlet to its outlet is defined

$$K_{con} = \frac{p_i + \frac{1}{2}\rho v_i^2 - p_o - \frac{1}{2}\rho v_o^2}{\frac{1}{2}\rho v_i^2} = \frac{p_i - p_o}{\frac{1}{2}\rho v_i^2} + \left(1 - x_o^2\right) \tag{2.35}$$

Referring to equations (2.22) and (2.23) the static pressure difference term in equation (2.35) is expressed as

$$p_i - p_o = \Delta p_{fr} - \rho v_i^2\left(1 - x_o^2\right) \tag{2.36}$$

Substitute equation (2.36) into equation (2.35) to obtain

$$K_{con} = \frac{\Delta p_{fr}}{\frac{1}{2}\rho v_i^2} - \left(1 - x_o^2\right) \tag{2.37}$$

The first term on the right hand side of equation (2.37) can be calculated by either equations (2.31a-c) or equations (2.34a-c). The value of K_{con} can be smaller than nil which means that a total gain of mechanical energy occurs over the flattened tube. In figure 2.3 the condensation loss coefficient is presented for different values of x_o for a flattened tube with a length (L_t) of 9m and an equivalent diameter (d_e) of 0.019m for both friction factor models as a function of the outlet quality at different inlet Reynolds numbers.

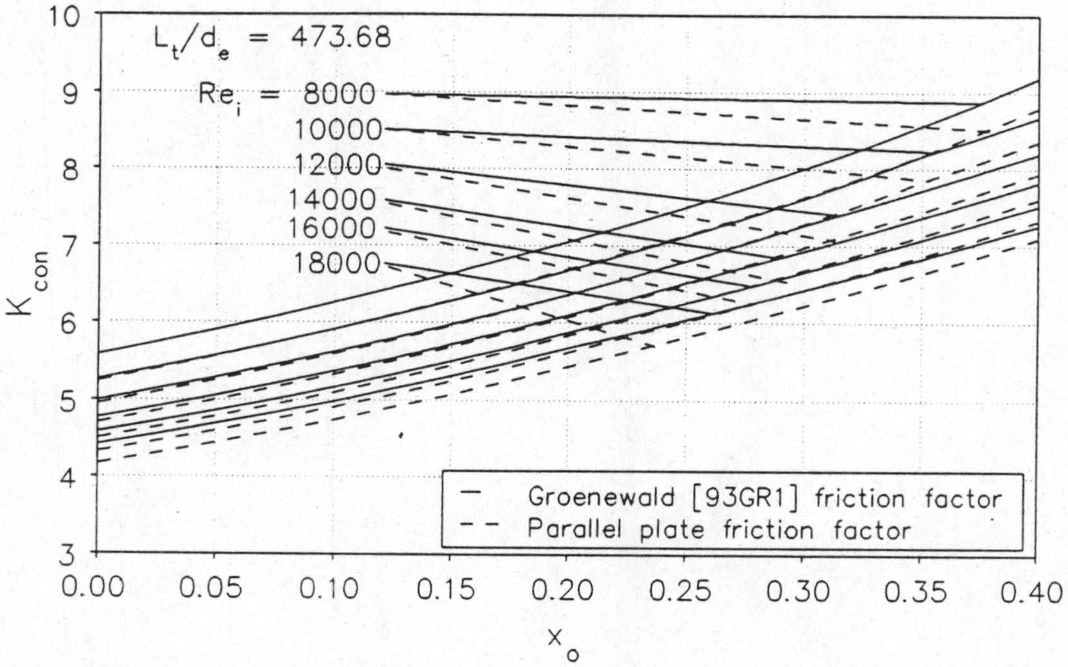

Figure 2.3: Condensation loss coefficients.

It can also be seen in figure 2.3 that the flow loss coefficient of Groenewald [93GR1] is higher than that of the parallel plate model, the maximum deviation being in the order of 5%.

2.5 ABRUPT CONTRACTIONS AND ABRUPT EXPANSIONS OF FLOW AREA

2.5.1 ABRUPT CONTRACTIONS

When a fluid experiences a sudden contraction of flow area as shown in figure 2.4, flow separation occurs at the sharp rectangular edge of the contraction due to the inertia forces acting on the fluid. This separation gives a recirculation vortex at the duct wall.

A jet stream, called the *vena contracta*, is formed between the separation vortices.

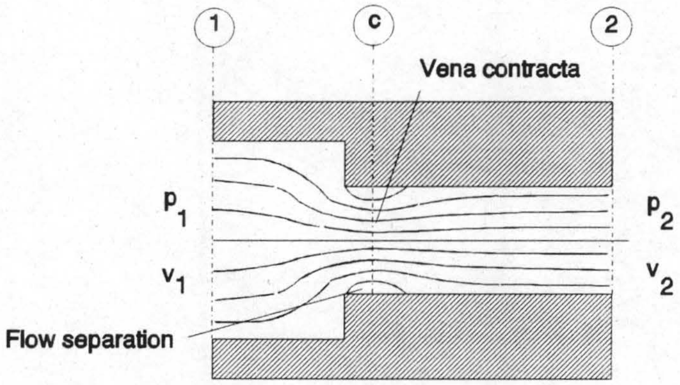

Figure 2.4: Sudden contraction of duct cross-sectional area.

Further downstream the flow reattaches to the wall again. After the point of reattachment the flow starts to develop its velocity profile. Across the sudden contraction the fluid experiences a loss of its mechanical energy which can be ascribed mainly to the jet contraction. The frictional irreversible energy conversions occurring up to the jet formation during the contraction and after reattachment of streamlines also contribute to the loss.

Define the area contraction ratio

$$\sigma_{12} = \frac{A_2}{A_1} \tag{2.38}$$

and the jet contraction ratio

$$C_c = \frac{A_c}{A_2} \tag{2.39}$$

Weisbach [00WE1] investigated the jet contraction ratio as a function of the contraction of flow area. Polynomials were fitted through his data. For round tube inlets the jet contraction ratio is given by:

$$C_c = 0.61375 + 0.13318\sigma_{12} - 0.26095\sigma_{12}^2 + 0.51146\sigma_{12}^3 \tag{2.40a}$$

while for inlets of parallel plate ducts it is given by

$$C_c = 0.6144517 + 0.04566493\,\sigma_{12} - 0.336651\,\sigma_{12}^2 + 0.4082743\,\sigma_{12}^3 + 2.672041\,\sigma_{12}^4 - 5.963169\,\sigma_{12}^5 + 3.558944\,\sigma_{12}^6 \qquad (2.40b)$$

The two equations above are shown graphically in figure 2.5.

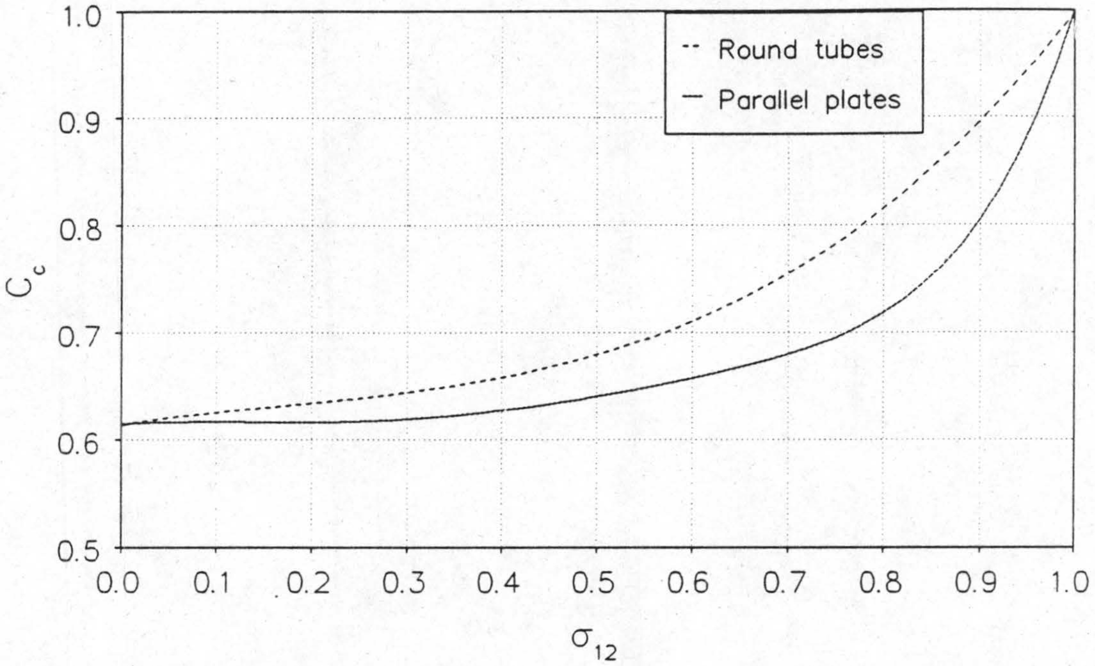

Figure 2.5: Jet contraction ratio of vena contracta.

The following authors present semi-analytical and empirical contraction loss coefficients:

Kays [50KA1]:

Kays derives an equation for the inlet loss coefficient, or contraction loss coefficient by assuming that no irreversible energy changes occur between sections 1 and c. Bernoulli's equation is applicable between the two sections. Between sections 1 and 2 the continuity equation and momentum equations are applied to give:

$$K_c = \frac{1 - \alpha_{e1}\sigma^2 C_c^2 - 2C_c + 2\alpha_{m3} C_c^2}{C_c^2} - \left(1 - \sigma^2\right) \qquad (2.41)$$

The energy correction factor, α_e, has been defined in equation (2.14). With the same variables the momentum correction factor, α_m, is defined as:

$$\alpha_m = \frac{1}{v^2 A} \int_A v_{loc}^2 \, dA \tag{2.42}$$

For fully turbulent flow at sections 1 and 2, α_{e1} and α_{m2} are approximately equal to 1. Equation (2.41) then becomes

$$K_c = \left(1 - \frac{1}{C_c}\right)^2 \tag{2.43}$$

Benedict, Carlucci and Swetz [66BE1]:

A loss coefficient equation is presented that consists of the sum of contributions of the contracting flow and the re-expansion up to the section where reattachment occurs:

$$K_c = \frac{1}{C_v^2 C_c^2} - \frac{2}{C_c} + 1 \tag{2.43}$$

Equation (2.43) was derived by Hughes and Safford [08HU1]. C_v is a velocity field correction factor of the vena contracta which is given in some references [00WE1], [00FR1] as C_v=0.975. Other publications neglect this influence and take the value as unity with the result that equation (2.44) is equal to equation (2.43). Furthermore Benedict et al [66BE1] conducted an experimental investigation to determine the contraction loss coefficient as a function of the flow area contraction ratio. The data was correlated by the following regression

$$\begin{aligned} K_c = {} & 0.57806 + 0.39543\sigma_{12} - 4.53854\sigma_{12}^2 \\ & + 14.24265\sigma_{12}^3 - 19.22214\sigma_{12}^4 + 8.54038\sigma_{12}^5 \end{aligned} \tag{2.45}$$

Idelchic [89ID1]:

The following approximation of the contraction loss coefficient for Reynolds numbers higher than 10^4 is presented by Idelchic [89ID1]:

$$K_c = \frac{1}{2}(1 - \sigma_{12}) \tag{2.46}$$

Idelchic adapted the above equation to describe his experimental data more accurately:

$$K_c = \frac{1}{2}(1 - \sigma_{12})^{\frac{3}{4}} \tag{2.47}$$

According to Idelchic the losses of mechanical energy that occur during the flow acceleration up to the vena contracta are negligible compared to those of the subsequent expansion.

Miller [71MI1], [78MI1]:

Miller postulates, like Idelchic, that the expansion primarily contributes to the contraction loss coefficient. He presents a graphical contraction loss coefficient which has been correlated with the following regression:

$$K_c = 0.62860 - 0.65431\sigma_{12} + 1.82875\sigma_{12}^2 - 4.38352\sigma_{12}^3 + 2.58042\sigma_{12}^4 \tag{2.48}$$

Engineering Science Data Unit [77EN1]:

Contraction loss coefficient data is given by the Engineering Science Data Unit in graphical form for duct Reynolds numbers greater than 10^5; the following polynomial has been fitted through the data

$$K_c = 0.583466 - 0.486125\sigma_{12} + 0.973659\sigma_{12}^2 - 3.006891\sigma_{12}^3 + 1.938821\sigma_{12}^4 \tag{2.49}$$

Figure 2.6 shows the graphical representation of the formulae of the above stated references. In the figure it can be clearly seen that the different contraction loss coefficient equations differ numerically. The experimental values of Augustin [95AU1] for σ_{12}=0 and σ_{12}=0.83 are also indicated in figure 2.6. The contraction loss coefficient for σ_{12}=0 will be designated K_0.

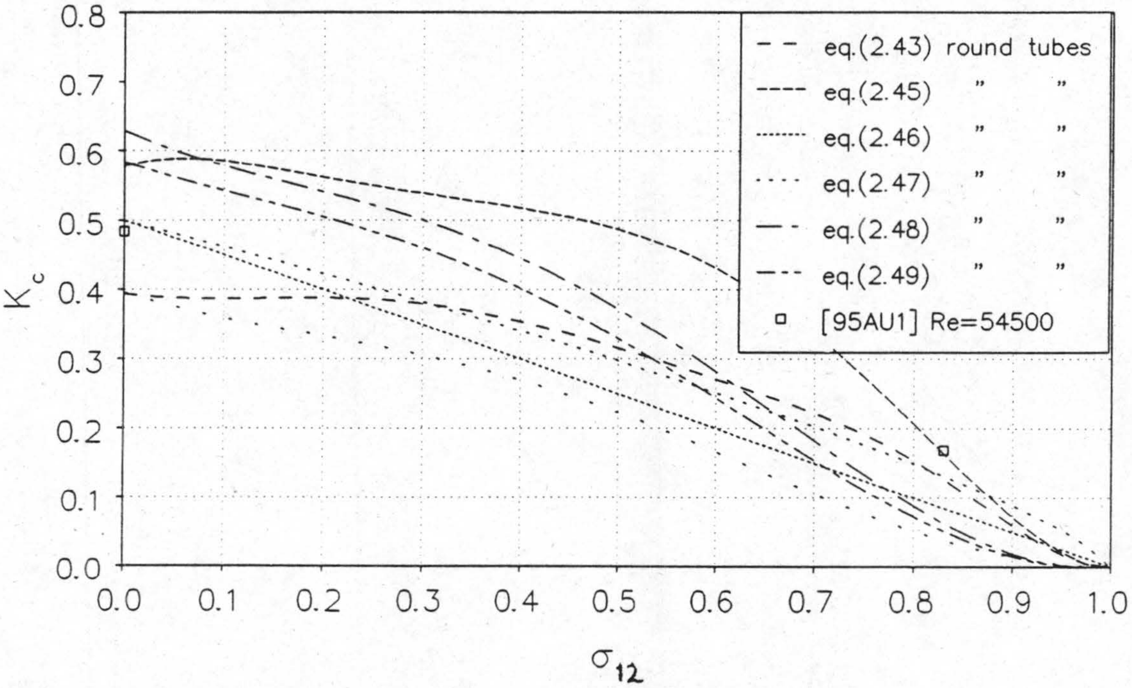

Figure 2.6: Contraction loss coefficients as function of the duct area contraction ratio.

2.5.2 ABRUPT EXPANSIONS

Consider flow experiencing a sudden expansion of the flow area as shown in figure 2.7.

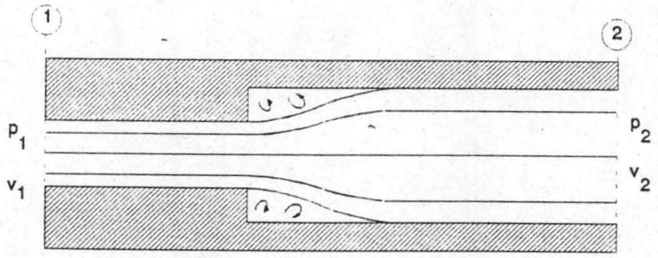

Figure 2.7: Flow experiencing a sudden expansion of flow area.

The following equation for the loss coefficient of flow experiencing a sudden expansion is proposed by Idelchic [86ID1]:

$$K_e = \left(1 - \frac{A_2}{A_1}\right)^2 = \left(1 - \sigma_{21}\right)^2 \tag{2.50}$$

2.6 FLOW APPROACHING AN INLET OBLIQUELY

Flow that enters a duct inlet obliquely, as shown in figure 2.8, has similar characteristics regarding flow separation to the case of flow undergoing a sudden contraction in flow area.

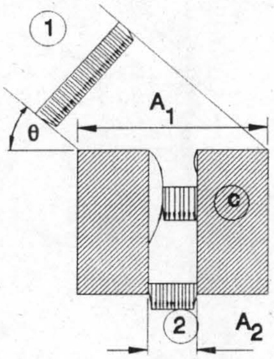

Figure 2.8: Flow approaching an inlet obliquely.

Flow approaches a screen of parallel plate ducts with a frontal area ratio (or porosity) of σ at an angle θ. If $\sigma_{12}=1$ the situation can be simplified to flow around a sharp bend. As indicated in figure 2.8, flow separation will occur at that inlet edge at which the flow approaches with a sharp angle. With a porosity smaller than unity the effects due to the contraction in flow area will also play a role. At first the case of unity porosity will be considered. As the flow is bent we actually have an increase in flow area. Separation occurs just after the inlet and a jet (vena contracta) is formed. Mohandes [79MO1] assumes a uniform velocity profile over the vena contracta and proposes that the jet contraction ratio for this case is given by the following function:

$$C_c = \frac{A_c}{A_2} = \sin\theta \tag{2.51}$$

where A_2 is the area of the duct downstream of the bend and A_c the flow area of the vena contracta. From conservation of momentum and assuming a uniform upstream and downstream velocity profile, the inlet loss coefficient can be derived as:

$$K_{i\theta} = \left(\frac{1}{\sin(\theta)} - 1\right)^2 \tag{2.52}$$

Augustin [95AU1] measured the velocity profile of the vena contracta for two bend angles for four different Reynolds numbers. It was found that the velocity profile is independent of the Reynolds number. Furthermore the velocity profile of the vena contracta was found to be non-uniform in contrast to the assumption of Mohandes. The experiments of Augustin also involved the determination of the inlet loss coefficient. Numerical solutions of the velocity profiles at the contraction obtained with the *PHOENICS* computer code (see appendix B for further details) are compared to the data of Augustin in figures B.9 and B.10 in appendix B. The two different numerical solutions presented in the figures are elaborated in appendix B.

Mohandes further gives the following correlation for the inlet loss coefficient for non-unity porosities based on the contraction loss coefficient of the specific porosity which correlates his experimental data.

$$K_{i\theta} = \left(K_c^{0.5} + \frac{1}{\sin(\theta)} - 1 \right)^2 \tag{2.53}$$

2.7 INLET LOSS COEFFICIENTS OF CONSECUTIVE LATERALS AT CONSTANT PITCH WITH NET PASSING FLOW

Consecutive laterals at constant pitch are found in the dividing header of an air-cooled condenser. Here the flow entering the laterals (or the finned tubes) experiences a loss in its total pressure dependent on the inlet geometry of the laterals and on the influence the laterals have on each other. Consider the situation of flow entering consecutive laterals at constant pitch at right angle to the general header flow direction shown in figure 2.9. At the inlet to the lateral the flow forms a vena contracta. This contraction can be ascribed to the area contraction but also to the small angle of approach. The contraction of flow area and the oblique approach will ensure the flow to separate at the lateral inlet edge as indicated in figure 2.9.

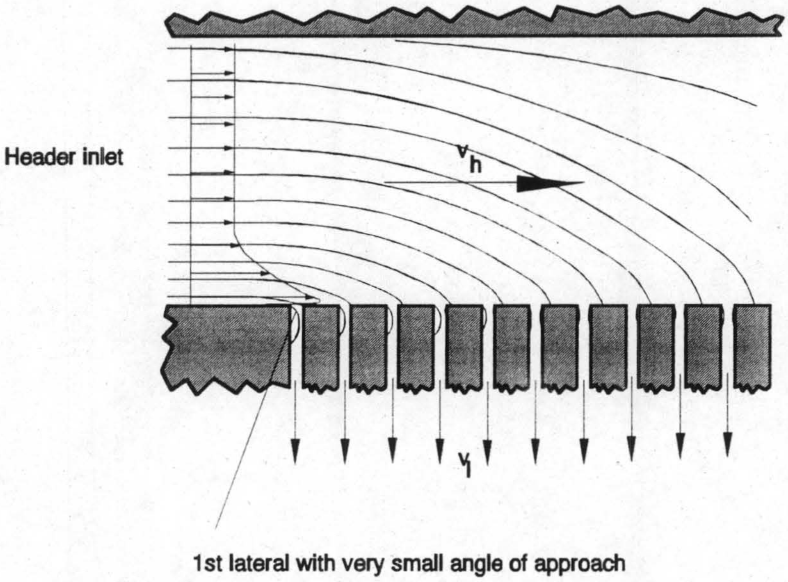

Figure 2.9: Lateral inlet configuration.

The extremely small angle of approach of the flow entering the first lateral can be seen in the figure. The flow into the remaining laterals approaches with a larger angle. The inlet loss coefficient of every lateral is defined as:

$$K_i = \frac{p_h - p_l}{\frac{1}{2}\rho v_l^2} + \alpha_{eh}\frac{v_h^2}{v_l^2} - 1 - f_D\frac{L_l}{d_{el}} \tag{2.54}$$

The lateral energy correction factor is taken as 1 because the point l is chosen in the region of fully developed turbulent flow in which an almost uniform velocity profile is found.

Nosova [59NO1] investigated the inlet loss coefficient found when flow from a net passing stream enters a single lateral. An increase of the inlet loss coefficient with an increasing header to mean lateral velocity ratio was observed. For multiple laterals it is difficult to determine the header energy correction factor, therefore in his experimental investigations Van Heerden [91VA1] only calculated the term

$$\left[K_i - \alpha_{eh} \frac{v_h^2}{v_l^2} \right] = \frac{p_h - p_l}{\frac{1}{2} \rho v_l^2} - 1 - f_D \frac{L_l}{d_{el}}$$

from his experimental readings. The application of this reduced inlet loss coefficient will be shown in the next chapter. Furthermore Van Heerden subtracted the normal inlet loss coefficient, K_0 of the laterals for a zero flow area contraction ratio. The remaining value will be called the header inlet to lateral velocity ratio dependent part of the inlet loss coefficient, or the K_{ivr} value which is

$$K_{ivr} = \left[K_i - \alpha_{eh} \frac{v_h^2}{v_l^2} \right] - K_0$$

Van Heerden [91VA1] investigated the inlet loss coefficients of several laterals at constant pitch consisting of both parallel plate ducts and round pipes. The experimental data of Van Heerden for 5 laterals with sharp inlet edges is shown in figure 2.10. It was found that the first lateral's inlet loss coefficient as a function of the header to mean lateral velocity ratio increased with a far greater gradient than those of the remaining laterals, even steeper than the inlet loss coefficient for a single lateral.

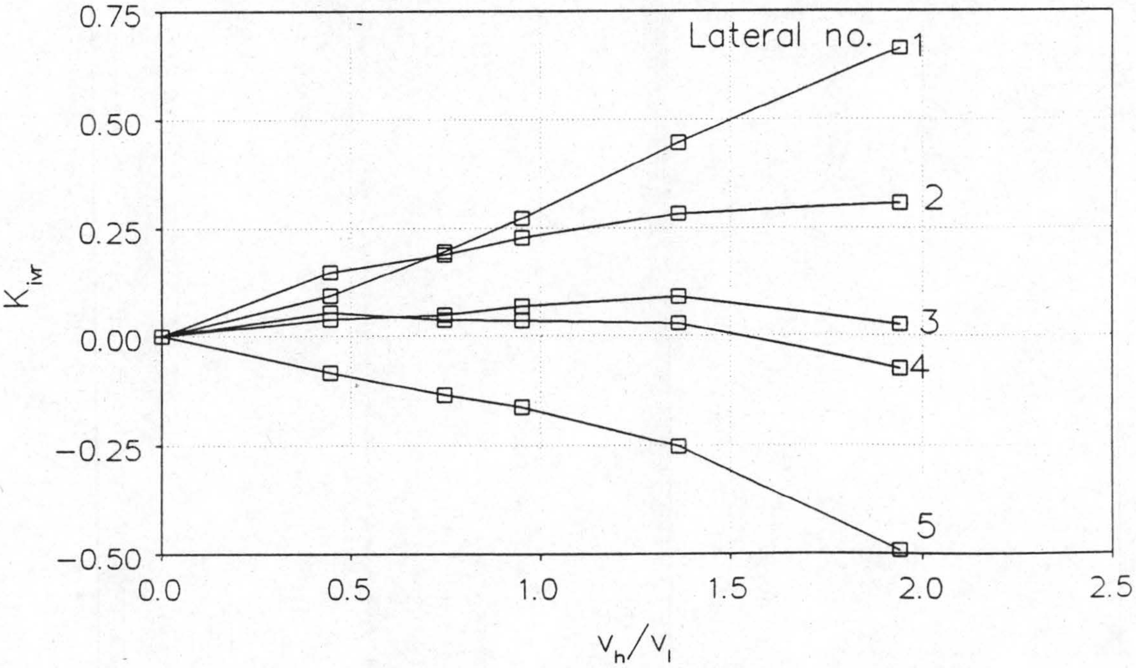

Figure 2.10: Experimental K_{ivr} values of Van Heerden for sharp lateral inlets.

Van Heerden's experimental apparatus consisted of a header width that was larger than the lateral height, giving a three-dimensional flow situation. For a header with the same height as that of the laterals the flow can be assumed to be two-dimensional. This flow situation was investigated numerically with the aid of the *PHOENICS* computer code as explained in appendix B. The trend of these K_{ivr} values, shown in figure B.13, is similar to that of Van Heerden's investigation.

CHAPTER 3

MANIFOLD SYSTEMS

3.1 INTRODUCTION

A flow manifold is used to divide flow into several ducts or to combine the flow coming from several ducts. This gives two basic types of manifolds: the dividing and the combining manifold. All manifold systems consist of one or combinations of these two. Figure 3.1 shows different manifold configurations encountered in heat exchangers.

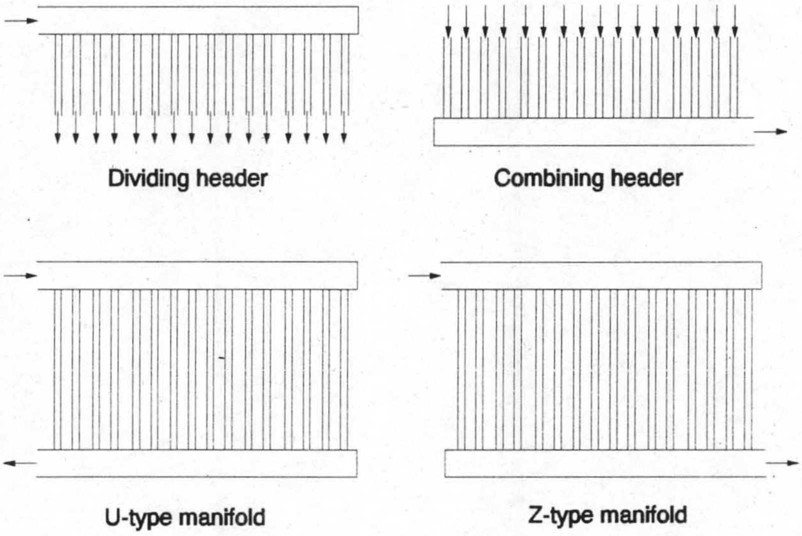

Figure 3.1: Manifold configurations.

Almost every heat exchanger in which heat is to be transferred to or from a process fluid, consists of a manifold system by which the exposed area of the fluid is increased in order to obtain a high heat transfer. The fluid enters the heat exchanger via a header from which it is then divided to into numerous smaller ducts or laterals, such as the finned tubes of an air-cooled condenser, in which the heat transfer takes place. A design criterion for heat exchanger manifold systems is to have a uniformly distributed flow through the laterals, because the laterals are usually identical with regard to heat transfer characteristics and geometry. It is therefore necessary to analyze the physics of flow through manifold systems. In this chapter we will present the governing manifold equations based on local header momentum balances. Based on these equations the solution methods presented by various authors are discussed.

3.2 DERIVATION OF THE HEADER CONTINUITY AND MOMENTUM DIFFERENTIAL EQUATIONS

The continuity and momentum equations describing the flow in the dividing and the combining header with constant cross-sectional are derived by applying a momentum balance over a control volume, which includes a single lateral inlet or outlet, as shown in figure (3.2).

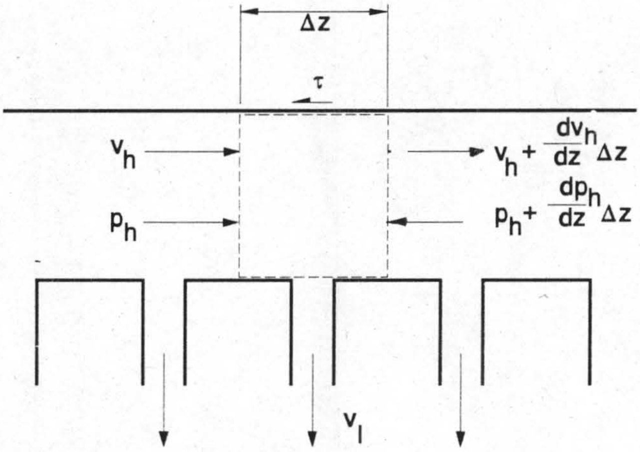

Figure 3.2: Header control volume.

For this control volume the continuity equation can be derived by applying the law of conservation of mass for incompressible flow:

$$\frac{d}{dz}\left(v_h\right)\Delta z A_h = -v_l A_l \tag{3.1}$$

where v_h and v_l are the mean header and lateral flow velocity in the indicated direction respectively. The momentum balance in the z-direction for the same control volume yields

$$\begin{aligned} p_h A_h - \left(p_h + \frac{d}{dz}(p_h)\Delta z\right)A_h - C\,\tau\,P_h\Delta z \\ = \left(\alpha_{mh} + \frac{d}{dz}(\alpha_{mh})\Delta z\right)\rho\left(v_h + \frac{d}{dz}(v_h)\Delta z\right)^2 A_h \\ + \alpha_{ml}\,\rho\, v_l A_l v_h - \alpha_{mh}\,\rho\, v_h^2 A_h \end{aligned} \tag{3.2}$$

where P_h is the header perimeter, τ the shear stress between the fluid and the header wall and C a factor which for $v_h > 0$, C = 1 and for $v_h < 0$, C = -1. The momentum correction factors, α_{mh} and α_{ml} are both based on the local mean header velocity. These factors provide for the non-uniformity of the local velocity profile of the header flow and the part of the header flow that enters the lateral respectively.

The header wall shear stress can be expressed in terms of the D'Arcy friction factor:

$$\tau = \frac{f_D}{4}\frac{1}{2}\rho v_h^2 \tag{3.3}$$

Substitute equations (3.1) and (3.3) into equation (3.2), ignore squares and higher orders of Δz and substitute equation (2.2) for the equivalent header diameter to obtain

$$\frac{dp_h}{dz} + \theta\,\rho\, v_h\frac{dv_h}{dz} + \rho\left(\frac{d\alpha_{mh}}{dz} + \frac{C}{2}\frac{f_D}{d_{eh}}\right)v_h^2 = 0 \tag{3.4}$$

where

$$\theta = 2\alpha_{mh} - \alpha_{ml} \tag{3.5}$$

Equation (3.4) is the general header momentum equation. When applying an integral momentum balance over the control volume boundary the identical equation can be derived if the same assumptions are made. The derivation thereof is presented by Bajura [71BA1].

If the header is regarded as a one dimensional continuum by assuming non-discrete lateral inlets or outlets, equation (3.4) can either be solved analytically (with certain assumptions and simplifications) or by means of a numerical integration scheme. For discrete lateral inlets or outlets, equation (3.4) can be discretized by considering the branching points separately, whereafter an iterative numerical solution algorithm can be applied.

3.3 THE LATERALS

The flow through each individual lateral is a function of the static pressure difference over that lateral and its flow resistance. The latter can be specified in terms of the sum of loss coefficients. In an iterative solution algorithm for manifold flow, the flow through every lateral is determined by the static pressure difference over the specific lateral which is the difference between the static pressure in the dividing header at the lateral inlet to that in the combing header at the lateral outlet. Consider a lateral as shown in figure 3.3.

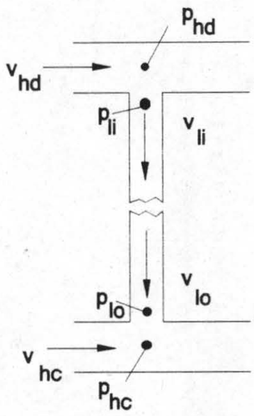

Figure 3.3: Lateral between two headers.

The total pressure loss the fluid experiences while flowing through a lateral from the dividing header to the combining header can be written as:

$$\Delta p_{totdc} = \Delta p_{toti} + \Delta p_{totlat} + \Delta p_{toto} \tag{3.6}$$

where Δp_{toti} is the fluid's loss in total pressure as it enters the lateral, Δp_{totlat} the loss in total pressure experienced in the lateral and Δp_{toto} its loss in total pressure experienced while leaving the lateral. These losses in total pressure can be expressed in terms of mean velocities, static pressures and loss coefficients as

$$\Delta p_{toti} = K_i \frac{1}{2} \rho v_{li}^2 = p_{hd} - p_{li} + \frac{1}{2} \rho \left(\alpha_{ed} v_{hd}^2 - v_{li}^2 \right) \tag{3.7}$$

$$\Delta p_{totlat} = K_{lat} \frac{1}{2} \rho v_{li}^2 = p_{li} - p_{lo} + \frac{1}{2} \rho \left(v_{li}^2 - v_{lo}^2 \right) \tag{3.8}$$

$$\Delta p_{toto} = K_o \frac{1}{2} \rho v_{lo}^2 = p_{lo} - p_{hc} + \frac{1}{2} \rho \left(v_{lo}^2 - \alpha_{ec} v_{hc}^2 \right) \tag{3.9}$$

where the subscripts refer to the positions shown in figure 3.3. The lateral inlet and outlet velocity profiles are assumed to be uniform. Therefore the energy correction factors are discarded. The distinction between the lateral inlet and outlet velocities provides for a phase change in the lateral.

Add equations (3.7) to (3.9) and solve for the static header to header pressure difference:

$$p_{hd} - p_{hc} = \left[\left(K_i - \alpha_{ed} \frac{v_{hd}^2}{v_{li}^2} \right) + K_{lat} \right] \frac{1}{2} \rho v_{li}^2 + \left(K_o + \alpha_{ec} \frac{v_{hc}^2}{v_{lo}^2} \right) \frac{1}{2} \rho v_{lo}^2 \tag{3.10}$$

The use of the terms

$$\left(K_i - \alpha_{ed} \frac{v_{hd}^2}{v_{li}^2} \right) \quad \text{and} \quad \left(K_o + \alpha_{ec} \frac{v_{hc}^2}{v_{lo}^2} \right)$$

eliminates the complicated determination of header energy correction coefficients from the header velocity profiles. These factors have been introduced in section 2.7 and will be called the *reduced* inlet and outlet loss coefficients respectively. For air-cooled condensers the lateral loss coefficient (K_{lat}) is replaced by the condensation loss coefficient (K_{con}) which has been introduced in section 2.4.3.

3.4 DISCUSSION OF SEVERAL SOLUTION METHODS FOR THE MANIFOLD HEADER MOMENTUM EQUATION AS PROPOSED IN THE LITERATURE

If the mass flow distribution through the laterals is known, the header velocity can be solved for by means of the continuity equation. The static pressure in the header can be determined by the momentum equation with the header velocity. The static pressure differences over every lateral calculated with equation (3.10) must be equal to the difference between the static pressure in the dividing header and that in the combining header at the respective lateral. This is only the case if the given mass flow distribution through the laterals has been chosen correctly. Because of the complexity of the differential equations involved and of numerous variables, it becomes clear that without simplifying assumptions the correct mass flow distribution through the laterals can only be obtained by the application of an iterative solution scheme for the discretized header momentum equation. In the literature some authors propose simplifications to be able to solve the equations analytically and some present numerical solution algorithms. We will discuss some of the more significant of these solution schemes found in the literature.

Bajura and Jones [76BA1]:

The header differential equation is derived by taking a surface integral of the momentum flowing through a header control volume similar to that shown in figure 3.2. The result is the same as equation (3.4). The dividing and combining header differential equations are combined by applying the continuity equation, and are non-dimensionalized to obtain a general manifold differential equation with respect to the header axial co-ordinate, z, in the form of

$$Q^{\prime}Q^{\prime\prime} + \Phi_1 Q^2 + 2\Phi_2 Q + M_1 Q Q^{\prime} + M_2 Q^{\prime} = \Phi_2 \tag{3.11}$$

where Q is a dimensionless flow parameter, Φ a friction term while M is a momentum coefficient. Constant lateral flow resistance and lateral pitch is assumed in the derivation of this equation. The equation is then solved with a numerical integration scheme. Experiments have been conducted by the above authors on manifold systems with a maximum of 20 laterals and a constant lateral pitch of 2.55 header diameters. This is not in the range of the pitch encountered in air-cooled condensers, where values of down to 0.001 header diameters are found. The numerical integration of the differential equation compares well with the experimental data. Data is also given for the momentum correction factors, $\theta_d = 1.05$ and $\theta_c = 2.6$. The model proposed by Bajura and Jones cannot incorporate the phase change that occurs in the laterals of air-cooled condensers.

Datta and Majumdar [80DA1],[83DA1]; Majumdar [80MA1]:

The same governing differential equations are used as in Bajura and Jones [76BA1]. A finite difference solution method is employed in solving them, using a one dimensional staggered grid with each pressure point at the lateral inlet or outlet while the velocities are calculated at positions between the branches. A modification on the SIMPLE algorithm, called the SNIP algorithm which was proposed by Spalding [76SP1], is applied to solve the header differential equation. The algorithm starts with an axial mean header velocity distribution obtained with the continuity equation by assuming a uniformly lateral mass flow distribution and an arbitrarily chosen static pressure distribution in the header. From the latter the mean header flow velocities are then calculated. With these calculated velocities a new pressure field is determined. These steps are repeated until a convergence criterion is met. Then a new lateral flow distribution is calculated by applying the dividing to combining header static pressure difference. This new mass flow distribution will however most probably not comply with the conservation of mass, therefore the flow rate through each lateral is corrected with a uniform correction summand, which is determined by taking the sum of the lateral flow rates, subtracting the total mass flow from that sum and dividing the result by the number of laterals. It has been found by Van Heerden [91VA1] and confirmed by the current author that the header pressure iteration algorithm is unnecessary because the choice of the lateral mass flow distribution, which was used to calculate the axial mean header velocity distribution, will only be confirmed after a converged solution for the static header pressure distribution is obtained. The solutions are compared with the experimental data of Bajura and Jones [76BA1] and good agreement is obtained. The authors also give a manifold analysis for the two-phase flow situation in a boiler [83DA1].

Bassiouny and Martin [84BA1] [84BA2]:

A solution method is presented to calculate both the dividing and combining header velocity and pressure distribution in plate heat exchanger manifolds in U- and Z-type arrangements. The momentum equation is simplified by assuming the momentum correction factor, θ_h, to be constant for the dividing and the combining header, and frictionless flow for both headers. It is further assumed that laterals have identical flow resistances, K_l. The dividing and combining headers are combined with the flow continuity and an ordinary differential equation is obtained which is of the following form for a manifold in U-configuration:

$$\frac{d^2 v_h}{dz^2} - m^2 v_h = 0 \tag{3.12}$$

and a manifold in Z-configuration

$$\frac{d^2(1 - v_{hd})}{dz^2} - m^2(1 - v_{hd}) = \frac{\theta_{hd}}{K_l}\left(\frac{N A_l}{A_{hd}}\right)^2 \qquad (3.13)$$

where

$$m^2 = \left[\left(\frac{\theta_{hc}}{\theta_{hd}}\right)\left(\frac{A_{hd}}{A_{hc}}\right) - 1\right]\frac{\theta_{hc}}{K_l}\left(\frac{N A_l}{A_{hd}}\right)^2 \qquad (3.14)$$

If m^2 is zero we have a uniform distribution for the U-configuration. This is possible if K_l is extremely high or if

$$\left(\frac{\theta_{hc}}{\theta_{hd}}\right)\left(\frac{A_{hd}}{A_{hc}}\right) = 1$$

For the Z-configuration a close to uniform distribution can only be achieved with a high K_l-value. Experimental data confirmed the proposed model. It must be stressed that this analysis is not applicable for condensers, because the model does not provide for a phase change in the laterals.

Schrey [95SC1]:

Schrey introduces an equation by which the maximum steam flow rate through an air-cooled condenser can be determined for which no dead zones occur in any lateral. This design equation can however only be applied if a part of the condenser is in Z-configuration. The equation and an example calculation to illustrate its application and shortcomings are presented in appendix E.

3.5 VALUES FOR THE MOMENTUM CORRECTION FACTORS

The header momentum correction factor gradient, $d\alpha_{mh}/dz$, and the overall header momentum correction factor, θ, must be given in order to solve the header momentum equation. Bajura et al [73BA1] present a graph of the overall header momentum correction factor as a function of the lateral to header diameter ratio for a dividing and a combining flow junction. It is however not clear how to apply the diameter ratio in the case of non-circular laterals. Furthermore it cannot be determined to what extent the lateral pitch influences the correction factors, because the data is valid for a single lateral branching. A numerical investigation of the header velocity profiles and the local values of θ with the aid of the *PHOENICS* computer code is shown in appendix B. The geometry of the dividing and the combining header has been chosen to resemble the headers of a typical air-cooled condenser. It is found that the value for $d\alpha_{mh}/dz$ can be neglected. We will take $\theta_d = 0.99$ and $\theta_c = 2.24$, according to the numerical analysis presented in appendix B.

3.6 PRESSURE DISTRIBUTION IN A DIVIDING AND A COMBINING HEADER

The pressure in a dividing or a combining header varies due to frictional effects and due to changes in momentum. The pressure change due to frictional effects is always decreasing in the flow direction while the change in momentum causes an increase in pressure in the flow direction for the dividing header and a decrease in pressure in the flow direction for the combining header. In most manifold systems the frictional effects are significantly smaller than the effects due to the change in momentum. Therefore the pressure in the dividing header is expected to increase in the flow direction while the pressure in the combining header is expected to decrease in the flow direction. This has been confirmed by the numerical analysis conducted on the *PHOENICS* code which is presented in appendix B. In figure B.18 the dimensionless pressure distributions, which were calculated with the code, are shown for the dividing and the combining headers with reverse flow in the latter. Thus the pressure difference from the dividing to the combining header can either converge or diverge for the U-configuration, depending on the magnitude of the pressure change along the headers, and diverge for the Z-configuration.

3.7 NUMERICAL DISCRETE SOLUTION SCHEME ADAPTED FOR AN AIR-COOLED CONDENSER MANIFOLD

An air-cooled condenser consists of a manifold where the finned tubes form the laterals. The major difference of an air-cooled condenser manifold system compared to the manifolds found in other applications, is due to the condensation in the laterals. Only a small fraction, or none if complete condensation takes place, of the steam entering the lateral flows out of the lateral into the combining header; in extreme cases the steam entering the lateral condenses fully before reaching the lateral outlet. The header momentum equation will be discretized in one dimensional staggered grid form as proposed by Majumdar [80MA1]. The mass flow rate out of every individual lateral is calculated by subtracting the condensation rate from the entering mass flow rate. The header velocity distributions are calculated via continuity and the header static pressure distribution with the momentum equation.

3.7.1 DISCRETISATION OF THE HEADER CONTINUITY AND MOMENTUM EQUATIONS

The dividing and the combining header can be discretized into uniform increments including a single lateral inlet or outlet. Figure 3.4 shows a discretized header.

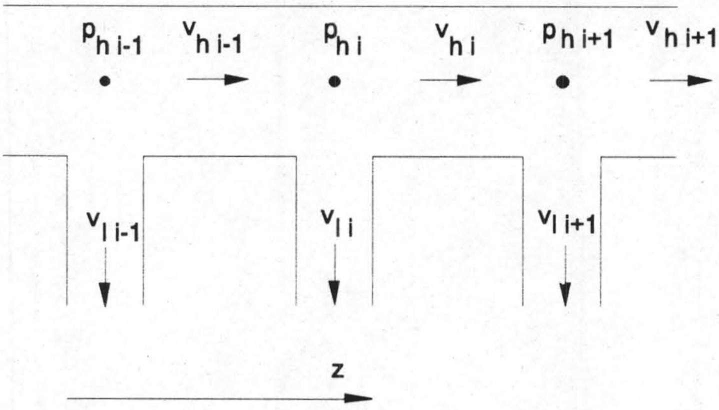

Figure 3.4: Discretized header.

Recall the header continuity equation

$$\frac{d}{dz}\left(v_h\right)\Delta z A_h = -v_l A_l \tag{3.15}$$

Discretizing the above equation by integration over the increment yields:

$$v_{h\,i+1} - v_{h\,i} = v_{l\,i}\frac{A_l}{A_h} \tag{3.16}$$

The lateral inlet velocity and the lateral outlet velocity are related as follows:

$$v_{lo\,i} = v_{li\,i} - \frac{m_{cl\,i}}{\rho A_l} \tag{3.17}$$

where $m_{cl\,i}$ is the condensation rate in the lateral.

Equation (3.4) can be rewritten:

$$\frac{dp_h}{dz} + \frac{\theta}{2}\rho\frac{d(v_h^2)}{dz} + \rho\left(\frac{d\alpha_{mh}}{dz} + \frac{C}{2}\frac{f_D}{d_{eh}}\right)v_h^2 = 0 \tag{3.18}$$

Equation (3.18) can be discretized by applying the staggered grid method in which pressures are calculated at the lateral inlet or outlet sections and velocities between these section as indicated in figure 3.4. Integrate equation (3.18) and make use of the upwind scheme given in Patankar [80PA1] for $v_{h\,i} > 0$:

$$p_{h\,i+1} - p_{h\,i} + \frac{\theta}{2}\rho\left(v_{h\,i}^2 - v_{h\,i-1}^2\right) + \rho\Delta z\left(\frac{d\alpha_{mh}}{dz} + \frac{1}{2}\frac{f_D}{d_{eh}}\right)v_{h\,i}^2 = 0 \tag{3.19a}$$

and for $v_{h\,i} < 0$.

$$p_{h\,i+1} - p_{h\,i} + \frac{\theta}{2}\rho\left(v_{h\,i+1}^2 - v_{h\,i}^2\right) + \rho\Delta z\left(\frac{d\alpha_{mh}}{dz} - \frac{1}{2}\frac{f_D}{d_{eh}}\right)v_{h\,i}^2 = 0 \tag{3.19b}$$

Equations (3.19a) and (3.19b) are valid for the dividing and the combining header.

The difference in static pressure over a lateral from the dividing to the combing header is calculated according to equation (3.10)

$$\begin{aligned}\Delta p_{hdc} &= p_{hd\,i} - p_{hc\,i}\\ &= \left[\left(K_i - \alpha_{ed}\frac{v_{hd\,i}^2}{v_{li\,i}^2}\right) + K_{con}\right]\frac{1}{2}\rho\, v_{li\,i}^2 + \left(K_o + \alpha_{ec}\frac{v_{hc\,i}^2}{v_{lo\,i}^2}\right)\frac{1}{2}\rho\, v_{lo\,i}^2 \qquad (3.20)\end{aligned}$$

A condensation rate has to be specified for the laterals. This can be either of constant value for all laterals or dependent on the individual lateral. In this work the condensation rate is taken as a constant for reasons of simplicity. This assumption can be justified by the almost identical heat transfer rates experienced by the individual laterals of an air-cooled condenser.

3.7.2 SOLUTION ALGORITHM

The solution algorithm is as follows, based on the proposed algorithm of Datta and Majumdar [80DA1] and similar to that of Van Heerden [91VA1]:

1) Start with a uniform mass flow rate through the laterals. The condensation rate in each lateral must be specified as either a fixed value or some function of the lateral inlet velocity.
2) Calculate the velocity distributions in the dividing and the combining header according to equations (3.16) and (3.17) respectively.
3) Calculate the static pressure difference over the first lateral with equation (3.20).
4) Calculate the static pressure distribution in the combining header with equation (3.19).
5) Calculate the static pressure distribution in the dividing header with equation (3.19) by setting the pressure value at the first node equal to the sum of the value of the pressure difference over the first lateral and the combining header pressure at the same node.
6) Calculate the pressure difference over every lateral by subtracting the respective combining header pressure from the dividing header pressure. With the pressure

difference over each lateral known, a new mass flow distribution is to be calculated.

7) The sum of the new lateral mass flow rates (m^*_{lat}) through the individual laterals will not comply with the specified total lateral mass flow rate (m_{tot}), therefore the lateral mass flow rates have to be corrected. A constant correction factor which is determined according to

$$C_{corr} = \frac{\sum m^*_{lat\,i} - m_{tot}}{N}$$

is subtracted from all the new calculated lateral mass flow rates.

8) With this new lateral mass flow distribution repeat the procedure from step 2) until a convergence criterion is met. In this work the criterion is taken as a sufficiently small value for C_{corr}.

In appendix F the mass flow distributions through the laterals of an air-cooled condenser section obtained by making use of this algorithm are presented.

CHAPTER 4

EXPERIMENTAL INVESTIGATION OF INLET LOSS COEFFICIENTS

4.1 INTRODUCTION

In this chapter the experimental apparatus and procedure to investigate the inlet loss coefficients of flow into one or more flat profile ducts (laterals) with different flow approach conditions is described and the results are presented graphically. A photograph of the experimental apparatus is shown in figure 4.1.

Figure 4.1: Photograph of experimental apparatus.

4.2 DESCRIPTION OF EXPERIMENTAL APPARATUS

The top view of the entire apparatus, as it is attached to the outlet of a low speed wind tunnel, is shown diagrammatically in figure 4.2.

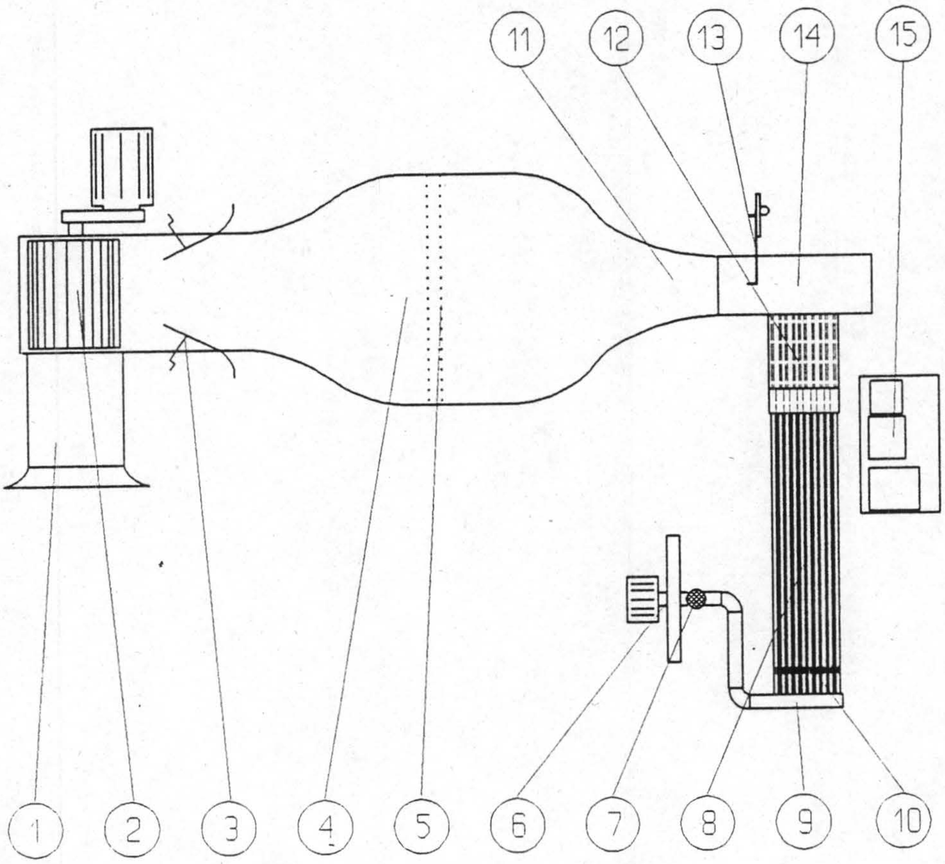

Legend:

1: Wind tunnel fan inlet
2: Wind tunnel fan (centrifugal)
3: Flow adjustment flaps
4: Expansion chamber
5: Screen
6: Suction fan (centrifugal)
7: Suction fan flow adjustment valve
8: Aluminium pipes for flow measurement
9: Suction manifold
10: Pipe flow adjustment valves
11: Wind tunnel converging section
12: Lateral inlet box
13: Pitot static tube
14: Header
15: Data acquisition system

Figure 4.2: Plan view of entire apparatus.

The main part of the apparatus, the lateral box, consists of 10 laterals with which flat finned tube inlets of an air-cooled condenser can be simulated. Referring to the assembly drawing in figure 4.3, this lateral inlet box consists of 10 parallel rectangular ducts or laterals, 400mm long, 10mm wide and 190mm high; created by eleven 30mm× 400mm×196mm PVC blocks placed into parallel grooves of 30mm width, 400mm length and 3mm depth machined into the top and bottom aluminium plates at a 40mm pitch.

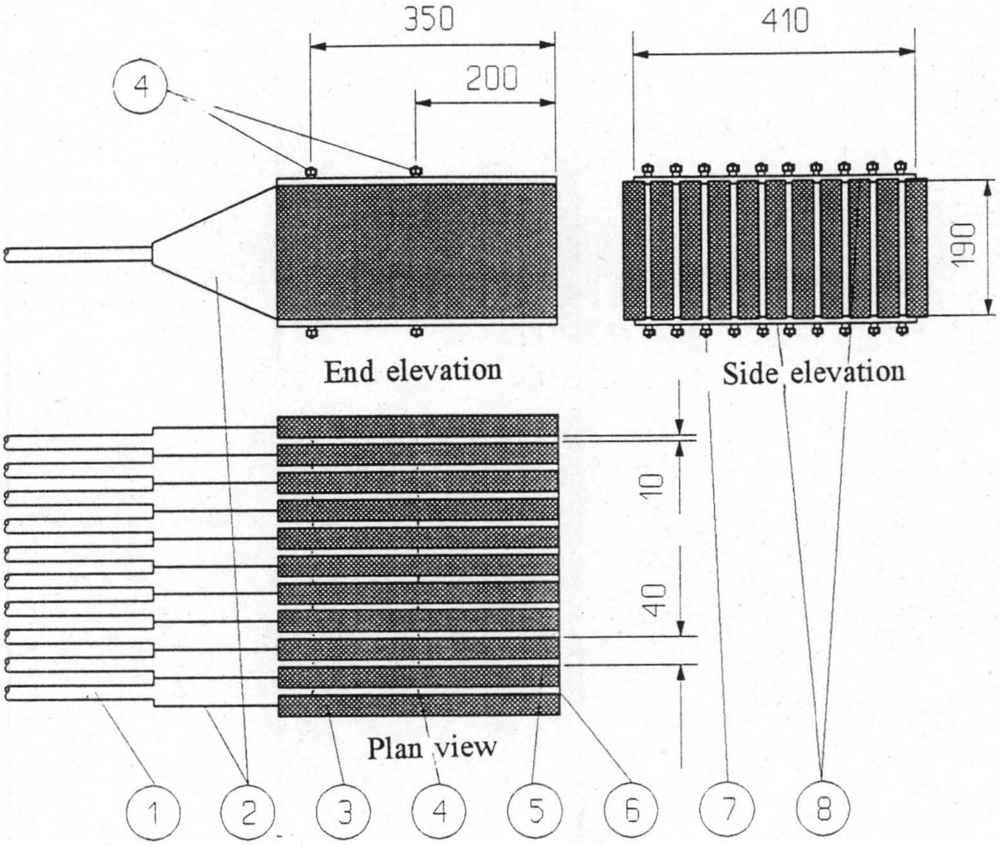

Legend:
1: Calibrated aluminium pipe (for flow measurement)
2: Lateral outlet manifold connecting each individual lateral leading to calibrated aluminium pipes
3: PVC blocks
4: Pressure tappings in top and bottom aluminium plates
5: Lateral
6: Lateral inlet face
7: Pressure tapping fitting
8: Top and bottom aluminium plates with 30mm×3mm grooves at 40mm pitch

Figure 4.3: Assembly drawing of lateral inlet box with connecting manifold.

The edges of the PVC blocks forming the inlets of the laterals are machined to have sharp 90° edges. The frontal face of the lateral inlet section has a total width of 410mm. The inlet section can be fitted perpendicular to the outlet section of a low speed wind tunnel as shown in figure 4.2, which can supply air velocities up to 40m/s. Other inlet configurations described in sections 4.7, 4.8 and 4.9.can also be mounted.

Three basic header configurations can be achieved by fitting the lateral inlet box to the outlet of the low speed wind tunnel, the latter simulating the dividing header of an air-cooled condenser:

1) Open two dimensional header configuration:

This configuration will be called the *standard configuration*. It is shown in figure 4.4. The header consists of two plates arranged as an extension of the top and bottom aluminium plates of the lateral inlet box to restrict the header flow entering the laterals to flow only parallel to the planes formed by the plates. There is no wall at the plane opposite the lateral inlets, therefore the static pressure in that plane, which is equal to the ambient atmospheric pressure, is used as the reference header pressure. This configuration has been investigated numerically in appendix B.

2) Closed header configuration:

The plane opposite to the lateral inlets is closed by a wall fitted with pressure tapping points situated directly opposite each lateral to measure the static header pressure. The wall is also indicated in figure 4.4.

3) Three dimensional header configuration:

The detachable wind tunnel outlet section is removed to enlarge the header flow area. Furthermore the top and bottom plates are removed and plates are fitted in line with the lateral inlet face to enlarge it so that flow can enter from the top and bottom sections. The configuration is shown in figure 4.5.

A centrifugal fan sucks air through the laterals via a manifold that collects the flow from the calibrated aluminium pipes which are connected to a manifold collecting the flow from every lateral outlet individually. These aluminium pipes are used to determine the mass flow rate or the air velocity through each respective lateral. Each pipe is fitted with two pressure tapping points situated 1m apart with the upstream pressure tapping point more than 10 diameters downstream of the lateral outlet manifold. The mass flow rate is determined by measuring the pressure difference over this 1m section and using the specific pipe's calibration regression. More information about the calibration of the aluminium pipes is given in appendix C.

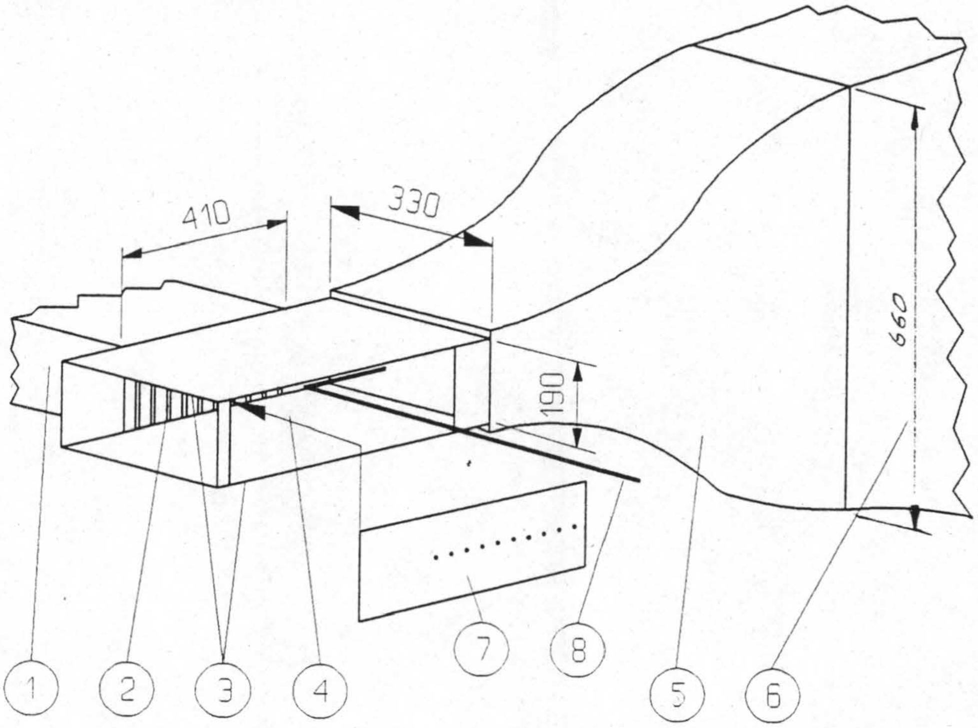

Legend:
1: Lateral inlet box
2: Lateral inlets
3: Top and bottom plates
4: Header
5: Detachable converging section
6: Fixed wind tunnel outlet section
7: Wall for closed configuration
8: Pitot static tube

Figure 4.4: Lateral inlet box attached to wind tunnel outlet in two dimensional configuration indicating the difference between open and closed header.

Every lateral has two pairs of static pressure tappings, that face each other on the top and bottom aluminium plates, situated at 200mm and 350mm from the lateral inlet face respectively. The pairs give an average pressure reading for both pressure tapping locations.

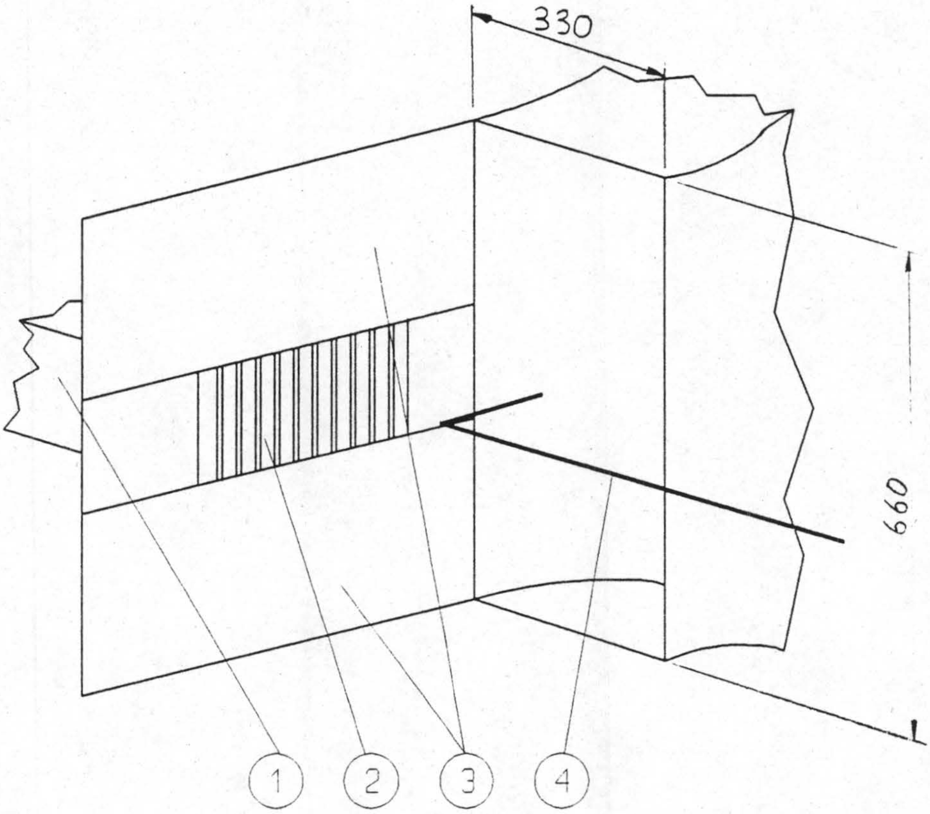

Legend:

1: Lateral inlet box	3: Extension plates of wind tunnel outlet
2: Lateral inlets	4: Pitot static tube

Figure 4.5: Lateral inlet box attached to wind tunnel outlet in open three dimensional configuration.

Figure 4.6 shows a diagram of the data acquisition system. Every pressure tapping on the lateral inlet box and the aluminium pipes is connected via a plastic pipe to a computer operated *Furness Control* valve selector box which connects a specific pressure channel to two *HBM* pressure transducers, one for the range 0 - 1 kN/m^2 and the other for greater differential pressures up to 10 kN/m^2. The latter is used to determine the static pressure difference between the static pressure and the ambient atmospheric pressure for each upstream aluminium pipe pressure tapping. The other transducer can be connected either differentially to give the differential pressure between two tapping points or with a certain selector box connection it can give a differential reading with respect to the ambient atmospheric pressure as well.

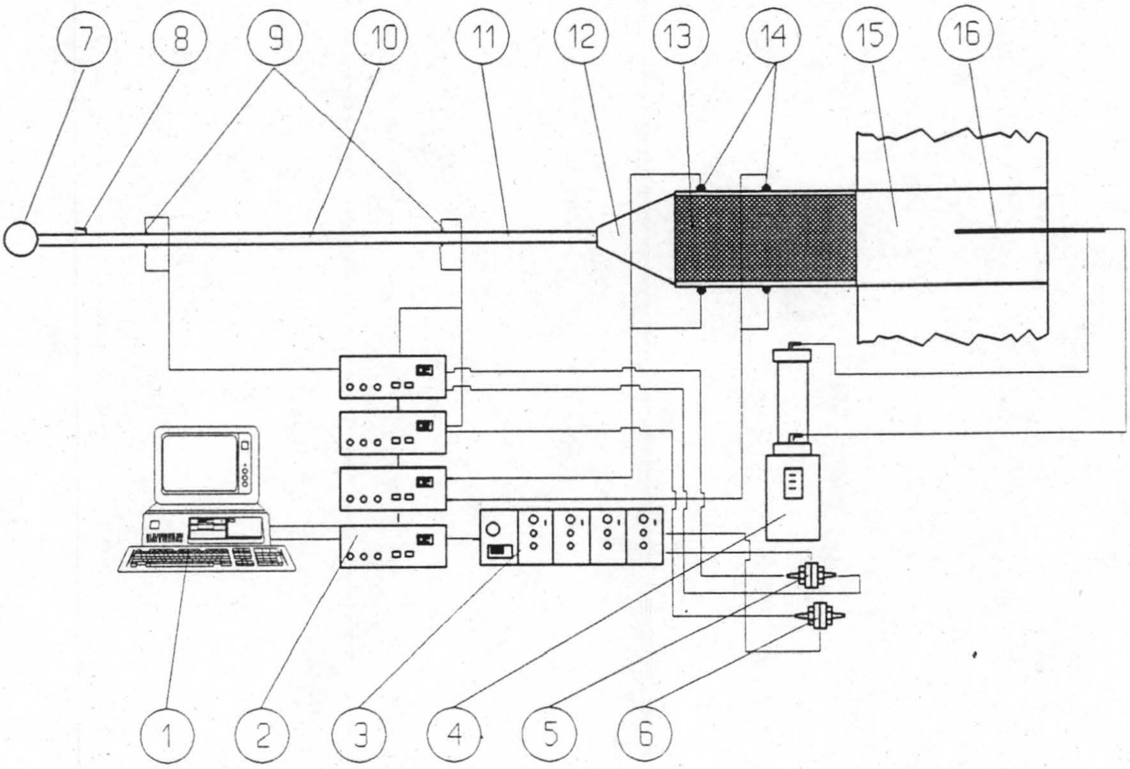

Legend:

1: *Olivetti M24* personal computer with *PC30* ADDA card
2: *Furness Control* pressure selector boxes
3: *HBM* bridge amplifier
4: *Betz* differential manometer
5: *HBM* pressure transducer (range: 0 - 1000N/m^2)
6: *HBM* pressure transducer (range: 0 - 10000N/m^2)
7: Collecting manifold leading to suction fan
8: Individual flow adjustment valve
9: Aluminium pipe differential pressure tapping points
10: Calibrated aluminium pipe
11: Pipe inlet section of 10 diameters
12: Connection manifold from lateral section outlet to aluminium pipe
13: Lateral inlet box
14: Downstream lateral pressure tapping points
15: Wind tunnel outlet forming the header section
16: Pitot static tube facing into wind tunnel outlet for header velocity measurement

Figure 4.6: Diagram of data acquisition system.

The pressure transducers are connected to *HBM* bridge amplifier channels which supply a voltage signal that can be converted to a pressure reading by using the calibration relationship of each pressure transducer. A linear regression is used to describe this curve; the calibration readings are obtained by using the pressure reading of a *Betz* manometer, which is connected to one point of the transducer, together with the respective amplified voltage signal of the transducer.

The personal computer used to operate the valve selector boxes and reading the amplifier signals is of the type *Olivetti M24* fitted with a *PC30 ADDA* card. A data acquisition program was written to operate the *Furness Control* valve selector box according to a prescribed valve selection sequence to select the valves in order to log the current pressure data. As the computer calculates the lateral mass flow rates and thereby the lateral velocities immediately, it is possible to adjust the mass flow rate through every lateral during the experiment by setting the individual flow adjustment valves. This is necessary as the lateral velocity is to be held constant during a full experiment manually, because the changes of the experimental conditions influence the lateral mass flow rates.

Air temperatures are read with a mercury thermometer and the absolute atmospheric pressure with a mercury barometer.

4.3 DETERMINATION OF THE EXPERIMENTAL INLET LOSS COEFFICIENT

Referring to the locations indicated in figure 4.7, the energy equation for the flow between points h in the header and l in the lateral can be written in terms of the inlet loss coefficient

$$\frac{p_h}{\rho} + \alpha_{eh}\frac{v_h^2}{2} = \frac{p_l}{\rho} + \alpha_{el}\frac{v_l^2}{2} + f_D\frac{L_l}{d_{el}}\frac{v_l^2}{2} + K_i\frac{v_l^2}{2} \tag{4.1}$$

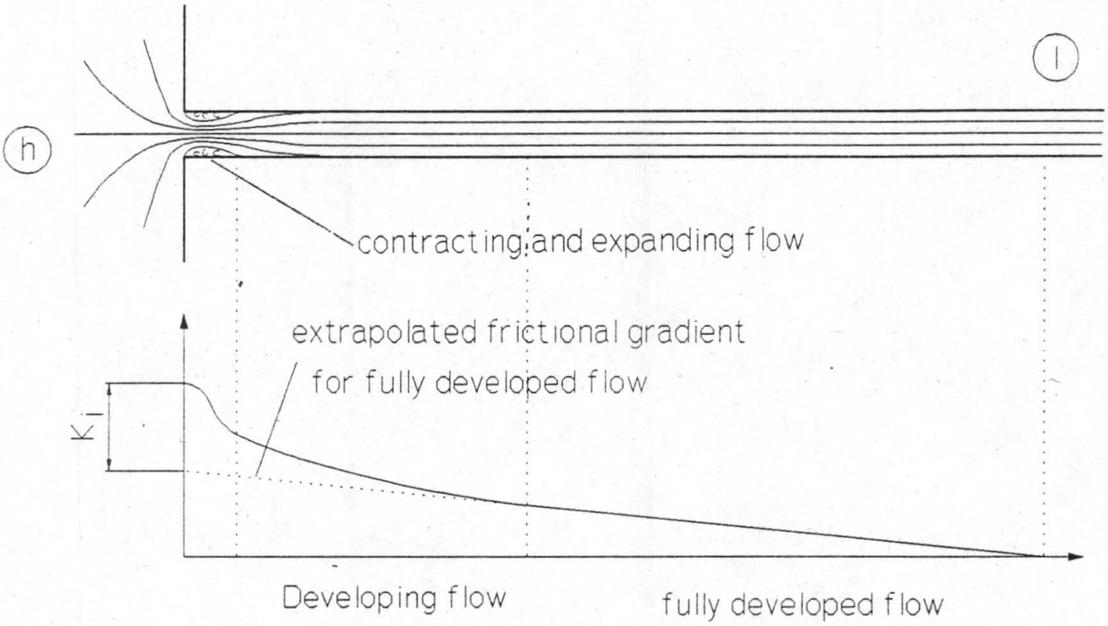

Figure 4.7: Diagram of a lateral inlet section to define positions.

Point l is situated at a downstream lateral position where the lateral flow has developed its fully turbulent velocity profile. According to Daugherty et al [89DA1], fully developed turbulent flow is found at about 50 diameters from the entrance of a round pipe. If the equivalent diameter concept is used the flow is expected to be fully developed at nearly 1m from the lateral inlet. Because of the cost factor involved the two pressure tapping points were situated closer, at 10.5 equivalent diameters (0.2m) and at 18.4 equivalent diameters (o.35m) from the lateral inlet. In appendix D it is shown that the friction factors of the individual laterals determined via the measured pressure difference correspond within ±10% to equation (2.11) which is valid for fully developed turbulent flow. The point at 0.35m was used during the experiments.

If the flow entering the lateral was normal and the lateral inlet edges were sharp as was the case in most of the experiments, the inlet loss coefficient would be equal to the contraction loss coefficient, K_c as defined in chapter 2. In the present investigation allowance was made for any header flow and the lateral inlet edges were to be rounded at a later stage, therefore we define a general inlet loss coefficient. This inlet loss coefficient is expressed in terms of the loss in total pressure of the fluid that remains after the total pressure loss due to the constant frictional pressure gradient encountered in fully developed flow has been extrapolated from point 1 up to the lateral inlet. The inlet loss coefficient thus includes the effects of the varying frictional total pressure drop of the developing flow just after the point of reattachment.

Because of the nearly uniform velocity profile encountered in fully developed turbulent flow at point l, α_l, is assumed to be unity. Solving equation (4.1) for the inlet loss coefficient yields

$$K_i = \frac{p_h - p_l}{\frac{1}{2}\rho v_l^2} + \alpha_{eh}\frac{v_h^2}{v_l^2} - 1 - f_D\frac{L_l}{d_{el}} \qquad (4.2)$$

The friction factor is calculated with the aid of the implicit friction factor equation for parallel plates which was derived from the logarithmic law using the equivalent diameter concept as presented in White [91WH1] and given in equation (2.11) in this work.

In the graph of the non-dimensionalized total pressure line accompanying the diagram in figure 4.7 the different drops in total pressure are indicated. Often uncertainty remains about the definition of the header velocity; the header energy correction coefficient, α_h, is even more difficult to determine, especially for the case of a dividing header with several laterals branching off it, as it is only applicable to that part of the header flow that enters the lateral to be investigated. For a configuration with many laterals and a header open to atmosphere, for instance, uncertainties prevail because an unquantifiable amount of ambient air can be sucked into the airstream leaving the wind tunnel, thus the continuity equation does not only involve the mass flow entering the upstream laterals and that entering the header. This problem can be resolved simply by subtracting the term including v_h from the inlet loss coefficient which reduces the calculation of the reduced inlet loss coefficient to

$$K_i - \alpha_{eh} \frac{v_h^2}{v_l^2} = \frac{p_h - p_l}{\frac{1}{2} \rho v_l^2} - 1 - f_D \frac{L_l}{d_{el}} \tag{4.3}$$

The pressure tapping at 200mm is used together with that at 350mm to determine an experimental friction factor which can be compared with the parallel plate friction factor given in equation (2.11) in order to give an indication as to what extent the flow is developed. The experimental friction factor is calculated with the following equation:

$$f_D = \frac{\Delta p_{\Delta L}}{\frac{\rho v_l^2}{2} \frac{\Delta L}{d_{el}}} \tag{4.4}$$

where $\Delta p_{\Delta L}$ is the pressure drop over the length, ΔL between the two lateral pressure tapping points at 200mm and 350mm from the lateral inlet, which is equal to 150mm. Although this length is rather short and gives small pressure difference readings in the order of $20 N/m^2$ the experimental data agrees reasonably well with the existing correlation of equation (2.11) as is shown in appendix D.

The header inlet velocity v_{hi} is determined with a pitot static tube inserted into the flow with its tip at a distance of 0.1 m upstream of the first lateral and in the middle of the wind tunnel outlet. The following equation is used to convert the pitot static pressure difference to a velocity reading:

$$v_{pitot} = C_{pitot} \sqrt{\frac{2 \Delta p_{pitot}}{\rho}} \tag{4.5}$$

where C_{pitot} is the pitot tube correction factor which is given as 1.01 for this specific pitot static tube. Figure 4.8 shows the almost uniform velocity profile at the header inlet for a header inlet to lateral velocity ratio of approximately unity, as measured with the pitot static tube. The pitot static tube is positioned in the centre of the header. As shown in figure 4.8 it can be seen that the local velocity at this point is about 1% higher than the mean header velocity. The header inlet velocity may then be obtained by multiplying the local velocity reading in the centre of the header by 0.99, yielding:

$$v_{hi} = 0.99 \times 1.01 \sqrt{\frac{2\,\Delta p_{pitot}}{\rho}} = 0.9999 \sqrt{\frac{2\,\Delta p_{pitot}}{\rho}} \qquad (4.6)$$

During every experiment the velocity of each lateral is adjusted to a value in the order of 10 to 11 m/s. This corresponds to a lateral Reynolds number of the order of 13000.

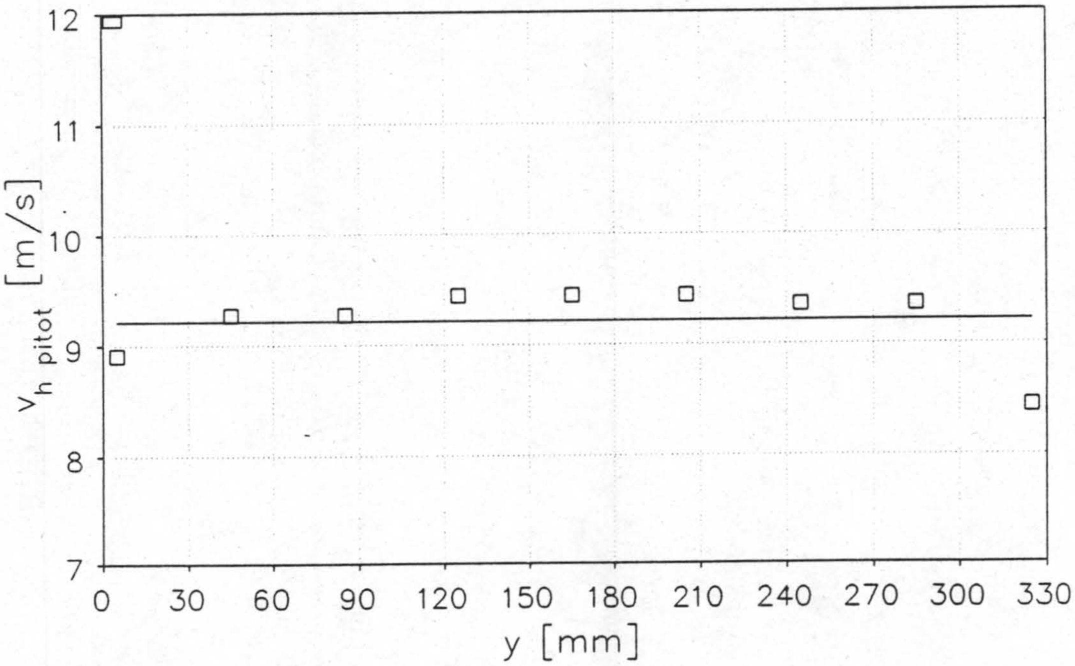

Figure 4.8: Header inlet velocity profile.

A sample calculation for the calculation of the inlet loss coefficients is presented in appendix D.

4.4 NORMAL INLET LOSS COEFFICIENTS OF EACH LATERAL

The normal inlet loss coefficient of each lateral for ideal flow, K_0, is now determined experimentally. This is achieved by considering a particular lateral and by closing the remaining 9 with masking tape. The face area of the lateral inlet box is made larger by attaching plates at the up- and downstream sides. This configuration resembles an infinitely small contraction of flow area thereby giving a zero area contraction ratio. Although the flow in the laterals is approximated by flow between infinite parallel plate, the entering flow still separates from the smaller inlet edges found at the aluminium plates. In order to investigate the extent of this flow separation on the inlet loss coefficient, two configurations as shown in figure 4.9 are investigated.

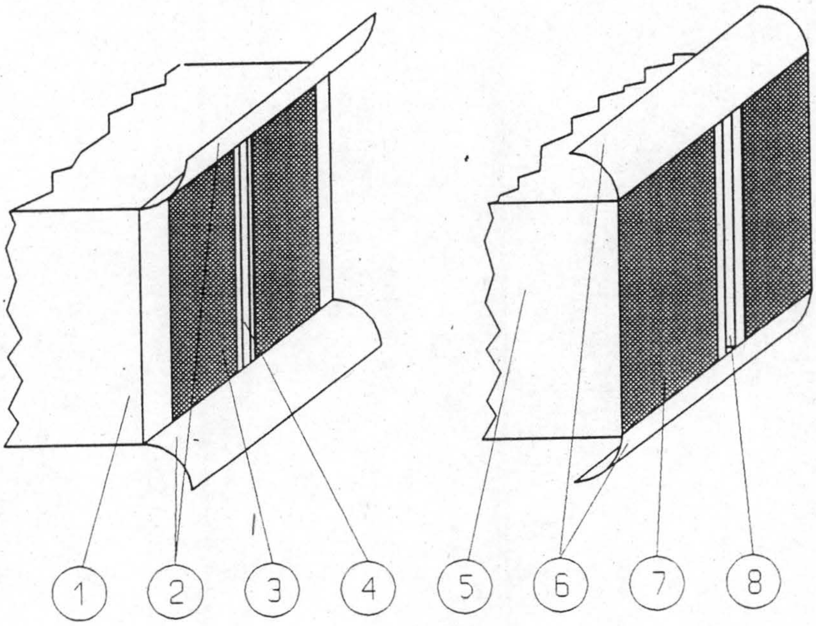

Legend
1,5: Lateral inlet box
2: Inlet rounding fitted two dimensionally, i.e. the flow enters tangential to the top and bottom plates.
3,7: Masking tape used to close remaining lateral inlets
4,8: Lateral to be investigated
6: Inlet roundings fitted three dimensionally, i.e. the flow enters tangentially to the inlet face, thereby causing flow separation from the top and bottom lateral walls.

Figure 4.9: Two and three dimensional configurations for individual laterals.

The two dimensional configuration consists of inlet roundings fitted tangentially to the lateral top and bottom walls to minimize the flow separation in those situations. In the three dimensional configuration the inlet roundings are fitted tangentially to the lateral inlet face in order to maximize the flow separation there. The average K_0 values of each lateral of three experimental runs for both configurations are presented graphically in figure 4.10, while the data for this experiment and those to follow is presented in appendix D.

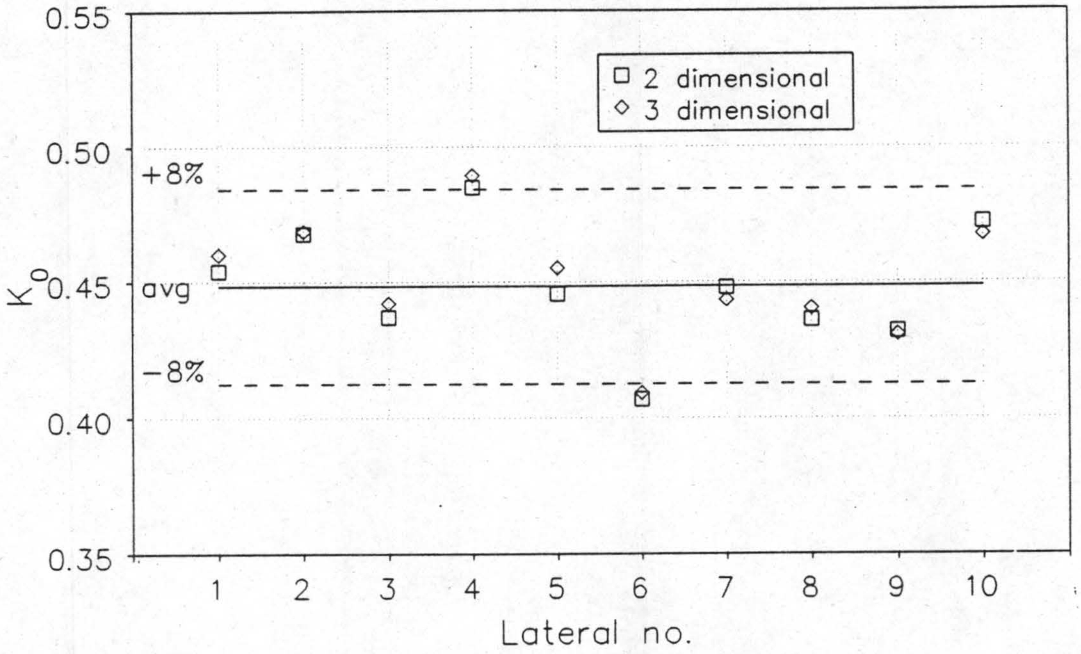

Figure 4.10: Normal inlet loss coefficient, K_0, of the ten laterals.

Figure 4.10 shows that the difference in magnitude of the contraction loss coefficients for both configurations is negligible, the values of the two dimensional configuration will be used for later applications. Due to the differences in magnitude of the experimentally determined K_0 values for each lateral, the reduced lateral inlet loss coefficients (as defined in equation (4.3)) of the experiments discussed in sections 4.5 to 4.9are compared by subtracting the K_0 value of the respective lateral to obtain the header inlet to lateral inlet velocity ratio dependent part of the inlet coefficient:

$$K_{ivr} = K_i - \alpha_{eh}\frac{v_h^2}{v_l^2} - K_0 = f\left(\frac{v_{hi}}{v_l}\right) \tag{4.7}$$

4.5 INLET LOSS COEFFICIENTS FOR SHARP INLETS WITH A PASSING FLOW

The lateral inlet box is attached at a right angle to the outlet section of the wind tunnel as previously shown diagrammatically in figure 4.4. A two dimensional flow condition, which means that no flow can enter from the top or bottom of the inlet section at the lateral face, is obtained by using two plates indicated in figure 4.4.

4.5.1 SINGLE LATERAL WITH SHARP INLET IN PASSING FLOW

In this experiment the inlet loss coefficient of a single lateral, (lateral no.1) is investigated for the two dimensional open configuration. The remaining nine are closed by means of smooth adhesive tape. The mean lateral velocity is kept at around 10.8m/s by adjusting the mass flow with the flow adjustment valve while the header velocity is increased in discrete steps from 0 to about 25m/s. The experimental K_{ivr} value is shown in figure 4.11 as a function of the header inlet to lateral velocity ratio, hereafter called the velocity ratio. The data is compared with data of Van Heerden [91VA1] and Nosova [59NO1]. The data of both these authors compares well with the data of this investigation up to v_{hi}/v_l=1.5.

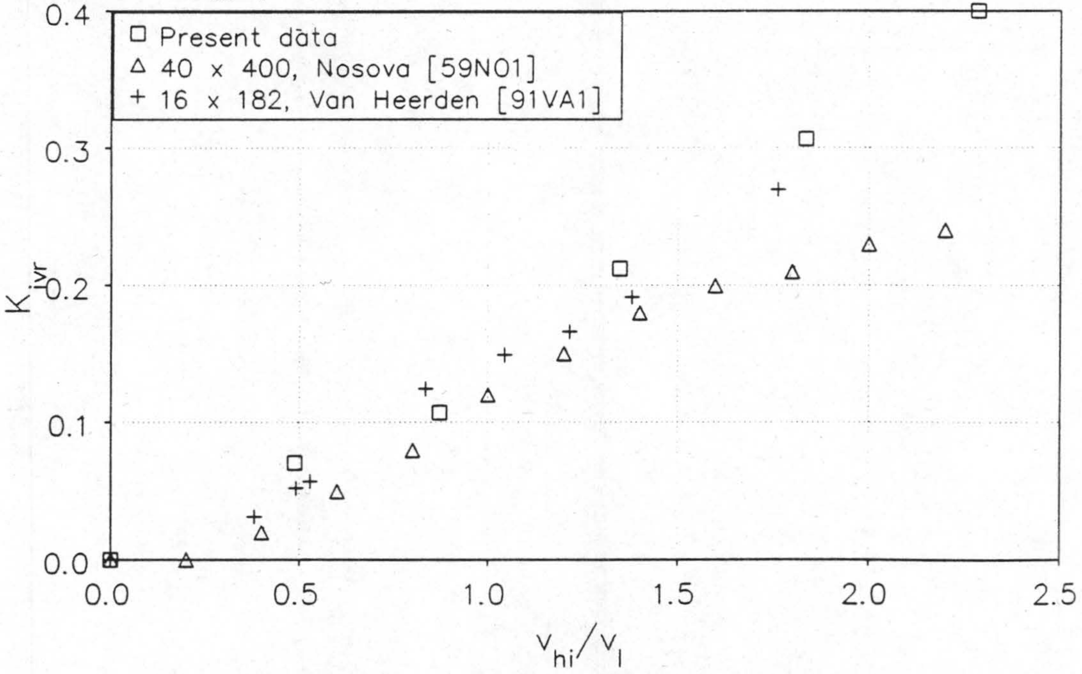

Figure 4.11: Single lateral with sharp inlet, two dimensional configuration.

4.5.2 10 LATERALS IN PASSING FLOW (STANDARD CONFIGURATION)

Figure 4.12 shows the experimentally determined inlet loss coefficient plotted against the header inlet to lateral velocity ratio of 10 consecutive laterals arranged in the two dimensional open configuration. For comparison with further experiments this configuration is called the *standard configuration* (abbreviated std.). Air-cooled condensers are designed with a unity velocity ratio, therefore the same values are plotted again in figure 4.13 for a velocity ratio scale of 0 to about 2.3 to show more clearly the K_{ivr} values around the design region. In both graphs the K_{ivr} value of the first lateral increases almost linearly as a function of the velocity ratio.

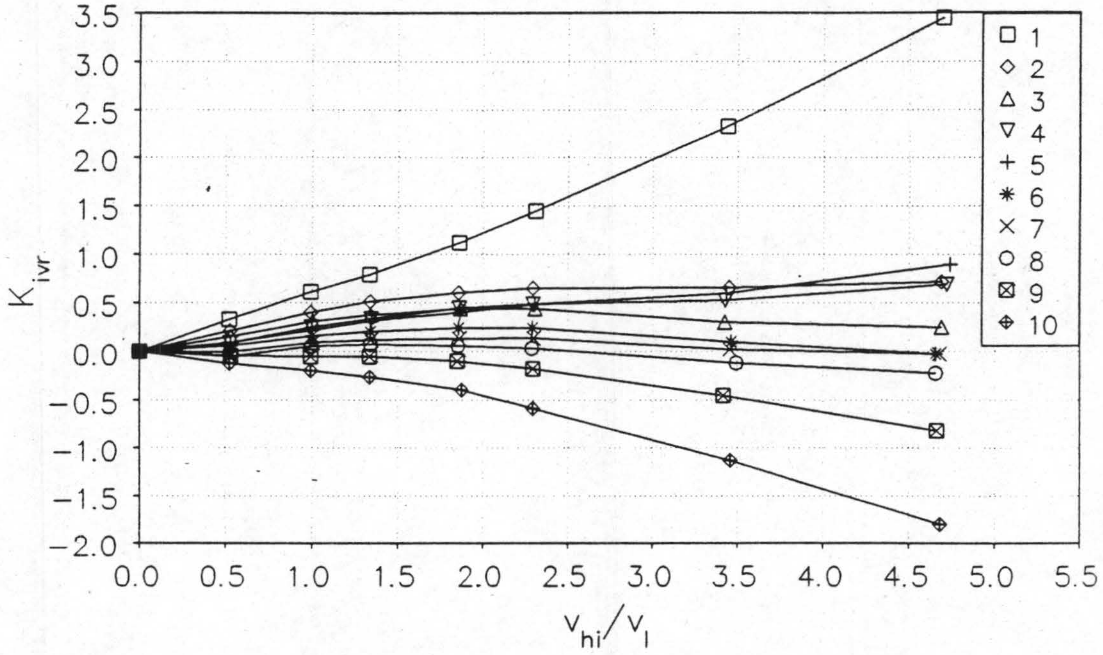

Figure 4.12: 10 Laterals in open two dimensional configuration (Standard configuration).

The K_{ivr} values of the second to the sixth lateral also increase as a function of the velocity ratio, at a rate considerately less than the first lateral's gradient. The seventh to the eighth lateral's K_{ivr} values remain nearly constant. The K_{ivr} values of the ninth and the tenth lateral, which is also the last lateral, decrease as a function of the velocity ratio.

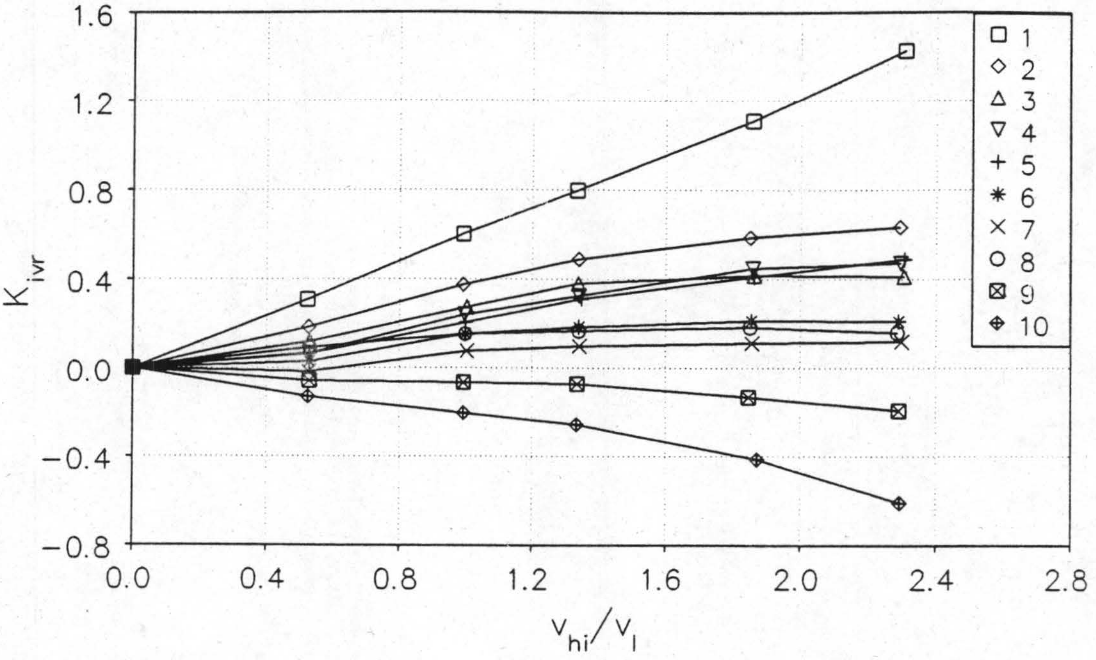

Figure 4.13: 10 Laterals (velocity ratio < 2.3) in open two dimensional configuration.

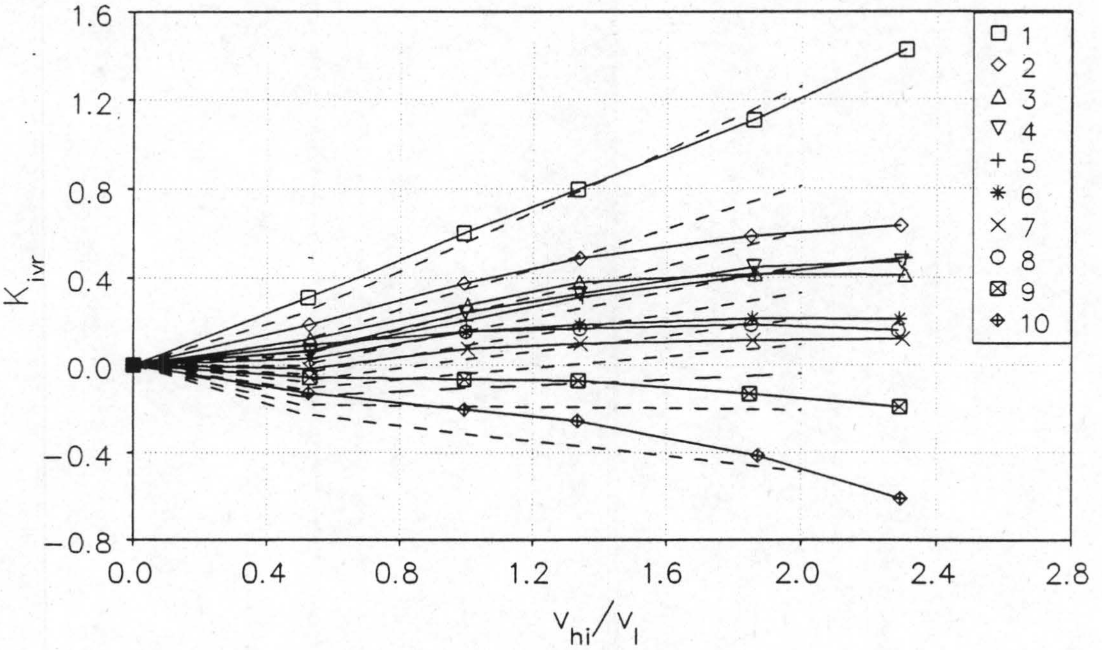

Figure 4.14: Comparison of experimental data with numerical solution.

In figure 4.14 the K_{ivr} values of the standard experimental configuration is compared with the numerical solution obtained with the aid of the *PHOENICS* code, which is shown in appendix B. There is good agreement in the magnitude and the trends of the dimensionless pressures as a function of the header inlet to lateral velocity ratio. The decrease of the K_{ivr} value of the downstream laterals with increasing velocity ratio is confirmed by the numerical solution.

The data presented up to now is for the two dimensional case in which the flow into the laterals is restricted to enter only from the direction parallel to the planes formed by the top and bottom aluminium plates. Furthermore the side opposite to the lateral inlets is open to the atmosphere so that the header pressure is equal to the ambient atmospheric pressure for every lateral. In order to investigate the effect of the above, two other configurations, which have been presented in figures 4.4 and 4.5, are investigated with ten laterals open, in order to compare the K_{ivr} values to the those of the open two dimensional configuration. The experimental results for the closed two dimensional and the open three dimensional inlet configurations are shown in figures 4.15 and 4.16 respectively.

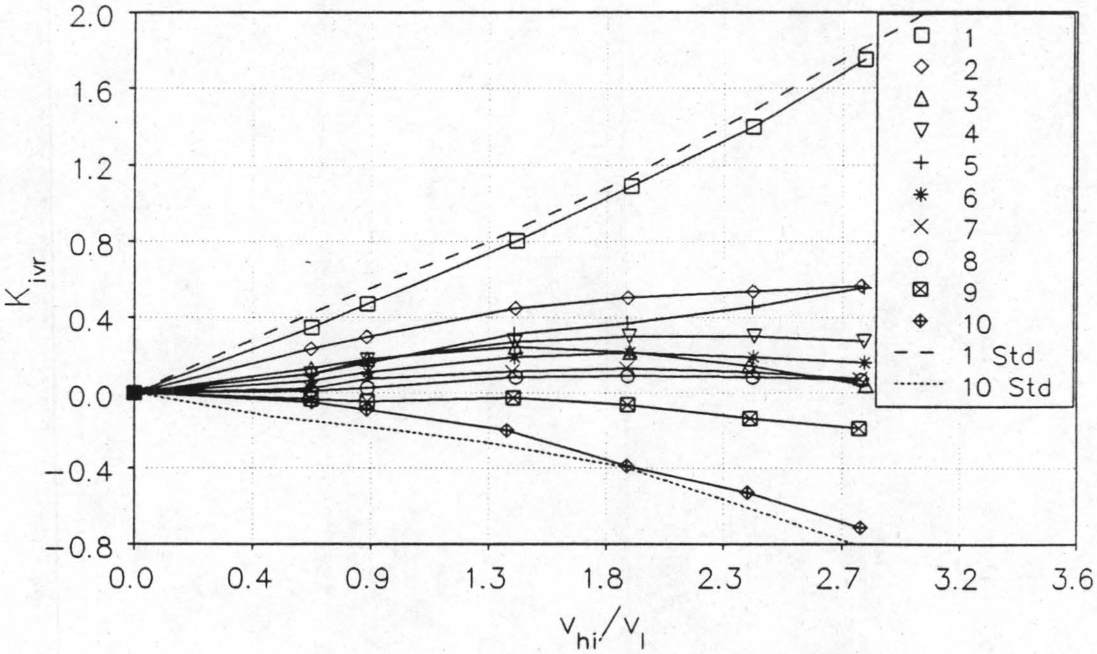

Figure 4.15: Inlet loss coefficients for closed two dimensional configuration with 10 laterals.

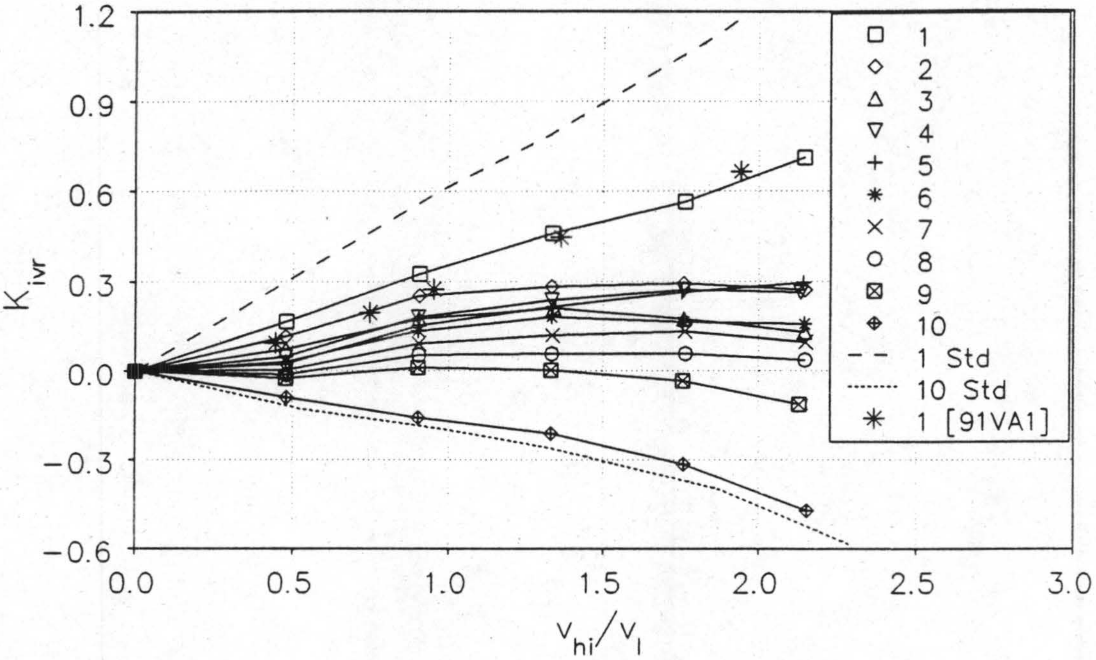

Figure 4.16: Inlet loss coefficients for three dimensional configuration with 10 laterals.

For the closed two dimensional configuration good agreement with the standard configuration is obtained, therefore the open configuration is used in most of the further experiments as this simplifies determining the reference header pressure, which is simply set as atmospheric. The three dimensional configuration gives a linearly increasing K_{ivr} value with about half the gradient of that of the two dimensional configuration for the first lateral. The data for the first of five laterals of Van Heerden [91VA1] (who also used a three dimensional configuration) compares reasonably with that of the first lateral of the three dimensional configuration as can be seen in figure 4.16, although his configuration consisted of 16mm×182mm laterals at a pitch of 52mm.

4.5.3 FIVE LATERALS WITH SHARP INLETS IN PASSING FLOW

In order to investigate whether the upstream laterals can be modelled accurately by the apparatus with its rather limited number of laterals (in air-cooled condensers the number is orders higher), an experiment has been conducted with the last five laterals blocked off with masking tape so that only the first five remain open. The results are shown graphically in figure 4.17. The trend of the first lateral's K_{ivr} value compares well with that of the first lateral of ten, while again the fifth (this time the last) lateral has a decreasing K_{ivr} value as the last two in the case of the ten laterals. Therefore it seems that the limited number of laterals does not affect the inlet loss coefficients.

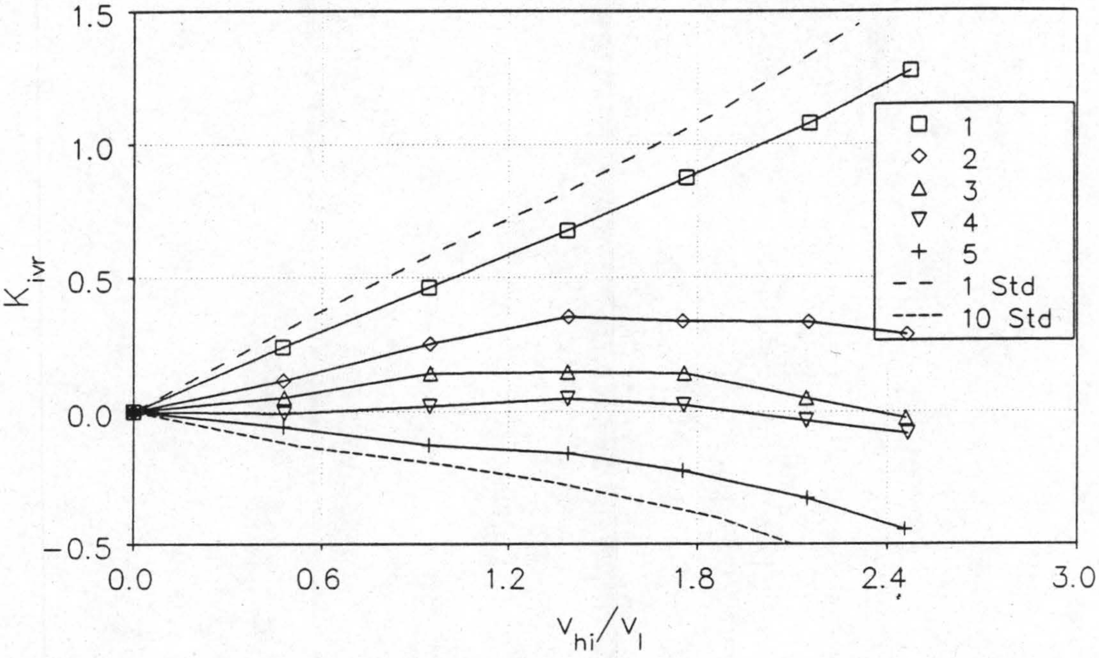

Figure 4.17: Five laterals at 40mm pitch, open two dimensional configuration.

4.5.4 FIVE LATERALS AT A PITCH OF 80mm

Figure 4.18 shows the data of the case where every second lateral is blocked so that five laterals at a pitch of 80mm remain open. The first lateral's K_{ivr} values have the same trend as with the 40mm pitch, their magnitude, however, is far smaller. The header velocity profile just before the first lateral is most likely less distorted, therefore the local velocity at the lateral inlet is smaller leading to a smaller inlet loss coefficient. The inlet loss coefficient of the last lateral remains nearly constant for the investigated velocity ratio range, different to the trend found at the 40mm pitch.

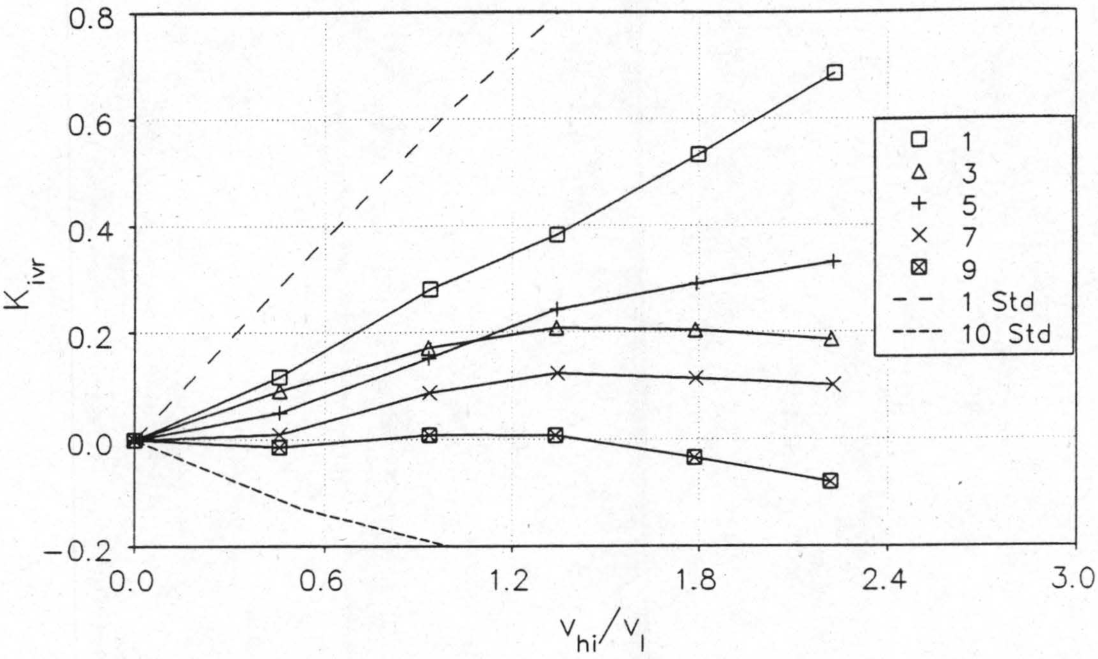

Figure 4.18: Five laterals at 80mm pitch, open two dimensional configuration.

4.5.5 UPSTREAM BACKWARD FACING STEPS

The aim of an upstream backward facing step is to allow the separated stream to flowmore directly into the first lateral, thereby avoiding the sharp turn the flow experiences while entering the first lateral. Figure 4.19 shows the step of height a and upstream distance b.

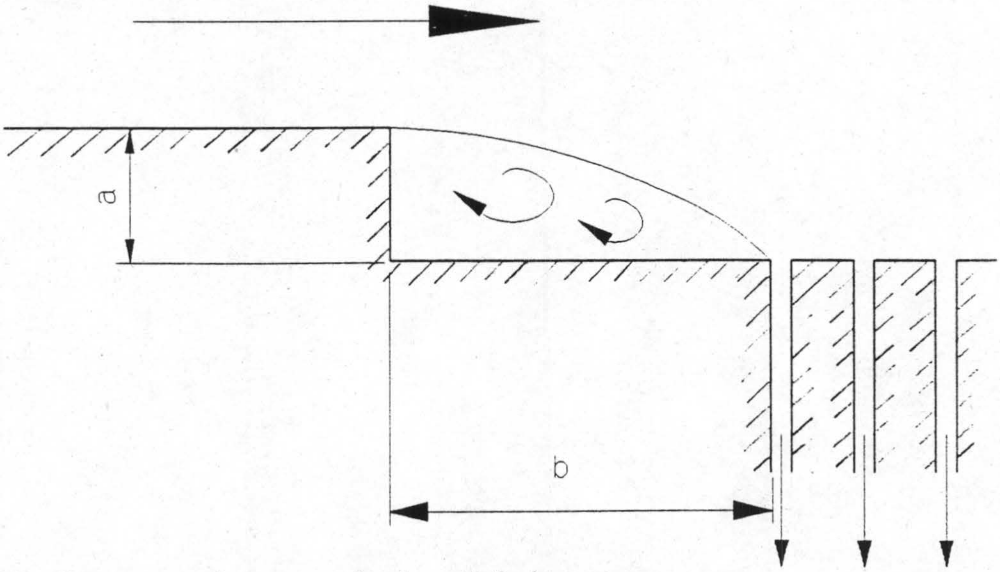

Figure 4.19: Geometry of upstream backward facing step.

The data for different upstream distances with two step heights is presented in figures 4.20 to 4.25.

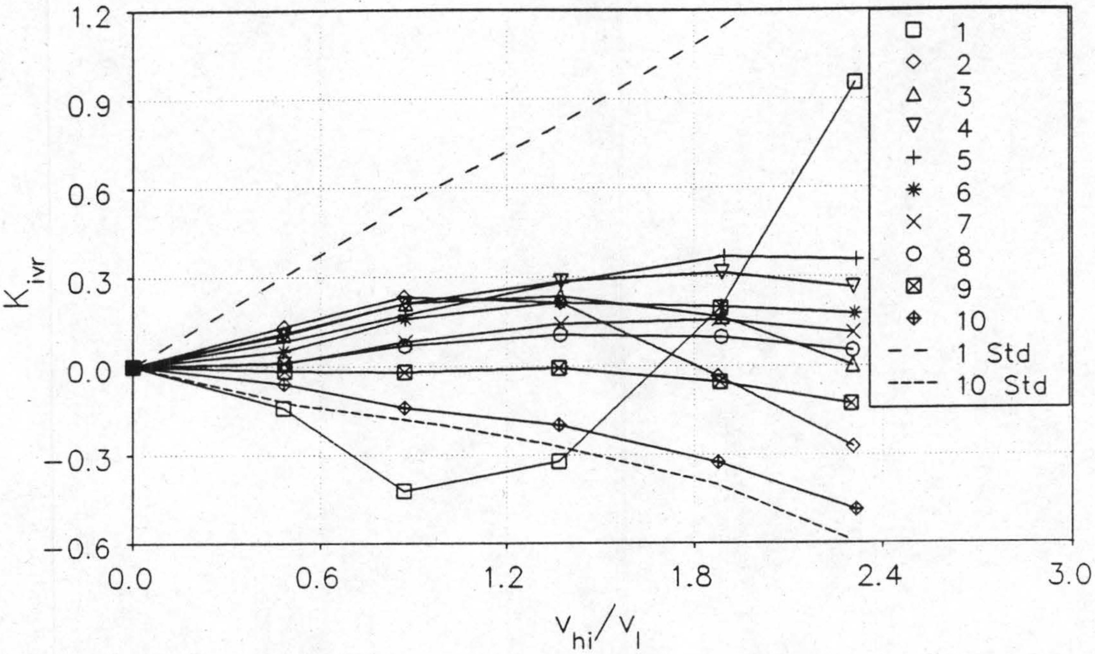

Figure 4.20: Upstream backward facing step; a=10mm, b=15mm, open two dimensional configuration.

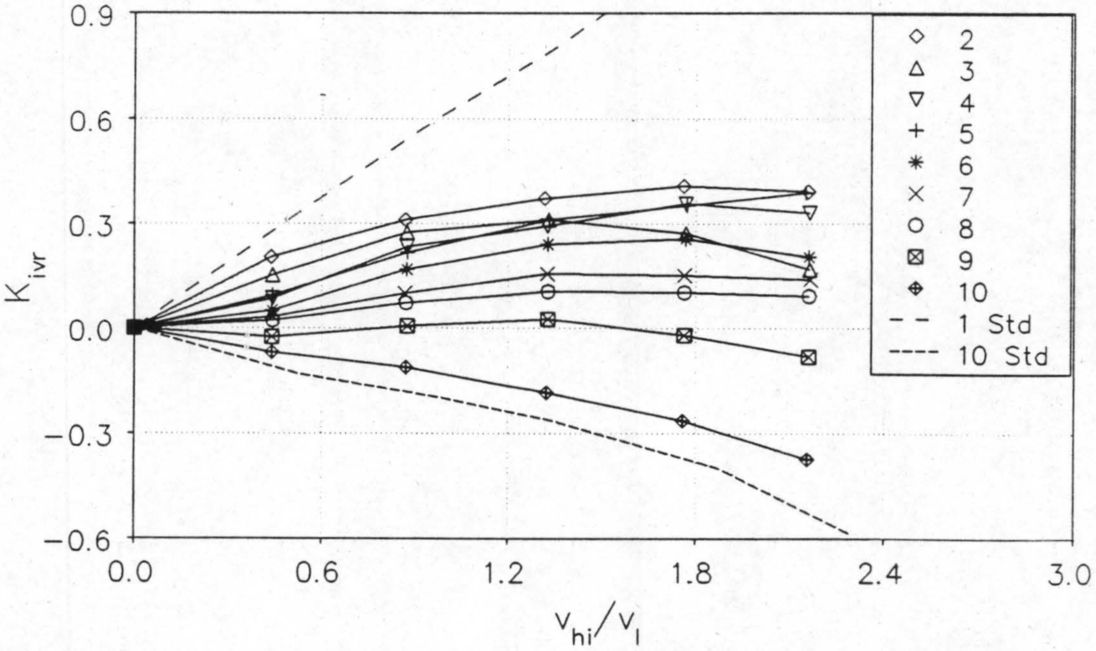

Figure 4.21: Upstream backward facing step; a=10mm, b=55mm, open two dimensional configuration.

A significant reduction in the loss coefficient is achieved with this configuration as is shown in figures 4.20, 4.21 and 4.24 and 4.25. The last lateral's K_{ivr} value behaves as

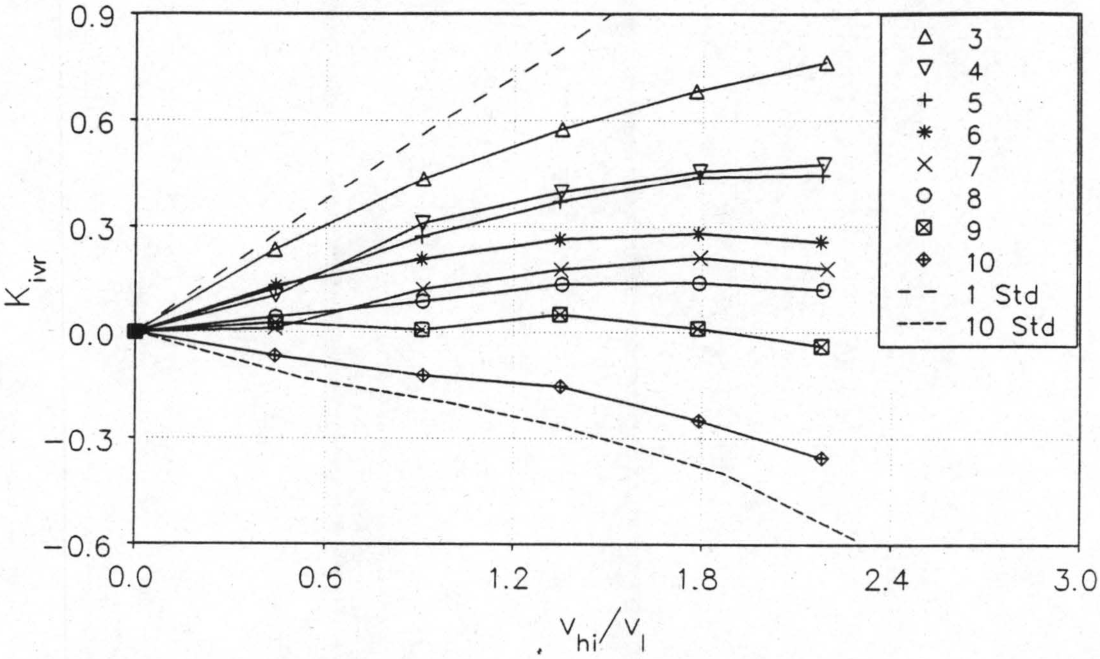

Figure 4.22: Upstream backward facing step; a=10mm, b=100mm, open two dimensional configuration.

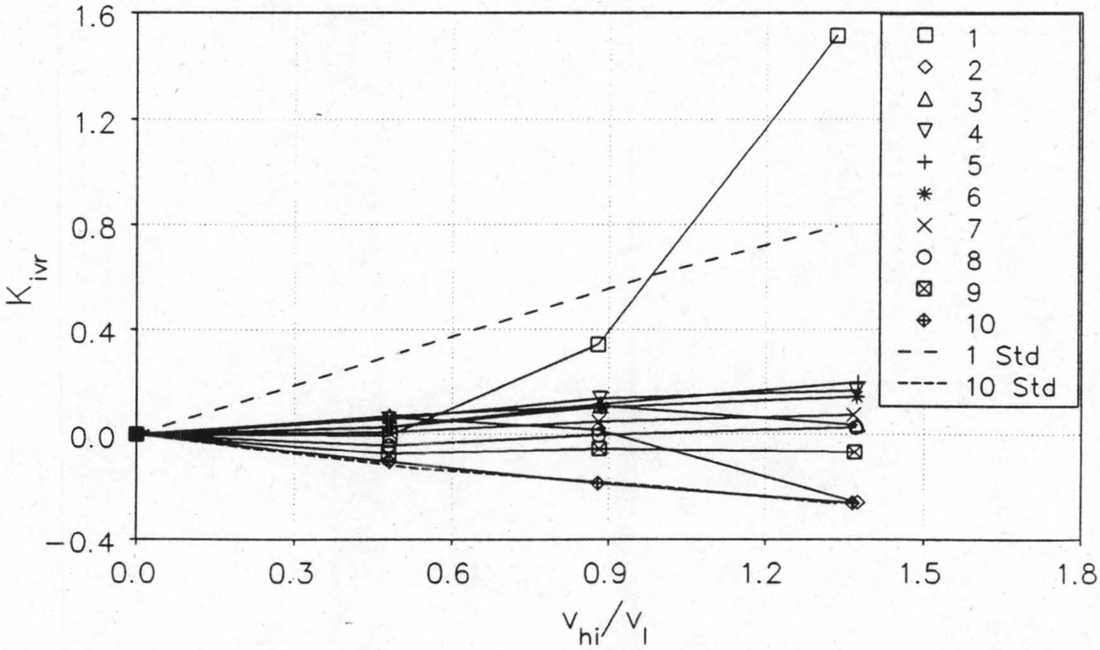

Figure 4.23: Upstream backward facing step; a=20mm, b=15mm, open two dimensional configuration.

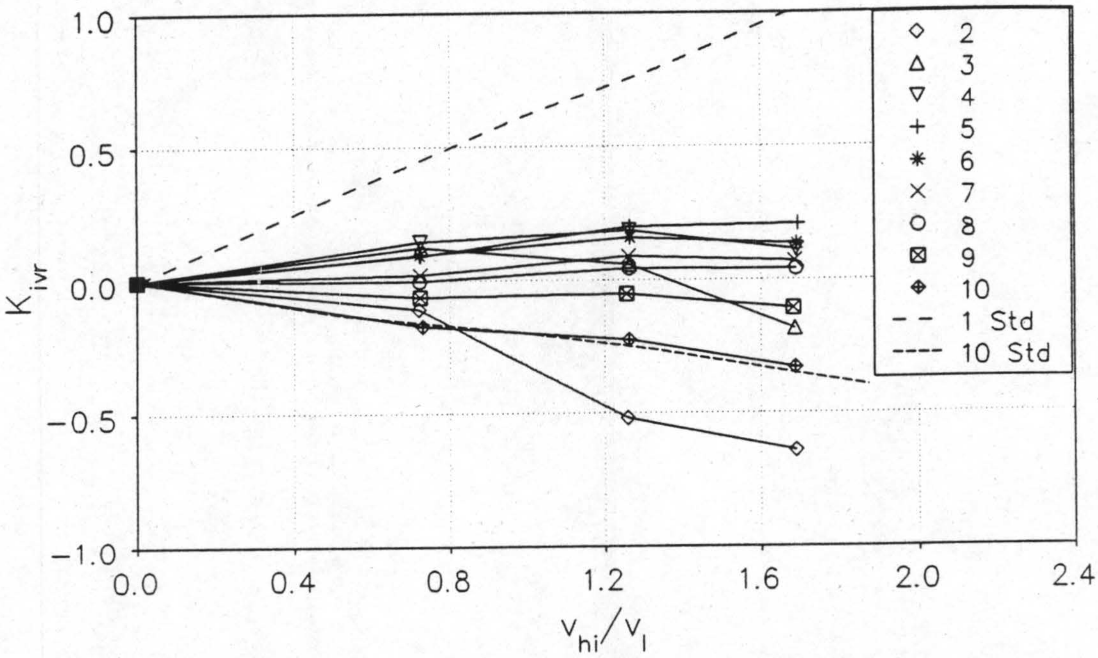

Figure 4.24: Upstream backward facing step; a=20mm, b=55mm, open two dimensional configuration.

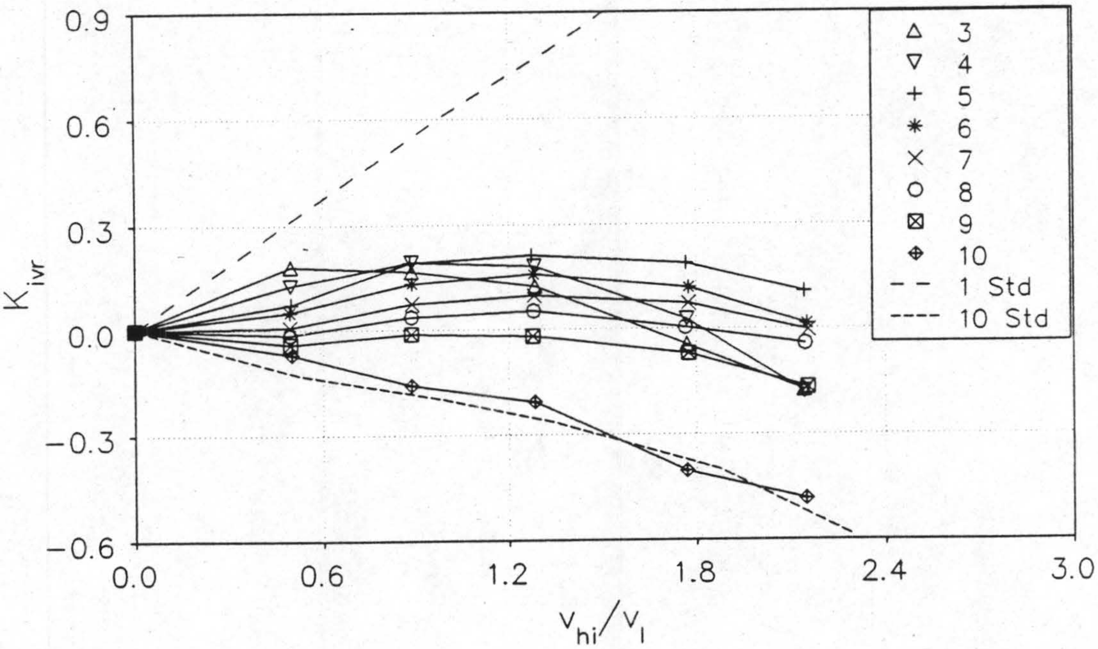

Figure 4.25: Upstream backward facing step; a=20mm, b=100mm, open two dimensional configuration.

4.5.6 UPSTREAM TRIANGULAR RAMP AND WALL LIKE STRIP

The first configuration consists of a triangular ramp placed at two different upstream distances. In the second, the ramp is replaced by a 10mm high sheet metal strip at the same distances. Again the aim is to create a vortex in order to facilitate the flow into the first lateral, as indicated in the diagram of the configuration shown in figure 4.26. The experimental data for both configurations is presented in figures 4.27 to 4.30.

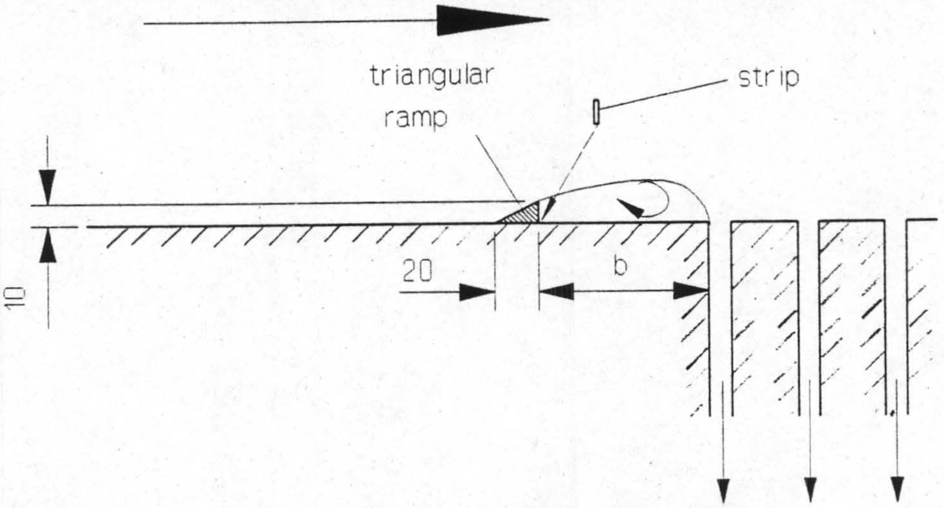

Figure 4.26: Diagram of upstream ramp and sheet metal strip.

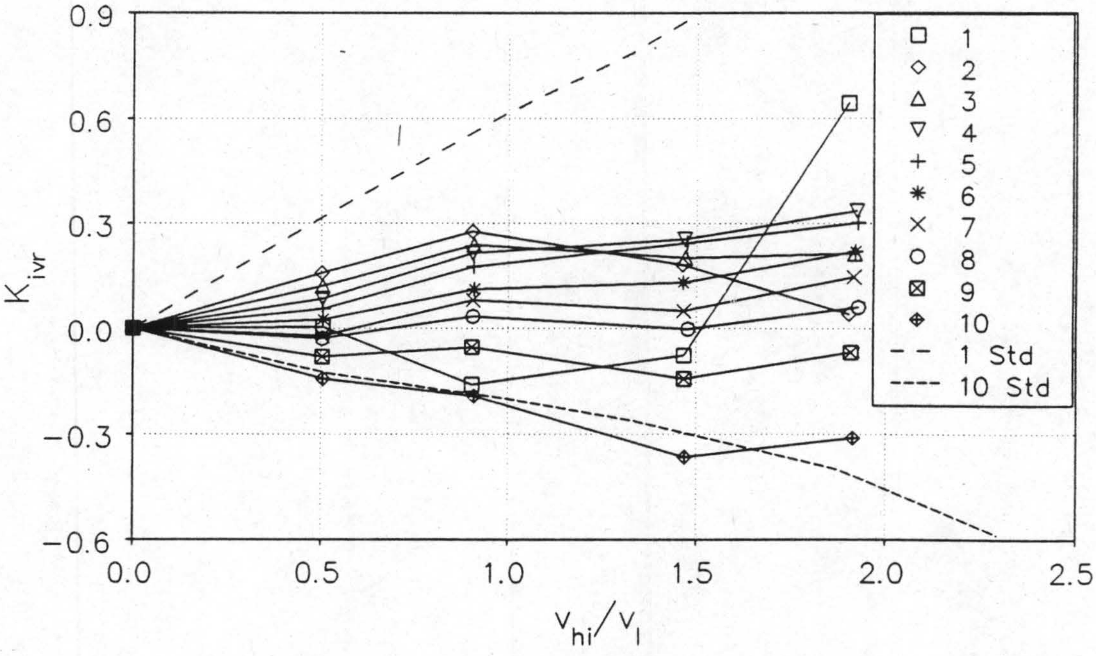

Figure 4.27: Upstream triangular ramp; b=40mm, open two dimensional configuration.

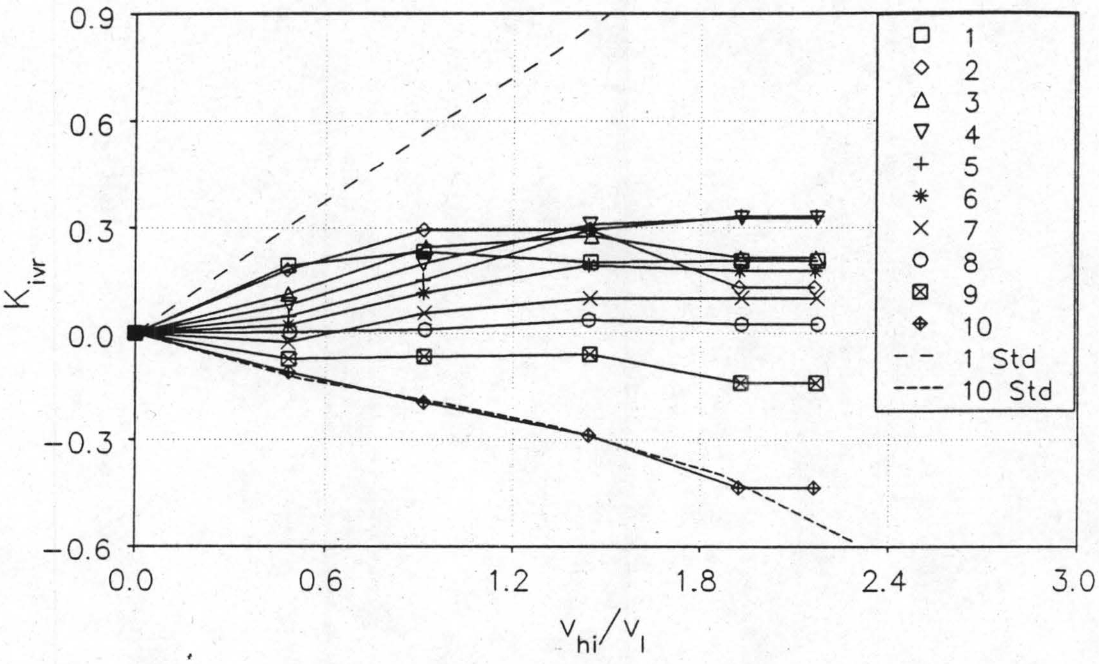

Figure 4.28: Upstream triangular ramp; b=80mm, open two dimensional configuration.

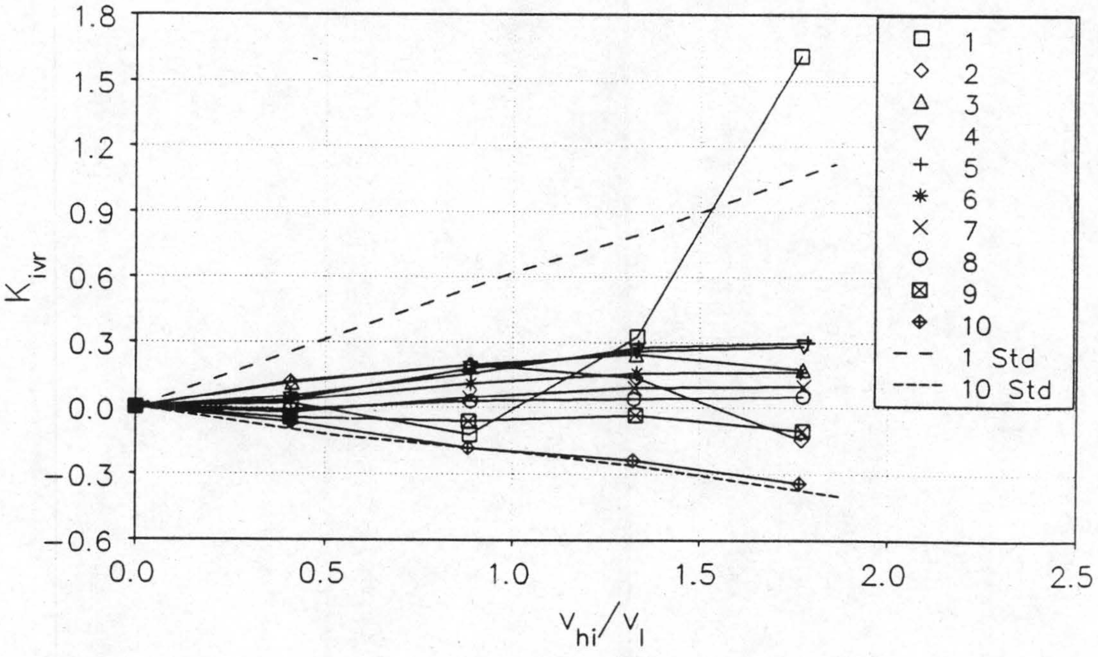

Figure 4.29: Upstream wall like strip; b=40mm, open two dimensional configuration.

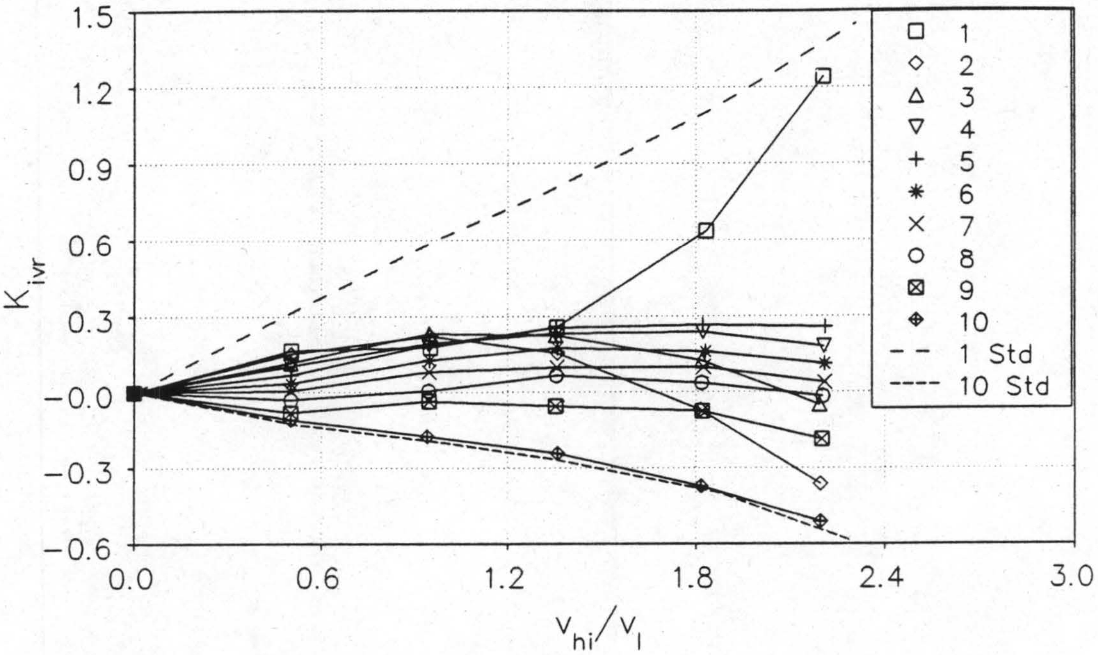

Figure 4.30: Upstream wall like strip; b=80mm, open two dimensional configuration.

For both the ramp and the strip configuration, the best results are for the upstream distance of 80mm. The ramp, however, gives more uniform K_{ivr} values for all laterals except the last which has the same K_{ivr} values as in the standard configuration.

4.5.7 IRON GRID ON LATERAL INLETS

A configuration to both improve the inlet loss coefficient and reduce erosion is investigated. A grid is used to shield the lateral inlets against the droplets of saturated water moving at high velocity (up to 80m/s), which are encountered in the dividing header of a practical air-cooled condenser. The grid consists of industrial walkway material with the same pitch as that of the laterals. The configuration is illustrated in figure 4.31. Three sub-configurations of this are investigated. In the first the ramp was left out. The respective K_{ivr} values are presented in figure 4.32. The ramp is then situated at two upstream positions. Figure 4.33 and figure 4.34 present the experimental data for both cases. It must be noted that the K_{ivr} values include the grid resistance.

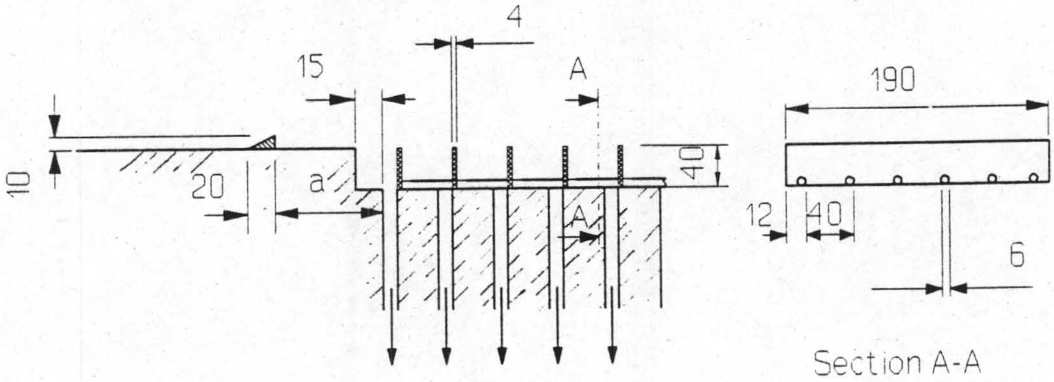

Figure 4.31: Lateral inlets fitted with grid and vortex generator.

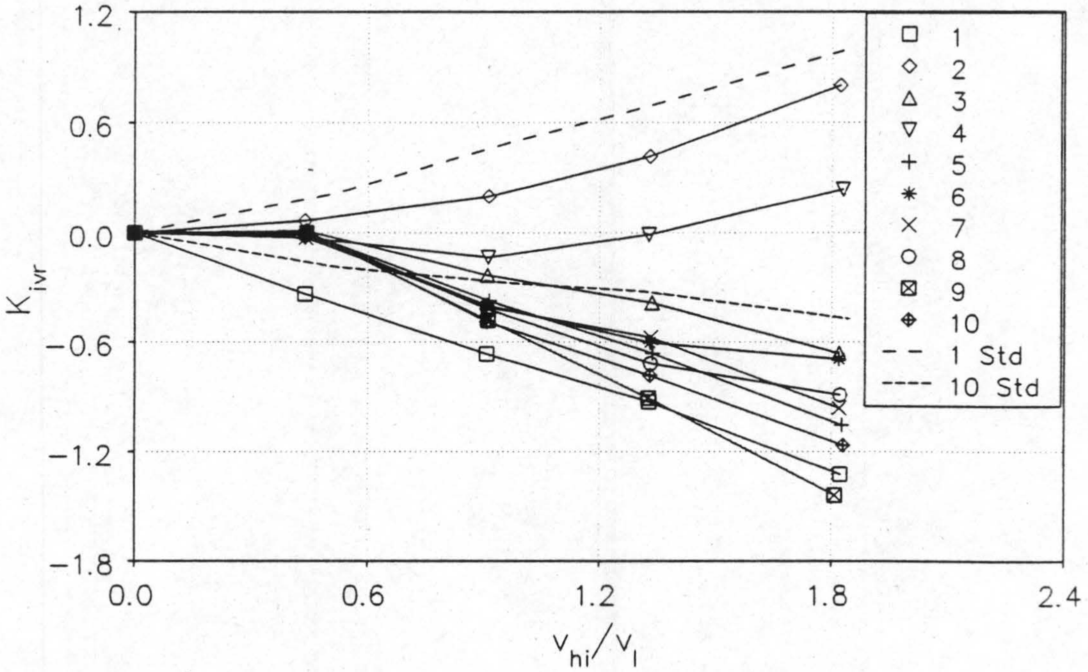

Figure 4.32: Grid configuration without upstream ramp, open two dimensional configuration.

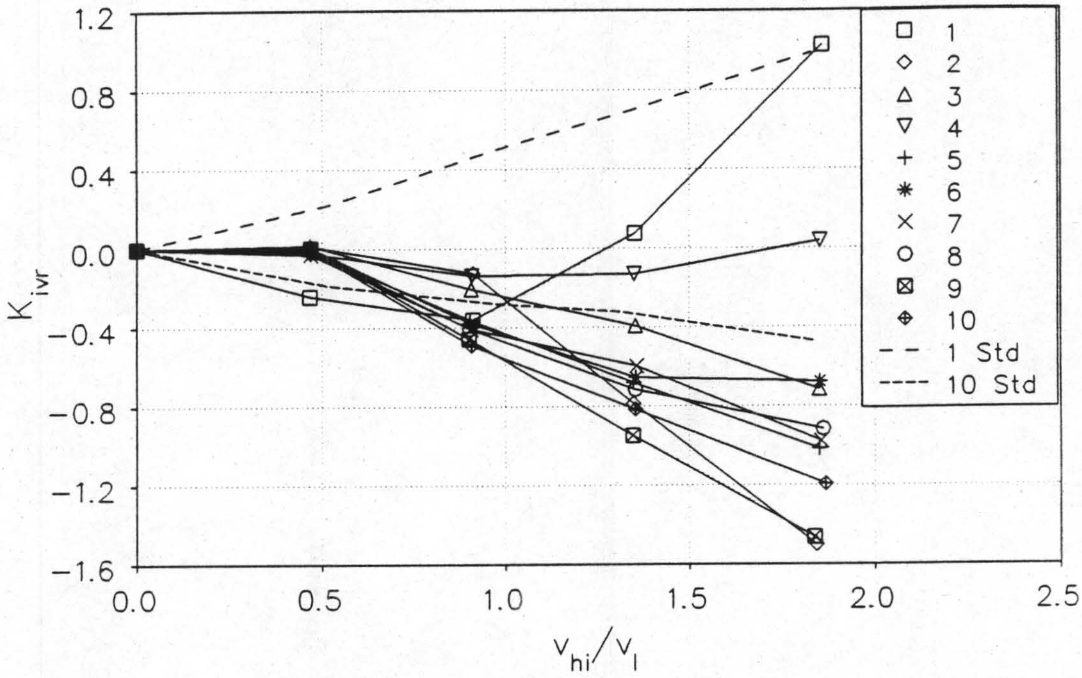

Figure 4.33: Grid configuration with upstream ramp; a = 40mm, open two dimensional configuration.

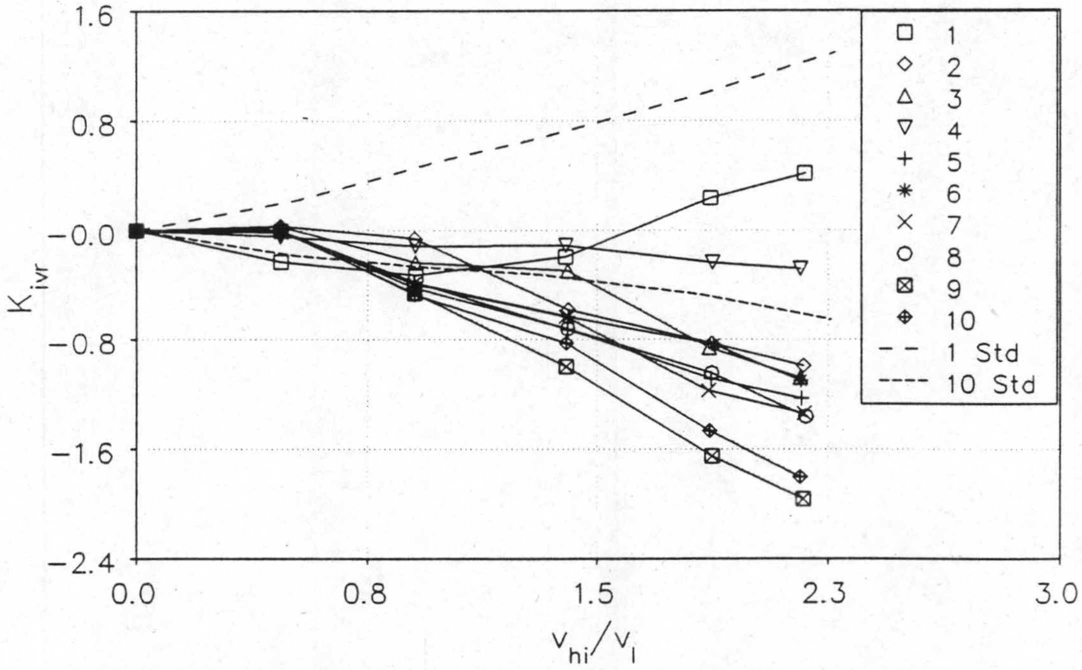

Figure 4.34: Grid configuration with upstream ramp; a = 80mm, open two dimensional configuration.

A reduction of the K_{ivr} values for all ten laterals is achieved with this configuration. The upstream ramp gives very favourable K_{ivr} values for both the positions at 60mm and 80mm. In this investigation the grid resistance is found to be negligible.

4.6 ROUNDED LATERAL INLETS

In practical applications where finned tubes are welded into the header wall, the welding seam forms a rounded inlet as shown in figure 4.35. The sharp edges of the experimental lateral inlets were machined away with a round cutting tool with a 3mm radius. A reduction of the inlet loss coefficient is expected as a result of this rounding because flow separation at the lateral inlet is reduced. The inlet loss coefficient of every individual lateral is determined experimentally in the same fashion as explained in section 4.4. The data is shown in figure 4.36. The designation K_{0r} will be used for the normal inlet loss coefficients of the rounded configuration, and the K_{ivr} values as defined in equation (4.9) are determined by subtracting that value. The K_{ivr} values of ten rounded laterals with a passing airstream are presented in figure 4.37. This will be called the *standard rounded configuration*. The values are compared to the K_{ivr} values of the first and the tenth lateral of the standard configuration.

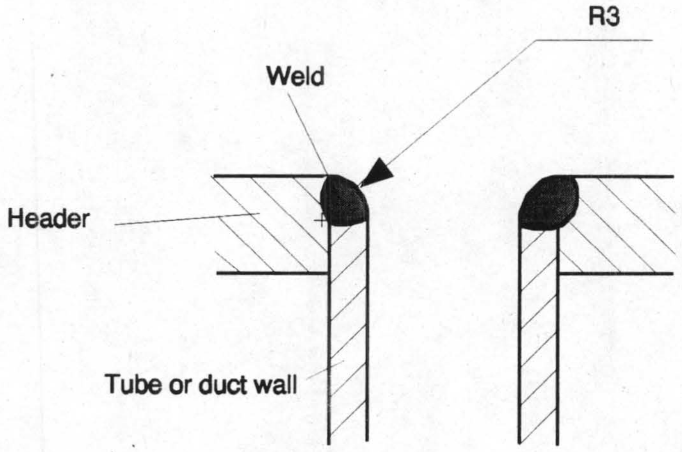

Figure 4.35: Diagram of rounded lateral inlets.

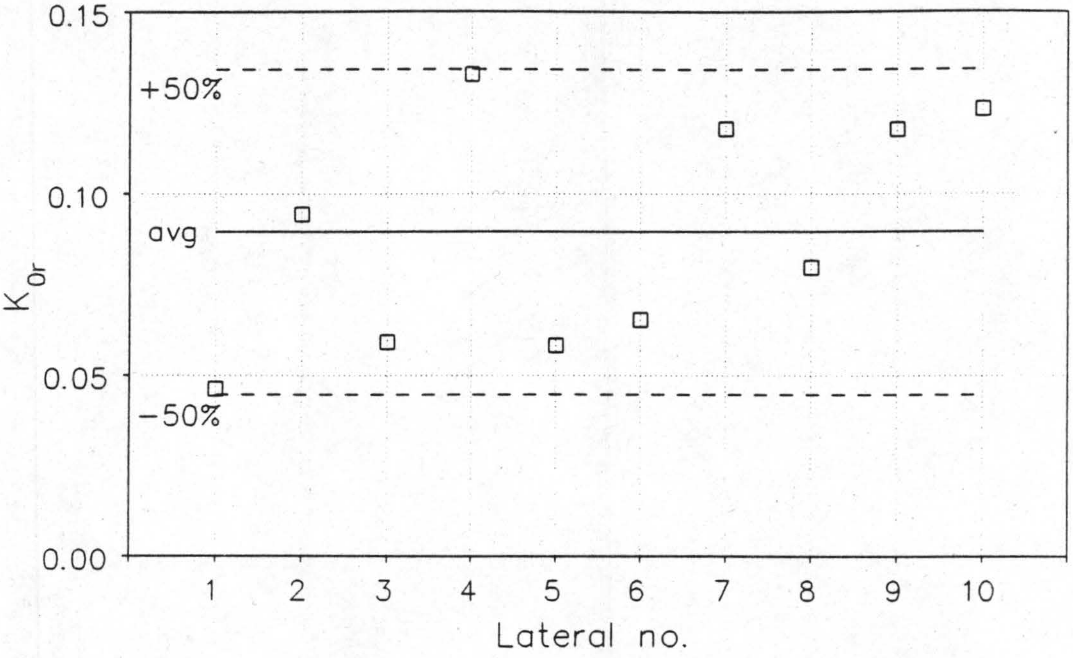

Figure 4.36: Normal inlet loss coefficients for rounded lateral inlets, with 3mm radius.

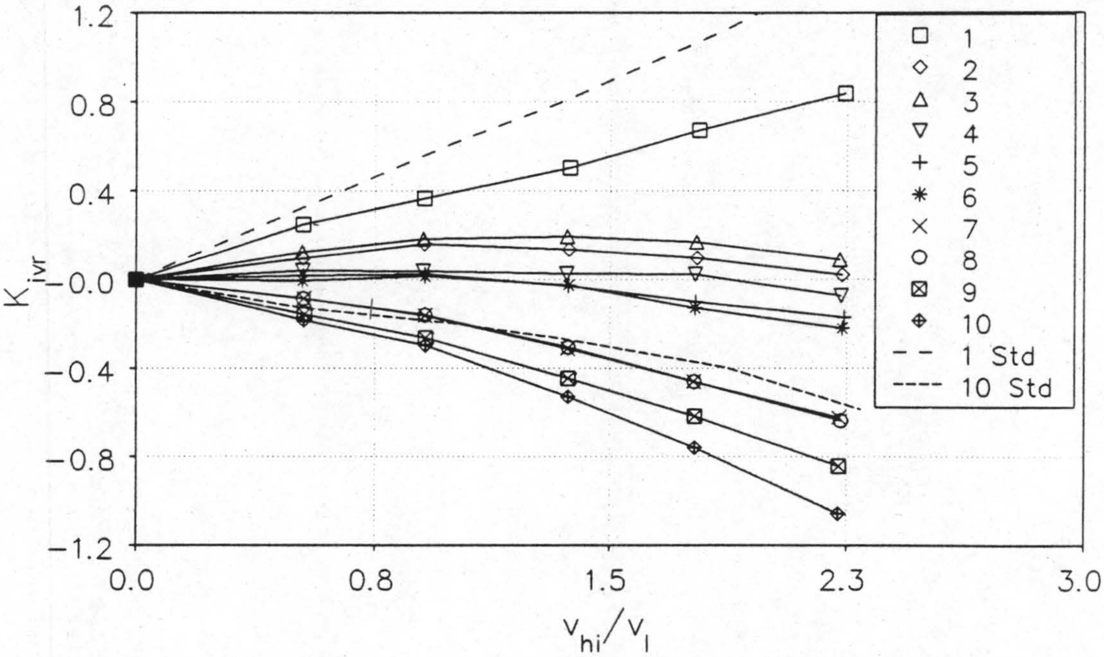

Figure 4.37: 10 laterals at 40mm pitch with 3mm inlet rounding in passing flow, open two dimensional configuration.

The three dimensional configuration described in section 4.5.2 was investigated and the resulting K_{ivr} values are presented in figure 4.37. As in the sharp inlet case, the three dimensional configuration's K_{ivr} values of the first lateral are smaller than those of the two dimensional case.

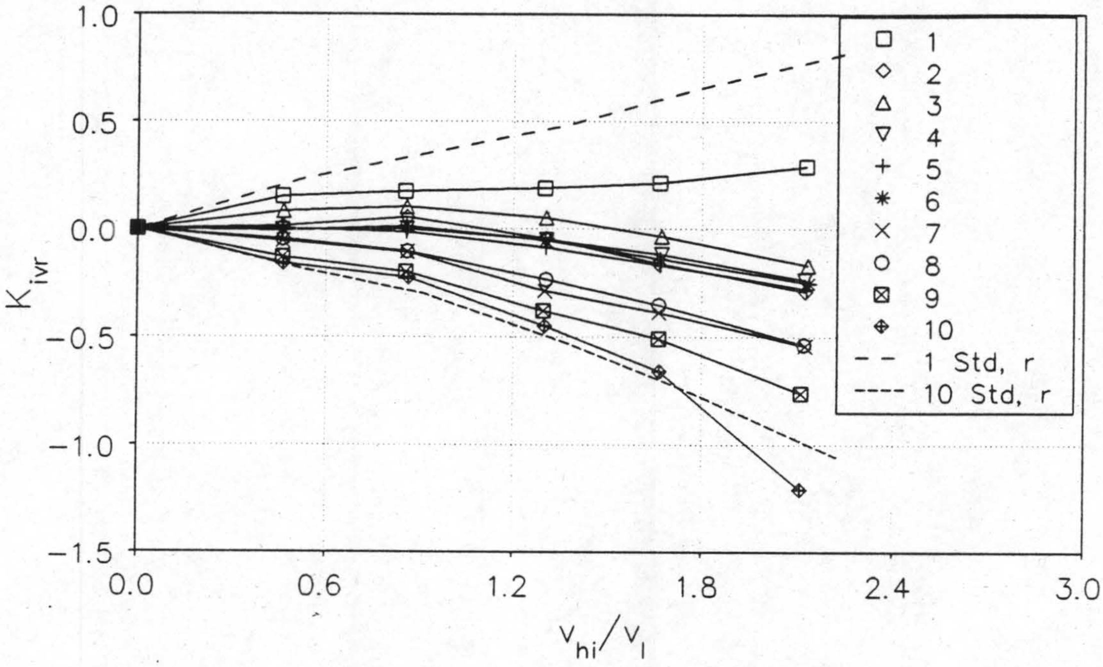

Figure 4.38: Ten laterals in open three dimensional configuration, rounded lateral inlets.

To reduce losses, the influence of two of the most effective devices found in the case of sharp inlets (a 20mm backward facing step 100mm upstream of the first lateral and the triangular ramp placed at a distance of 80mm upstream of the first lateral) are investigated for the two dimensional configuration. The K_{ivr} values for both cases are presented in figures 4.39 and 4.40 respectively. In this investigation the open two dimensional header configuration is used again. A very favourable reduction is achieved with the 20mm step upstream of the first lateral. The triangular ramp also yields lower inlet loss coefficients.

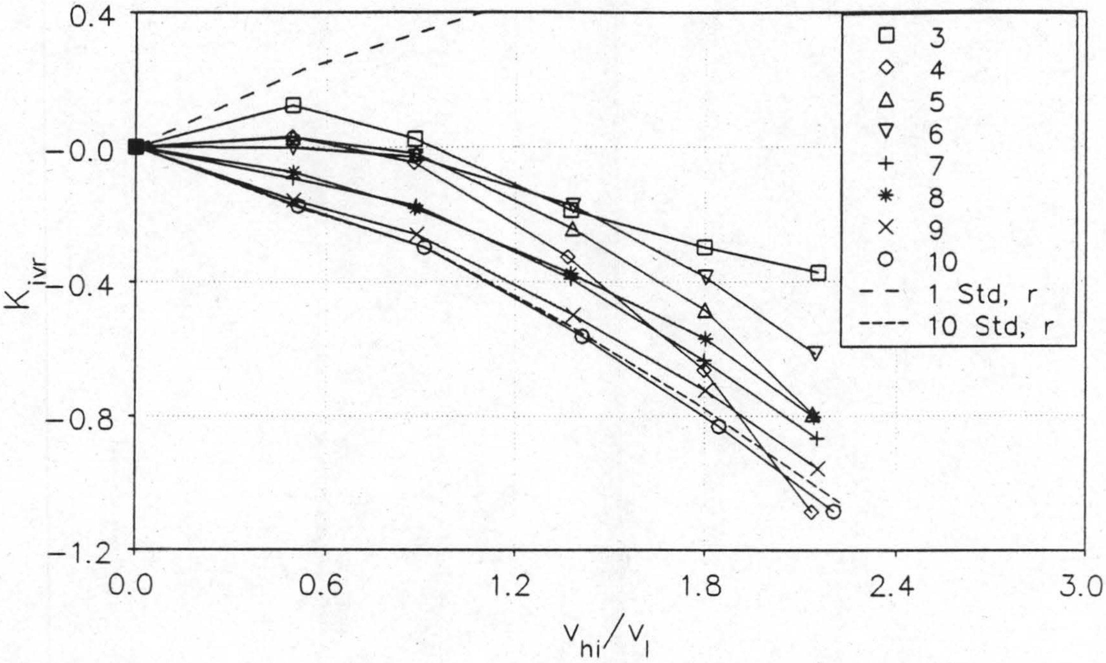

Figure 4.39: 20mm Backward facing step' 100mm before first lateral, open two dimensional configuration, rounded lateral inlets.

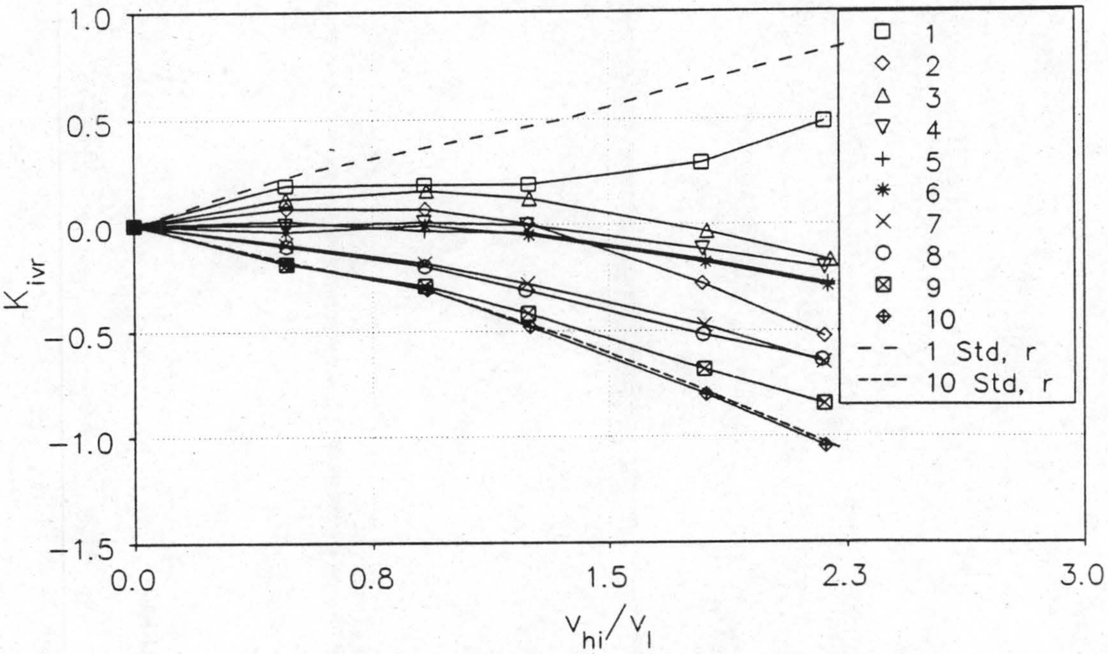

Figure 4.40: Triangular ramp 80m before first lateral, open two dimensional configuration, rounded lateral inlets.

4.7 DIVIDING MANIFOLD CONFIGURATION

The following experiment was conducted to investigate the inlet loss coefficient of the last lateral of a header without nett flow passing it. Both the sharp and the rounded experimental lateral inlets were investigated. The experimental configuration is shown in figure 4.41. A 100mm wide header which has an opening at 100mm upstream of the first lateral with rounded inlet edges to assure a nearly uniform velocity distribution in its inlet is fitted onto the lateral inlet box. The header width is of the same dimension than the lateral height, thus the flow enters parallel to the planes formed by the top and bottom plates of the lateral inlet box, so that the flow can be considered to be two-dimensional.

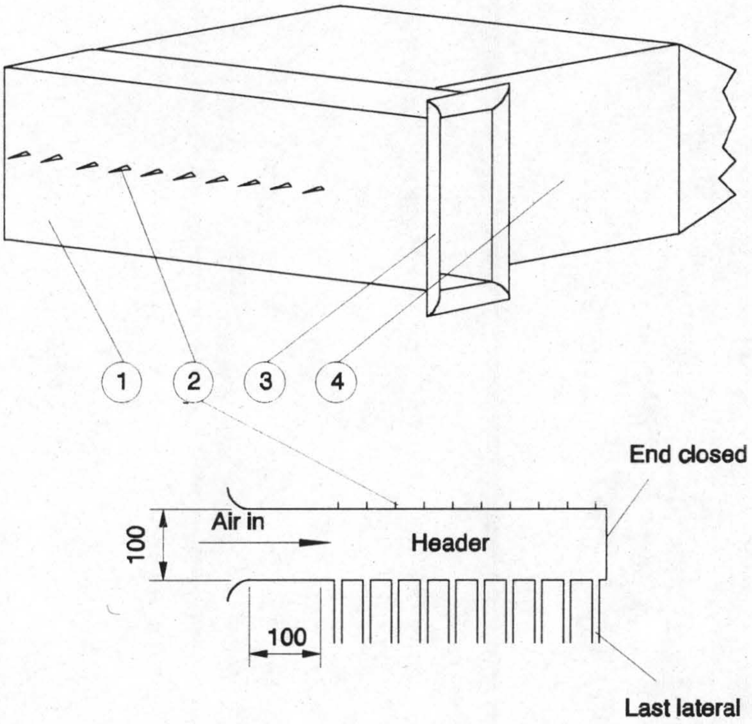

Legend:
1: Dividing header mounted onto lateral inlet box
2: Header pressure tapping points situated opposite every lateral inlet
3: Rounded inlet
4: Lateral inlet box

Figure 4.41: Dividing manifold configuration.

With air being sucked through the ten laterals at a nearly uniform lateral inlet velocity, the header mean inlet velocity is almost equal to the mean lateral velocity, as can be shown with the aid of the continuity equation. The experimental K_{ivr} values are shown in figure 4.42, where they are compared to the closed two dimensional header standard configuration. It must be noted that the header pressure tapping points are situated on the wall opposite their respective laterals.

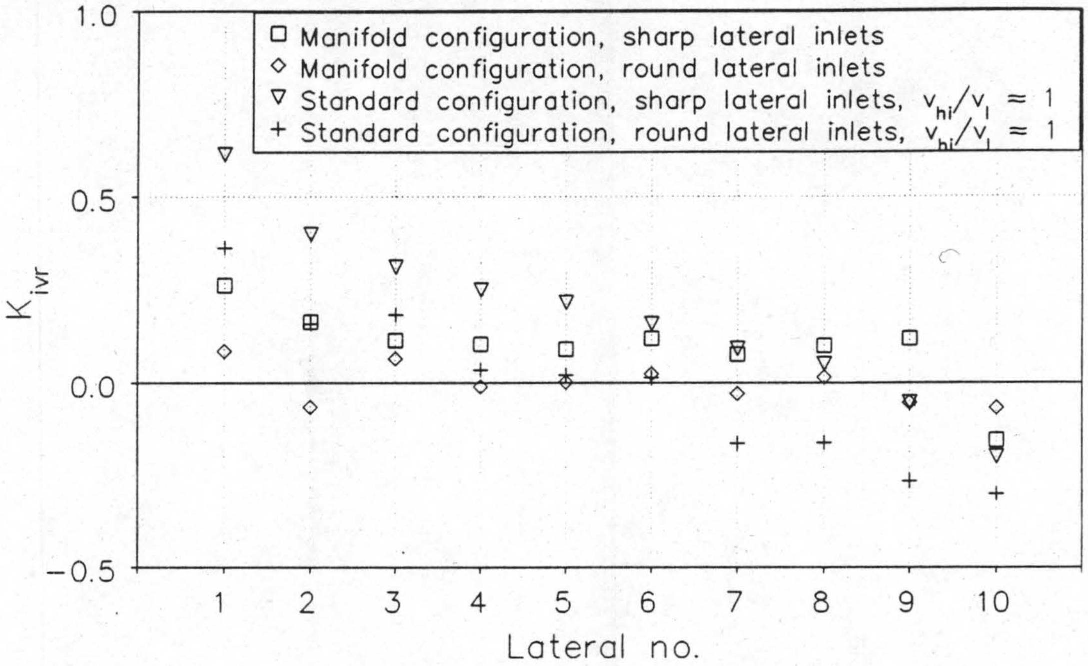

Figure 4.42: K_{ivr} values of manifold configuration compared to data of the standard configuration for sharp and rounded lateral inlets.

4.8 MISCELLANEOUS LATERAL CONFIGURATIONS

The lateral inlet loss coefficients of a single lateral or several laterals for different configurations with reference to figure 4.43 were investigated. These configurations are used to model the transition found at the position where the air-cooled condenser combining header becomes the dephlegmator dividing header. In the experiments described in this section air is sucked through a single lateral or several laterals while all or part of the remaining laterals are used in reverse by disconnecting their respective aluminium pipes from the suction manifold leading to the suction fan, so that the ambient air can flow reversely through them; thereby the air is supplied to the sucking lateral or laterals. We use the lateral numbers shown in figure 4.43 to describe the flow situations that will be investigated. The number of laterals used in the experiments to follow is changed by shifting the adjustable wall as indicated in figure 4.43. We name the numbers of the laterals which are in sucking mode while the remaining open laterals can then be accepted to be disconnected from the fan manifold with their aluminium pipe open so that ambient air is supplied to the header through them.

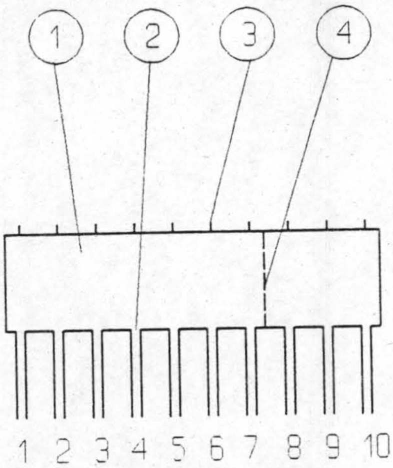

Legend:
1: Header
2: Lateral inlets
3: Pressure tapping points opposite lateral inlets
4: Adjustable wall

Figure 4.43: Fully closed header configuration with adjustable side wall.

4.8.1 FIRST FIVE OF TEN LATERALS SUCKING

The inlet loss coefficient of the first five laterals of ten are investigated. The second five are used to supply the air to the dividing header. The experimental K_{ivr} values are shown in figure 4.44. From continuity, using the area of the header and that of the laterals, the axial combining header inlet velocity to lateral velocity ratio is 0.5. The data of the standard configuration for the velocity ratio of 0.52 of lateral no. 1 and 10 are compared in figure 4.44 with that of lateral no.5 and 1 respectively, as now the nett header flow is into the opposite direction and we consider only a total of five laterals instead of ten. The K_{ivr} value of lateral no.5 is far greater than that of lateral no.1 of the standard configuration, while the K_{ivr} value of lateral no. 1 compares well with that of lateral no.10 of the standard configuration.

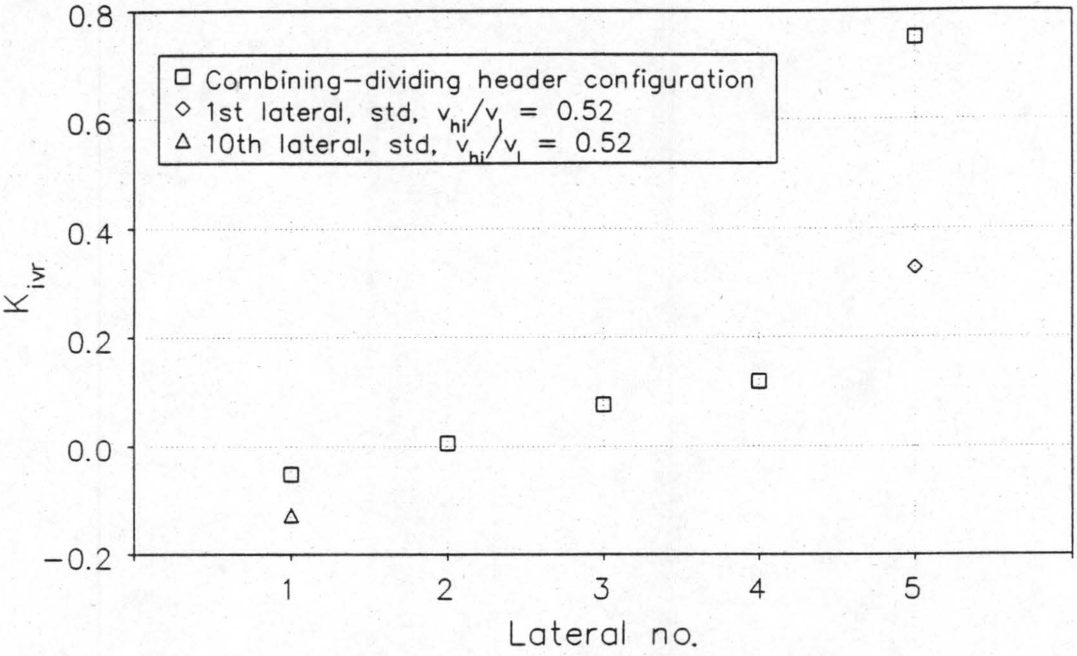

Figure 4.44: Five laterals sucking from combining-dividing header.

4.8.2 SINGLE LATERAL OF SEVEN LATERALS SUCKING

Figure 4.45 shows the experimental K_{ivr} values of the first and the fourth of seven laterals respectively as a function of the lateral Reynolds number.

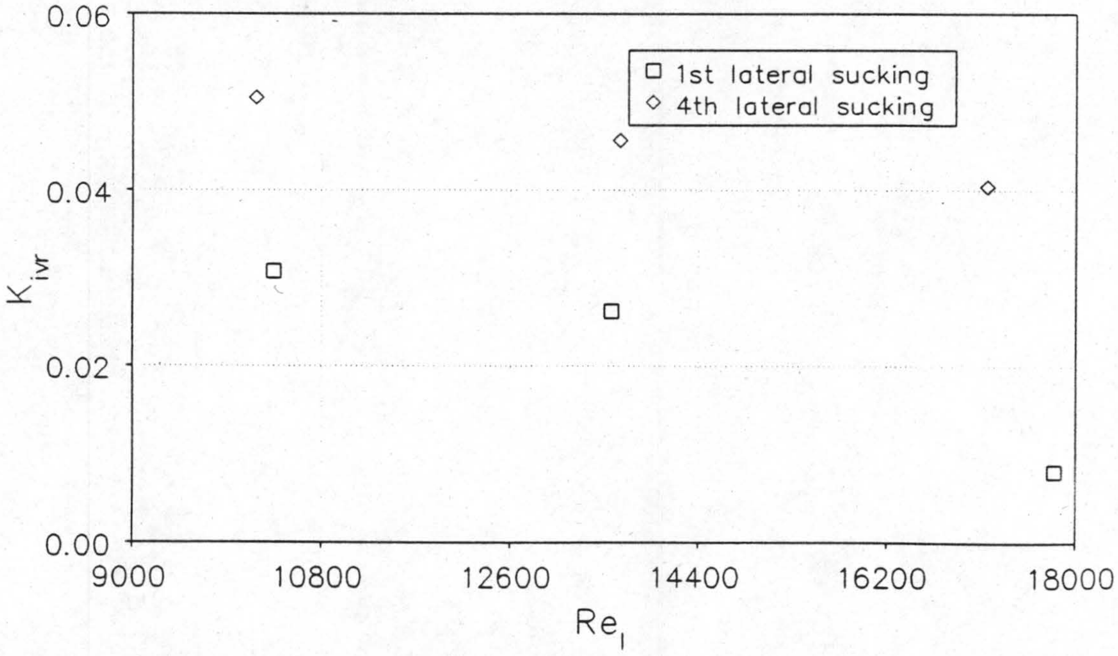

Figure 4.45: First and fourth of seven laterals in suction mode, totally closed header.

The K_{ivr} values differ less than 12% from the K_0 values of the respective laterals for both configurations.

4.9 FLOW ENTERING THE LATERAL INLET FACE AT AN ANGLE

The influence of the approach angle of the incoming flow (θ) on the inlet loss coefficient of the lateral inlet box is investigated in the following experiment. Three flow directing sections of θ = 30°,60° and 90° respectively can be attached onto the lateral box as shown schematically in figure 4.46. The flow directing sections have rounded entrances to allow for a uniform velocity distribution in the inlet. Their large cross sectional flow areas, the rather low flow velocities encountered in them, together with their inlet rounding make allowance for the assumption that the Bernoulli equation (i.e. no irreversibilities) can be used to describe the flow in the inlet section, meaning that the inlet loss coefficients can be calculated by comparing the energy levels of the downstream lateral pressure tapping to that of the ambient atmosphere. Therefore the total upstream pressure is taken as equal to the ambient static atmospheric pressure:

$$p_{atm} = p_h + \frac{1}{2} \rho v_h^2$$

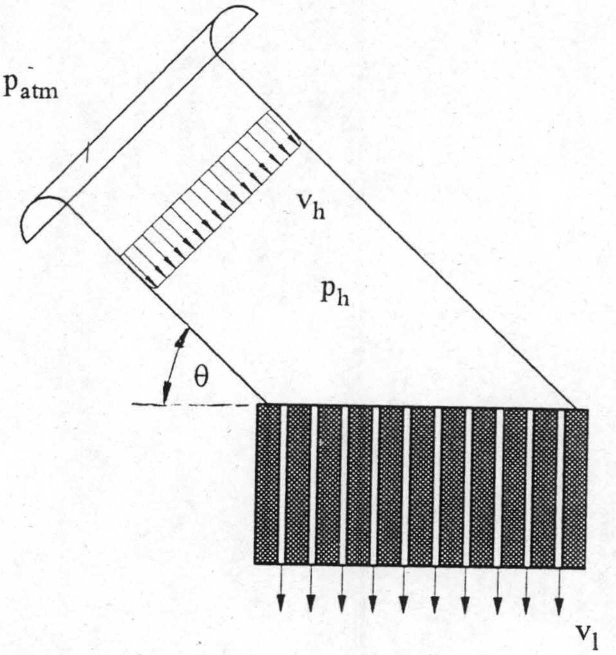

Figure 4.46: Flow directing section fitted to lateral inlet box.

The inlet loss coefficients for the three angles are shown graphically in figure 4.47.

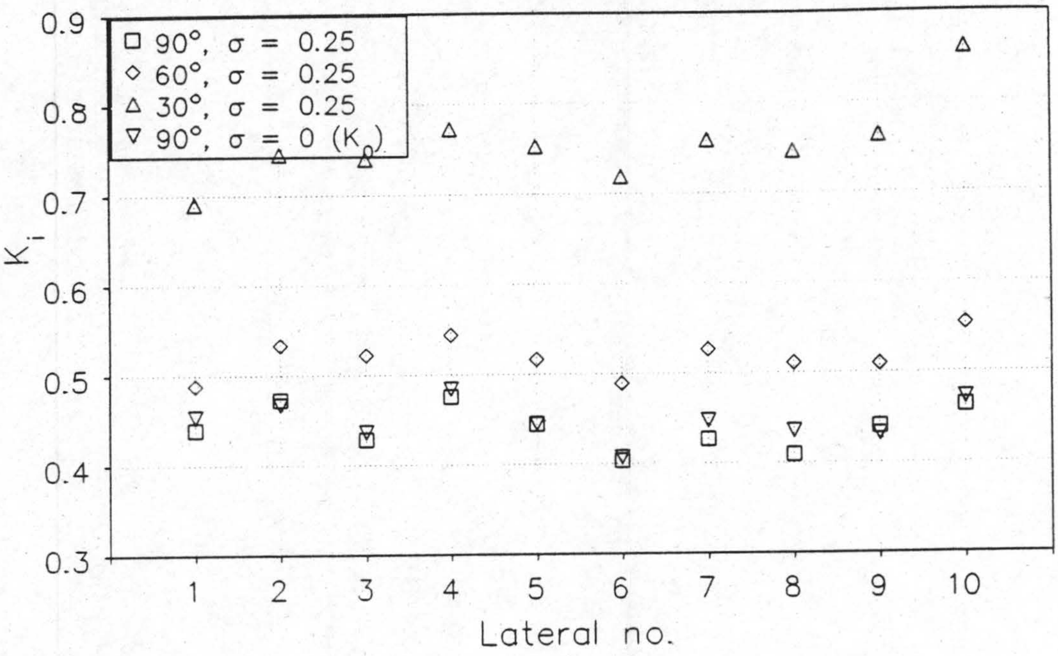

Figure 4.47: Inlet loss coefficients of oblique entering flow.

It can be seen that the flow approaching with a 30° angle gives a far higher inlet loss coefficient than the 60° and the 90° angles. The reciprocal of the average inlet loss coefficient values are compared in figure 4.48 with the Mohandes [79MO1] correlation and data for a inlet face contraction ratio of nil presented by Augustin [95AU1]. It can be seen that the correlations of Mohandes for both cases does not describe the trend of the present experimental data or that of Augustin. The present data for an inlet face area contraction ratio of 0.25 can be correlated by the following equation:

$$\frac{1}{K_i} = 2.3 \sin^{0.9}(\theta) \qquad (4.8)$$

Mohandes investigated the entrance losses of the parallel plate ducts between the fins of finned tubes. These ducts have a small equivalent diameter, therefore the Reynolds number is often in the laminar or transitional range and not in the turbulent range, as is the case in the present investigation. This could explain the deviation of the present data from the correlation of Mohandes.

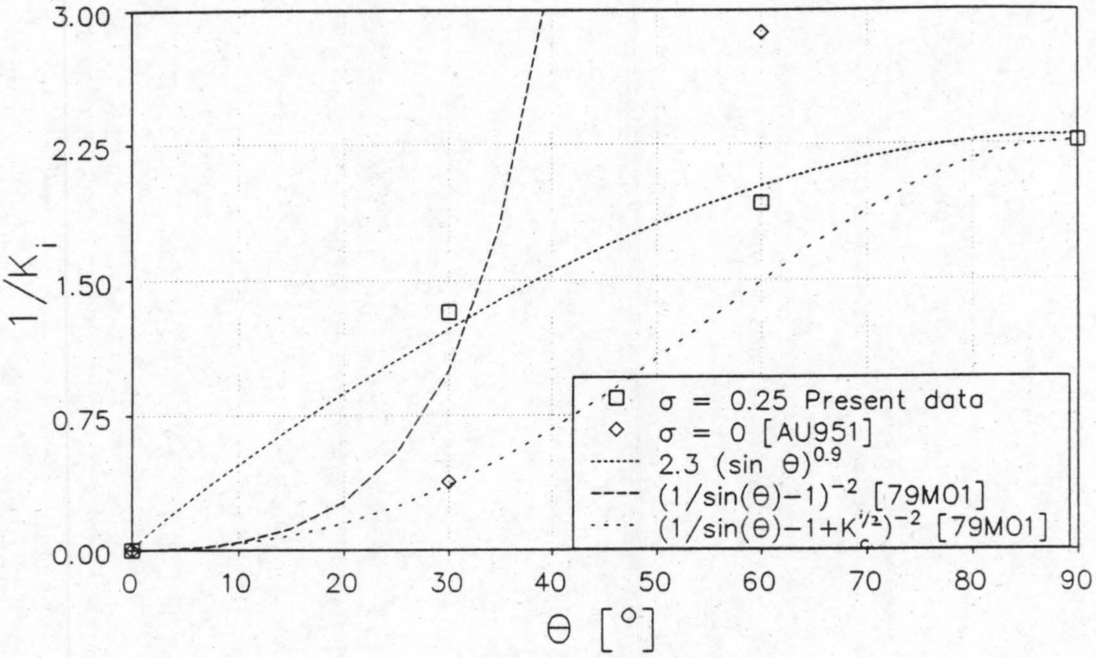

Figure 4.48: Reciprocal of inlet loss coefficients as a function of the angle of approach. (K_c is the experimentally determined normal contraction loss coefficient for σ=0.25)

4.10 APPLICATION OF THE EXPERIMENTAL DATA IN THE DESIGN OF AIR-COOLED CONDENSERS

The length of the lateral inlet face in the experimental configuration is limited to a maximum of 10 times the lateral pitch. Air-cooled condenser headers can have a length of over 1000 times the lateral pitch. In the present experimental investigation it has been shown in section 4.5.3 that the inlet loss coefficients of the first three laterals do not differ significantly if two or seven sucking laterals are situated downstream of the third lateral, as long as the lateral pitch for both configurations is the same. From this the assumption is made that the K_{ivr} values of the first three laterals behave as measured in the experiments for any header length longer than that of the respective experimental configuration. In figures 4.49 and 4.50 the K_{ivr} values of the three dimensional sharp and rounded inlet standard configurations are plotted as a function of the non-dimensionalized header distance for the velocity ratios of approximately unity. The K_{ivr} values of the remaining laterals except the last two will be taken as the values corresponding to the respective dimensionless lateral position and the header inlet to lateral inlet velocity ratio.

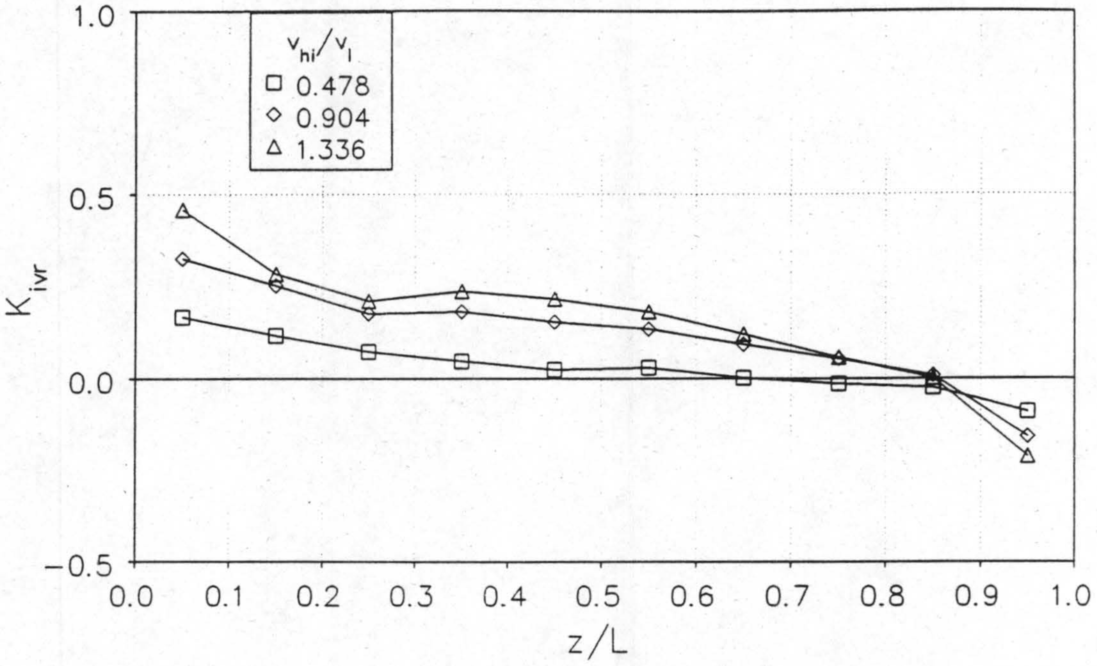

Figure 4.49: K_{ivr} values for sharp inlet standard configuration (three-dimensional).

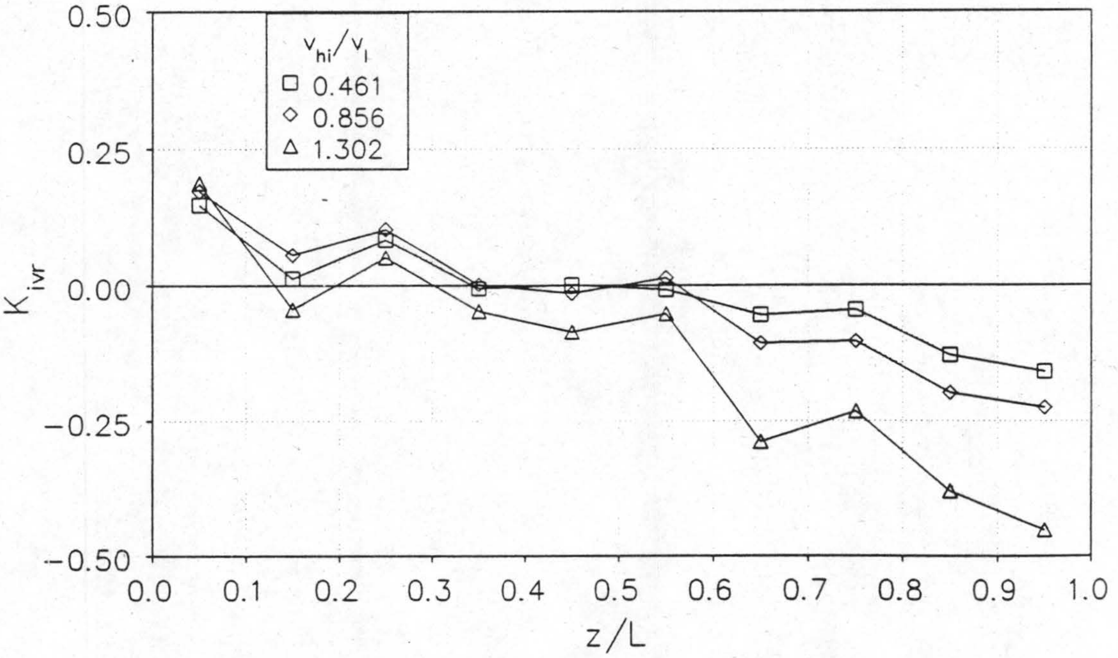

Figure 4.50: K_{ivr} values for rounded inlet standard configuration (three-dimensional).

For a dividing header with an open end the K_{ivr} values of the last two laterals again will be taken as those measured with the experimental configuration resembling the respective header configuration the closest. For a dividing header with a closed end the K_{IVT} values of section 4.7 will be used, although the size of the header of a typical industrial air-cooled condenser is most likely far greater than that used in the experiment.

CHAPTER 5

AIR-COOLED CONDENSER HEADER DESIGN METHOD WITH ASSUMED MASS FLOW DISTRIBUTION THROUGH THE LATERALS

5.1 INTRODUCTION

In this chapter a simplified design method to avoid the formation of dead zones in the finned tubes of an air-cooled condenser which consists of bundles with single rows of flattened finned tubes (laterals) is be presented. In this method the flow through only two laterals has to be considered. The two laterals is the one at which a dead zone is expected to occur, which will be referred to as the *critical* lateral, and one of the remaining laterals. The maximum condensation ratio for a specified dividing to combining header area ratio can be determined with this approach. In the Z-configuration only the first lateral can be the critical one because of a diverging dividing to combining header pressure difference. It is possible that in the U-configuration either the first or the last lateral can be the critical one because the pressure difference over the laterals may increase or decrease. These two laterals, the first and the last of the analyzed condenser section, are therefore considered as the two required in the design approach. Identical condensation rates in the laterals are assumed.

5.2 DERIVATION OF THE DESIGN METHOD

Consider an air-cooled condenser in either parallel (U) or reverse (Z) steam flow configuration with N laterals at both sides of the A-frame. Figure 5.1(a) shows such a condenser in Z-configuration determined by the directions of the header velocities. The U-configuration is described by taking negative values for the combining header velocities, as shown in figure 5.1(b).

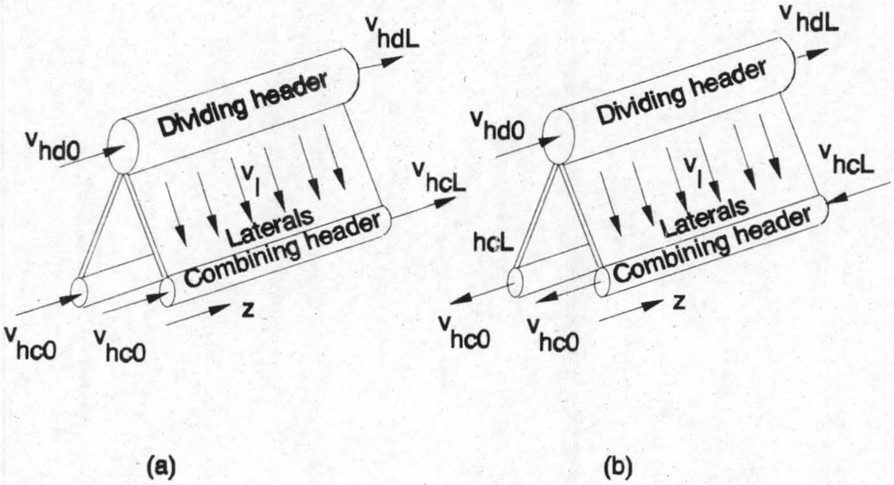

Figure 5.1: Diagram of an air-cooled condenser sections in (a) Z-configuration and (b) U-configuration.

Ignoring the header gradient of the momentum correction factor in equation (3.4), the static pressure gradient in the dividing and the combining header can be written as:

$$\frac{dp_h}{dz} = -\rho\,\theta\,v_h\,\frac{dv_h}{dz} - \frac{C}{2}\,\frac{\rho}{d_h}\,f_D\,v_h^2 \tag{5.1}$$

where $C = 1$ for $v_h > 0$ and $C = -1$ for $v_h < 0$.

Integrate equation (5.1) to obtain an expression for the pressure change over the full header length of the dividing header:

$$p_{hdL} - p_{hd0} = \frac{1}{2}\rho\,\theta_d\left(v_{hd0}^2 - v_{hdL}^2\right) - \Delta p_{dfr0L} \tag{5.2}$$

while the pressure change over the combining header is

$$p_{hcL} - p_{hc0} = \frac{1}{2}\rho\,\theta_c\left(v_{hc0}^2 - v_{hcL}^2\right) - \Delta p_{cfr0L} \tag{5.3}$$

The subscript 0 indicates the header inlet position, whereas the header outlet position is indicated by L. The last term in equations (5.2) and (5.3) is the pressure change over the respective headers due to frictional effects and is defined as:

$$\Delta p_{fr0L} = \frac{C}{2} \frac{\rho}{d_h} \int_0^{L_h} f_D v_h^2 \, dz \tag{5.4}$$

Both f_D and v_h have to be expressed as a function of z to determine the integral in equation (5.4). Note that the value of Δp_{fr0L} may be positive as found in the combining header of the U-configuration.

For an air-cooled condenser with bundles consisting of a single row of laterals we define

$$A_{hd} = \frac{A_{hdtot}}{2} \tag{5.5}$$

where A_{hdtot} is the total dividing header cross-sectional area at the specific section (two rows of laterals branch off from the dividing header to both sides of the A-frame). The header pressure is a function of the local axial header velocity, v_{hd} and v_{hc}, which can be determined via the continuity equation for the dividing header as

$$\frac{dv_{hd}}{dz} = -v_{li} \frac{A_l}{A_{hd} \Delta z} \tag{5.6}$$

and for the combining header as

$$\frac{dv_{hc}}{dz} = v_{lo} \frac{A_l}{A_{hc} \Delta z} \tag{5.7}$$

where v_{li} and v_{lo} are the respective lateral inlet and outlet steam velocities as a function of z, which are determined from the specified mass flow distribution through the laterals.

Define m_{hd0} as the total mass flow entering the dividing header of the air-cooled condenser and provide for a net mass flow leaving a dividing header with an open end which will be named m_{hdL}. The steam mass flow rates entering one row of laterals of the air-cooled condenser section is defined as:

$$m_{ltot} = \frac{\left(m_{hd0} - m_{hdL}\right)}{2} \tag{5.8}$$

Let Γ be the condensation ratio of that row, and define the condensation rate of the row of laterals as:

$$m_{ltotc} = \Gamma\, m_{ltot} \tag{5.9}$$

The condensation rate in an individual lateral is:

$$m_{lc} = \frac{m_{ltotc}}{N} \tag{5.10}$$

Because of the assumption of an identical condensation rate in every lateral the outlet steam mass flow rate of any lateral is expressed as:

$$m_{lo} = m_{li} - m_{lc} \tag{5.11}$$

Define the ratio of the dividing header flow area to the combining header flow area:

$$\sigma = \frac{2\,A_{hd}}{A_{hc}} = \frac{A_{hdtot}}{A_{hc}} \tag{5.12}$$

Subtracting equation (5.3) from equation (5.2) yields:

$$\begin{aligned}\Delta p_{hL} - \Delta p_{h0} = {} & \frac{1}{2}\rho\left(\theta_d\left(v_{hd0}^2 - v_{hdL}^2\right) - \theta_c\left(v_{hc0}^2 - v_{hcL}^2\right)\right) \\ & - \left(\Delta p_{dfr0L} - \Delta p_{cfr0L}\right)\end{aligned} \tag{5.13}$$

where

$$\Delta p_{hL} = p_{hdL} - p_{hcL}$$

$$\Delta p_{h0} = P_{hd0} - p_{hc0}$$

are the respective static pressure differences over the last and the first lateral of the air-cooled condenser section.

The dividing header velocities at z = 0 and z = L, v_{hd0} and v_{hdL} respectively, are given for both the U and the Z-configuration as

$$v_{hd0} = \frac{m_{hd0}}{2 \rho A_{hd}} \tag{5.14}$$

$$v_{hdL} = \frac{m_{hdL}}{2 \rho A_{hd}} \tag{5.15}$$

The combining header velocities at z = 0 and z = L, v_{hc0} and v_{hcL} respectively, are given for the U-configuration as

$$v_{hc0} = -(1 - \Gamma) \frac{m_{ltot}}{\rho A_{hc}} - \frac{m_{hcL}}{\rho A_{hc}} \tag{5.16}$$

$$v_{hcL} = -\frac{m_{hcL}}{\rho A_{hc}} \tag{5.17}$$

and for the Z-configuration as

$$v_{hc0} = \frac{m_{hc0}}{\rho A_{hc}} \tag{5.18}$$

$$v_{hcL} = \frac{m_{hc0}}{\rho A_{hc}} + (1 - \Gamma) \frac{m_{ltot}}{\rho A_{hc}} \tag{5.19}$$

where m_{cL} and m_{c0} provide for net mass flow rates entering the combining header of the U and the Z-configuration respectively.

The static pressure difference over the first and the last lateral can be calculated by equation (3.11) which is rewritten in terms of the present nomenclature:

$$p_{hd} - p_{hc} = \Bigg(\left(\left[K_i - \alpha_{ed} \frac{v_{hd}^2}{v_{li}^2} \right] + K_{con} \right) \frac{1}{2} \rho v_{li}^2 + \left[K_o + \alpha_{ec} \frac{v_{hc}^2}{v_{lo}^2} \right] \frac{1}{2} \rho v_{lo}^2 \tag{5.20}$$

The lateral inlet and outlet velocities have to be specified in equation (5.20). These velocities can be determined via continuity if the mass flow through the laterals is given. Mass flow distributions through the laterals as a function of the condensation ratio and the header distance will therefore be presented. The design specification stipulates that no dead zone may form in any lateral. This means that the smallest flow through a lateral must be equal to or greater than the lateral condensation rate. In this analysis the minimum mass flow rate through a lateral will be taken as the lateral condensation rate.

5.3 LINEAR FUNCTIONS FOR THE MASS FLOW DISTRIBUTION THROUGH THE LATERALS

Van Heerden [91VA1] proposes the following function for the mass flow distribution through the laterals:

$$m_{li} = a\frac{z}{L_h} + b \tag{5.21}$$

Although this linear function is not expected to describe the mass flow distribution through the laterals accurately, it provides for either the first or the last lateral being the critical one. For the case of the condenser being in Z-configuration, with the diverging pressure difference over the laterals, a linear increasing function might even give a good approximation of the flow distribution through the laterals. This linear mass flow distribution function can assume three different forms specified in the following cases, for which expressions for the factors a and b will be given:

Case 1: Linearly increasing flow distribution where the first lateral has the smallest mass flow rate.

$$a = 2(1-\Gamma)\frac{m_{ltot}}{N}$$

$$b = \Gamma\frac{m_{ltot}}{N}$$

Case 2: Linearly decreasing flow distribution where the last lateral has the smallest mass flow rate.

$$a = 2(\Gamma - 1)\frac{m_{ltot}}{N}$$

$$b = (2 - \Gamma)\frac{m_{ltot}}{N}$$

Case 3: The flow is distributed uniformly through the laterals.

$$a = 0$$

$$b = \frac{m_{ltot}}{N}$$

From equation (5.11) it follows that

$$m_{lo} = a\frac{z}{L_h} + b - \Gamma\frac{m_{ltot}}{N} \tag{5.22}$$

The lateral inlet velocity can be derived as:

$$v_{li} = \frac{1}{\rho A_l}\left(a\frac{z}{L_h} + b\right) \tag{5.23}$$

while the lateral outlet velocity is:

$$v_{lo} = \frac{1}{\rho A_l}\left(a\frac{z}{L_h} + b - \Gamma\frac{m_{ltot}}{N}\right) \tag{5.24}$$

The inlet and outlet velocity of the first and the last lateral can be calculated by equations (5.23) and (5.24). These velocities are substituted into equation (5.20) to calculate the pressure difference over both laterals. These pressure differences are then substituted into equation (5.13). Van Heerden ignored the effect of the pressure losses due to frictional effects.

The second case of Van Heerden implies that the last lateral is the critical one. This is only possible in the U-configuration where the static pressure in the dividing and in the combining header increases along the header axial direction. If the gradient in the combining header is higher than that in the dividing header, the pressure difference over the last lateral will be smaller than that over the first. This pressure difference can be sufficiently small to give a lower mass flow through the last lateral than through the first, despite the higher inlet loss coefficient of the first lateral.

5.4 QUANTIFICATION OF THE PRESSURE LOSS DUE TO FRICTIONAL EFFECTS ENCOUNTERED IN THE HEADERS

The following analysis will give an indication of the magnitude of the frictional pressure loss in a header if the mass flow entering or exiting the laterals is uniform. The friction factor and the header velocity in equation (5.4) have to be rewritten in terms of z in order to determine the integral. In general the mass flow distribution into the laterals of an air-cooled condenser does not deviate too much from the ideal uniform distribution. Therefore the pressure loss due to frictional effects in the dividing header can be quantified by assuming a uniform mass flow distribution into the laterals. The model is similar to that of a finned tube in which the steam mass flow is condensed uniformly along the tube length, which is described in section 2.4. For simplicity the flow will be regarded as turbulent throughout the header, this simplification is allowable because the header Reynolds number is in the high turbulent range due to the large header diameters. The same approximation will be used for the combining header.

The Blasius friction factor for fully developed turbulent flow (equation (2.9)) in terms of the header Reynolds number is

$$f_D = \frac{0.3164}{Re_h^{0.25}} \tag{5.25}$$

The header Reynolds number can be written as a function of z:

$$Re_h = \frac{R_{hL} - Re_{h0}}{L_h} z + Re_{h0} \tag{5.26}$$

Rewrite equation (5.4) in terms of the header Reynolds number:

$$\Delta p_{fr0L} = \frac{C}{2} \frac{0.3164\,\mu^2 L_h}{(Re_{hL} - Re_{h0})\,\rho\, d_h^3} \int_{Re_{h0}}^{Re_{hL}} Re_h^{1.75}\, d(Re_h) \qquad (5.27)$$

The integral can be determined and the pressure loss due to frictional effects over the full header length is

$$\Delta p_{fr0L} = \frac{C}{2} \rho\, v_{h0}^2 \frac{L_h}{d_{eh}} \frac{1}{\frac{Re_{hL}}{Re_{h0}} - 1} \frac{0.115055}{Re_{h0}^{0.25}} \left(\left(\frac{Re_{hL}}{Re_{h0}} \right)^{2.75} - 1 \right) \qquad (5.28)$$

The constant C assumes the value 1 for header flow in the positive z-direction and -1 for flow in the negative z-direction. For the case of $Re_{h0} < 0$, Re_{h0} and v_{h0} must be replaced by Re_{hL} and v_{hL} respectively.

5.5 ADOPTION OF UNIFORM MASS FLOW DISTRIBUTION FUNCTION IN ORDER TO INVESTIGATE CRITICAL LATERAL FLOWS

For the U-configuration the effect of the first lateral experiencing a larger inlet loss coefficient than the other laterals is not described convincingly by the linear increasing or decreasing mass flow distributions through the laterals. It can rather be expected that the first lateral has the critical mass flow rate (full condensation) while the mass flow rate through the other laterals is nearly uniformly distributed because the inlet loss coefficients tend to be similar. This uniform mass flow through each lateral is then greater than the constant condensation rate. The third case of the model proposed by Van Heerden [92VA1] describes a uniform distribution. However no critical lateral can be identified as the flow distribution is fully uniform. This model will be adjusted to allow for a critical lateral.

For the critical lateral, which will be either the first or the last lateral, a mass flow rate equal to the lateral condensation rate is specified. With this mass flow rate the lateral inlet velocity can be calculated. Because of full condensation the lateral outlet velocity is nil. The mass flow rate through the remaining laterals is calculated by assuming a fully uniform mass flow distribution through the laterals. The condensation rates in these laterals are equal to that of the critical one. Therefore the steam mass flow rates leaving these laterals can be determined by the difference between the inlet mass flow rate and the condensation rate. The inlet and outlet velocities of that lateral can then be calculated via continuity. With the inlet and outlet velocities now known for the first and the last lateral, the pressure difference over these two laterals can be calculated by equation (5.20). The inlet and outlet velocities of the dividing and the combining header are determined via continuity.

For a uniform mass flow distribution the pressure distribution in the dividing and the combining headers can be calculated according to equations (5.2) and (5.3).

5.6 SAMPLE CALCULATION TO DEMONSTRATE THE DESIGN METHOD

The application of the proposed design method introduced in section 5.4 will be demonstrated by means of a sample calculation. Consider a section of an A-frame, single finned tube row air cooled steam condenser in U-configuration as shown in figure 5.2.

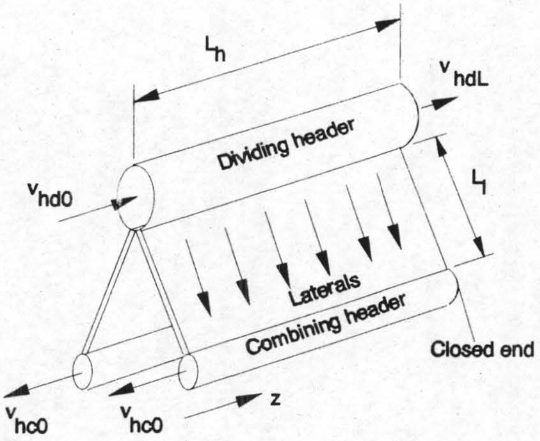

Figure 5.2: Air-cooled condenser section.

The calculation will be performed with the assumption that the first lateral is the critical one, while the mass flow rate is assumed to be uniformly distributed through all of the remaining laterals. Steam at 60°C enters the dividing header with a flow rate of 12kg/s. The specifications of the condenser are as follows:

Length of the headers,	L_h	=	10m
Lateral pitch,	Δz	=	0.04m
Number of laterals on two sides of the A-frame,	2N	=	2×250
Dividing header diameter,	d_{hd}	=	1.2500m
Dividing header area,	$2A_{hd}$	=	$1.2272m^2$
Combining header diameter,	d_{hc}	=	0.3125m
Combining header area,	A_{hc}	=	$0.07670m^2$
Header area ratio,	σ	=	A_{hd}/A_{hc} = 16.0
Length of lateral,	L_l	=	9m
Lateral height (see fig.2.2),	h	=	0.19m
Lateral width,	w	=	0.01m

The lateral inlets are rounded with a 3mm radius. It is required to find the condensation ratio for which no dead zone will occur in any lateral.

Because of the implicitness of the equations involved, the solution of the condensation ratio will be used in the sample calculation:

$\Gamma = 0.950977$

The thermo-physical properties for saturated steam at 60°C are calculated according to equations (A.2) and (A.3):

$$\rho = -4.062329056 + 0.10277044\,T - 9.76300388\times10^{-4}\,T^2 + 4.475240795\times10^{-6}\,T^3 - 1.004596894\times10^{-8}\,T^4 + 8.9154895\times10^{-12}\,T^5$$

$$= -4.062329056 + 0.10277044\times(333.15) - 9.76300388\times10^{-4}\times(333.15)^2 + 4.475240795\times10^{-6}\times(333.15)^3 - 1.004596894\times10^{-8}\times(333.15)^4 + 8.9154895\times10^{-12}\times(333.15)^5 = 0.13023\text{kg/m}^3$$

$$\mu = 2.562435\times10^{-6} + 1.816683\times10^{-8}\ T + 2.579066\times10^{-11}\ T^2 - 1.067299\times10^{-14}\ T^3$$
$$= 2.562435\times10^{-6}+ 1.816683\times10^{-8}\times(333.15) +2.579066\ 10^{-11}\times(333.15)^2$$
$$- \ 1.067299\ \times10^{-14}\times(333.15)^3 = 1.10825 \times 10^{-5}\ \text{Ns/m}^2$$

The lateral cross sectional area is:

$$A_l = w \times 2 \times h = 0.19 \times 2 \times 0.005 = 0.019\text{m}^2$$

In order to calculate the wall Reynolds number of condensing flow in a duct consisting of parallel plates the area of these parallel plates is determined:

$$A_{lw} = 2 \times w \times L_l = 2 \times 0.19 \times 9 = 3.42\text{m}^2$$

The condensation rate of the condenser is:

$$2m_{ltotc} = \Gamma\ (2m_{ltot}) = 2 \times 0.950977 = 11.4117\text{kg/s}$$

This gives a condensation rate in a single lateral of:

$$m_{lc} = \frac{2\ m_{ltotc}}{2\ N} = \frac{11.4117}{2 \times 250} = 0.022823\text{kg/s}$$

As the first lateral is identified as the critical one, the mass flow through it is taken as condensation rate.

The dividing and the combining headers are closed at z=L; this means that $v_{hdL} = 0$ and $v_{hcL} = 0$. The steam velocity at the dividing header inlet is:

$$v_{hd0} = \frac{m_{hd0}}{\rho\ 2\ A_{hd}} = \frac{12.0}{0.13023 \times 1.22718} = 75.086\text{m/s}$$

At the end of this condenser section the dividing and combining header velocities are zero because the headers are closed at z = L. Therefore the combining header steam velocity at z=0 can be calculated as:

$$v_{hc0} = -\frac{(1-\Gamma)2\,m_{ltot}}{2\,\rho\,A_{hc}} = -\frac{(1-0.950977)\times 12}{2\times 0.13023\times 0.076699} = -29.4475\text{m/s}$$

The velocity is negative because of the U-configuration.

The condensation loss coefficient will be determined by equation (2.37), with the frictional pressure loss according to section 2.4.1 which is the approach of Groenewald [93GR1]. Calculate the wall Reynolds number according to equation (2.28):

$$Re_w = \frac{m_{lc}\,d_{el}}{A_{li}\,\mu} = \frac{0.022823\times 0.019}{(2\times 0.19\times 9)\times 1.10825\times 10^{-5}} = 11.4411$$

The coefficients of equations (2.27a) and (2.27b) are:

$$\begin{aligned} A &= 1.041\times 10^{-3}\,Re_w - 2.011\times 10^{-7}\,Re_w^3 + 1.0649 \\ &= 1.041\times 10^{-3}\times 11.4411 - 2.011\times 10^{-7}\times (11.4411)^3 + 1.0649 \\ &= 1.07651 \end{aligned}$$

$$\begin{aligned} B &= 59.3153\,Re_w + 1.5995\times 10^{-2}\,Re_w^3 + 290.1479 \\ &= 59.3153\times 11.4411 + 1.5995\times 10^{-2}\times (11.4411)^3 + 290.1479 \\ &= 992.735 \end{aligned}$$

$$\begin{aligned} C &= 1 + 6.56\times 10^{-4}\,Re_w^2 = 1 + 6.56\times 10^{-4}\times (11.4411)^2 \\ &= 1.0859 \end{aligned}$$

Static pressure change over the first lateral:

The lateral inlet velocity is calculated as:

$$v_{li} = \frac{m_{lc}}{\rho\,A_l} = \frac{0.022823}{0.13023\times 0.0019} = 92.239\text{m/s}$$

For the first lateral $v_{lo} = 0$.

From the lateral inlet velocity the lateral inlet Reynolds number can be calculated as:

$$
\begin{aligned}
Re_{li} &= \frac{\rho\, v_{li}\, d_{el}}{\mu} \\
&= \frac{0.13023 \times 92.239 \times 0.019}{1.10825 \times 10^{-5}} \\
&= 20594.04
\end{aligned}
$$

Because of full condensation, $Re_{lo} = 0$ and $x_o = 0$; the quality at the transition from turbulent to laminar flow is:

$$x_{tr} = \frac{2300}{Re_{li}} = \frac{2300}{20594.04} = 0.111683$$

The condensation loss coefficient,

$$K_{con} = \frac{\Delta p_{fr}}{\frac{1}{2}\rho\, v_{li}^{2}} - \left(x_o^2 - 1\right)$$

can now be calculated. The first term of the right hand side in above equation for turbulent inflow and full condensation can be calculated with equation (2.31b) of the Groenewald [93GR1] model:

$$
\begin{aligned}
\frac{\Delta p_{fr}}{\frac{1}{2}\rho v_{li}^{2}} &= \frac{L_1}{d_{el}}\frac{1}{x_o - 1}\times\left[\frac{0.3164}{Re_{li}^{0.25}}\right. \\
&\quad\times\left(\frac{A}{2.75}\left(x_{tr}^{2.75}-1\right)+\frac{B}{1.75\,Re_{li}}\left(x_{tr}^{1.75}-1\right)\right) \\
&\quad\left.+\frac{48\,C}{Re_{li}}\left(x_o^{2}-x_{tr}^{2}\right)\right] \\
&= \frac{9}{0.019}\times\frac{1}{(0)-1}\times\left[\frac{0.3164}{(20594.04)^{0.25}}\right. \\
&\quad\times\left(\frac{1.07651}{2.75}\left((0.111677)^{2.75}-1\right)+\frac{992.737}{1.75\times 20594.04}\left((0.111683)^{1.75}-1\right)\right) \\
&\quad\left.+\frac{48\times 1.0859}{20594.04}\left((0)^{2}-(0.111683)^{2}\right)\right] \\
&= 5.237845
\end{aligned}
$$

Calculate the condensation loss coefficient:

$$
\begin{aligned}
K_{con} &= \frac{\Delta p_{fr}}{\frac{1}{2}\rho v_{li}^{2}} - \left(1 - x_o^{2}\right) \\
&= 5.237845 - \left(1 - (0)^{2}\right) \\
&= 4.237845
\end{aligned}
$$

The dividing header inlet to lateral inlet velocity ratio is:

$$
\frac{v_{hdi}}{v_{li}} = \frac{75.086}{92.239} = 0.81404
$$

For a three dimensional inlet header configuration with rounded lateral inlets, the K_{ivr} value for this velocity ratio can be interpolated from the experimental values of table D.47 which are shown figure 4.38, as 0.168824 for the first lateral. The average K_{0r} value for laterals with 3mm inlet roundings is 0.08950. Calculate

$$
K_i - \alpha_{ed}\frac{v_{hd}^{2}}{v_{li}^{2}} = K_{0r} + K_{ivr} = 0.08950 + 0.168824 = 0.258324
$$

Because of a zero outlet velocity the outlet loss coefficient is not considered.

Calculate the static pressure difference over the first lateral:

$$p_{hd0} - p_{hc0} = \left[\left(K_i - \alpha_{ed}\frac{v_{hd}^2}{v_{li}^2}\right) + K_{con}\right]\frac{1}{2}\rho v_{li}^2$$

$$= \left[0.259324 + 4.237845\right]\frac{1}{2} \times 0.13023 \times (92.239)^2$$

$$= 2490.8902 \mathrm{N/m}^2$$

Static pressure change over the last lateral:

By assuming a uniform mass flow distribution through the laterals, the last lateral's inlet velocity is calculated as:

$$v_{li} = \frac{2\, m_{ltot}}{2\, N\, \rho\, A_l} = \frac{12}{2 \times 250 \times 0.13023 \times 0.0019} = 96.994 \mathrm{m/s}$$

Its outlet velocity is:

$$v_{lo} = v_{li} - \frac{m_{lc}}{\rho\, A_l} = 96.994 - \frac{0.022823}{0.13023 \times 0.0019} = 4.755 \mathrm{m/s}$$

The respective lateral inlet and outlet Reynolds numbers are:

$$Re_{li} = \frac{\rho\, v_{li}\, d_{el}}{\mu} = \frac{0.13023 \times 96.994 \times 0.019}{1.10825 \times 10^{-5}} = 21655.7$$

and

$$Re_{lo} = \frac{\rho\, v_{lo}\, d_{el}}{\mu} = \frac{0.13023 \times 4.755 \times 0.019}{1.10825 \times 10^{-5}} = 1060.6$$

Calculate the condensation loss coefficient. Again the first term of the right hand side of equation (2.37) is calculated first. The outlet quality is:

$$x_o = \frac{Re_{lo}}{Re_{li}} = \frac{1060.6}{21655.7} = 0.049023$$

and the quality at the transition from turbulent to laminar flow is:

$$x_{tr} = \frac{2300}{Re_{li}} = \frac{2300}{21655.7} = 0.10621$$

Again equation (3.31b) is used, as the steam leaves the lateral with $Re_{lo}<2300$.

$$\frac{\Delta p_{fr}}{\frac{1}{2}\rho v_{li}^2} = \frac{L_l}{d_{el}}\frac{1}{x_o - 1}$$

$$\times \left(\frac{0.3164}{Re_{li}^{0.25}}\left(\frac{A}{2.75}\left(x_{tr}^{2.75}-1\right) + \frac{B}{1.75\,Re_{li}}\left(x_{tr}^{1.75}-1\right)\right) + \frac{48\,C}{Re_{li}}\left(x_o^2 - x_{tr}^2\right)\right)$$

$$= \frac{9}{0.019}\,\frac{1}{(0.049023 - 1)}$$

$$\times \left[\frac{0.3164}{(21655.7)^{0.25}}\left(\frac{1.0765}{2.75}\left((0.10621)^{2.75} - 1\right) + \frac{992.737}{1.75\times(21655.7)}\left((0.10621)^{1.75} - 1\right)\right) + \frac{48\times 1.0859}{21655.7}\left((0.049023)^2 - (0.10621)^2\right)\right]$$

$$= 5.419226$$

The condensation loss coefficient can be calculated according to equation (2.37):

$$K_{con} = \frac{\Delta p_{fr}}{\frac{1}{2}\rho v_{li}^2} - \left(1 - x_o^2\right) = 5.419226 - \left(1 - (0.049023)^2\right) = 4.42163$$

For the last lateral, as we have a closed header the K_{ivr} value is -0.09526, taken as the average value from table D.54. Calculate

$$K_i - \alpha_{ed}\frac{v_{hd}^2}{v_{li}^2} = K_{0r} + K_{ivr} = 0.0895 - 0.09526 = -0.00576$$

Because of the high aspect ratio of the laterals, the area expansion ratio from the lateral to the combining header is taken as w/Δz = 0.1/0.4 = 0.25 for which from equation (2.50):

$$K_o = \left(1 - \frac{A_l}{A_{hc}}\right)^2 = \left(1 - 0.25\right)^2 = 0.5625$$

The static pressure difference over the last lateral is calculated as:

$$p_{hdl} - p_{hcl} = \left[\left(K_i - \alpha_{ed}\frac{v_{hd}^2}{v_{li}^2}\right) + K_{con}\right]\frac{1}{2}\rho v_{li}^2 + \left(K_o + \alpha_{ec}\frac{v_{hc}^2}{v_{lo}^2}\right)\frac{1}{2}\rho v_{lo}^2$$

$$= \left[-0.00576 + 4.4216\right] \times \frac{1}{2} \times 0.13023 \times (96.994)^2$$

$$+ \left(0.5625 + 0\right) \times \frac{1}{2} \times 0.13023 \times \left(4.755\right)^2$$

$$= 2705.93 \mathrm{N/m}^2$$

The combining header velocity (v_{hc}) is nil at the last lateral.

Header momentum equations:

The momentum correction coefficients are obtained from the numerical solution of header flow shown in appendix E. The respective momentum correction factors for the dividing and the combining header are $\theta_d = 0.99$ and $\theta_c = 2.24$.

The pressure loss due to frictional effects for both headers is now calculated according to equation (5.32). Firstly consider the dividing header. At z = 0 the header Reynolds number is:

$$Re_{hd0} = \frac{\rho v_{hd0} d_{hd}}{\mu} = \frac{0.13023 \times 75.086 \times 1.25}{1.108251 \times 10^{-5}} = 1.10291 \times 10^6$$

The dividing header Reynolds number at $z = L_h$ is 0 as the header is closed. Calculate the pressure change over the dividing header due to frictional losses according to equation (5.28)

$$\Delta p_{dfr0L} = \frac{C}{2}\rho v_{hd0}^{2} \frac{L_h}{d_{hd}} \frac{1}{\frac{Re_{hdL}}{Re_{hd0}} - 1} \frac{0.115055}{Re_{hd0}^{0.25}} \left(\left(\frac{Re_{hdL}}{Re_{hd0}} \right)^{2.75} - 1 \right)$$

$$= \frac{1}{2} \times 0.13023 \times (75.086)^2 \times \frac{10}{1.25} \times \frac{1}{\frac{0}{1.10291 \times 10^6} - 1}$$

$$\times \frac{0.115055}{(1.10291 \times 10^6)^{0.25}} \times \left(\left(\frac{0}{1.10291 \times 10^6} \right)^{2.75} - 1 \right) = 10.427 \text{ N/m}^2$$

The combing header Reynolds number at $z = 0$ is

$$Re_{hc0} = \frac{\rho v_{hc0} d_{hc}}{\mu} = \frac{0.13023 \times 29.447 \times 0.31250}{1.108251 \times 10^{-5}} = 1.08036 \times 10^5$$

At $z = L_h$ $Re_{hcL} = 0$ as the velocity is nil. Calculate the pressure change over the combining header due to frictional losses

$$\Delta p_{cfr0L} = \frac{C}{2}\rho v_{hc0}^{2} \frac{L_h}{d_{hc}} \frac{1}{\frac{Re_{hcL}}{Re_{hc0}} - 1} \frac{0.115055}{Re_{hc0}^{0.25}} \left(\left(\frac{Re_{hcL}}{Re_{hc0}} \right)^{2.75} - 1 \right)$$

$$= \frac{-1}{2} \times 0.13023 \times (29.419)^2 \times \frac{10}{0.31250} \times \frac{1}{\frac{0}{1.08036 \times 10^5} - 1}$$

$$\times \frac{0.115055}{(1.08036 \times 10^5)^{0.25}} \times \left(\left(\frac{0}{1.08032 \times 10^5} \right)^{2.75} - 1 \right) = -11.464 \text{N/m}^2$$

Now we can solve equation (5.13). The left hand side of the equation is:

$$\begin{aligned} \text{LHS} &= \left(p_{hdL} - p_{hcL}\right) - \left(p_{hd0} - p_{hc0}\right) \\ &= 2705.96 - 2490.89 \\ &= 215.07 \text{N/m}^2 \end{aligned}$$

and the right hand side gives:

$$
\begin{aligned}
\text{RHS} &= \frac{1}{2}\rho\left(\theta_d\left(v_{hd0}^2 - v_{hdL}^2\right) - \theta_c\left(v_{hc0}^2 - v_{hcL}^2\right)\right) \\
&\quad - \left(\Delta p_{dfr0L} - \Delta p_{cfr0L}\right) \\
&= \frac{1}{2} \times 0.13023 \\
&\quad \times \left((0.99) \times \left((75.086)^2 - (0)^2\right) - (2.24)\left((-29.447)^2 - (0)^2\right)\right) \\
&\quad - \left(10.43 - (-11.46)\right) \\
&= 215.07\text{N/m}^2
\end{aligned}
$$

which is equal to the left hand side. This means that the correct value of Γ has been chosen.

5.7 THE APPLICABILITY OF THE DESIGN METHOD

The sample calculation which is presented in section 5.6 shows how, if a total mass flow rate through all the laterals of a section of an air-cooled condenser is specified, the maximum condensation rate is calculated for a specific header area ratio with the design method. In this section the relationship between σ and Γ for a condenser section with a specified total mass flow rate of 12kg/s through its laterals, identical to the mass flow rate used in the sample calculation, is investigated. The dividing header dimensions are kept constant while the combining header diameter is varied in order to change σ. The properties of the steam are the same as in the sample calculation. The effect of sharp edged lateral inlets and rounded lateral inlets is also investigated. The inlet loss coefficients used in the calculations are interpolated from the values of tables D.26 and D.8 for the respective geometries.

Firstly a condenser section in U-configuration as shown in figure 5.2 is investigated. The combining header is closed at $z = L$, while the dividing header may allow for a nett mass flow leaving it. Two situations are now compared:

Situation (1):

A mass flow rate of 12kg/s enters the dividing header. There is no nett outflow at the dividing header end.

Situation (2):

A mass flow rate of 24kg/s enters the dividing header. The nett outflow at the dividing header end is 12kg/s.

Figure 5.3 shows the relationship between Γ and σ for situations (1) and (2) for the case of the first lateral and the case of last lateral being the critical one calculated with the design method. Furthermore the relationship between Γ and σ obtained by applying the numerical solution algorithm presented in section 3.7.2 is presented in figure 5.3. In the numerical solution the relationship is determined by choosing a value for Γ which gives an entering mass flow rate into any lateral which is equal to the lateral condensation rate for a fixed value of σ. The mass flow distributions through the laterals obtained with the numerical method are shown in appendix F. Rounded lateral inlets are used in the numerical solution.

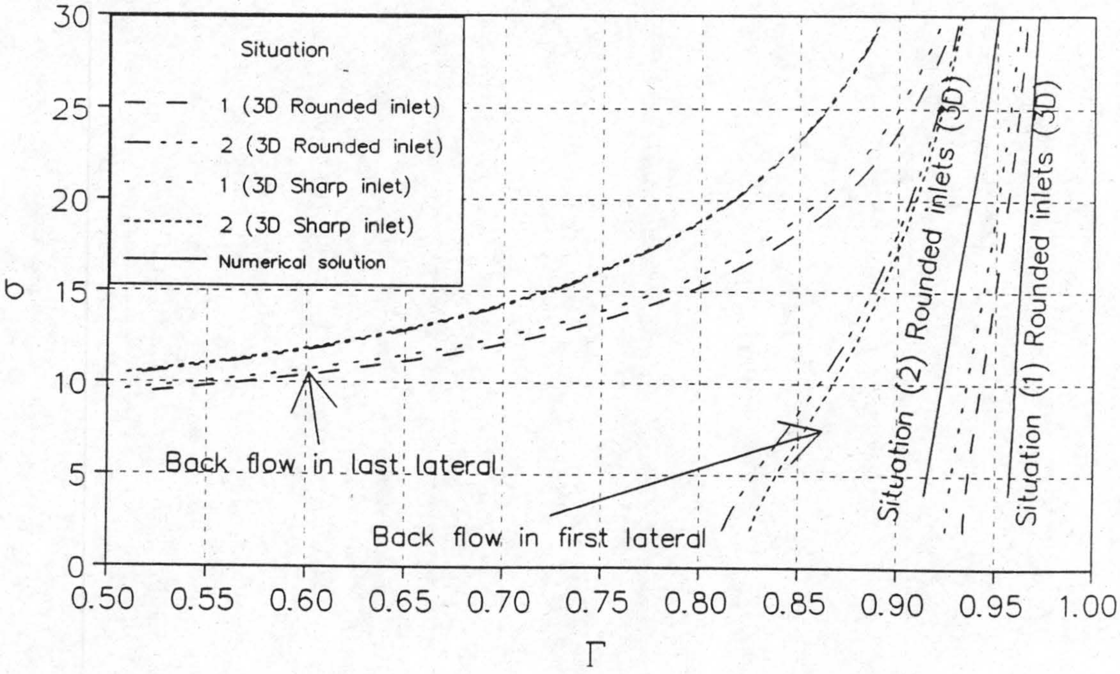

Figure 5.3: Γ to σ design regions for situations (1) and (2), $d_{hd} = 1.25$m.

It can be seen in figure 5.3 that the inlet geometry does not severely affect the relationship between σ and Γ. If there is a nett outflow from the dividing header, the allowable values for Γ are decreased. Figure 5.3 can be used as a design chart by choosing a value for Γ between the respective two lines indicating the first and the last laterals as critical for a fixed value for σ. It must be noted that this design chart is dependent on the condenser configuration and the specified mass flow rate. Furthermore figure 5.3 shows that the numerical solution allows greater Γ than the proposed design method. The numerical solution does not predict the last lateral to be the critical one for this investigated condenser section. This means that no back flow occurs if the value for Γ is smaller than the maximum allowable value calculated by taking the first lateral as the critical one.

For situation (2) the dividing header inlet velocity is found to be 1.63 times the inlet velocity of the first lateral. The pressure change over the dividing header is a quadratic function of the dividing header velocity and thus a higher dividing header velocity influences the maximum allowable condensation ratio significantly. In order to reduce the dividing header velocity the cross-sectional header flow area can be increased. The relationship between Γ and σ calculated with the design method for a dividing header diameter increased from 1.25m to 1.8m are shown in figure 5.4.

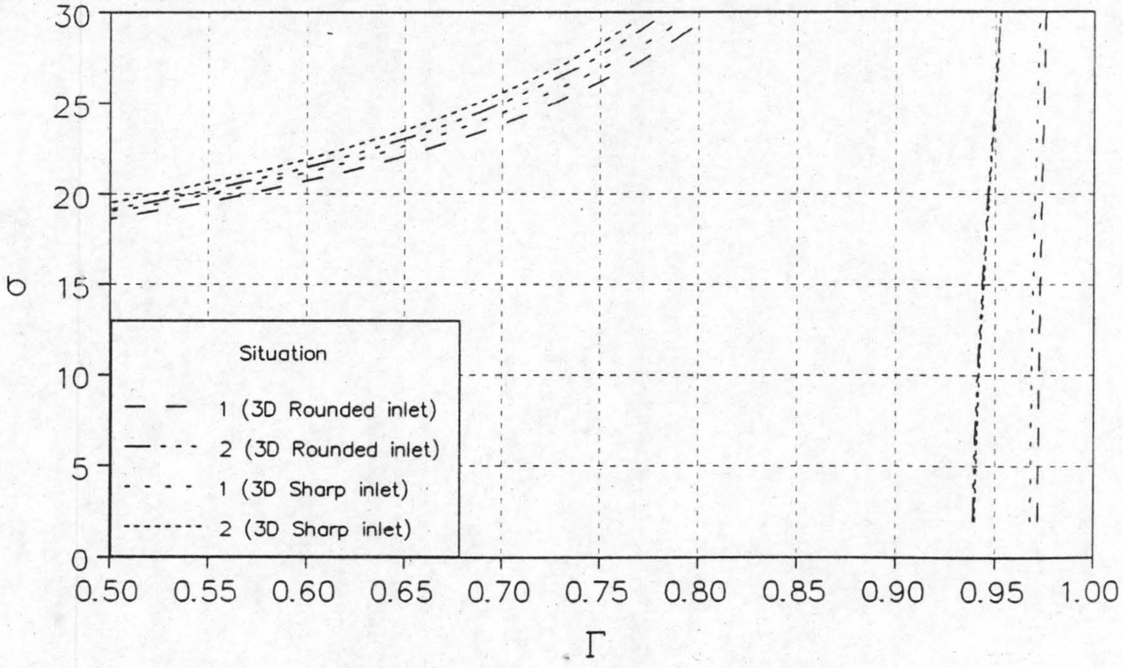

Figure 5.4: Γ to σ design regions for the two situations, d_{hd} = 1.8m.

The graph in figure 5.4 shows that for d_{hd} = 1.8m a higher value for Γ is allowed for situations (1) and (2) than for the case with d_{hd} = 1.25m. The difference between the solutions of Γ of situations (1) and (2) is also decreased.

If the condenser section is configured in Z-configuration, it is expected that the assumption of a uniform mass flow distribution through the laterals can deviate significantly from the actual distribution due to the increasing pressure difference over the laterals with increasing z. An air-cooled condenser section similar to that shown in figure 5.2 but configured in Z-configuration is now investigated. The condenser dimensions and the total mass flow rate entering the laterals are equal to that used in the sample calculation in section 5.6. The combining header is closed at z = 0 and there is no nett outflow at the dividing header end. Figure 5.5 shows the relationship between Γ and σ calculated with the design method for this configuration. The results obtained by the numerical solution are also presented in figure 5.6. Although the equations of the design method can be solved for small values of Γ, the numerical solution does not yield these low values for Γ. This shows that the assumption of a uniformly distributed mass flow through the laterals is not valid for small values of Γ for the Z-configuration. Figure F.4 in appendix F shows that by decreasing Γ, only the non-uniformity of the flow distribution through the laterals increases and no back flow occurs.

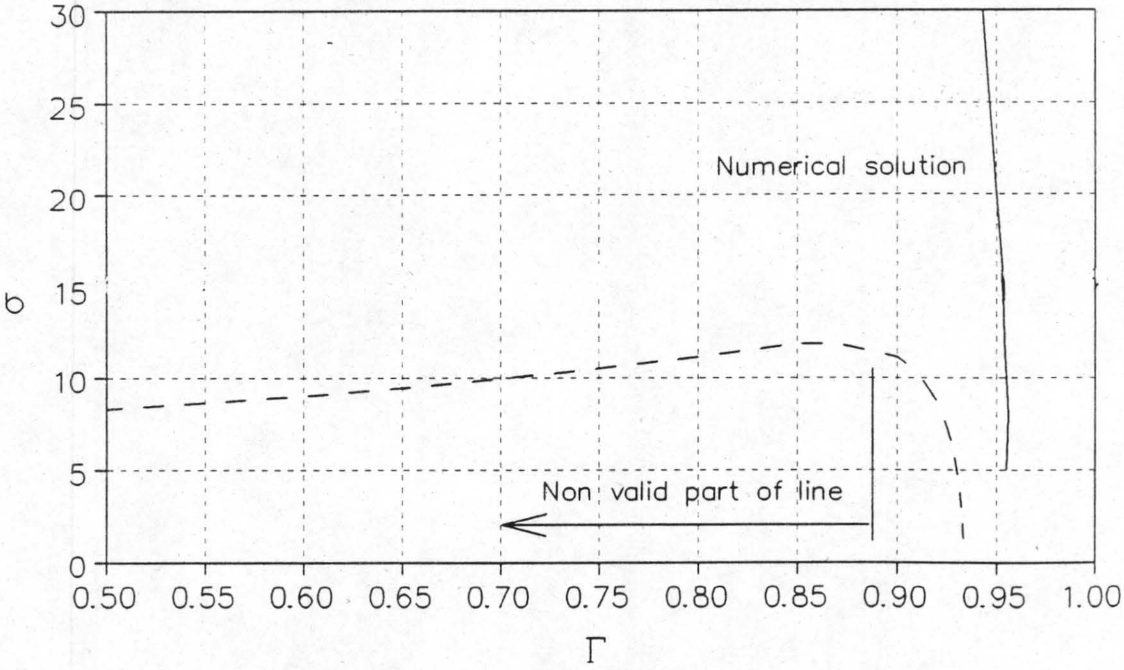

Figure 5.5: Γ to σ design regions for the Z-configuration, situation (1), d_{hd} = 1.25m.

It is shown that for both the U and the Z-configurations, the numerical solution always predicts a higher allowable Γ than the proposed design method. Thus the proposed design method is more conservative and can be applied with confidence.

CHAPTER 6

CONCLUSION AND DISCUSSION

The inlet loss coefficients of consecutive laterals, spaced at a relatively small pitch, through which flow from a header with a net passing flow is branched off perpendicularly, vary in respect to the position of the lateral and the header flow velocity. It has been found experimentally and confirmed by a numerical analysis that the upstream lateral has the highest inlet loss coefficients which increases with increasing header flow velocity. With most of the geometrical modifications which have been investigated experimentally, a decrease of the inlet loss coefficient of the upstream lateral has been achieved. These modifications included an backward facing step, a wall like strip and a triangular ramp placed upstream of the first lateral. An iron grid placed at the lateral inlets does not only give lower inlet loss coefficients, but also protects against potential erosion at the lateral inlets induced by high velocity droplets of condensate which occur in the dividing header of air-cooled condensers. The finned tubes in a practical air-cooled condenser are welded to the header. If the welding seams form an inlet rounding of 3mm radius, the inlet loss coefficients are decreased significantly compared to a sharp edge at the inlet.

In existing air-cooled steam condensers the formation of a dead zone in the upstream lateral may be explained by a higher inlet loss coefficient of that lateral, since the inlet loss coefficient forms part of the flow resistance impeding the steam flow entering the lateral. Many of the modifications presented in this work can be used in increasing the efficiency of existing condensers.

The design method for determining the flow characteristics of the steam side of air-cooled condensers which has been proposed in chapter 5, has been found to be more conservative than the numerical analysis. The latter solution allowed for higher condensation ratios for a specific header area ratio. Therefore, the proposed method can be applied to design an air-cooled steam condenser functioning efficiently with regard to the steam flow distribution through the finned tubes.

For the analyzed geometries the effect of the inlet loss coefficients only becomes significant if the maximum value for the condensation ratio is to be determined. If however the condensation loss coefficients (K_{con}) are lower, may it be due to a lower lateral condensation rate or a lower lateral inlet Reynolds number, the inlet loss coefficients becomes more significant. Therefore they cannot be neglected.

It must be emphasized that the condensation rates in the finned tubes were assumed to be identical in all analyses presented in this work. If this assumption is however not valid, as can be the case if the air flow distribution over the bundles was not uniform, a modification of the analyses, taking into account the different condensation rates in the finned tubes, has to be made to allow for these differences.

The U-configuration does not necessarily give a better flow distribution through the finned tubes than the Z-configuration, depending on the geometrical condenser configuration. This is found when the pressure change along the combining header is considerably higher than that along the dividing header.

The change in static pressure in the combining header can be considerably higher than that in the dividing header, especially if the combining header outlet velocity is high due to a low condensation ratio or a high header area ratio. Therefore this change, which is a function of the overall momentum correction factor of the dividing header (θ_c), can be the most significant parameter in the design of the steam flow distribution through the condenser and an accurate value of θ_c is required. For the case investigated numerically in appendix B, θ_c was found to be 2.24. This value has been used for all cases that have been investigated in this work. The value for the overall momentum correction coefficient of the dividing header can be taken as the numerically determined 0.99, because it compares well with the value of 1.05 which was used by Bajura and Jones [76BA1].

REFERENCES

00FR1 Freeman, J.R., *The Discharge of Water through Fire Hoses and Nozzles*, Trans. ASCE, no.21, pp.303-482, 1888.

00WE1 Weisbach, J., *Mechanics of Engineering*, Van Nostrand Book Company, New York, 1872.

08HU1 Hughes, H.J. and Safford, A.t., *Hydraulics*, Macmillan Book Company, New York, 1908.

11BL1 Blasius, H., *Das Ähnlichkeitsgesetz bei Reibungsvorgängen in Flüssigkeiten*, Forschg. Ing.-Wesen, vol.131, Berlin, 1911.

32NI1 Nikuradse, J., *Gesetzmäßigkeit der Turbulenten Strömung in Glatten Rohren*, Forschg. Arb. Ing.-Wes., no.356,1932.

39CO1 Colebrook, C.F., *Turbulent Flow in Pipes with Particular Reference to the Transition Region between the Smooth and Rough Pipe Laws,* J. Institution of Civil Engineers, vol.11, pp.133-156, 1939.

50KA1 Kays, W.M., *Loss Coefficients for abrupt Changes in Flow Cross Section with Low Reynolds Number Flow in Single and Multiple-Tube Systems*, Trans., ASME, vol.72, pp.1067 - 1074, 1950.

59NO1 Nosova, M.M. et al., *Resistance of Inlet and Exit Orifices in the Presence of a Passing Stream*, Promyshlennaya Aerodinamika, no.15, pp.20 - 37, 1959.

66BE1 Benedict, R.P., Carlucci, N.A. and Swetz, S.D., *Flow Losses in Abrupt Enlargements and Contractions*, Trans. ASME, vol.1, pp.73-81, 1966.

71BA1 Bajura, R.A., *A Model for Flow Distribution Manifolds*, Trans. ASME, J. Engineering for Power, Paper no.70-Pwr-3, pp.7-14,1971.

71MI1 Miller, D.S., *Internal Flow, A Guide to Losses in Pipe and Duct Systems*, The British Hydromechanics Research Association, Cranfield, 1971.

73BA1 Bajura, R.A., LeRose, V.F., and Williams,L.E., *Fluid Distribution in Combining, Dividing and Reverse Flow Manifolds*, ASME Paper 73-PWR-1, 1973.

77EN1 Engineering Science Data Unit, *Pressure Losses in Flow through a Sudden Contraction of Duct Area*, Item no.78007, London, 1977.

76BA1 Bajura, R.A., and Jones, E.H., *Flow Distribution Manifolds*, Trans. ASME, J. Fluid Engineering, vol.98, pp.656 - 666, 1976.

76SP1 Spalding, D.B., *Basic Equations of Fluid Mechanics and Heat and Mass Transfer, and Procedures for their Solution*, Imperial College, Mechanical Engineering Department, Report no.HTS/76/6, 1976.

78MI1 Miller, D.S., *Internal Flow Systems*, The British Hydromechanics Research Association, Cranfield, 1978.

79MO1 Mohandes, M.A., *The Flow Through Heat Exchanger Banks*, Ph.D. thesis, Oxford University, 1979.

80DA1 Datta, A.B. and Majumdar, A.K., *Flow Distribution in Parallel and Reverse Flow Manifolds*, Int. J. Heat and Fluid Flow, vol.2, no.4, pp.253 - 262, 1980.

80MA1 Majumdar, A.K., *Mathematical Modelling of Flow in Dividing and Combining Flow Manifolds*, Applied Mathematical Modelling, vol.4, pp.424 - 431, 1980.

80PA1 Patankar, S.V., *Numerical Heat Transfer and Fluid Flow*, McGraw-Hill Book Company, New York,1980.

80SP1 Spalding, D.B., *Mathematical Modelling of Fluid-Mechanics, Heat Tansfer and Chemical Reaction Process: A Lecture Course*, HTS/80/1, Imperial College, London, 1980.

81BS1 British Standards Institution, BS1042, *Methods of Measurement of Fluid Flow in Closed Conduits*, Part 1, London, 1981.

83HA1 Haaland, S.E., *Simple and Explicit Formulas for the Friction Factor in Turbulent Flow*, Trans. ASME, J. of Fluids Engineering, vol.105, no.3, pp. 89-90, 1983.

84BA1 Bassiouny, M.K. and Martin, H., *Flow Distribution and Pressure Drop in Plate Heat Exchangers*, Chemical Engineering Science, vol.39, no.4, 1984.

84BA2 Bassiouny, M.K. and Martin, H., *Flow Distribution and Pressure Drop in Plate Heat Exchangers*, Chemical Engineering Science, vol.39, no.4, 1984.

87RO1 Rosten, H.I., and Spalding, D.B., *The PHOENICS Equations*, TR/99, CHAM, Wimbledon, 1987.

87RO2 Rosten, H.I., and Spalding, D.B., *The PHOENICS Beginners Guide*, TR/100, CHAM, Wimbledon, 1987.

87RO3 Rosten, H.I., and Spalding, D.B., *The PHOENICS Reference Manual*, TR/200, CHAM, Wimbledon, 1987.

89ID1 Idelchic, I.E., *Flow Resistance: a Design Guide for Engineers*, Hemisphere Publishing Corporation, New York, 1989.

89DA1 Daugherty, R.L., Franzini, J.B. and Finnemore, E.J., *Fluid Mechanics with Engineering Applications*, McGraw-Hill Book Company, 1980.

89KR1 Kröger, D.G., *Cooling Towers Performance Evaluation and Design*, Department of Mechanical Engineering, Stellenbosch University, Stellenbosch, 1989.

91VA1 Van Heerden, E., *Steam Flow Distribution in Air-Cooled Condensers*, M.Eng. Thesis, Department of Mechanical Engineering, Stellenbosch University, Stellenbosch, 1992.

91WH1 White, F.M., *Viscous Fluid Flow*, McGraw-Hill, New York, 1991.

93GR1 Groenewald, W., *Heat Transfer and Pressure Change in an Inclined Air-Cooled Flattened Tube During Condensation of Steam*, M.Eng. Thesis, Stellenbosch University, Stellenbosch, 1993.

95AU1 Augustin, C.H., *Eintrittverluste bei scharfkantigen Querschnittsänderungen in rechteckigen Kanälen bei gerader und geneigter Einströmung*, Diplomarbeit, Technische Universität Hamburg-Harburg, 1995.

95FA1 Fahlsing, P.M., *Benefits of Variable Speed Drives Applied on Dry Condensing at the Wyodak Power Station*, PWR-vol.28, 1995 Joint Power Generation Conference, vol.3, ASME, 1995.

95SC1 Schrey, H.G., *Design Particularities of Forced Draft Air-Cooled Condensers*, Dry Cooling Systems Symposium, Chinese Society for Electrical Engineering, Wutai Mountain, China, August 17-19, 1995.

APPENDIX A

THERMO-PHYSICAL PROPERIES OF AIR AND SATURATED STEAM

Equations for the properties of air and steam are given by Kröger [89KR1]:

Air viscosity:

$$\mu = 2.287973\times10^{-6} + 6.259793\times10^{-8}\times T_a - 3.131956\times10^{-11}\times T_a^2 + 8.15038\times10^{-15}\times T_a^3 \qquad (A.1)$$

Saturated steam density:

$$\rho = -4.062329056 + 0.10277044\ T - 9.76300388\times10^{-4}T^2 + 4.475240795\times10^{-6}T^3 - 1.0045964894\times10^{-8}T^4 + 8.9154895\times10^{-12}T^5 \qquad (A.2)$$

Saturated steam viscosity:

$$\mu = 2.562435\times 10^{-6}+1.816683\times10^{-8}T+2.579066\times10^{-11}T^2 - 1.067299\times 10^{-14}T^3 \qquad (A.3)$$

APPENDIX B

NUMERICAL SOLUTION OF DIFFERENT FLOW SITUATIONS WITH THE AID OF THE *PHOENICS* COMPUTER CODE

B.1 INTRODUCTION

Inlet geometries and flow around a bend for two dimensional flow situations was investigated with the aid of the *PHOENICS* computer code. Furthermore the velocity profiles and pressure distributions in a dividing and a combining header found in a typical air-cooled condenser were studied. Incompressible, adiabatic single phase flow was assumed in all simulations.

B.2 THE *PHOENICS* COMPUTER CODE

PHOENICS is a computer code with which fluid flow, heat transfer, chemical reaction and related phenomena can be analyzed numerically. A full description of the *PHOENICS* computer code is given by Rosten and Spalding [87RO1], [87RO2] and [87RO3]. Simulations can be conducted on various scales. For example an industrial heat exchanger as a whole may be simulated or only one small tube thereof can be investigated. *PHOENICS* simulations are based on mathematical deductions from established physical principles. In this work we will only use fluid flow simulations. Solutions are provided to the discretized versions of sets of differential equations having the general form:

$$\underbrace{\frac{\partial}{\partial t}(\rho\,\phi)}_{\text{transient}} + \operatorname{div}\big(\underbrace{\rho\,v\,\phi}_{\text{convection}} - \underbrace{\Gamma_\phi \nabla \phi}_{\text{diffusion}}\big) = \underbrace{S}_{\text{source}} \qquad \text{(B.1)}$$

where t is the time, ρ the density, ϕ the conserved property of the fluid such as mass, enthalpy, momentum per unit mass, turbulence energy etc and **v** the velocity vector. Furthermore Γ_ϕ denotes the exchange coefficient of ϕ while S is the source rate. A staggered grid formulation is employed by the computer code together with the *SIMPLEST* pressure correction algorithm as described by Spalding [80SP1]. The flow situation to be analyzed is broken up into a grid that is composed of cells. The velocities are calculated at the cell boundaries and the pressures in the centres of the cells. The sizes of the cells may differ from each other, as long as the grid lines that make up the cells are continuous. The computer code makes provision for several turbulence models. The K-ε model for turbulence is used in this work. The code also provides for the logarithmic wall function for turbulent boundary layers, which was specified for every wall found in the flow situations to be analyzed.

B.3 TWO DIMENSIONAL FLOW AROUND A 60° AND A 30° SHARP BEND

When a two dimensional stream flows around a sharp bend in a duct as shown schematically in figure B.1, a separation of the stream lines occurs at the bend due to the inertia forces acting on the fluid.

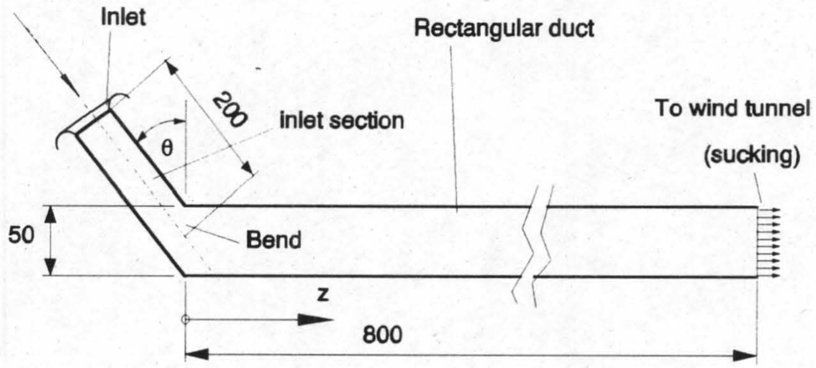

Figure B.1: Experimental configuration to investigate flow around a bend.

This flow separation forms a vena contracta just after the bend. Augustin [95AU1] investigated this vena contracta experimentally. In his experiments a 50mm wide and 500mm high rectangular duct was fitted with two inlet sections directing the flow at θ=30° and at θ=60° respectively into the duct as shown in figure B.1. These two flow situations created by the two angles will be investigated with the aid of the *PHOENICS* code. Augustin used a duct with a relatively large aspect ratio to give an approximately two dimensional flow situation.

B.3.1 BOUNDARY CONDITIONS, GRID AND FLUID PROPERTIES USED IN COMPUTER SIMULATION

Figure B.2 shows the boundary conditions specified for the code for the flow situations created by the two bend angles.

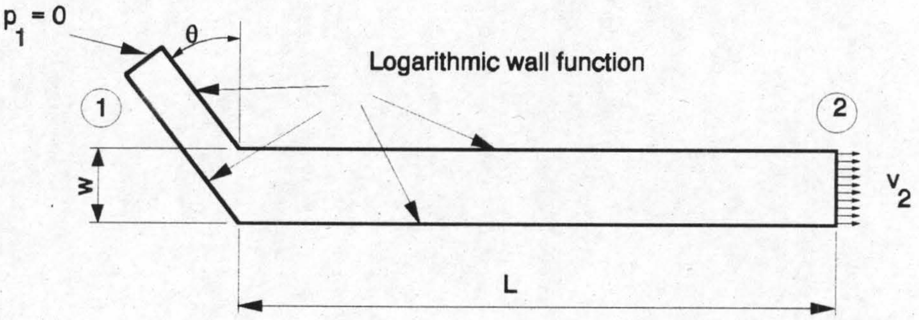

Figure B.2: Boundary conditions of flow around a bend.

A uniform velocity profile is specified as boundary condition over the duct outlet and a constant pressure boundary over the duct inlet. The logarithmic wall function is defined at the duct walls. The centre-line length of the section upstream of the bend is 200mm and the length of the downstream section is 800mm. These are the same lengths that were used in Augustin's apparatus to allow for flow development. The grid configurations for both angles are shown in figure B.3.

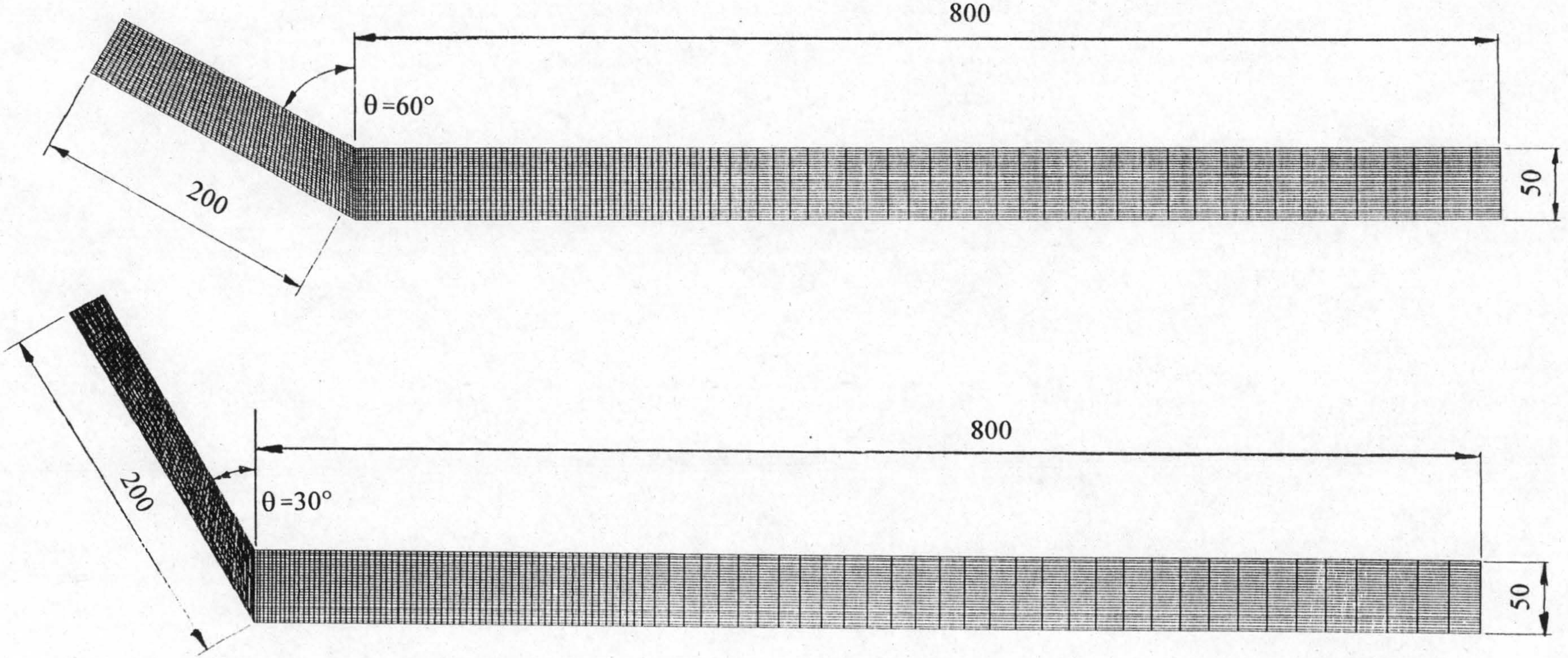

Figure B.3: Grid layout for 60° and 30° bend flow situation.

Augustin investigated the influences of four different Reynolds numbers in the turbulent range based on the equivalent diameter of the downstream duct, namely in the order of around 10000, 50000, 100000 and 150000. He found that the velocity profiles just after the bend are not significantly dependent on the Reynolds number. We will therefore only specify one Reynolds number for the numerical investigation. The duct outlet velocity will be specified such that the Reynolds number of the flow downstream of the bend has a value of 50000. From the definition of the Reynolds number this outlet velocity is given by

$$v_o = \frac{\mu \, Re}{\rho \, d_e} \tag{B.2}$$

Air at 300K and at a pressure of 101325N/m^2 is used as fluid. The viscosity is calculated according to equation (A.1):

$$\begin{aligned}\mu &= 2.287973\times10^{-6} + 6.259793\times10^{-8}\times T_a - 3.131956\times10^{-11}\times T_a^{\,2} \\ &\quad + 8.15038\times10^{-15}\times T_a^{\,3} \\ &= 2.287973\times10^{-6} + 6.259793\times10^{-8}\times(300) - 3.131956\times10^{-11}\times(300)^2 \\ &\quad + 8.15038\times10^{-15}\times(300)^3 \\ &= 1.8468\times10^{-5}\text{Ns/m}^2\end{aligned}$$

Furthermore from the ideal gas law the density is:

$$\rho = \frac{p}{R\,T} = \frac{101325}{287.1 \times 300} = 1.1764\,\text{N/m}^2$$

The width, w, of the duct downstream of the bend is 0.05m. The approximate equivalent diameter is calculated according to equation (2.3):

$$d_e = 2w = 2\times0.05 = 0.1\text{m}$$

The mean outlet velocity is calculated according to equation (B.2):

$$v_o = \frac{\mu \, Re}{\rho \, d_e} = \frac{1.8468 \times 10^{-5} \times 50000}{1.1764 \times 0.1} = 7.8496\text{m/s}$$

B.3.2 NUMERICAL RESULTS

In figures B.4 and B.5 the velocity vectors of the converged computer solution at the bend are shown for the two angles respectively. It can be seen that for the 60° angle no visible flow separation occurs, while for the 30° angle a recirculation vortex as a result of flow separation is formed. The flow separation does however only occur a short distance downstream of the edge of the bend, and not directly at the edge as would be expected. A small step, which is indicated in figure B.6 is introduced by adding a row of cells to the upstream inlet section and thereby widening it. This is justifiable because in the experiments of Augustin a poor alignment between the inlet section and the downstream duct could have occurred to form a small step.

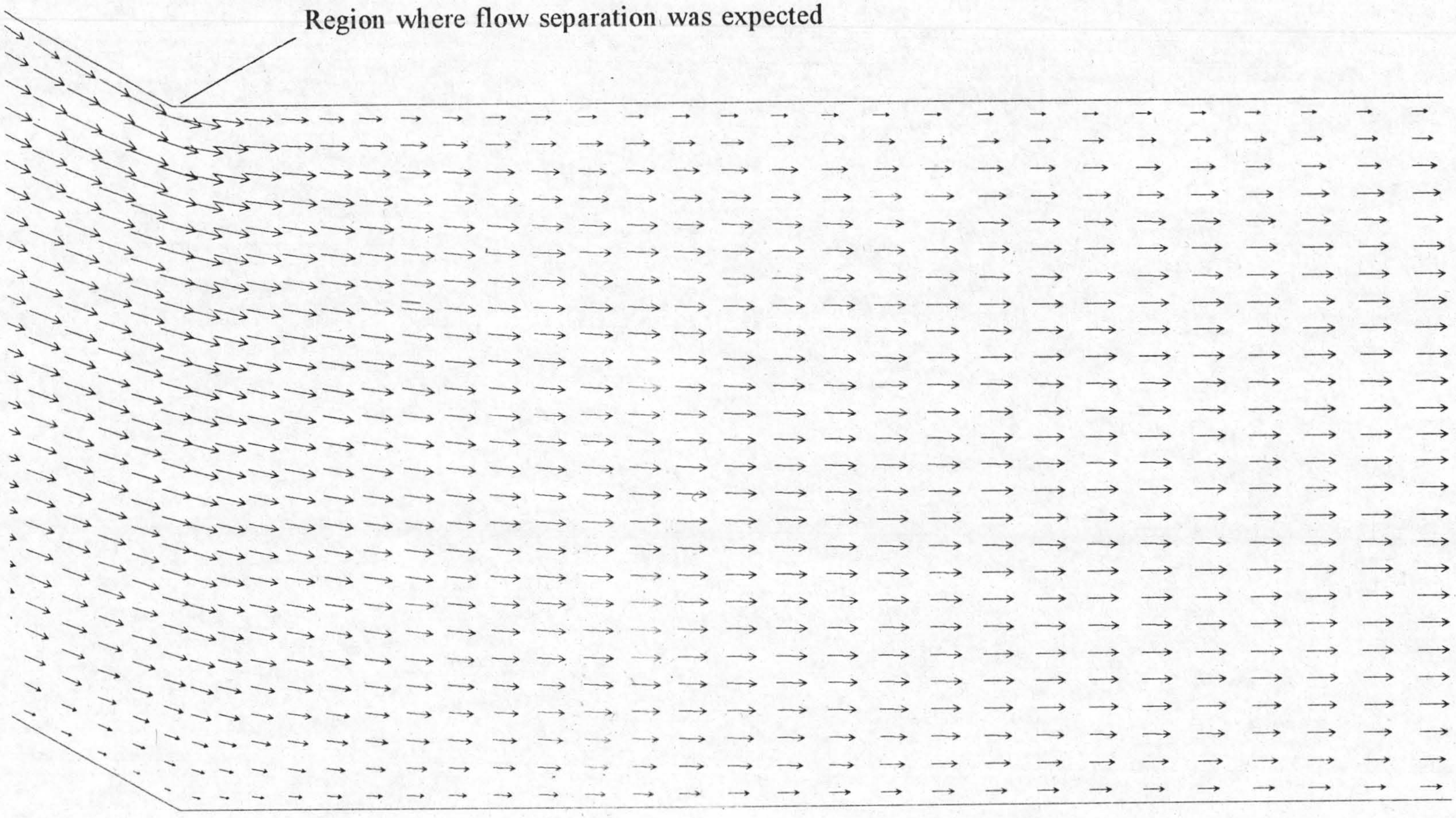

Figure B.4: Velocity vector plot at 60° bend.

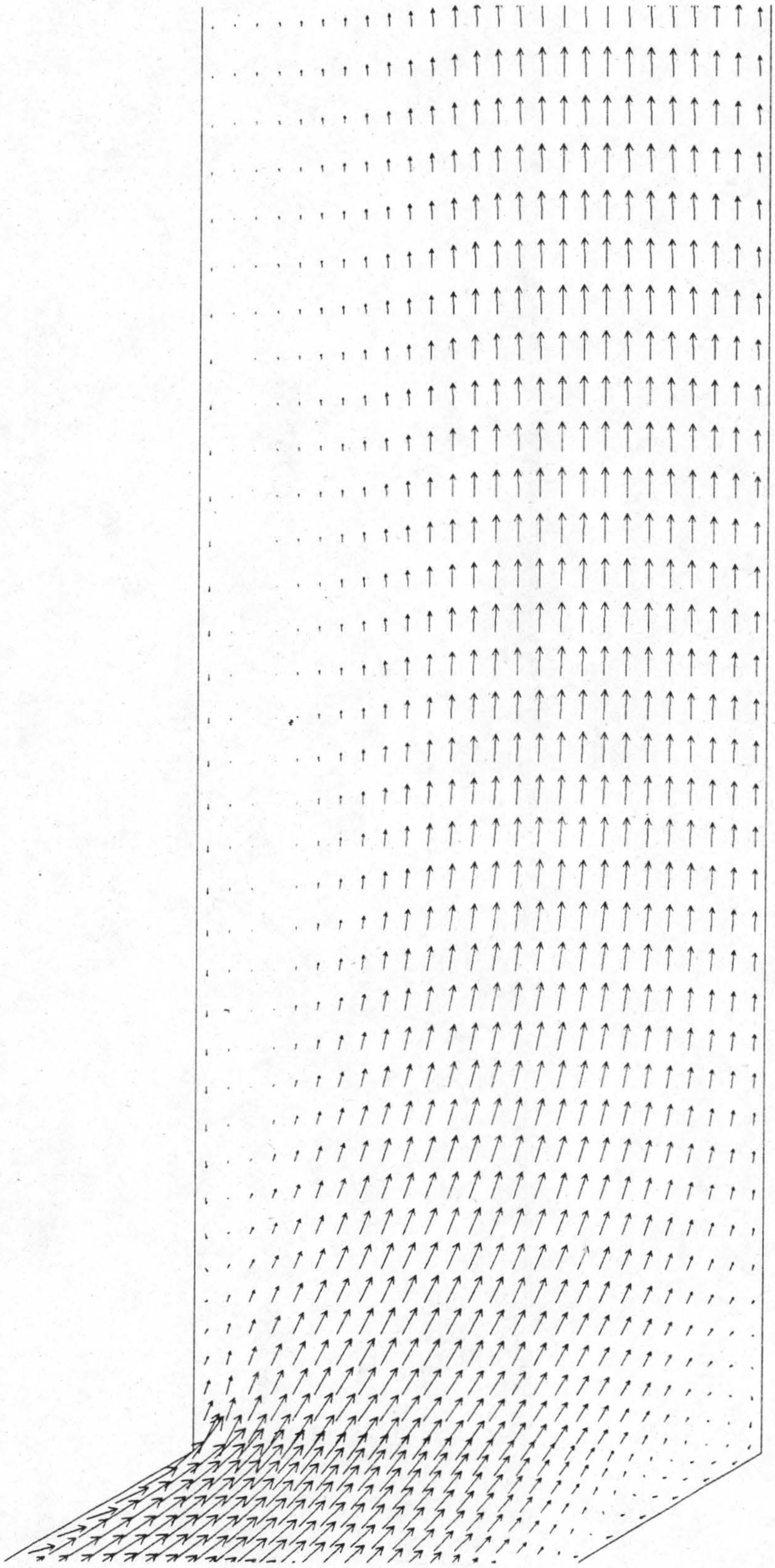

Figure B.5: Velocity vector plot at 30° bend.

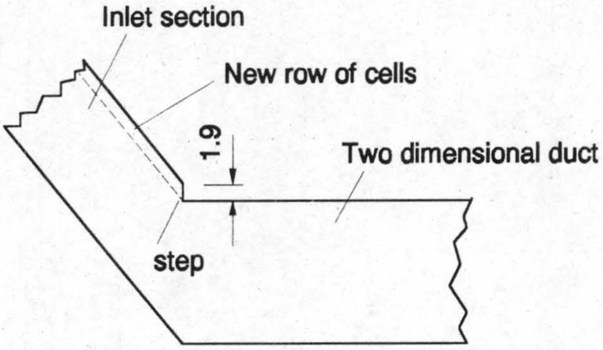

Figure B.6: Configuration of a step at the bend.

The step has a height of 1.9mm. The resulting vector plots for both bend angles can be seen in figures B.7 and B.8. The step gives a little noticeable flow separation for the 60° bend while for the 30° bend the vortex formed due to the separation is greater than that of the case without the step.

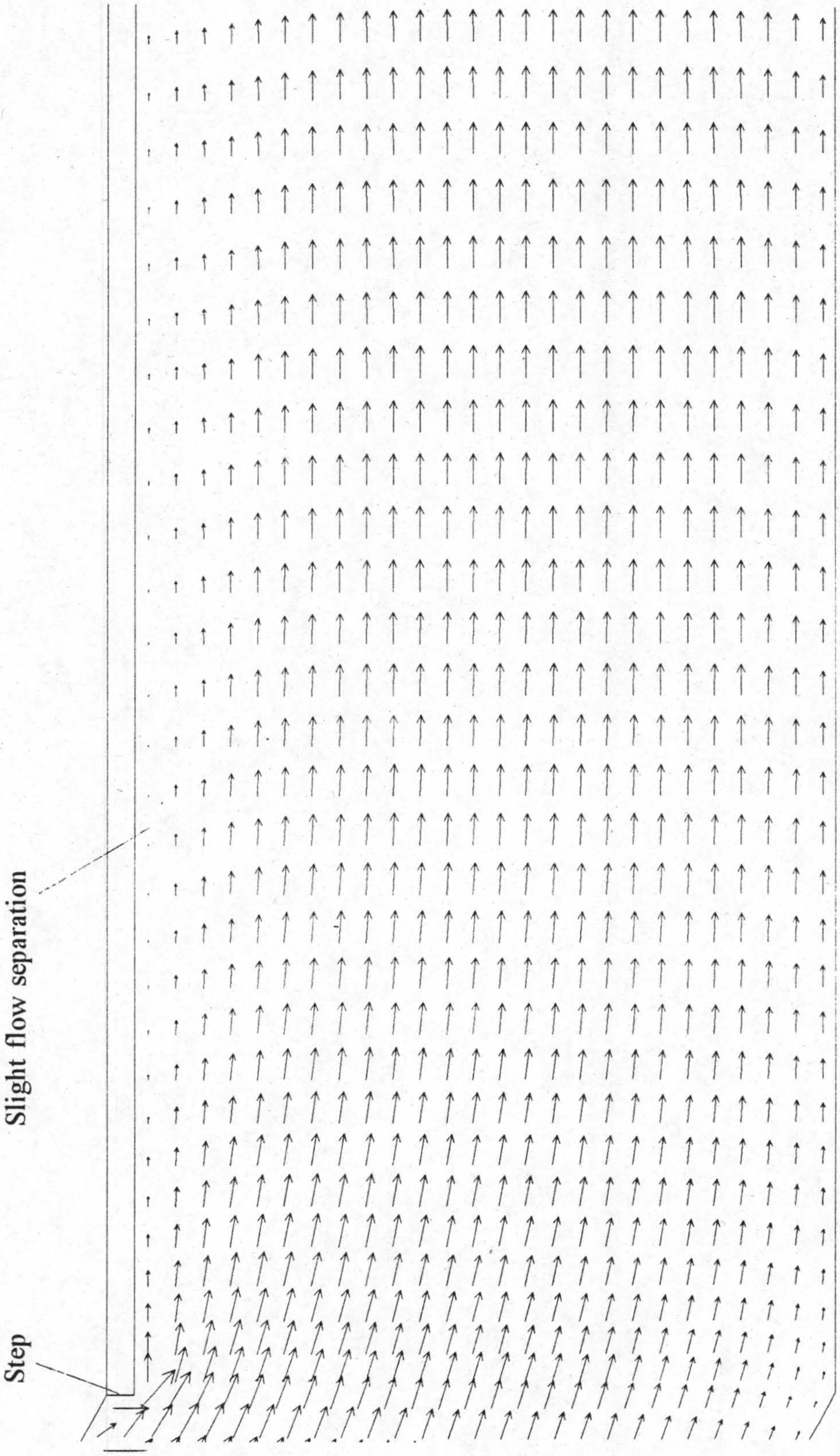

Figure B.7: Velocity vector plot at 60° bend with step.

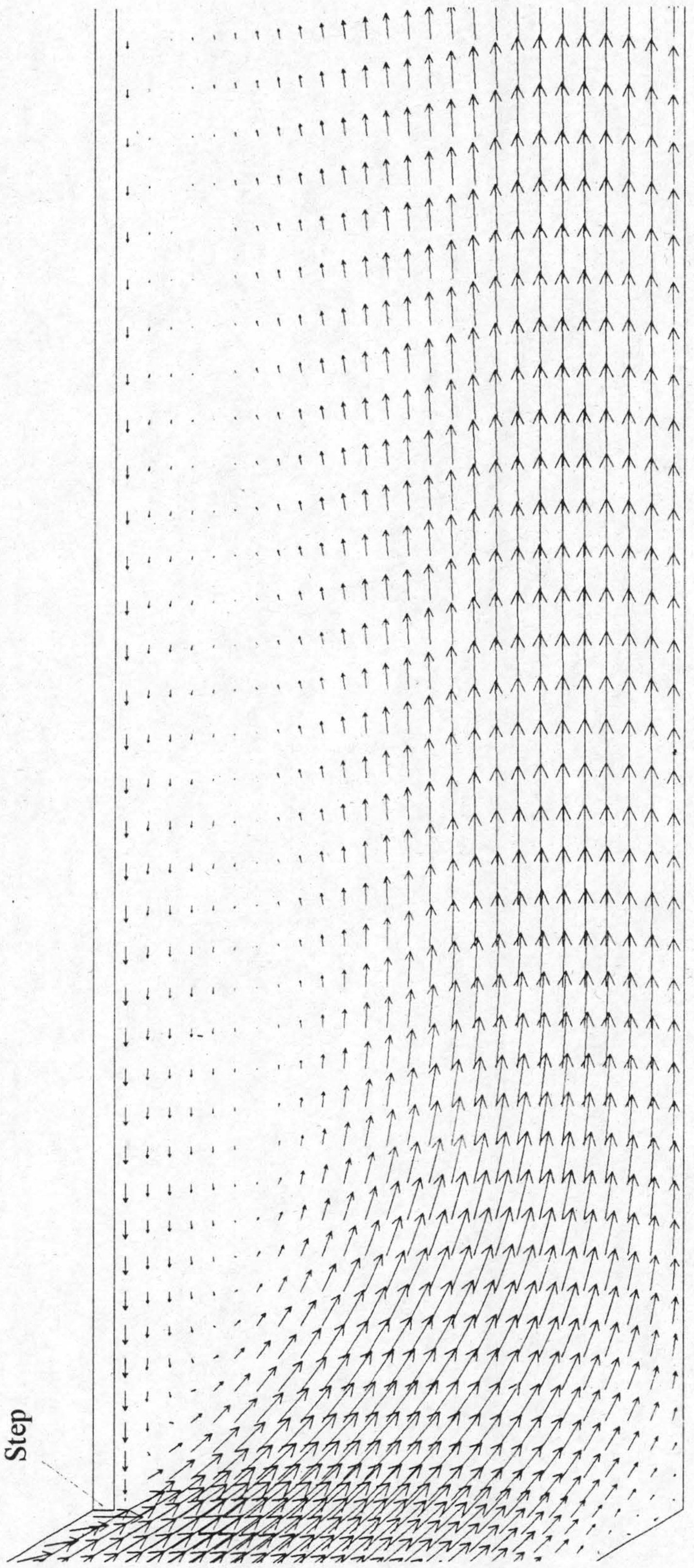

Figure B.8: Velocity vector plot at 30° bend with step.

In figures B.9 and B.10 the velocity profiles at the vena contracta calculated by the code are compared to the experimental data of Augustin.

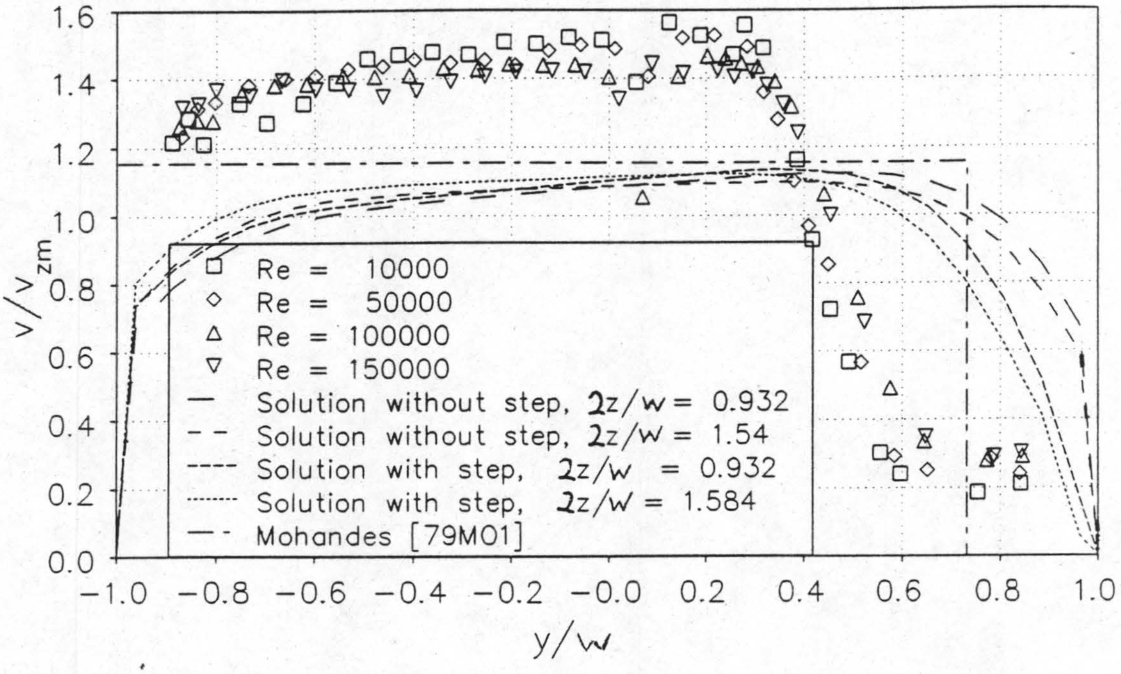

Figure B.9: Velocity profile at vena contracta of 60° bend angle.

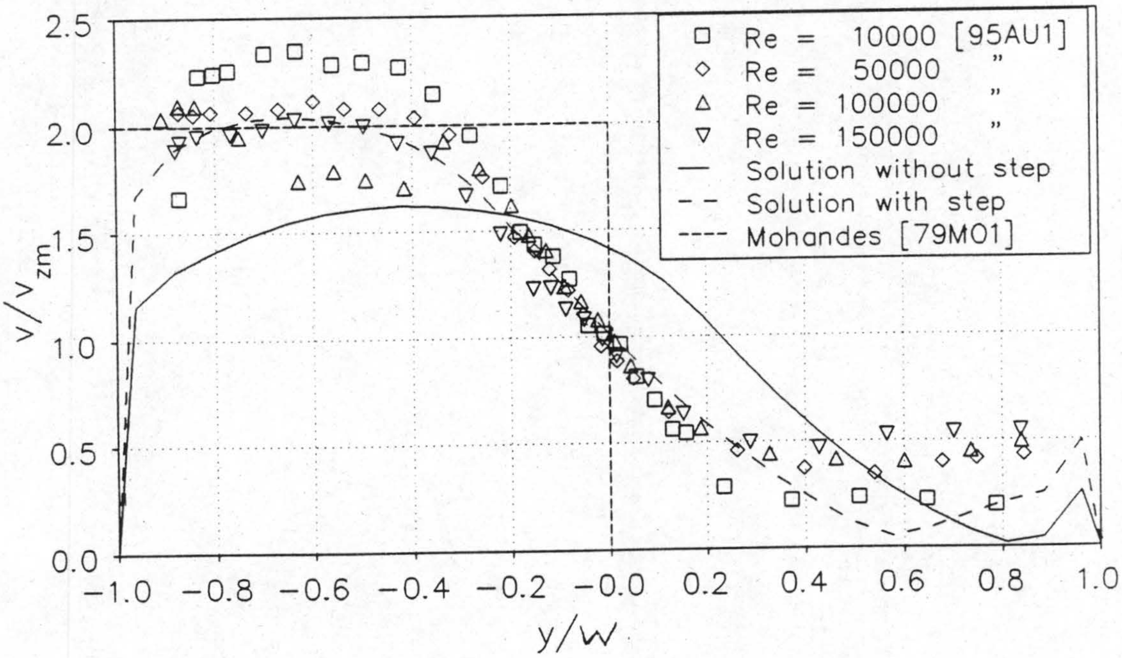

Figure B.10: Velocity profile at vena contracta of 30° bend angle.

The numerically determined profiles are situated at the same location in the duct as those of the experimental investigation. For the 30° bend the velocity profile calculated with the step geometry agrees well with the experimental data, whereas the case without the step gives a wider vena contracta. For the 60° bend however the step has only a small effect on the velocity profile, although the small recirculation zone is formed. The forms of the numerically determined velocity profiles at the vena contracta are similar to those determined by the experiments for both bend angles.

A possible explanation of the absence of flow separation at the 60° bend without the step can be, that with the staggered grid method employed in the *PHOENICS* code, where pressures and velocities are not calculated at the same points, abrupt changes such as sharp bends could yield inaccurate solutions. Furthermore the boundary layer theory employed in the code can also not respond to the calculated pressure gradient at the bend. The K-ε is also not particularly accurate in recirculation zones.

Augustin also determined the loss coefficient quantifying the loss of mechanical energy that the flow around the bend experiences. This loss coefficient is calculated as follows:

$$K = \frac{p_1 + \frac{1}{2}\rho v_1^2 - p_2 - \frac{1}{2}\rho v_2^2}{\frac{1}{2}\rho v_2^2} - f_{D2}\frac{L_2}{d_{e2}} + f_{D1}\frac{L_1}{d_{e1}}\frac{v_1^2}{v_2^2} \tag{B.3}$$

The loss coefficients determined from the pressure data of the numerical solution are compared to those determined from the experimental data of Augustin and are tabulated in table B.1. The values are not in good agreement which is attributed to the shortcomings of the numerical solution.

Table B.1: Comparison of numerically and experimentally determined loss coefficients.

θ [°]	K (Augustin)	K (without step)	K (with step)
60	0.36181	0.56191	0.59122
30	3.00717	1.79882	2.94165

B.4 NUMERICAL INVESTIGATION OF A TWO DIMENSIONAL DIVIDING HEADER WITH 10 LATERALS

A two dimensional header with 10 laterals at constant pitch branching off at right angle to the longitudinal header direction was investigated with the aid of the *PHOENICS* code. This same configuration was investigated experimentally, as explained in chapter 4, where it is called the *standard configuration*.

B.4.1 BOUNDARY CONDITIONS, GRID AND FLUID PROPERTIES USED IN COMPUTER SIMULATION

The dimensions and the boundary conditions entered into the computer code to describe the flow situation are shown in figure B.11.

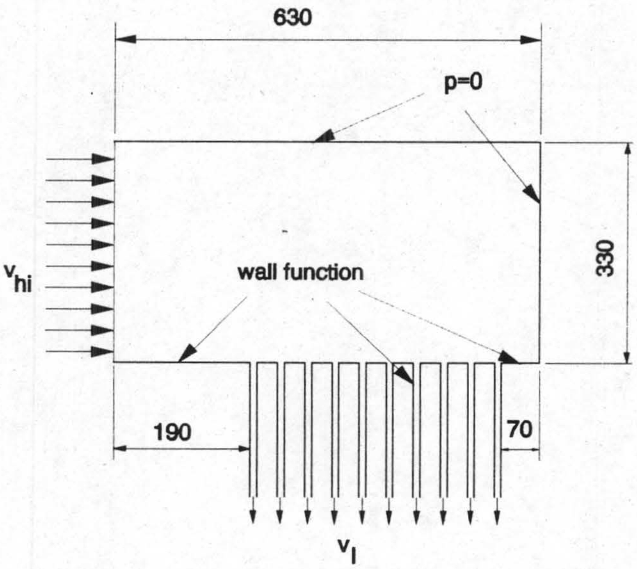

Figure B.11: Dimensions and boundary conditions of the numerical dividing header analysis.

The laterals have been given a length, L, of 200mm which coincides with the first lateral pressure tapping pair of the experimental apparatus described in chapter 4. The laterals have a width (w) of 10mm and they are situated at a pitch of 40mm along the header wall. The cross-sectional header width is 330mm, resembling the experimental apparatus. The magnitude of the mean velocity specified over every lateral outlet is v_l=11m/s. The header inlet velocity, v_{hi}, is given four values, namely 5.5m/s, 11m/s, 17.5m/s and 22m/s. In the experimental configuration the header plane opposite the laterals and its outlet are open to the atmosphere and the header pressure is assumed to be that of the surrounding atmosphere. Therefore a zero pressure boundary is specified at the same planes in the numerical investigation. The grid configuration is shown in figure B.12. Because of the relatively large overall dimensions in comparison to the lateral width, the laterals are described by only five cell columns perpendicular to the header flow direction and the space between the laterals by 15.

Again air at 101235N/m^2 and 300K is specified as fluid for which $\mu = 1.8468 \times 10^{-5}$Ns/m^2 and $\rho = 1.1764$kg/m^3 as calculated in the previous section.

The code yields pressures in the centres of the cells, therefore the pressures at the outlet planes of every lateral are calculated by extrapolation, using the pressure data of the two last cells of the cell column in the centre of the respective lateral.

As in the experimental investigation, the reduced inlet loss coefficient according to section 2.7 is calculated from the numerical data by the following equation:

$$K_i - \alpha_{eh} \frac{v_h^2}{v_l^2} = \frac{p_h - p_l}{\frac{1}{2} \rho v_l^2} - f_D \frac{L}{d_e} - 1 \qquad \text{(B.3)}$$

The header pressure (p_h) is taken as the pressure specified as zero at the header boundary opposite the lateral inlet. Thereby the same pressure difference as in the experiment will be used.

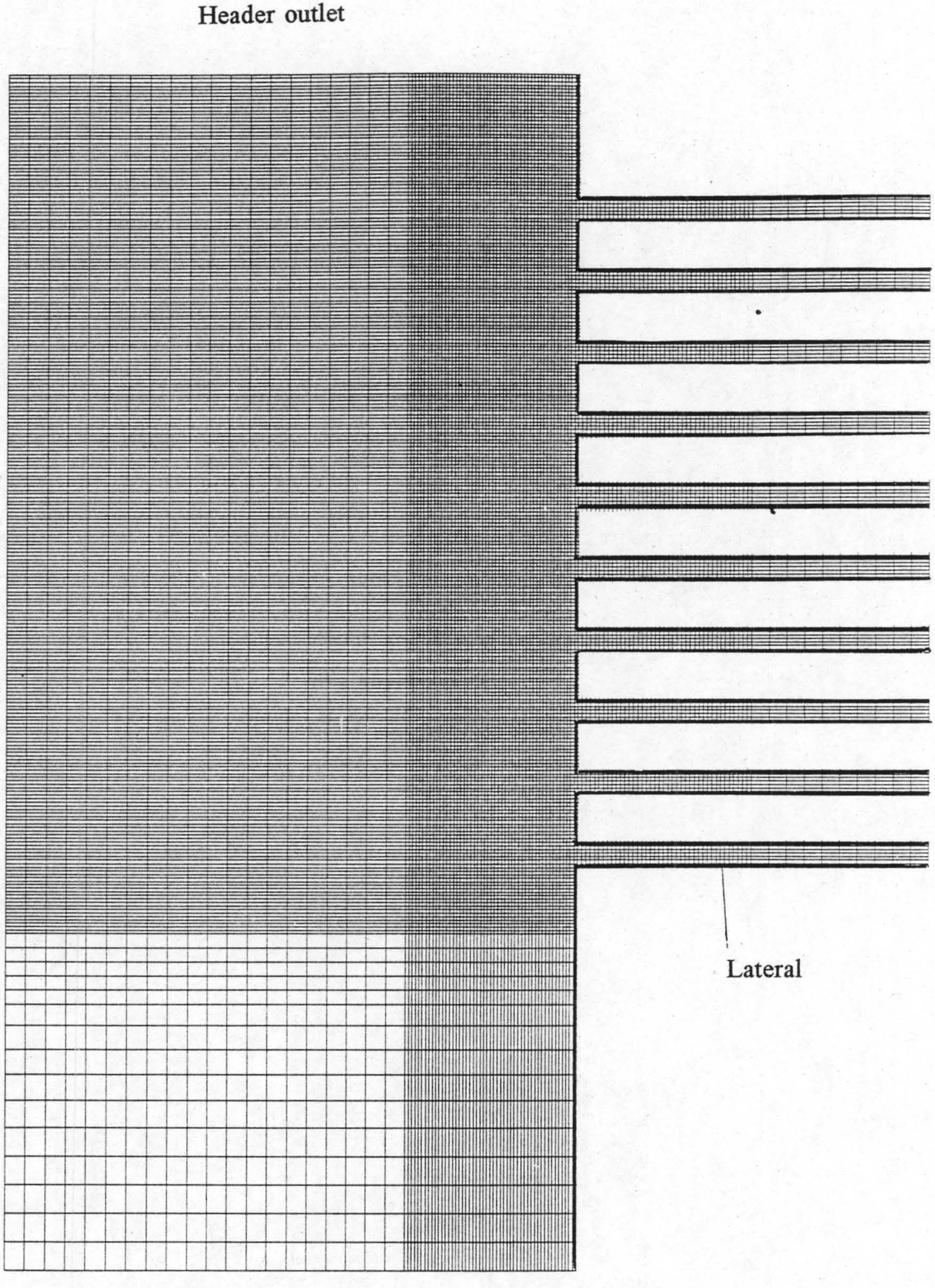

Figure B.12: Grid configuration of two dimensional dividing header simulation.

In order to obtain the K_0 value (the inlet loss coefficient of a single lateral with a zero area contraction ratio), only a single lateral is simulated while the remaining nine laterals are "closed" by specifying a wall at their inlets. The K_0 value is taken as the reference inlet loss coefficient, so that the presentation of the inlet loss coefficients can be compared with that of the experimental investigation.

B.4.2 NUMERICAL RESULTS

The numerically determined pressures at the lateral ends are tabulated in table B.2.

Table B.2: Extrapolated static pressures (in N/m^2) 200mm downstream of inlets.

v_{hi} [m/s]	0	5.5	11.0	17.5	22.0
lateral 1	-124.2	-140.8	-164.0	-187.9	-213.5
2	-124.2	-132.0	-148.9	-164.8	-181.7
3	-124.2	-127.3	-141.2	-153.8	-167.1
4	-124.2	-124.1	-135.2	-145.7	-156.5
5	-124.2	-121.4	-130.5	-138.8	-147.5
6	-124.2	-119.0	-126.0	-132.4	-139.1
7	-124.2	-116.6	-121.4	-126.0	-130.7
8	-124.2	-114.1	-116.6	-119.0	-121.3
9	-124.2	-111.5	-110.9	-110.3	-109.5
10	-124.2	-108.5	-101.8	-96.1	-89.9

The numerical pressure data agrees well with the experimental data tabulated in the seventh column of table D.6. The two may be compared because the lateral velocities of the computer simulation and the experiment are very close. The experimental pressure readings taken at the 200mm pressure tapping pair will be used in the comparison and not those taken at the point 350mm from the inlet. The K_{ivr} values are calculated as follows from the numerical pressure data:

$$
\begin{aligned}
K_{ivr} &= K_i - \alpha_{eh}\frac{v_h^2}{v_l^2} - K_0 \\
&= \frac{p_h - p_l}{\frac{1}{2}\rho v_l^2} - f_D\frac{L}{d_e} - 1 - \left(\frac{p_{h0} - p_{l0}}{\frac{1}{2}\rho v_l^2} - f_D\frac{L}{d_e} - 1\right) \\
&= \frac{p_h - p_l - (p_{h0} - p_{l0})}{\frac{1}{2}\rho v_l^2}
\end{aligned}
\qquad (B.4)
$$

The friction factors in equation (B.4) are identical because of identical specified lateral Reynolds numbers. From the computer program output the normal inlet loss coefficient is $K_0 = 0.446$ which is very close to the average experimentally determined value of 0.4483. Figure B.13 shows the K_{ivr} values of every lateral as a function of the header inlet to lateral velocity ratio.

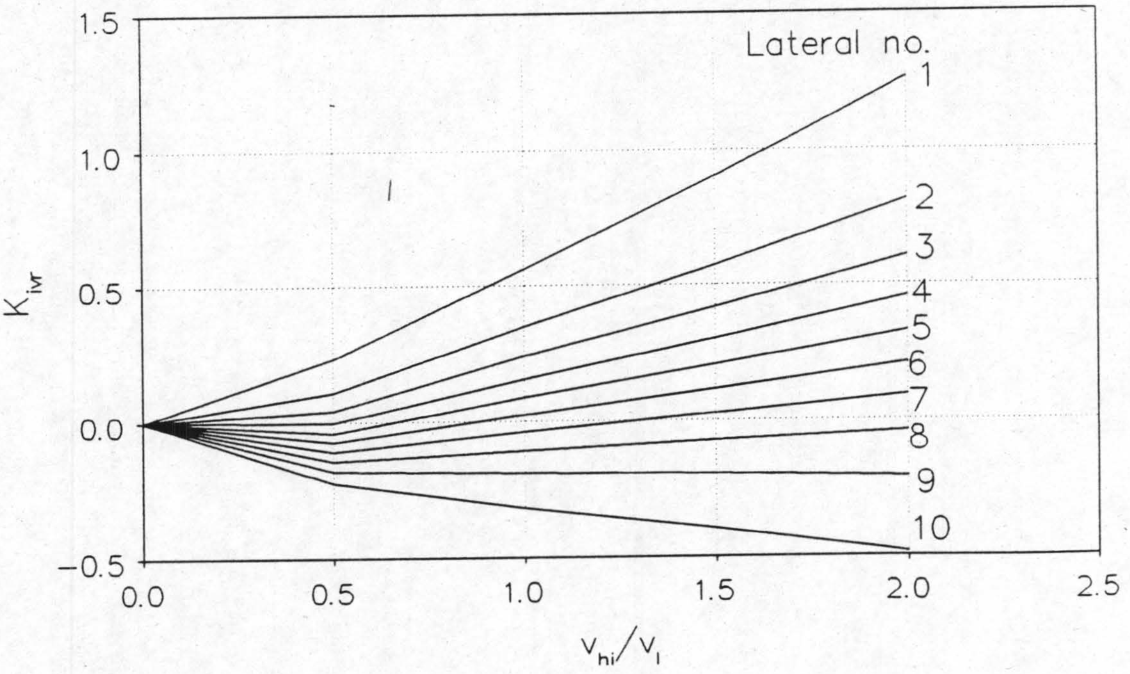

Figure B.13: K_{ivr} values calculated from computer solution.

B.5 NUMERICAL INVESTIGATION OF THREE DIMENSIONAL HEADER SIMULATION TO DETERMINE MOMENTUM CORRECTION FACTORS

Data for the overall momentum correction factor (θ) which is given in equation (3.5), of the dividing and the combining header of typical air-cooled condensers could not be found in literature. The *PHOENICS* code was employed to calculate the flow in a dividing and a combing header of a typical air-cooled condenser. With the velocity vectors and the longitudinal static pressure distribution, values of the momentum correction factors can be determined. Figure B.14 shows the dividing or combining header that was simulated.

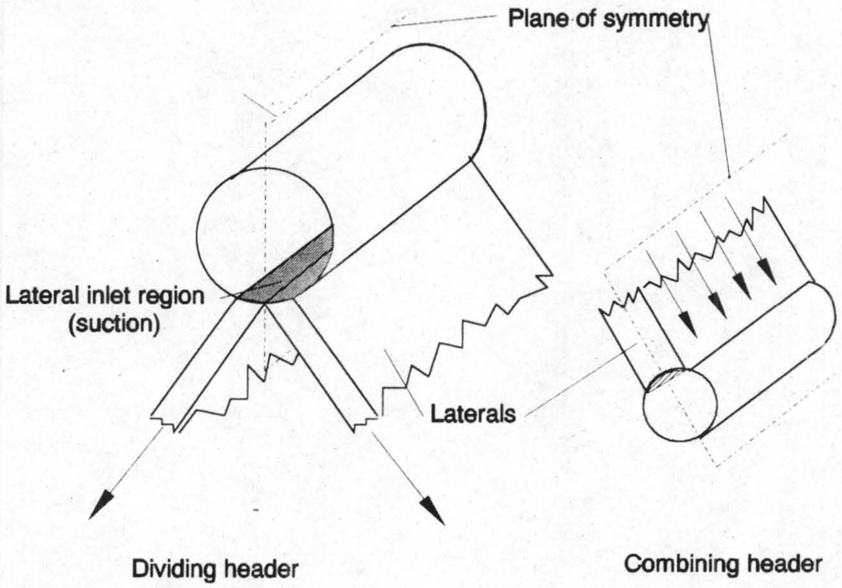

Figure B.14: Diagram of the dividing and combining header configuration.

A three-dimensional cylindrical grid configuration is used to describe the header geometry. Due to symmetry only one half of a header needs to be considered. The case of a uniform mass flow distribution into or out of the laterals was studied. The pitch at which the laterals are spaced is relatively small compared to the overall header dimensions. Therefore the model is simplified by assuming a continuous suction or outflow over the span of the header wall to which the laterals are attached. This suction or outflow velocity (v_w) is then calculated as a fraction of the specified lateral inlet or outlet velocity (v_l) by continuity according to the ratio of the lateral width (w) and pitch (Δz):

$$w\, v_l = \Delta z\, v_w \tag{B.5}$$

With the magnitude of the velocity vector components in the longitudinal header direction (v_{hz}) for each cell determined by the computer code, the local longitudinal header momentum correction coefficient (α_{mh}) can be calculated by the following approximation:

$$\alpha_{mh} \approx \frac{\sum_{i=1}^{n} v_{hzi}^2 \Delta A_i}{v_h^2 A_h} \tag{B.6}$$

From continuity the mean longitudinal header velocity as a function of the longitudinal header distance (z) and the lateral height (h) is given by

$$v_h = v_w \frac{A_w}{A_h} = v_w \frac{(L - z)h}{\frac{\pi}{4n} d_h^2} \tag{B.7}$$

where L is the length of the header over which the suction or inflow occurs. The constant n assumes the value 2 for the dividing header and 1 for the combining header for the case of a single row A-frame condenser configuration.

With the solution for the longitudinal header pressure distribution known it is possible to calculate the local value of the overall momentum correction coefficient (θ) by discretizing equation (3.4) as follows:

Recall equation (3.4):

$$\frac{dp_h}{dz} + \theta \rho \frac{1}{2} \frac{d}{dz}\left(v_h^2\right) + \rho \left(\frac{d\alpha_{mh}}{dz} + \frac{C}{2} \frac{f_D}{d_{eh}} \right) v_h^2 = 0$$

with C = 1 for $v_h > 0$ and C = -1 for $v_h < 0$.

The local friction factor is calculated according to equation (2.13):

$$f_D = \frac{0.3164}{Re_h^{0.25}} = 0.3164\left(\frac{\mu}{\rho\, v_h\, d_h}\right)^{0.25}$$

Discretize equation (3.4) as follows:

$$0 = p_{h\,i+1} - p_{h\,i} + \theta\,\frac{\rho}{2}\left(v_{h\,i+1}^2 - v_{h\,i}^2\right)$$
$$+\rho\left(\frac{d\alpha}{dz} + \frac{C}{2}\,\frac{0.3164}{d_h}\left(\frac{\mu}{\rho\, v_{h\,i}\, d_h}\right)^{0.25}\right)\left(z_{i+1} - z_i\right)v_{h\,i}^2$$

and solved for θ:

$$\theta \approx \frac{p_{h\,i+1} - p_{h\,i} + \rho\left(\frac{d\alpha}{dz} + \frac{C}{2}\,\frac{0.3164}{d_h}\left(\frac{\mu}{\rho\, v_{h\,i}\, d_h}\right)^{0.25}\right)\left(z_{i+1} - z_i\right)v_{h\,i}^2}{\frac{\rho}{2}\left(v_{h\,i+1}^2 - v_{h\,i}^2\right)} \qquad \text{(B.8)}$$

B.5.1 PROPERTIES, DIMENSIONS, BOUNDARY CONDITIONS AND GRID CONFIGURATION

The physical properties of saturated steam at 60°C (333.15K) are calculated according to equations (A.2) and (A.3)

$$\rho = -4.062329056 + 0.10277044\,T - 9.76300388\times10^{-4}T^2 + 4.475240795\times10^{-6}T^3$$
$$-1.004596894\times10^{-8}T^4 + 8.9154895\times10^{-12}T^5$$
$$= -4.062329056 + 0.10277044\times(333.15) - 9.76300388\times10^{-4}\times(333.15)^2$$
$$+ 4.475240795\times10^{-6}\times(333.15)^3 - 1.004596894\times10^{-8}\times(333.15)^4$$
$$+ 8.9154895\times10^{-12}\times(333.15)^5 = 0.13023\text{kg/m}^3$$

$$\mu = 2.562435\times10^{-6} + 1.816683\times10^{-8}T + 2.579066\times10^{-11}T^2 - 1.067299\times10^{-14}T^3$$
$$= 2.562435\times10^{-6} + 1.816683\times10^{-8}\times(333.15) + 2.579066\times10^{-11}\times(333.15)^2$$
$$- 1.067299\times10^{-14}\times(333.15)^3 = 1.1083\times10^{-5}\text{Ns/m}^2$$

The header dimensions and configuration together with the boundary conditions are in figure B.15.

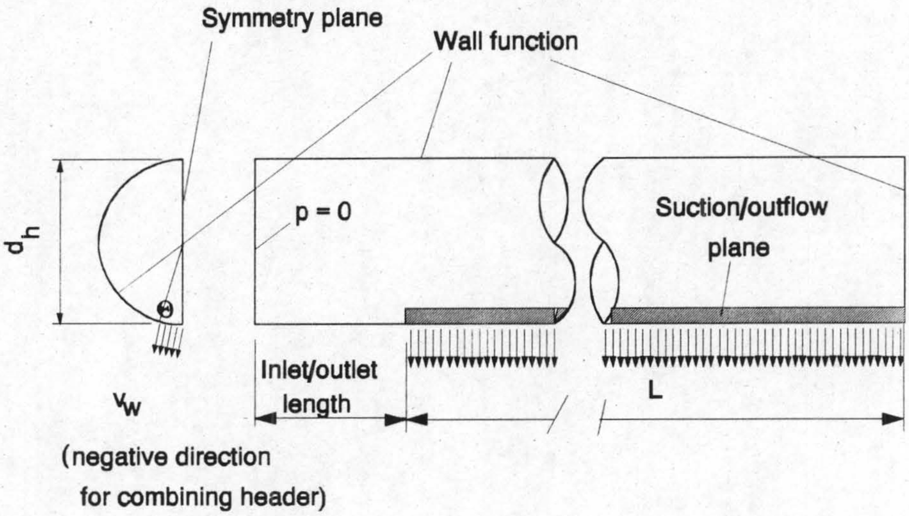

Figure B.15: Header configuration and boundary conditions.

Lateral (flattened tube) specifications:

Lateral width, w:	0.01m
Lateral height, h:	0.19m
Lateral pitch, Δz:	0.04m
Lateral equivalent diameter, d_{el}:	0.019m

Dividing header analysis:

Two dividing header lengths are used to investigate the effect of the ratio of the suction velocity to the header inlet velocity.

The wall suction is specified in such a way that it would be equivalent to a lateral Reynolds number in the order of 15000 for the case of discrete laterals consisting of laterals with dimensions as specified above:

A lateral inlet velocity of 65m/s gives a lateral Reynolds number of

$$\begin{aligned} Re_l &= \frac{\rho\, v_l\, d_{el}}{\mu} \\ &= \frac{0.132 \times 65 \times 0.019}{1.1 \times 10^{-5}} \\ &= 14820 \end{aligned}$$

For a continuous wall suction the suction velocity is

$$v_w = \frac{v_l}{\dfrac{\Delta z}{2h}} = \frac{65}{\dfrac{0.04}{0.01}} = 16.25\text{m/s}$$

The header dimensions are as follows:

Length with suction (L): 25m / 33m
Inlet length: 2m / 2.64m
Number of longitudinal increments: 108
Header Diameter (d_h): 2m
Angle over which suction occurs (Θ): 0.06057π radians

Combining header analysis

We specify that 90% of the lateral steam flow is condensed. Therefore the velocity of the vapour exiting the lateral into the combining header is only 10% of that of the suction velocity of the dividing header. Because of the continuous outflow model:

$v_w = 0.1 \times 16.25 = 1.625\text{m/s}$

We consider only one half of the combining header. Therefore only half the lateral width is used to determine the angle over which suction occurs.

The header dimensions are as follows:
Length with suction (L): 25m
Outlet length: 2m
Number of longitudinal increments: 108
Header Diameter (d_h): 0.7071m
Angle over which suction occurs (Θ): 0.08502π radians

Boundary conditions:

The logarithmic wall function is specified for all solid walls. Over the suction/outflow area a uniformly distributed velocity (v_w) is specified. The inlet plane has been given a fixed pressure of 0.

Grid configuration:

The grid configurations in the polar plane of the dividing header and the combining header are shown in figures B.16 and B.17 respectively.

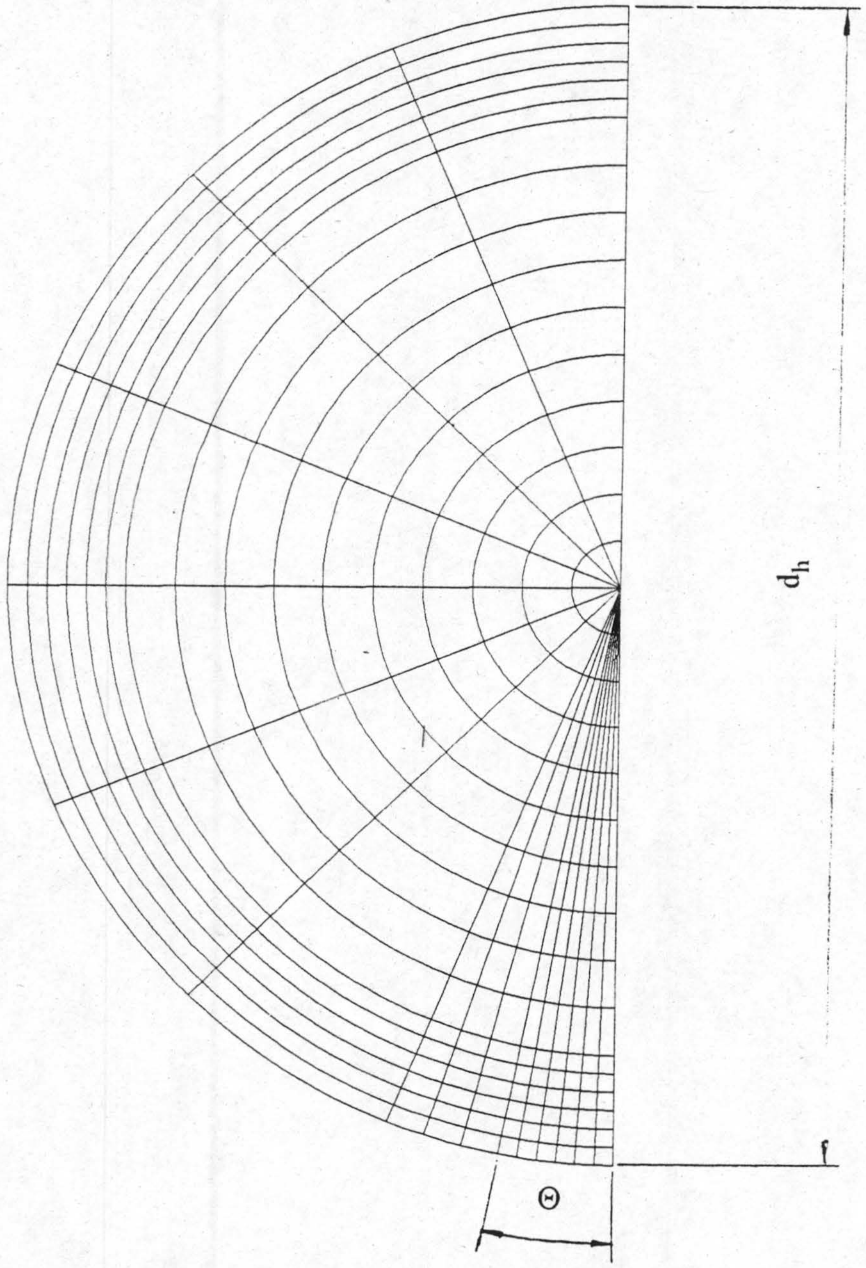

Figure B.16: Dividing header grid in polar plane.

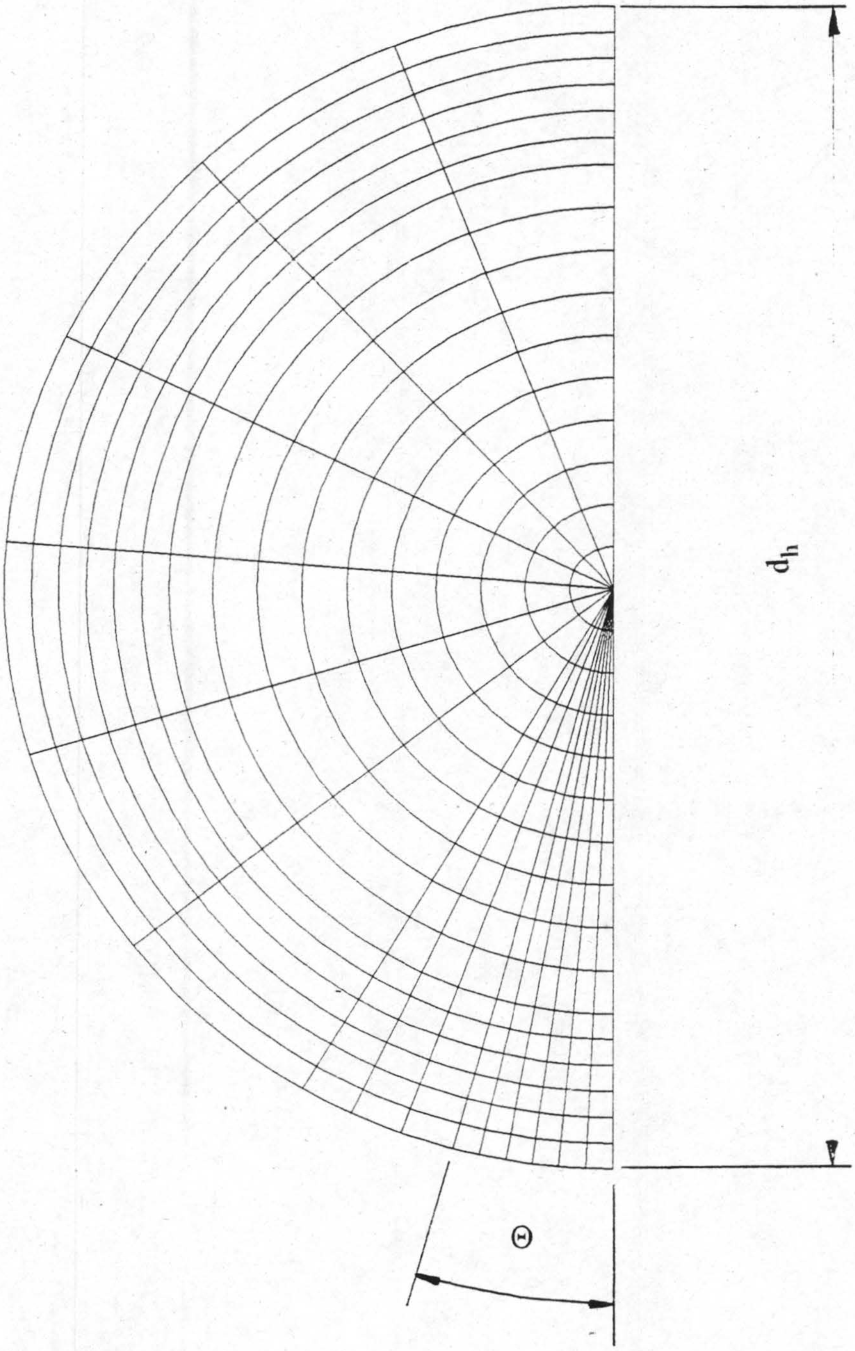

Figure B.17: Combining header grid in polar plane.

There are 108 equidistantly spaced planes in the longitudinal direction for both headers.

B.5.2 RESULTS

The non-dimensionalized header static pressure distribution is shown in figure B.18.

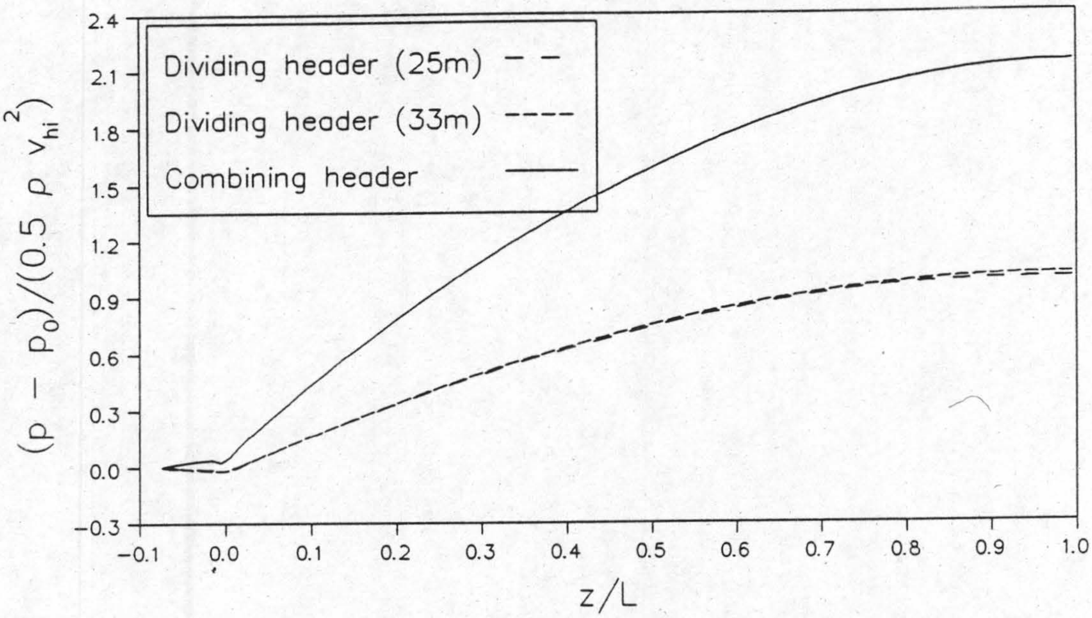

Figure B.18: Non-dimensionalized static pressure distributions in headers.

For the two dividing headers and one combining header configuration the header momentum correction factor (α_{mh}) is shown in figure B.19 together with the overall header momentum correction factor (θ). It can be seen that for the dividing header the value of the coefficient is constant and very close to unity independent of the distance and the header length. The momentum correction factor of the combining header for this specific geometry has a slight gradient but its value is also around unity.

Because of these small gradients the term $d\alpha_{mh}/dz$ of equation (B.3) has been ignored for both the dividing and the combining header in the determination of the overall header momentum correction factor.

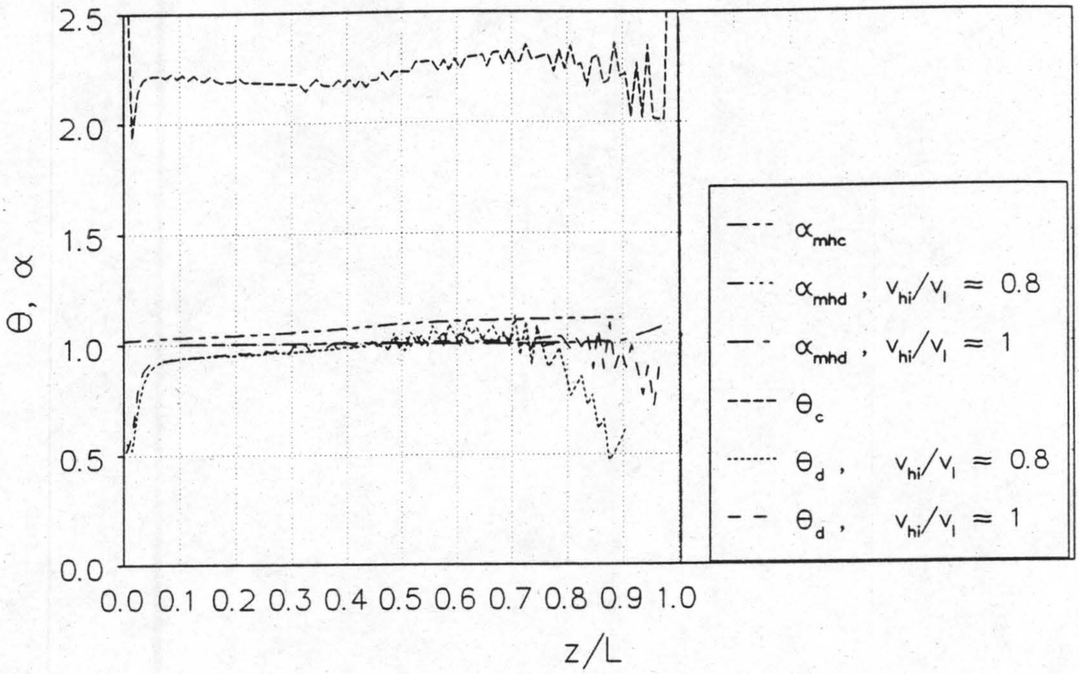

Figure B.19: Header momentum correction factors (α_{mh},θ_h).

The drastically changing gradient of θ is explained by the sometimes identical numerical values for the pressures at two adjacent planes in the longitudinal direction because of the limited number of decimals the *PHOENICS* code output consists of. Thus the incremental pressure difference in equation (B.8) is nil and the other terms contribute to the sudden change of the otherwise relatively constant value of θ. The overall header length of the dividing header does not influence the average value of θ. These average values are θ_{hd} = 0.99 and θ_{hc} = 2.24 for the above configuration.

APPENDIX C

CALIBRATION OF ALUMINIUM PIPES

The calibration facility is shown schematically in figure C.1.

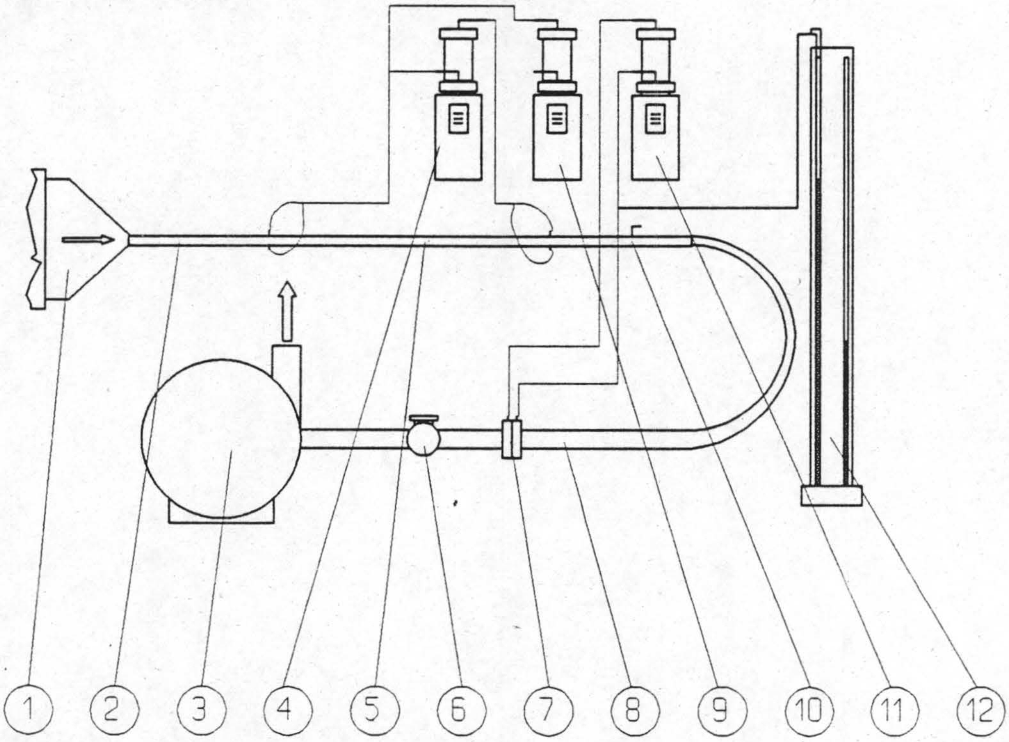

Legend:

1) Outlet manifold connecting a single lateral of experimental apparatus to the aluminium pipe.
2) 0.25m aluminium pipe inlet section for flow development.
3) Suction fan.
4) Betz manometer for measuring pressure difference over 1m section aluminium pipe.
5) 1m section of aluminium pipe.
6) Large flow adjustment valve just before suction fan.
7) Orifice according to BS1042.
8) 2m pipe section upstream orifice for flow development.
9) Betz manometer for measuring absolute pressure in test section.
10) Butterfly valve for individual pipe flow adjustment.
11) Betz manometer for measuring pressure difference over orifice.
12) Water manometer to determine absolute upstream orifice pressure.

Figure C.1: Aluminium pipe calibration facility.

The air leaving each lateral flows through an aluminium pipe connected to the lateral. Each of these aluminium pipes has two pressure tapping points situated 1m apart. Over this length a pressure difference is measured. This pressure difference can be quantified by the following equation:

$$\Delta p_p = f_D \frac{L_p}{d_p} \frac{1}{2} \rho_p v_p^2 \tag{C.1}$$

where f_D is the D'Arcy friction factor, L_p, is the distance between the two pressure tappings of the pipe, ρ_p, is the density of the air flowing through the pipe and v_p is the mean air velocity in the pipe. By solving equation (C.1) for the pipe velocity, the mass flow rate through the pipe can be determined with a known pressure difference over the 1m section of the aluminium pipe.

The inner diameters, d_p, of the 10 aluminium pipes used in the experimental investigation are listed in table C.1.

Table C.1: Aluminium pipe inner diameters.

Pipe no.	d_p [mm]
1	28.41
2	28.41
3	28.38
4	28.29
5	28.34
6	28.38
7	28.30
8	28.38
9	28.38
10	28.37

During the calibration, air was sucked through the pipes and the pressure differences over the 1m pipe length and over an orifice plate, manufactured according to British Standards BS1042 [84BS1] and situated downstream of the flow leaving the pipe, were measured. The absolute pressures at the orifice's and each pipe's upstream pressure tapping point are measured in order to determine the air density.

Sample calculation of calibration point:

The following sample calculation shows how the mass flow through a pipe is calculated by using the pressure difference over the orifice plate and the absolute upstream pressure.

Orifice dimensions:

Pipe diameter, d_{po}:	46.75mm
Throat diameter:	30.00mm
Diameter ratio, β:	0.64278

Measured values:

Atmospheric pressure,	p_{atm}	= 100940N/m^2
Thermocouple voltage,	V	= 0.744mV
Pressure difference over orifice,	Δp_o	= 1854N/m^2
Absolute pressure before orifice,	h_{o1}	= 529mm water (below atmospheric pressure)
Pressure difference over pipe,	Δp_p	= 618N/m^2
Absolute pressure upstream pipe,	h_{p1}	= 200.8 mm water (below atmospheric pressure)

Calculations:

The air temperature is determined by converting the thermocouple reading

$$T_a = 273.15 + 25.29036 \times V = 273.15 + 25.29036 \times 0.744 = 291.966\text{K}$$

The pressure upstream of the orifice is

$$p_{o1} = p_{atm} - \rho_{Water} g h_{o1} = 100940 - 998.34 \times 9.7962 \times 0.529 = 95766.4\text{N/m}^2$$

Asuuming air to be an ideal gas, the upstream density is determined as

$$\rho_{o1} = \frac{p_{o1}}{R\,T_a} = \frac{95766.4}{(287.08)(291.966)} = 1.14256\text{kg/s}$$

The temperature dependent dynamic viscosity can be empirically obtained from equation

(A.3)

$$\mu = 2.287973\times10^{-6} + 6.259793\times10^{-8}\times T_a - 3.131956\times10^{-11}\times T_a^2 + 8.15038\times10^{-15}\times T_a^3$$

$$= 2.287973\times10^{-6} + 6.259793\times10^{-8}\times291.97 - 3.131956\times10^{-11}\times(291.97)^2 + 8.15038\times10^{-15}\times(291.97)^3 = 1.80975\times10^{-5}\text{Ns/m}^2$$

According to BS1042 it has to be ascertained that the pressure ratio before the orifice plate is greater than 0.75:

$(p_{o1} - \Delta p_o)/p_{o1} = (95766.4 - 618)/95766.4 = 0.9935$,

which satisfies the condition.

The expansion factor is calculated with the following empirical formula given in BS1042:

$$\varepsilon = 1 - (0.41 + 0.35\,\beta^4)\,\Delta p_o/(k_{air}p_{o1})$$

$$= 1 - (0.41 + 0.35 \times 0.64278^4) \times 1854/(1.4 \times 95766.4)$$

$$= 0.993504$$

From BS1042 the velocity approach factor is

$$E = (1 - \beta^4)^{-0.5} = (1 - (0.64278)^4)^{-0.5} = 1.09811$$

Due to the iterative solution procedure we will use the converged solution to estimate the initial Reynolds number:

$Re_o = 46679.336$

According to BS1042 the approximate discharge coefficient is calculated using this Reynolds number

$$C_1 = 0.5959 + 0.0312\beta^{2.1} - 0.184\beta^8 + 0.0029\beta^{2.5}(10^6/Re_o)^{0.75}$$

$$= 0.5959 + 0.0312\times0.64278^{2.1} - 0.184\times0.64278^8 + 0.0029\times0.64278^{2.5}(10^6/46679.336)^{0.75}$$

$$= 0.612437$$

Since the orifice diameter is smaller than 50mm the discharge coefficient must be

corrected by a factor F_B. From figure 1(a) of BS1042: Section 1.2: 1984, with $\beta = 0.64278$ the factor $F_A = 1.0113$ can be read. The factor F_B is given by
$F_B = 0.5(F_A - 1) + 1 = 0.5(1.0113 - 1) + 1 = 1.00565$

From BS1042 the corrected discharge factor is
$C = C_1 F_B = 0.612437 \times 1.00565 = 0.615897$

According to BS1042 the air approach velocity to the orifice plate is calculated according to

$$v_{o1} = C\,E\,\beta^2\,\varepsilon\left(\frac{2\Delta p_o}{\rho_{o1}}\right)^{0.5} = 0.615897\times1.09811\times(0.64278)^2\times0.993514\left(\frac{2\times1854}{1.14256}\right)^{0.5}$$
$$= 15.81550\text{ m/s}$$

The corrected Reynolds number is
$Re_o = \rho_{o1} v_{o1} d/\mu = 1.14256\times15.81550\times0.04675/(1.80975\times10^{-5}) = 46679.37$
which is very close to the initial value.

With this converged solution the air mass flow rate can now be calculated
$m = \rho_{o1} v_{o1} \pi d_{po}^2/4 = 1.14256\times15.81550\times\pi\times(0.04675)^2/4 = 0.0310181\text{kg/s}$

With the given mass flow rate the friction factor for the particular Reynolds number in the aluminium pipe (in this case pipe 1) can be calculated by using the definition of the D'Arcy friction factor:

$$f_D = \frac{\Delta p_p}{\frac{L_p}{d_p}\frac{1}{2}\rho v_p^2} \tag{C.2}$$

The upstream pipe pressure is
$p_p = p_{atm} - \rho_{Water} g h_p = 100940 - 998.34\times9.7962\times0.2008 = 98976.19\text{N/m}^2$

which yields a density of

$$\rho_p = \frac{p_p}{R\,T_a} = \frac{98976.19}{(287.08)\,(291.966)} = 1.18085\,\text{kg/s}$$

The mean velocity in the pipe is

$v_p = m/(\rho_p \pi d_p{}^2/4) = 0.0310181/(1.18085\times\pi\times(0.02841)^2/4) = 41.4369\text{m/s}$

A pipe friction factor can now be calculated

$$f_D = \frac{\Delta p_p}{\frac{L}{d_p}\,\frac{1}{2}\,\rho_p\,v_p^2}$$

$$= \frac{618}{\frac{1}{0.02841}\times\frac{1}{2}\times 1.18085\times(41.4369)^2} = 0.017319$$

The corresponding Reynolds number is

$Re_p = \rho_p v_p d_p/\mu = 1.180852\times 41.4369\times 0.02841/(1.80975\times 10^{-5}) = 76813.1$

The friction factor data as a function of the Reynolds number of each pipe are listed in tables C.3 to C.12, together with the experimental readings. Figures C.2 to C.11 represent the friction factor calibration data graphically as a function of the Reynolds number.

Linear logarithmic regression functions in the form of

$$f_D = a\,Re_p{}^b$$

have been fitted through the calibration data for each pipe.

In order to calculate the mass flow rate with given pressure difference over the 1m pipe section the following explicit formula, obtained by substituting equation (C.2) into equation (C.1) and making use of the continuity equation:

$$m = \rho_p \pi \frac{d_p}{4} v_p = \rho_p \pi \frac{d_p}{4} \left(\frac{2\, d_p}{a\, \rho_p L_p} \left[\frac{\mu}{\rho_p d_p} \right]^b \right)^{\frac{0.5}{1\; + 0.5\, b}} \tag{C.3}$$

Both coefficients, a and b are listed in table C.2 for the 10 pipes.

Table C.2: Regression coefficients of calibrated pipes.

Pipe no.	a	b
1	0.43569	-0.28778
2	0.17762	-0.19276
3	0.17704	-0.19345
4	0.20098	-0.20615
5	0.15356	-0.18041
6	0.12428	-0.15727
7	0.13806	-0.16814
8	0.38551	-0.27493
9	0.31390	-0.25510
10	0.38384	-0.27977

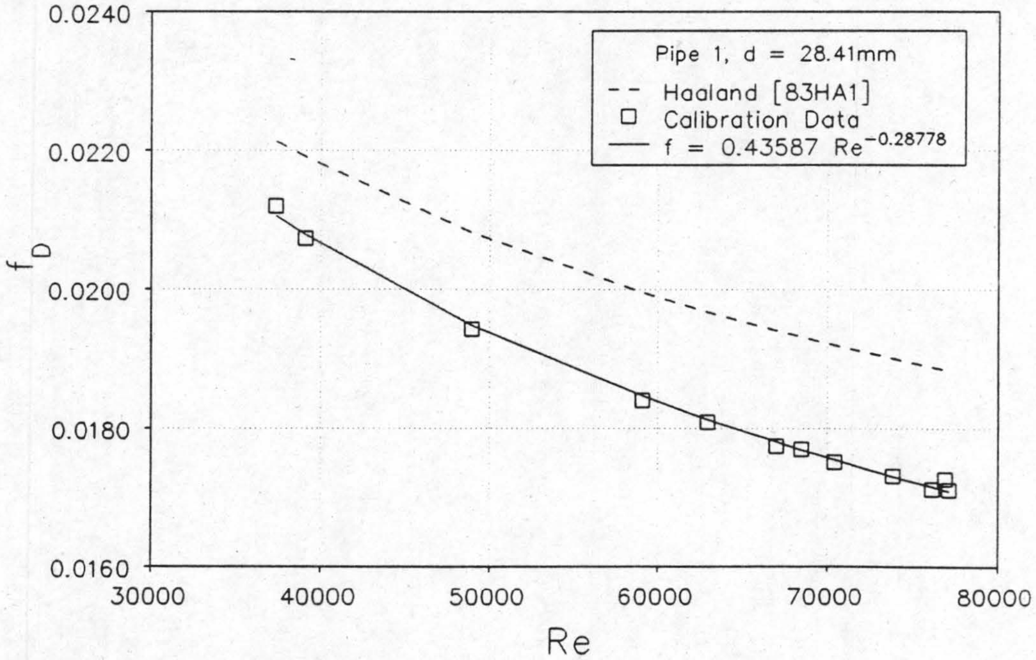

Figure C.2: Calibration data of pipe no.1.

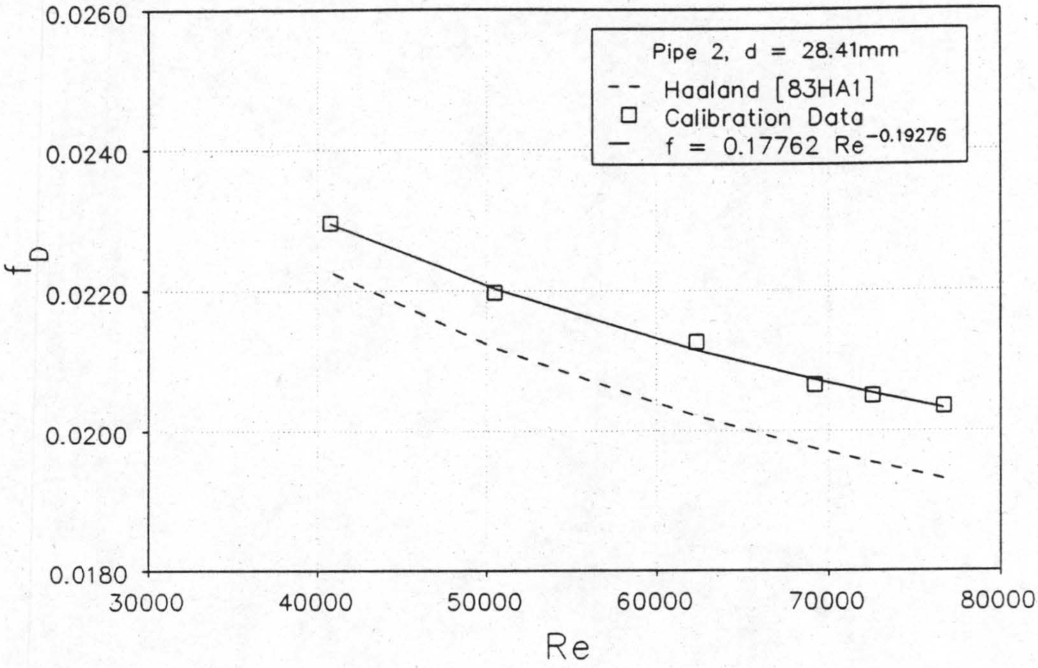

Figure C.3: Calibration data of pipe no.2.

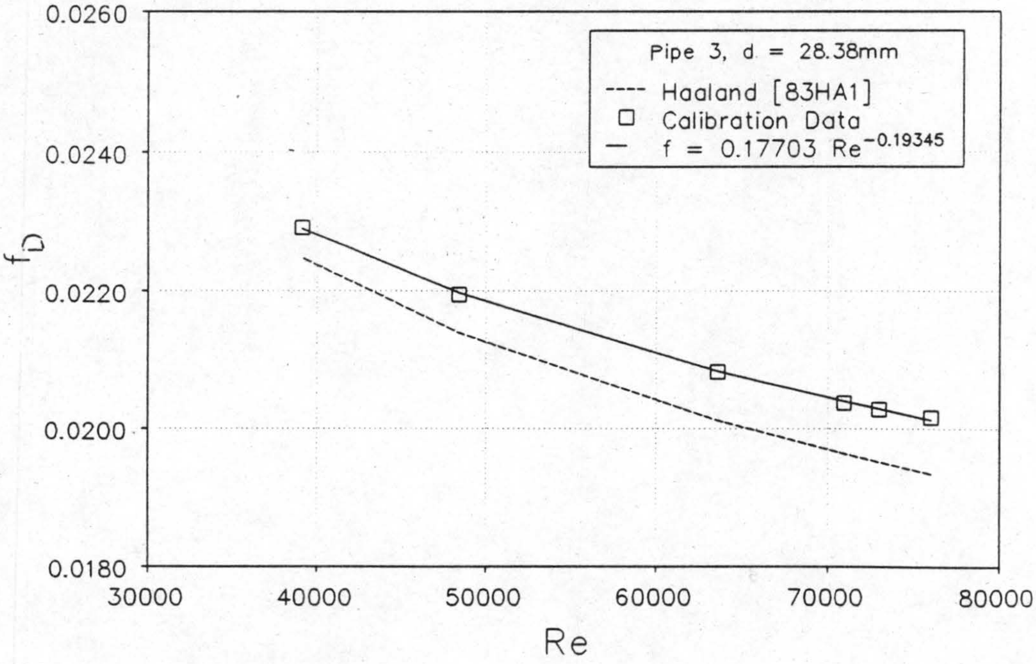

Figure C.4: Calibration data of pipe no.3.

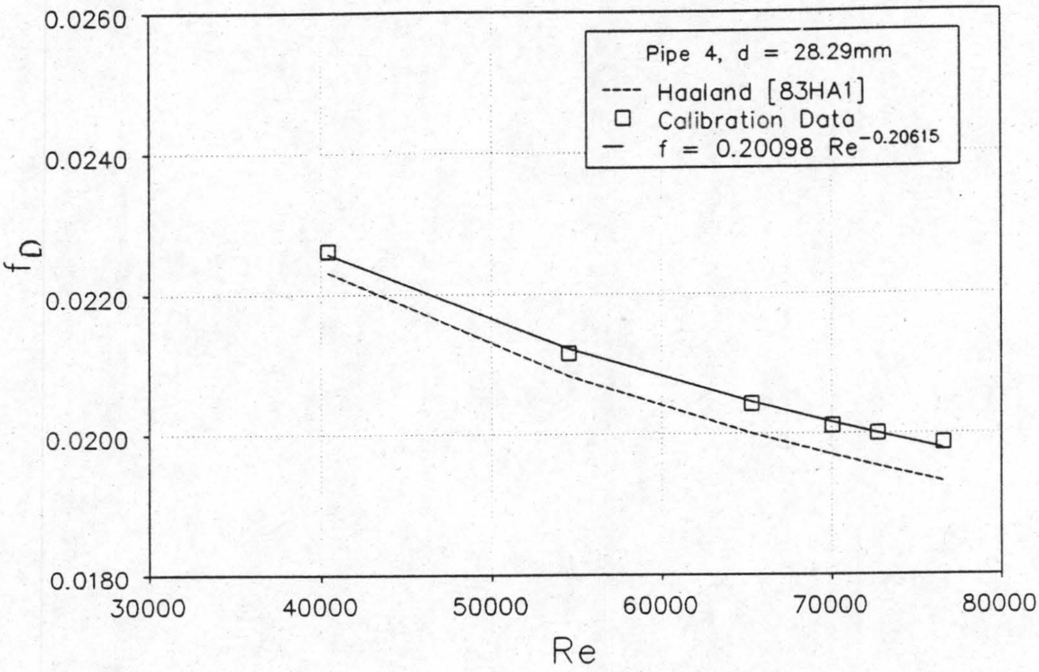

Figure C.5: Calibration data of pipe no.4.

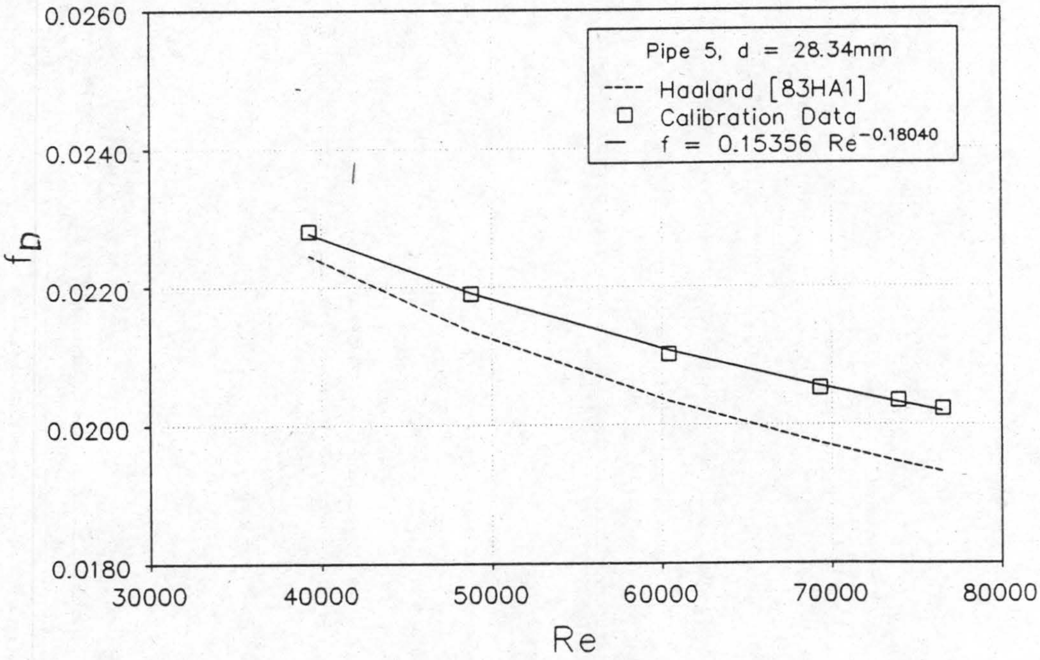

Figure C.6: Calibration data of pipe no.5,

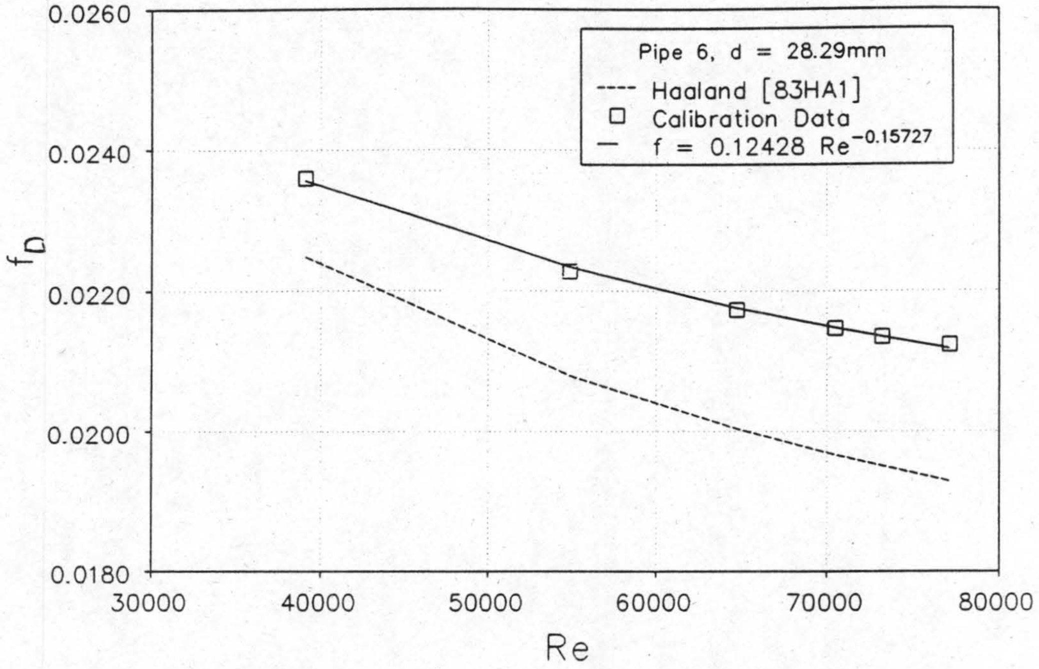

Figure C.7: Calibration data of pipe no.6.

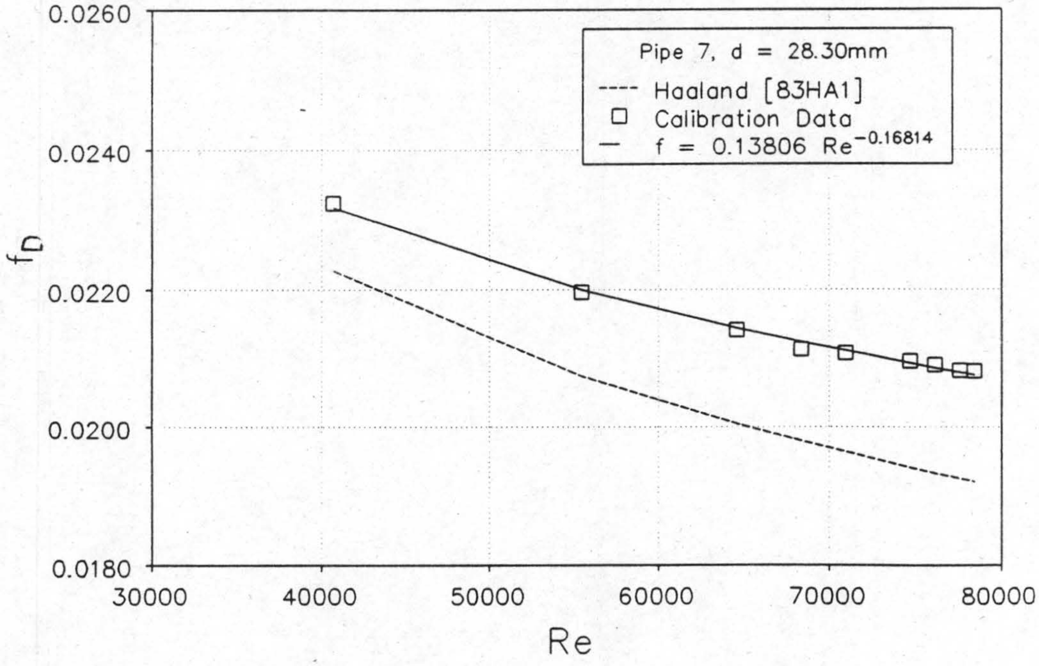

Figure C.8: Calibration data of pipe no.7.

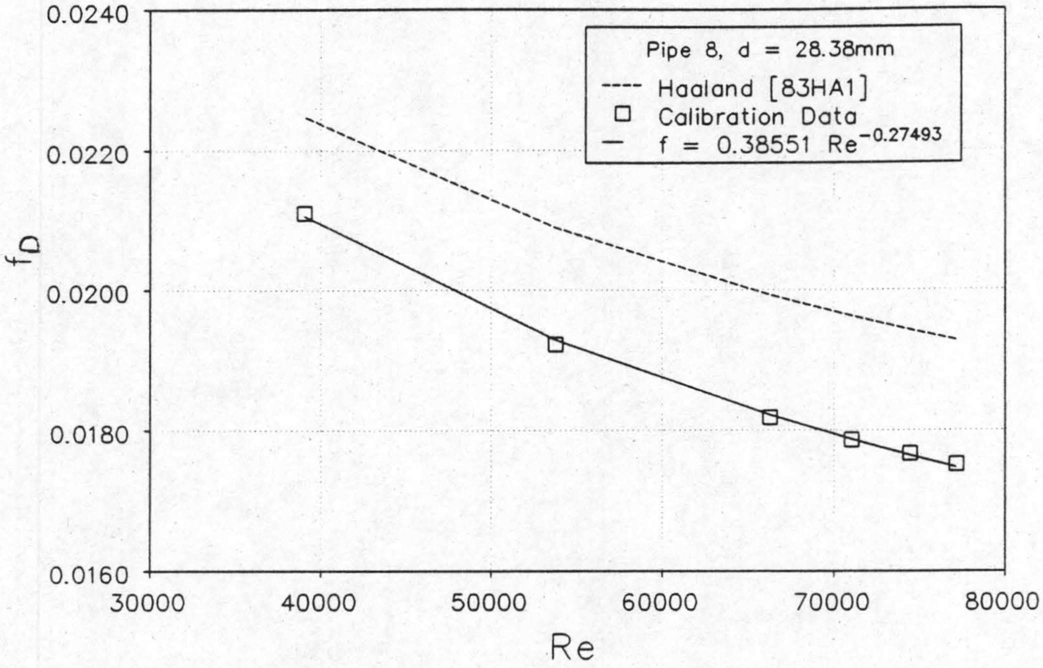

Figure C.9: Calibration data of pipe no.8.

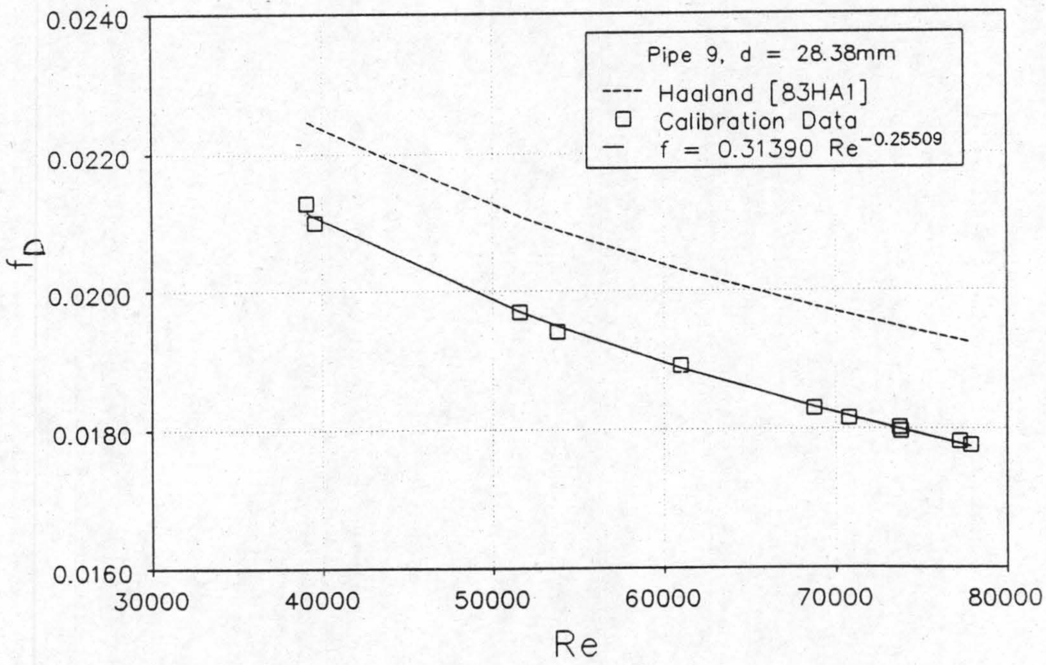

Figure C.10: Calibration data of pipe no.9.

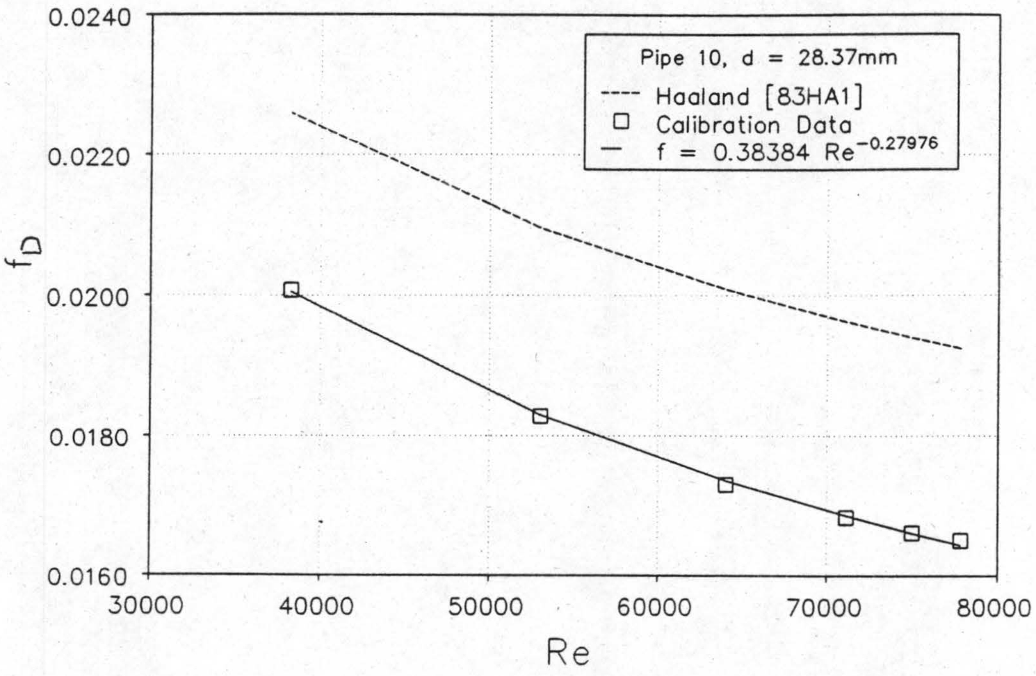

Figure C.11: Calibration data of pipe no. 10.

The deviation of the calibration friction factors of the pipes from the friction factor given by Haaland can be explained by the inaccurate machining of the pressure tapping points. Repeatability was obtained in the calibration of pipes no.1, no.7 and no.9. Thus the calibration data was reliable.

Table C.3: Calibration Values of Pipe no.1.

Thermo-couple reading [mV]	Δp_o [N/m^2]	p_{atm}-p_{o1} [mmH$_2$O]	Δp_p [N/m^2]	p_{atm}-p_{p1} [mm H$_2$O]	m [kg/s]	Re	f_D
p_{atm} = 100940 N/m^2, t_a = 19°C							
0.744	1854	529	618	200.8	0.031069	76941.48	0.017261
0.743	1532	443	523	167.6	0.028432	70413.83	0.017502
0.742	1378	402	479	151.7	0.027054	67006.19	0.017733
0.742	1056	315	385	117.7	0.023855	59082.38	0.018394
0.741	712	218	278	80.8	0.019763	48952.41	0.019422
p_{atm} = 101210 N/m^2, t_a = 19°C							
0.705	1794	515	594	194.4	0.030680	76171.03	0.017118
0.705	442	135	187	51.2	0.015753	39111.46	0.020729
p_{atm} = 101150 N/m^2, t_a = 19°C							
0.751	1865	532	616	201.9	0.031180	77179.31	0.017108
0.750	1697	486	570	184.7	0.029847	73885.24	0.017306
0.749	1443	417	499.5	158.4	0.027671	68504.40	0.017691
0.748	1206	353	430	133.6	0.025429	62958.03	0.018079
0.747	406	128	176	47.4	0.015091	37365.45	0.021190

Table C.4: Calibration Values of Pipe no.2.

p_{atm} = 100945 N/m^2, t_a = 19°C							
Thermo-couple reading [mV]	Δp_o [N/m^2]	p_{atm}-p_{o1} [mm H$_2$O]	Δp_p [N/m^2]	p_{atm}-p_{p1} [mm H$_2$O]	m [kg/s]	Re	f_D
0.736	1838	522	722	188.4	0.030961	76711.88	0.020348
0.735	1632	468	650	168.6	0.029297	72594.67	0.0205
0.735	1473	426	594	153.2	0.027926	69195.67	0.020651
0.734	1180	347	495	124.4	0.025156	62336.73	0.021269
0.735	758	230	334	82.0	0.020373	50480.01	0.021971
0.735	486	152	227	53.8	0.016452	40764.59	0.022961

Table C.5: Calibration Values of Pipe no.3.

p_{atm} = 100950 N/m², t_a = 19°C							
Thermo-couple reading [mV]	Δp_o [N/m²]	p_{atm}-p_{o1} [mm H_2O]	Δp_p [N/m²]	p_{atm}-p_{p1} [mm H_2O]	m [kg/s]	Re	f_D
0.733	1798	518	704	183.3	0.030641	76014.92	0.020166
0.732	1648	479	652	169.1	0.029425	73003.02	0.020283
0.731	1550	452	618	159.7	0.028598	70954.04	0.020374
0.730	1228	365	506	128.6	0.025633	63603.47	0.020829
0.730	692	215	307	75.2	0.019503	48391.47	0.021945
0.729	445	141	209	49.5	0.01577	39132.42	0.022909

Table C.6: Calibration Values of Pipe no.4.

p_{atm} = 100955 N/m², t_a = 19°C							
Thermo-couple reading [mV]	Δp_o [N/m²]	p_{atm}-p_{o1} [mm H_2O]	Δp_p [N/m²]	p_{atm}-p_{p1} [mm H_2O]	m [kg/s]	Re	f_D
0.726	1813	523	710	188.0	0.030768	76606.31	0.019312
0.725	1620	470	643	169.4	0.029203	72714.47	0.019532
0.726	1495	436	599	157.2	0.028127	70030.11	0.019694
0.726	1289	382	528	136.9	0.026231	65310.95	0.019999
0.726	882	269	380	96.0	0.021909	54548.17	0.020819
0.725	472	149	222	53.1	0.016228	40407.05	0.022304

Table C.7: Calibration Values of Pipe no.5.

p_{atm} = 100960 N/m², t_a = 19°C							
Thermo-couple reading [mV]	Δp_o [N/m²]	p_{atm}-p_{o1} [mm H_2O]	Δp_p [N/m²]	p_{atm}-p_{p1} [mm H_2O]	m [kg/s]	Re	f_D
0.723	1815	517	718	187.2	0.030799	76562.33	0.020227
0.720	1682	483	672	174.4	0.029731	73922.35	0.020346
0.719	1466	425	595	153.4	0.027883	69332.67	0.020526
0.719	1095	325	461	116.8	0.024296	60413.32	0.021021
0.718	700	214	312	76.7	0.019625	48800.45	0.021894
0.718	446	140	210	50.2	0.015796	39280.44	0.022804

Table C.8: Calibration Values of Pipe no.6.

p_{atm} = 100965 N/m^2, t_a = 19°C							
Thermo-couple reading [mV]	Δp_o [N/m^2]	p_{atm}-p_{o1} [mm H_2O]	Δp_p [N/m^2]	p_{atm}-p_{p1} [mm H_2O]	m [kg/s]	Re	f_D
0.717	1844	515	760	184.0	0.03105	77107.38	0.021233
0.716	1654	486	688	166.7	0.029489	73237.71	0.021348
0.715	1521	432	640	153.8	0.028385	70499.44	0.021463
0.715	1271	366	546	130.2	0.026086	64788.86	0.021731
0.715	896	265	400	93.6	0.022094	54874.02	0.022272
0.714	442	136	214	48.0	0.015733	39077.75	0.023606

Table C.9: Calibration Values of Pipe no.7.

p_{atm} = 100970 N/m^2, t_a = 19°C							
Thermo-couple reading [mV]	Δp_o [N/m^2]	p_{atm}-p_{o1} [mm H_2O]	Δp_p [N/m^2]	p_{atm}-p_{p1} [mm H_2O]	m [kg/s]	Re	f_D
0.710	1855	519	760	185.6	0.031143	77594.41	0.02082
0.709	1709	482	708	172.0	0.02998	74700.25	0.02096
0.709	1530	435	641	155.2	0.028471	70939.5	0.021077
0.708	1255	363	539	129.2	0.025937	64630.39	0.021411
0.710	910	269	406	95.8	0.022263	55468.54	0.021958
0.709	477	147	230	52.2	0.016325	40677.68	0.023234
p_{atm} = 101150 N/m_2, t_a = 19°C							
0.732	1902	528	778	190.2	0.031512	78400.31	0.020806
0.729	1785	497	736	179.4	0.030603	76153.85	0.020897
0.730	1410	402	598	144.3	0.027479	68375.67	0.02113

Table C.10: Calibration Values of Pipe no.8.

p_{atm} = 100975 N/m^2, t_a = 19°C							
Thermo-couple reading [mV]	Δp_o [N/m^2]	p_{atm}-p_{o1} [mm H_2O]	Δp_p [N/m^2]	p_{atm}-p_{p1} [mm H_2O]	m [kg/s]	Re	f_D
0.709	1843	515	627	193.7	0.031053	77157.14	0.01751
0.707	1706	481	588	180.4	0.029959	74447.49	0.017669
0.706	1562	438	540	164.1	0.028579	71023.97	0.017861
0.706	1332	383	478	143.0	0.026679	66302.25	0.01818
0.706	857	255	331	94.3	0.021637	53772.14	0.019232
0.707	441	136	191	50.1	0.015721	39065.5	0.021112

Table C.11: Calibration Values of Pipe no.9.

p_{atm} = 100980 N/m^2, t_a = 19°C							
Thermo-couple reading [mV]	Δp_o [N/m^2]	p_{atm}-p_{o1} [mm H_2O]	Δp_p [N/m^2]	p_{atm}-p_{p1} [mm H_2O]	m [kg/s]	Re	f_D
0.703	1844	517	638	191.3	0.031067	77221.38	0.017816
0.703	1669	472	587	174.2	0.029659	73721.94	0.018015
0.703	1528	435	544	160.4	0.028461	70743.46	0.018156
0.701	857	255	334	93.1	0.021643	53802.24	0.019408
0.702	453	140	195	50.8	0.015929	39596.3	0.021002
p_{atm} = 101210 N/m^2, t_a = 19°C							
0.718	1878	514	648	194.8	0.031368	77892.69	0.017762
0.717	1672	463	587	174.9	0.029717	73797.41	0.017963
0.717	1438	403	518	151.9	0.02769	68764.31	0.0183
0.719	1116	319	420	119.8	0.02456	60984.05	0.018916
0.721	786	230	312	86.0	0.020777	51584.13	0.019696
0.723	442	136	192	49.8	0.015746	39087.57	0.021285

Table C.12: Calibration Values of Pipe no.10.

$p_{atm} = 100985\ N/m^2$, $t_a = 19°C$							
Thermo-couple reading [mV]	Δp_o $[N/m^2]$	p_{atm}-p_{o1} [mm H_2O]	Δp_p $[N/m^2]$	p_{atm}-p_{p1} [mm H_2O]	m [kg/s]	Re	f_D
0.702	1870	505	601	194.8	0.031301	77836.02	0.0165
0.701	1728	476	561	180.6	0.030164	75012.2	0.01661
0.700	1542	430	510	162.6	0.0286	71127.11	0.016828
0.699	1235	351	424	132.0	0.025761	64071.23	0.017297
0.700	831	243	306	90.9	0.021333	53053.71	0.018276
0.700	421	129	174	47.6	0.015378	38245.5	0.020082

APPENDIX D

SAMPLE CALCULATION AND TABULATION OF EXPERIMENTAL DATA

D.1 SAMPLE CALCULATION OF LATERAL VELOCITY AND THE INLET LOSS COEFFICIENT

The following calculation shows how the lateral velocity and the inlet loss coefficient are determined by the data acquisition computer program, which was written in the *PASCAL* code. The mass flow rate is determined by inserting the pressure differentials measured over the 1m aluminium pipe section into the respective pipe's calibration equation that is given in appendix C.

The data of the first line of table D.3 (single lateral in a passing stream) will be used in this sample calculation. Figure D.1 shows the respective positions of the header, the lateral and the aluminium pipe.

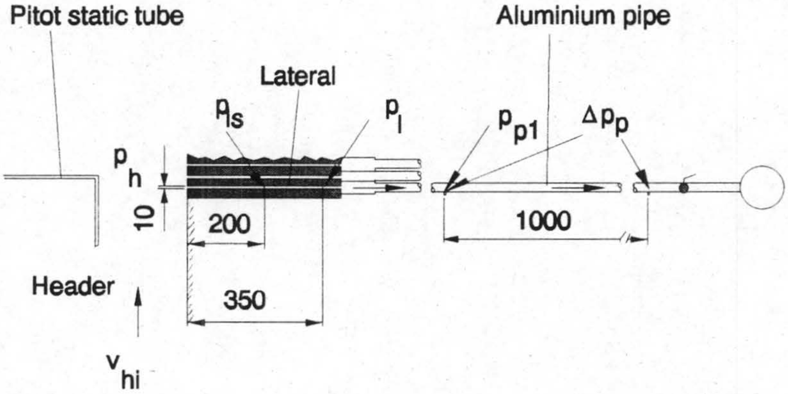

Figure D.1: Positions and dimensions of a single header, lateral and aluminium pipe combination.

Because of machining inaccuracies the widths of the laterals (w) deviate from the value of 10mm which is specified in the description of the apparatus in chapter 4. The measured distances are listed in table D.1. The measured lateral height (h) however, is 190mm.

Table D.1: Widths and equivalent diameters of laterals:

Lat. no.	w [m]	d_{el} [m]
1	0.01012	0.019216
2	0.00999	0.018982
3	0.00999	0.018982
4	0.01001	0.019018
5	0.00987	0.018765
6	0.00995	0.018910
7	0.01006	0.019108
8	0.01009	0.019162
9	0.01009	0.019162
10	0.01013	0.019234

Experimental readings:

Lateral (and aluminium pipe) no. : 1

Atmospheric pressure, $p_{atm} = p_{h_l}$: 100086 N/m^2

Air temperature, T_a : 28+273.15 = 301.15 K

Pressure difference over
aluminium pipe, Δp_p : 396.75 N/m^2

Upstream pressure in aluminium pipe, relative
to atmospheric pressure, $p_{atm} - p_{p1}$: 1174.95 N/m^2

Lateral pressure at 350mm tapping relative to
header pressure, $p_h - p_l$: 133.78 N/m^2

Lateral frictional pressure loss, Δp_l : 16.54 N/m^2

Pitot static pressure
difference, Δp_{pitot} : 14.97 N/m^2

Calculation of the mass flow rate:

The absolute upstream pressure in the aluminium pipe is

$$
\begin{aligned}
p_{p1} &= p_{atm} - (p_{atm} - p_{p1}) \\
&= 100086 - 1174.95 \\
&= 98911.05 \text{ N/m}^2
\end{aligned}
$$

The temperature dependent dynamic viscosity can calculated by equation (A.1)

$$
\begin{aligned}
\mu &= 2.287973\times10^{-6} + 6.259793\times10^{-8}\times T_a - 3.131956\times10^{-11}\times T_a^{\,2} \\
&\quad + 8.15038\times10^{-15}\times T_a^{\,3} \\
&= 2.287973\times10^{-6} + 6.259793\times10^{-8}\times301.15 - 3.131956\times10^{-11}\times(301.15)^2 \\
&\quad + 8.15038\times10^{-15}\times(301.15)^3 \\
&= 1.8521\times10^{-5} \text{ Ns/m}^2
\end{aligned}
$$

By taking air as an ideal gas, the density in the pipe section is calculated as

$$\rho_p = \frac{p_{p1}}{R\,T_a} = \frac{98911.05}{287.1\times(273.15+28)} = 1.14401 \text{ kg/m}^3$$

In appendix C the friction factor of a calibrated aluminium pipe is given in the form of

$$f_D = a\,Re_p^{\,b} \tag{D.2}$$

The constants in the above equation for aluminium pipe no.1 are taken from table C.2 as:

$a = 0.43569$

$b = -0.28778$

For the same pipe the internal diameter is

$d_p = 0.02841$ m

The mass flow rate through the aluminium pipe is calculated by equation (C.3):

$$
\begin{aligned}
m &= \rho_p A_p \left(\frac{2\,\Delta p_p\, d_p}{a\,\rho_p\, L_p} \left[\frac{\mu}{\rho_p\, d_p} \right]^{b} \right)^{\frac{1}{2+b}} \\
&= 1.14401 \times \frac{\pi}{4} (0.02840)^2 \\
&\times \left(\frac{2 \times 386.75 \times 0.02841}{0.43569 \times 1.14401 \times 1} \left[\frac{1.8522 \times 10^{-5}}{1.14401 \times 0.02841} \right]^{-0.28778} \right)^{\frac{1}{2-0.28778}} \\
&= 0.0232345 \mathrm{kg/s}
\end{aligned}
$$

Calculation of the inlet loss coefficient:

Because of a relatively small pressure drop over the lateral inlet, the air density in the header is assumed to be equal to the air density in the lateral. The two dimensional *open* header configuration allows for the header pressure to be taken as atmospheric. From the ideal gas law:

$$
\rho_l = \rho_h = \frac{p_{atm}}{R\,T_a} = \frac{100086}{287.1 \times 301.15} = 1.15760 \ \mathrm{kg/m^3}
$$

From conservation of mass the mean lateral velocity is calculated

$$
v_l = \frac{m}{\rho_l A_l} = \frac{0.0232315}{1.15760 \times 0.0019228} = 10.437 \ \mathrm{m/s}
$$

The Reynolds number in the lateral is

$$
\mathrm{Re}_l = \frac{\rho_l v_l d_{el}}{\mu} = \frac{1.1575967 \times 10.437 \times 0.01921647}{1.85222 \times 10^{-5}} = 12535
$$

The friction factor for parallel plates is calculated by the implicit equation (2.11):

$$
f_D = \left(2 \log_{10}\left(\mathrm{Re}_l\, f_D^{0.5} \right) - 1.19 \right)^{-2}
$$

from which

$f_D = 0.032794$

The experimental friction factor is calculated by equation (4.4):

$$f_D = \frac{\Delta p_1}{\frac{\Delta L_1}{d_{el}}\frac{1}{2}\rho_1 v_1^2}$$

$$= \frac{16.54}{\frac{0.15}{0.019216}\frac{1}{2}\times 1.14401 \times (10.437)^2}$$

$$= 0.03401$$

The difference between the theoretical and the experimentally determined friction factor can be ascribed to the small measured pressure difference and the relatively small length over which the pressure difference is measured. The pressure reading of this specific data point could have been effected by a small disturbance, e.g. a pressure pipe could have been moved during the reading, giving a small pulse onto the diaphragm of the pressure transducer.

In the section to follow, average values of the experimentally determined friction factor for each lateral will be compared to the values calculated by equation (2.11).

The reduced inlet loss coefficient can be determined by using equation (4.3)

$$K_i - \alpha_{eh}\frac{v_h^2}{v_1^2} = \frac{p_h - p_1}{\frac{1}{2}\rho v_1^2} - f\frac{L_1}{d_1} - 1$$

$$= \frac{133.78}{\frac{1}{2}\times 1.15760 \times (10.437)^2} - 0.032794 \times \frac{0.35}{0.0192165} - 1$$

$$= 0.52454$$

From equation (4.7) the velocity ratio dependent part of the inlet loss coefficient is

$$K_{ivr} = \left(K_i - \alpha_{eh}\frac{v_h^2}{v_1^2}\right) - K_0$$

$$= 0.524533 - 0.453944 = 0.070589$$

Calculation of the header inlet velocity:

The header inlet velocity is obtained by converting the pitot-static pressure difference with equation (4.6)

$$v_{hi} = 0.9999 \sqrt{\frac{2\Delta p_{pitot}}{\rho_h}} = 0.9999 \sqrt{\frac{2 \times 14.97}{1.15760}} = 5.09 \text{m/s}$$

D.2 COMPARISON OF THE EXPERIMENTAL FRICTION FACTOR BY THOSE CALCULATED WITH EQUATION (2.11)

The friction factors of each lateral is calculated with the pressure difference data for the two dimensional normal inlet loss coefficient, K_0 which is presented in table D.2. Figure D.2 shows a comparison between experimentally determined friction factors and those determined with equation (2.11). The good general agreement confirms that the parallel plate friction factor of equation (2.11) has to be used in the calculation of the inlet loss coefficients.

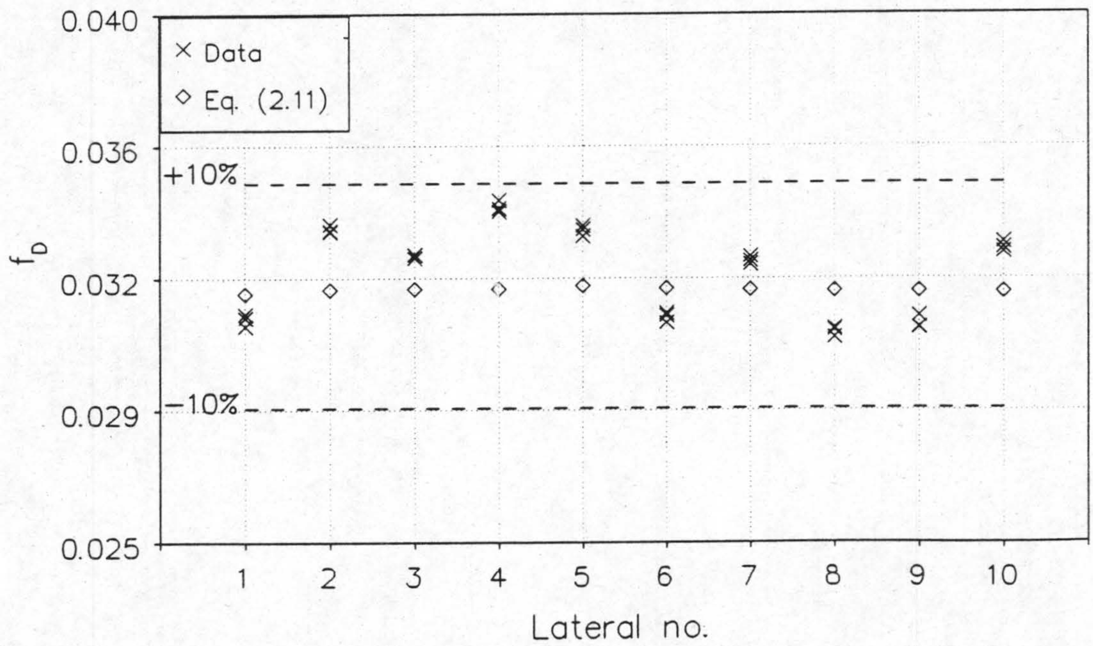

Figure D.2: Comparison of experimental and theoretical friction factors.

D.3 EXPERIMENTAL DATA

Table D.2: Normal inlet loss coefficient (K_0) of each lateral (sharp inlet), 2D configuration.

p_{atm}=99976N/m^2				t_a=23.5°C				
Lat no.	Δp_p [N/m^2]	p_{atm}-p_{p1} [N/m^2]	v_l [m/s]	p_h-p_l [N/m^2]	Δp_l [N/m^2]	f_D exp.	f_D eq.(2.11)	K_0
1	430.1	1296.6	11.1	145.8	17.4	0.0311	0.0321	0.4494
1	428.5	1290.4	11.0	145.5	17.5	0.0314	0.0321	0.4529
1	428.3	1297.9	11.0	145.9	17.6	0.0315	0.0321	0.4596
2	487.2	1203.1	11.0	147.4	19.2	0.0338	0.0322	0.4640
2	486.8	1203.1	11.0	147.4	19.3	0.0340	0.0322	0.4657
2	486.5	1202.0	11.0	147.9	19.1	0.0338	0.0322	0.4734
3	481.8	1190.0	11.0	144.7	18.6	0.0331	0.0322	0.4378
3	480.2	1184.5	11.0	144.0	18.6	0.0332	0.0322	0.4341
3	479.3	1189.7	11.0	144.0	18.6	0.0332	0.0322	0.4385
4	483.6	1213.6	11.0	147.5	19.3	0.0344	0.0322	0.4829
4	482.8	1217.9	11.0	147.5	19.4	0.0347	0.0322	0.4869
4	484.4	1215.6	11.0	147.9	19.4	0.0345	0.0322	0.4849
5	477.4	1168.4	11.0	146.9	19.4	0.0339	0.0323	0.4482
5	477.0	1174.4	11.0	146.5	19.5	0.0340	0.0323	0.4443
5	477.5	1171.9	11.0	146.6	19.3	0.0337	0.0323	0.4438
6	501.7	1158.3	11.0	142.9	17.7	0.0312	0.0322	0.4016
6	500.5	1156.3	11.0	143.0	17.8	0.0314	0.0322	0.4072
6	499.5	1155.3	11.0	143.0	17.8	0.0315	0.0322	0.4118
7	506.0	1178.9	11.0	144.2	18.3	0.0330	0.0322	0.4510
7	505.3	1187.8	11.0	143.6	18.4	0.0331	0.0322	0.4455
7	507.7	1182.2	11.0	144.5	18.3	0.0329	0.0322	0.4474
8	433.3	1245.0	11.0	143.2	17.2	0.0316	0.0322	0.4356
8	433.9	1249.6	11.0	143.4	17.2	0.0315	0.0321	0.4348
8	434.4	1247.7	11.0	143.7	17.1	0.0320	0.0321	0.4371
9	440.6	1240.9	11.0	143.8	17.3	0.0311	0.0321	0.4357
9	441.0	1239.4	11.0	143.8	17.5	0.0314	0.0321	0.4328
9	442.3	1241.6	11.0	143.8	17.4	0.0311	0.0321	0.4268
10	413.5	1259.5	11.0	145.8	18.5	0.0334	0.0321	0.4696
10	414.7	1259.2	11.0	146.0	18.5	0.0332	0.0321	0.4659
10	412.1	1264.1	11.0	146.0	18.5	0.0335	0.0321	0.4810

Table D.3: Normal inlet loss coefficient (K_0) of each lateral (sharp inlet), 3D configuration.

p_{atm}=99976N/m^2				t_a=23.5°C		
Lat no.	Δp_p [N/m^2]	p_{atm}-p_{p1} [N/m^2]	v_l [m/s]	p_h-p_l [N/m^2]	f_D	K_0
1	427.0	1285.0	11.0	145.5	0.0321	0.4609
1	427.5	1287.7	11.0	145.6	0.0321	0.4596
1	428.0	1287.4	11.0	145.8	0.0321	0.4596
2	484.5	1196.3	11.0	147.0	0.0322	0.4701
2	484.4	1199.7	11.0	147.0	0.0322	0.4707
2	486.5	1198.1	11.0	147.3	0.0322	0.4653
3	478.7	1185.4	11.0	144.1	0.0322	0.4424
3	479.4	1191.3	11.0	144.9	0.0322	0.4506
3	481.2	1186.8	11.0	144.2	0.0322	0.4328
4	479.9	1204.9	11.0	146.4	0.0322	0.4857
4	479.4	1204.3	11.0	147.0	0.0322	0.4949
4	479.8	1204.7	11.0	146.6	0.0322	0.4881
5	477.2	1171.0	11.0	147.4	0.0323	0.4568
5	476.9	1172.5	11.0	147.1	0.0323	0.4543
5	476.6	1171.2	11.0	147.1	0.0323	0.4543
6	500.8	1167.1	11.0	143.4	0.0322	0.4121
6	501.7	1163.7	11.0	143.6	0.0322	0.4114
6	503.0	1164.0	11.1	143.5	0.0322	0.4040
7	507.5	1188.3	11.0	144.0	0.0322	0.4422
7	507.8	1184.8	11.0	144.1	0.0322	0.4415
7	507.3	1182.5	11.0	144.3	0.0322	0.4460
8	434.3	1246.1	11.0	143.8	0.0321	0.4393
8	436.0	1255.6	11.0	144.5	0.0321	0.4408
8	435.4	1250.8	11.0	144.3	0.0321	0.4401
9	442.6	1244.4	11.0	144.1	0.0321	0.4290
9	441.6	1244.7	11.0	144.1	0.0321	0.4341
9	442.9	1245.3	11.0	144.1	0.0321	0.4285
10	413.9	1262.4	11.0	146.2	0.0321	0.4729
10	414.3	1261.2	11.0	145.8	0.0321	0.4653
10	414.5	1259.1	11.0	145.8	0.0321	0.4640

Table D.4: Average K_0-values, sharp inlet (fig.4.10).

lat. no.	2D	3D
1	0.4539	0.4600
2	0.4677	0.4687
3	0.4368	0.4420
4	0.4849	0.4896
5	0.4454	0.4551
6	0.4069	0.4092
7	0.4480	0.4432
8	0.4358	0.4401
9	0.4318	0.4305
10	0.4722	0.4674

Table D.5: Single lateral (no. 1), open 2D configuration, p_{atm}=100086N/m^2, t_a=28°C (fig.4.11).

run no.	Δp_{pitot} [N/m^2]	v_{hi} [m/s]	Δp_p [N/m^2]	$p_{atm}-p_{p1}$ [N/m^2]	v_l [m/s]	p_h-p_l [N/m^2]	Δp_l [N/m^2]	$K_i-\alpha_h(v_h/v_l)^2$	K_{ivr}
1	15.0	5.09	386.8	1175.0	10.44	133.8	16.5	0.4873	0.0706
2	49.2	9.22	395.1	1205.3	10.57	139.4	16.6	0.8726	0.1070
3	117.4	14.24	395.2	1208.8	10.57	146.2	16.8	1.3476	0.2123
4	216.7	19.35	393.9	1217.3	10.55	151.7	16.8	1.8347	0.3064
5	332.2	23.96	389.9	1219.3	10.49	155.9	16.9	2.2849	0.4001

Table D.6: 10 laterals, open 2D standard configuration, $p_{atm}=100565 N/m^2$ (fig.4.12).

Lat. no.	Δp_p [N/m^2]	$p_{atm}-p_{pl}$ [N/m^2]	v_l [m/s]	v_{hi}/v_l	p_h-p_l [N/m^2]	p_h-p_{ls} [N/m^2]	$K_i-\alpha_{eh}(v_h/v_l)^2$	K_{ivr}
run no.1	t_a=25°C				Δp_{pitot}=18.6 N/m^2, v_{hi}=5.62 m/s			
1	410.6	1277.2	10.75	0.5230	160.9	142.5	0.7812	0.3273
2	459.0	1187.6	10.68	0.5262	152.4	132.6	0.6734	0.2057
3	453.1	1172.6	10.64	0.5283	145.6	125.7	0.5887	0.1519
4	457.3	1196.6	10.66	0.5275	144.4	124.7	0.5651	0.0802
5	446.1	1136.2	10.64	0.5285	142.4	122.2	0.5340	0.0886
6	468.6	1133.2	10.63	0.5287	137.1	118.5	0.4612	0.0543
7	480.6	1159.0	10.66	0.5272	136.0	117.3	0.4417	-0.0063
8	410.5	1208.7	10.64	0.5286	131.1	114.9	0.3807	-0.0552
9	416.0	1220.4	10.64	0.5282	131.6	114.0	0.3851	-0.0467
10	396.7	1217.8	10.73	0.5240	130.6	112.5	0.3430	-0.1291
run no.2	t_a=25°C				Δp_{pitot}=66.4 N/m^2, v_{hi}=10.64 m/s			
1	408.7	1295.6	10.72	0.9921	179.3	161.6	1.0665	0.6126
2	462.6	1201.8	10.73	0.9913	166.6	146.7	0.8653	0.3975
3	450.1	1182.0	10.60	1.0031	155.0	135.1	0.7470	0.3102
4	459.6	1208.8	10.69	0.9952	156.5	136.8	0.7354	0.2505
5	447.0	1145.0	10.65	0.9987	151.2	131.8	0.6618	0.2164
6	470.3	1140.8	10.65	0.9982	144.6	127.1	0.5661	0.1592
7	476.4	1164.2	10.61	1.0022	141.2	122.3	0.5395	0.0915
8	412.6	1216.5	10.67	0.9970	139.0	119.6	0.4877	0.0519
9	420.5	1221.5	10.71	0.9931	132.7	114.8	0.3786	-0.0532
10	394.7	1212.4	10.70	0.9942	125.1	106.9	0.2722	-0.1999
run no.3	t_a=25°C				Δp_{pitot}=120.2 N/m^2, v_{hi}=14.30 m/s			
1	409.1	1307.8	10.72	1.3338	191.5	174.9	1.2449	0.7909
2	459.1	1208.3	10.68	1.3389	173.1	153.2	0.9823	0.5146
3	456.8	1188.7	10.69	1.3382	161.7	144.4	0.8102	0.3734
4	458.3	1214.1	10.67	1.3407	161.8	142.2	0.8221	0.3372
5	444.8	1150.8	10.62	1.3469	157.0	138.1	0.7609	0.3154
6	471.9	1144.3	10.67	1.3402	148.2	129.8	0.6120	0.2051
7	479.9	1167.1	10.66	1.3424	144.2	124.7	0.5669	0.1189
8	413.7	1218.0	10.68	1.3388	140.5	121.0	0.5037	0.0679
9	420.7	1221.6	10.71	1.3353	132.8	114.5	0.3784	-0.0534
10	396.5	1208.7	10.73	1.3337	121.5	104.0	0.2091	-0.2631

Table D.6 continued:

Lat. no.	Δp_p [N/m^2]	$p_{atm}-p_{p1}$ [N/m^2]	v_1 [m/s]	v_{hi}/v_1	p_h-p_1 [N/m^2]	p_h-p_{ls} [N/m^2]	$K_i-\alpha_{eh}(v_h/v_1)^2$	K_{ivr}
run no.4	t_a =25°C				Δp_{pitot} =230.6 N/m^2, v_{hi} =19.81 m/s			
1	405.3	1327.5	10.67	1.8577	211.2	193.9	1.5705	1.1165
2	460.4	1215.0	10.70	1.8517	179.8	160.1	1.0743	0.6066
3	452.7	1191.4	10.64	1.8628	164.4	145.4	0.8736	0.4369
4	457.7	1221.3	10.66	1.8584	169.0	150.2	0.9336	0.4487
5	446.3	1157.1	10.64	1.8623	163.3	145.5	0.8479	0.4025
6	472.9	1147.0	10.69	1.8543	150.8	131.9	0.6466	0.2397
7	481.7	1168.4	10.68	1.8558	145.5	126.2	0.5784	0.1304
8	415.2	1218.1	10.71	1.8506	140.6	122.6	0.4959	0.0601
9	421.8	1218.7	10.73	1.8470	129.9	110.7	0.3302	-0.1016
10	387.5	1196.7	10.58	1.8720	109.5	90.9	0.0731	-0.3990
run no.5	t_a =25°C				Δp_{pitot} =351.8 N/m^2, v_{hi} =24.47 m/s			
1	401.5	1347.1	10.61	2.3075	230.8	212.7	1.9022	1.4483
2	458.6	1217.1	10.68	2.2919	181.9	162.7	1.1176	0.6499
3	451.3	1191.0	10.62	2.3046	164.0	144.5	0.8751	0.4384
4	458.2	1224.0	10.67	2.2938	171.7	152.1	0.9705	0.4856
5	444.5	1161.8	10.62	2.3053	168.1	149.8	0.9306	0.4851
6	473.6	1147.2	10.69	2.2882	151.0	131.9	0.6462	0.2393
7	479.2	1167.9	10.65	2.2986	145.0	125.8	0.5830	0.1350
8	415.5	1216.1	10.71	2.2846	138.6	121.0	0.4651	0.0293
9	418.5	1212.4	10.68	2.2915	123.6	105.7	0.2529	-0.1789
10	393.0	1185.8	10.67	2.2932	98.6	79.3	-0.1157	-0.5878
run no.6	t_a =25°C				Δp_{pitot} =786.6 N/m^2, v_{hi} =36.59 m/s			
1	403.9	1406.8	10.64	3.4394	290.5	273.3	2.7784	2.3244
2	453.3	1215.5	10.61	3.4495	180.3	162.5	1.1266	0.6589
3	456.2	1183.7	10.68	3.4259	156.7	138.3	0.7382	0.3014
4	458.9	1227.1	10.68	3.4272	174.8	155.6	1.0129	0.5280
5	447.0	1170.4	10.65	3.4365	176.6	156.6	1.0436	0.5981
6	463.2	1134.4	10.57	3.4629	138.2	119.6	0.5033	0.0964
7	474.5	1158.8	10.59	3.4554	135.9	116.2	0.4667	0.0187
8	399.9	1200.5	10.48	3.4926	123.0	104.8	0.3125	-0.1233
9	420.6	1194.4	10.71	3.4160	105.6	87.1	-0.0251	-0.4569
10	387.3	1148.4	10.58	3.4576	61.2	40.7	-0.6606	-1.1327

Table D.6 continued:

Lat. no.	Δp_p [N/m^2]	$p_{atm}-p_{p1}$ [N/m^2]	v_l [m/s]	v_{hi}/v_l	p_h-p_l [N/m^2]	p_h-p_{ls} [N/m^2]	$K_i-\alpha_{eh}(v_h/v_l)^2$	K_{ivr}
run no.7		t_a =25°C			Δp_{pitot} =1464.0 N/m^2, v_{hi} =49.92 m/s			
1	403.6	1480.8	10.63	4.6964	364.5	344.8	3.9012	3.4473
2	456.8	1220.9	10.65	4.6863	185.7	167.4	1.1851	0.7174
3	453.9	1179.1	10.65	4.6867	152.1	133.4	0.6819	0.2452
4	451.8	1234.9	10.58	4.7168	182.7	162.7	1.1765	0.6917
5	439.1	1186.1	10.54	4.7356	192.4	172.2	1.3369	0.8915
6	476.1	1130.1	10.73	4.6544	134.0	113.1	0.3809	-0.0260
7	481.4	1157.8	10.67	4.6771	134.8	114.8	0.4198	-0.0282
8	416.6	1199.2	10.73	4.6535	121.7	102.9	0.2083	-0.2276
9	420.3	1169.8	10.71	4.6618	81.0	64.6	-0.3887	-0.8205
10	392.3	1104.4	10.67	4.6806	17.2	-2.0	-1.3326	-1.8047

Table D.7: 10 laterals, closed 2D configuration, p_{atm}=100110 N/m^2, (fig.4.15):

Lat. no.	Δp_p [N/m^2]	$p_{atm}-p_{pl}$ [N/m^2]	v_l [m/s]	v_{hi}/v_l	p_h-p_l [N/m^2]	$K_i-\alpha_{eh}(v_h/v_l)^2$	K_{ivr}
run no.1		p_h=100079.7N/m^2		t_a=29°C	Δp_{pitot}=29.3N/m^2, v_{hi}=7.13 m/s		
1	394.1	1218.8	10.56	0.6750	154.0	0.7965	0.3425
2	446.6	1139.9	10.60	0.6725	149.3	0.6979	0.2302
3	443.9	1123.0	10.60	0.6723	140.7	0.5637	0.1269
4	448.7	1143.6	10.62	0.6711	142.3	0.5834	0.0985
5	434.0	1083.6	10.56	0.6752	138.7	0.5424	0.0970
6	459.9	1083.2	10.61	0.6721	134.7	0.4677	0.0608
7	471.6	1121.1	10.63	0.6703	134.9	0.4690	0.0210
8	404.9	1162.2	10.62	0.6713	132.9	0.4448	0.0089
9	408.1	1141.0	10.60	0.6726	129.3	0.3978	-0.0340
10	383.3	1171.4	10.58	0.6735	130.3	0.4211	-0.0510
run no.2		p_h=100071.9N/m^2		t_a=29°C	Δp_{pitot}=50.8N/m^2, v_{hi}=9.39m/s		
1	396.9	1226.9	10.61	0.8849	163.4	0.9223	0.4683
2	448.3	1134.9	10.62	0.8834	154.1	0.7621	0.2944
3	442.2	1114.5	10.58	0.8869	143.4	0.6150	0.1783
4	446.2	1136.2	10.59	0.8863	146.2	0.6567	0.1719
5	432.4	1076.0	10.54	0.8907	142.2	0.6046	0.1592
6	457.1	1065.5	10.58	0.8875	136.9	0.5134	0.1065
7	468.0	1103.3	10.59	0.8861	137.1	0.5177	0.0697
8	403.7	1150.1	10.60	0.8853	133.5	0.4617	0.0259
9	408.6	1132.9	10.61	0.8848	128.6	0.3845	-0.0473
10	385.4	1155.8	10.62	0.8838	128.5	0.3805	-0.0916
run no.3		p_h=100060.2N/m^2		t_a=30°C	Δp_{pitot}=134.8N/m^2, v_{hi}=15.32m/s		
1	390.0	1247.8	10.51	1.4577	181.1	1.2558	0.8019
2	441.4	1137.4	10.55	1.4521	161.0	0.9101	0.4424
3	439.1	1130.6	10.55	1.4512	146.3	0.6776	0.2408
4	443.8	1147.4	10.57	1.4487	151.5	0.7535	0.2686
5	434.7	1100.0	10.58	1.4475	152.6	0.7557	0.3102
6	455.1	1085.4	10.56	1.4499	141.4	0.5945	0.1876
7	471.3	1119.4	10.65	1.4385	140.7	0.5585	0.1105
8	398.1	1146.5	10.53	1.4545	134.9	0.5170	0.0812
9	407.1	1142.5	10.60	1.4454	129.2	0.4036	-0.0282
10	394.9	1178.6	10.78	1.4205	124.6	0.2710	-0.2011

Table D.7 continued:

Lat. no.	Δp_p [N/m^2]	p_{atm}-p_{p1} [N/m^2]	v_l [m/s]	v_{hi}/v_l	p_h-p_l [N/m^2]	K_i-$\alpha_{eh}(v_h/v_l)^2$	K_{ivr}
run no.4		p_h=100048.5 N/m^2		t_a=30°C	Δp_{pitot}=228.6N/m^2, v_{hi}=19.94m/s		
1	391.6	1273.1	10.53	1.8936	200.4	1.5443	1.0904
2	445.3	1160.4	10.60	1.8818	166.2	0.9682	0.5005
3	439.1	1137.9	10.56	1.8896	144.7	0.6526	0.2158
4	443.7	1160.3	10.57	1.8869	153.2	0.7809	0.2960
5	436.8	1111.7	10.61	1.8800	157.0	0.8119	0.3665
6	454.3	1089.7	10.55	1.8898	142.6	0.6182	0.2113
7	469.7	1130.2	10.63	1.8768	141.3	0.5755	0.1275
8	402.9	1160.5	10.60	1.8812	137.0	0.5221	0.0862
9	407.3	1135.7	10.60	1.8816	127.0	0.3677	-0.0641
10	383.7	1150.6	10.61	1.8805	108.4	0.0807	-0.3914
run no.5		p_h=100038.7N/m^2		t_a=30°C	Δp_{pitot}=357.6N/m^2, v_{hi}=24.94 m/s		
1	394.4	1312.3	10.57	2.3591	221.7	1.8535	1.3995
2	443.3	1170.7	10.57	2.3595	167.5	1.0003	0.5326
3	445.3	1159.7	10.64	2.3453	141.9	0.5764	0.1396
4	441.6	1162.3	10.54	2.3658	152.6	0.7825	0.2976
5	435.0	1116.6	10.59	2.3564	161.7	0.8954	0.4500
6	454.9	1085.3	10.56	2.3615	141.4	0.5954	0.1885
7	469.3	1125.2	10.62	2.3480	139.9	0.5560	0.1081
8	400.9	1156.6	10.57	2.3591	136.1	0.5184	0.0826
9	408.3	1136.3	10.62	2.3495	122.5	0.2927	-0.1391
10	386.9	1142.0	10.66	2.3401	100.4	-0.0581	-0.5302
run no.6		p_h=100031.9N/m^2		t_a=30°C	Δp_{pitot}=496.4N/m^2, v_{hi}=29.39m/s		
1	393.0	1334.1	10.55	2.7855	243.1	2.2021	1.7482
2	445.0	1172.0	10.60	2.7736	170.2	1.0318	0.5641
3	437.2	1130.6	10.53	2.7907	132.6	0.4736	0.0369
4	443.1	1162.1	10.56	2.7820	151.3	0.7544	0.2695
5	432.7	1122.5	10.56	2.7841	167.5	1.0006	0.5552
6	453.9	1085.2	10.55	2.7855	139.0	0.5635	0.1566
7	468.9	1121.0	10.62	2.7676	137.5	0.5203	0.0723
8	402.2	1150.5	10.60	2.7739	135.5	0.5017	0.0658
9	408.6	1127.2	10.62	2.7666	119.3	0.2406	-0.1911
10	383.3	1120.6	10.60	2.7715	87.5	-0.2418	-0.7139

Table D.8: 10 laterals, open 3D configuration, p_{atm}=100343N/m^2 (fig.4.16).

Lat. no.	Δp_p [N/m^2]	p_{atm}-p_{p1} [N/m^2]	v_l [m/s]	v_{hi}/v_l	p_h-p_l [N/m^2]	K_i-$\alpha_{eh}(v_h/v_l)^2$	K_{ivr}
run no.1		t_a=24°C			Δp_{pitot}=16.0N/m^2, v_{hi}=5.22m/s		
1	419.6	1270.1	10.89	0.4791	153.8	0.6206	0.1667
2	477.1	1187.7	10.91	0.4780	152.5	0.5834	0.1156
3	474.5	1174.4	10.92	0.4779	147.4	0.5088	0.0721
4	481.0	1202.3	10.96	0.4759	150.1	0.5310	0.0461
5	466.1	1138.4	10.89	0.4788	144.7	0.4688	0.0234
6	494.0	1139.3	10.94	0.4768	143.2	0.4367	0.0298
7	502.3	1166.0	10.92	0.4777	143.0	0.4496	0.0016
8	427.8	1217.8	10.89	0.4789	140.3	0.4218	-0.0141
9	435.3	1228.6	10.92	0.4776	139.9	0.4063	-0.0255
10	406.4	1224.0	10.88	0.4795	136.8	0.3803	-0.0918
run no.2		t_a=24°C			Δp_{pitot}=57.0N/m^2, v_{hi}=9.84m/s		
1	418.8	1287.6	10.87	0.9054	164.5	0.7783	0.3243
2	473.1	1191.6	10.86	0.9065	160.5	0.7186	0.2509
3	472.3	1186.2	10.89	0.9045	153.8	0.6117	0.1749
4	476.8	1217.4	10.91	0.9028	158.0	0.6650	0.1802
5	462.8	1155.6	10.85	0.9073	152.6	0.5986	0.1531
6	492.2	1149.1	10.92	0.9018	149.9	0.5409	0.1340
7	498.5	1176.9	10.88	0.9053	148.1	0.5390	0.0910
8	426.8	1229.8	10.88	0.9051	144.5	0.4885	0.0526
9	434.2	1241.8	10.90	0.9029	141.9	0.4407	0.0089
10	408.0	1238.0	10.90	0.9030	132.7	0.3134	-0.1587
run no.3		t_a=24°C			Δp_{pitot}=124.0N/m^2, v_{hi}=14.52m/s		
1	418.4	1305.9	10.87	1.3365	173.5	0.9129	0.4589
2	475.1	1201.3	10.89	1.3340	163.4	0.7500	0.2822
3	467.6	1190.3	10.83	1.3414	154.6	0.6472	0.2105
4	474.3	1222.8	10.87	1.3356	161.0	0.7217	0.2368
5	461.8	1155.1	10.84	1.3398	156.5	0.6607	0.2153
6	489.2	1157.5	10.88	1.3346	152.2	0.5873	0.1804
7	496.8	1181.6	10.85	1.3379	149.5	0.5674	0.1194
8	427.3	1229.4	10.88	1.3341	145.0	0.4922	0.0564
9	433.3	1239.3	10.89	1.3332	141.1	0.4335	0.0018
10	407.0	1238.9	10.89	1.3339	128.6	0.2592	-0.2129

Table D.8 continued:

Lat. no.	Δp_p [N/m^2]	p_{atm}-p_{pl} [N/m^2]	v_l [m/s]	v_{hi}/v_l	p_h-p_l [N/m^2]	K_i-$\alpha_{eh}(v_h/v_l)^2$	K_{ivr}
run no.4		t_a=24°C			Δp_{pitot}=215.0N/m^2, v_{hi}=19.12m/s		
1	416.7	1313.7	10.84	1.7640	180.1	1.0190	0.5651
2	473.5	1211.2	10.86	1.7600	163.5	0.7590	0.2913
3	471.3	1202.0	10.87	1.7587	153.5	0.6123	0.1756
4	473.5	1228.1	10.86	1.7603	163.1	0.7555	0.2707
5	467.0	1181.1	10.90	1.7537	161.7	0.7089	0.2634
6	489.6	1162.1	10.89	1.7566	151.2	0.5714	0.1645
7	495.5	1189.2	10.84	1.7642	150.0	0.5797	0.1317
8	423.4	1242.2	10.83	1.7661	143.5	0.4920	0.0561
9	432.9	1247.8	10.89	1.7566	138.3	0.3963	-0.0355
10	406.2	1245.0	10.87	1.7585	121.2	0.1570	-0.3151
run no.5		t_a=24°C			Δp_{pitot}=318.0N/m^2, v_{hi}=23.25m/s		
1	417.1	1334.7	10.84	2.1444	190.4	1.1658	0.7118
2	471.2	1213.5	10.84	2.1462	161.3	0.7392	0.2715
3	468.6	1202.3	10.84	2.1458	149.3	0.5657	0.1290
4	477.0	1242.3	10.91	2.1324	163.7	0.7464	0.2615
5	464.1	1185.9	10.87	2.1402	162.8	0.7396	0.2942
6	486.0	1163.6	10.84	2.1452	149.5	0.5645	0.1576
7	494.4	1194.0	10.82	2.1483	147.1	0.5428	0.0949
8	423.9	1240.5	10.83	2.1465	142.1	0.4703	0.0344
9	435.7	1242.1	10.93	2.1283	133.8	0.3175	-0.1143
10	401.6	1223.3	10.80	2.1525	109.0	0.0008	-0.4714

Table D.9: Five laterals at 40mm pitch, open 2D configuration, p_{atm}=100740 N/m^2 (fig.4.17).

Lat. no.	Δp_p [N/m^2]	p_{atm}-p_{p1} [N/m^2]	v_l [m/s]	v_{hi}/v_l	p_h-p_l [N/m^2]	K_i-$\alpha_{eh}(v_h/v_l)^2$	K_{ivr}
run no.1		t_a=25°C			Δp_{pitot}=15.6N/m^2, v_{hi}=5.15m/s		
1	415.8	1273.4	10.82	0.4763	157.1	0.6928	0.2389
2	467.6	1184.3	10.79	0.4779	149.1	0.5814	0.1137
3	462.6	1169.1	10.76	0.4792	142.1	0.4889	0.0521
4	464.1	1192.9	10.74	0.4800	140.7	0.4764	-0.0085
5	458.0	1130.2	10.79	0.4779	136.4	0.3868	-0.0587
run no.2		t_a=25°C			Δp_{pitot}=60.6N/m^2, v_{hi}=10.15m/s		
1	412.6	1287.2	10.77	0.9419	170.9	0.9141	0.4602
2	464.2	1192.5	10.74	0.9445	157.3	0.7187	0.2510
3	461.1	1174.5	10.74	0.9450	147.5	0.5764	0.1396
4	465.9	1195.3	10.76	0.9429	143.1	0.5030	0.0181
5	458.1	1125.5	10.79	0.9407	131.8	0.3185	-0.1270
run no.3		t_a=25°C			Δp_{pitot}=130.9N/m^2, v_{hi}=14.92m/s		
1	411.4	1301.4	10.75	1.3872	185.1	1.1315	0.6776
2	463.1	1198.9	10.73	1.3906	163.7	0.8190	0.3513
3	463.3	1175.6	10.77	1.3855	148.6	0.5805	0.1438
4	465.8	1197.3	10.76	1.3864	145.0	0.5322	0.0473
5	454.9	1122.5	10.75	1.3882	128.8	0.2883	-0.1572
run no.4		t_a=25°C			Δp_{pitot}=210.1 N/m^2, v_{hi}=18.89m/s		
1	407.9	1313.0	10.70	1.7660	196.7	1.3305	0.8765
2	466.8	1199.1	10.77	1.7537	163.9	0.8018	0.3340
3	462.6	1175.0	10.76	1.7566	148.0	0.5760	0.1393
4	466.3	1195.8	10.77	1.7550	143.5	0.5078	0.0230
5	457.7	1118.9	10.78	1.7526	125.2	0.2240	-0.2215
run no.5		t_a=25°C			Δp_{pitot}=314.6N/m^2, v_{hi}=23.12m/s		
1	410.4	1328.1	10.74	2.1540	211.8	1.5340	1.0800
2	464.5	1198.1	10.75	2.1520	162.9	0.8000	0.3323
3	465.4	1169.7	10.79	2.1424	142.7	0.4845	0.0478
4	468.3	1192.4	10.79	2.1426	140.1	0.4489	-0.0359
5	457.1	1111.6	10.77	2.1462	117.9	0.1192	-0.3262

Table D.9 continued:

Lat. no.	Δp_p [N/m^2]	p_{atm}-p_{p1} [N/m^2]	v_1 [m/s]	v_{hi}/v_1	p_h-p_1 [N/m^2]	K_i-$\alpha_{eh}(v_h/v_1)^2$	K_{ivr}
run no.6		t_a =25°C			Δp_{pitot} =413.3N/m^2, v_{hi} =26.50m/s		
1	409.7	1340.8	10.72	2.4713	224.5	1.7283	1.2744
2	466.1	1195.4	10.77	2.4617	160.2	0.7511	0.2834
3	464.9	1164.6	10.79	2.4569	137.6	0.4123	-0.0245
4	466.0	1188.4	10.76	2.4626	136.1	0.4012	-0.0837
5	458.8	1104.0	10.80	2.4546	110.3	0.0019	-0.4435

Table D.10: Five laterals at 80mm pitch, open 2D configuration, p_{atm}=100740N/m^2 (fig.4.18).

Lat. no.	Δp_p [N/m^2]	$p_{atm}-p_{pl}$ [N/m^2]	v_l [m/s]	v_{hi}/v_l	p_h-p_l [N/m^2]	$K_i-\alpha_{eh}(v_h/v_l)^2$	K_{ivr}
run no.1		t_a=25°C			Δp_{pitot}=14.7N/m^2, v_{hi}=4.99m/s		
1	421.6	1267.5	10.91	0.4574	151.2	0.5717	0.1177
3	473.9	1175.5	10.90	0.4578	148.5	0.5276	0.0909
5	467.8	1140.9	10.91	0.4574	147.1	0.4963	0.0509
7	500.9	1166.1	10.90	0.4579	143.2	0.4580	0.0100
9	436.7	1229.8	10.93	0.4564	141.1	0.4173	-0.0145
run no.2		t_a=25°C			Δp_{pitot}=60.6N/m^2, v_{hi}=10.15m/s		
1	417.8	1277.2	10.85	0.9351	160.9	0.7345	0.2805
3	474.9	1181.5	10.91	0.9297	154.5	0.6082	0.1715
5	466.3	1147.4	10.89	0.9317	153.7	0.5976	0.1521
7	498.4	1170.8	10.87	0.9336	147.8	0.5359	0.0879
9	432.8	1230.0	10.88	0.9327	141.3	0.4397	0.0079
run no.3		t_a=25°C			Δp_{pitot}=125.1N/m^2, v_{hi}=14.58m/s		
1	418.0	1284.2	10.85	1.3432	167.9	0.8354	0.3814
3	471.8	1182.9	10.87	1.3407	155.9	0.6446	0.2078
5	462.9	1152.5	10.85	1.3440	158.8	0.6877	0.2422
7	495.5	1172.3	10.83	1.3456	149.4	0.5709	0.1229
9	433.3	1230.2	10.89	1.3392	141.4	0.4393	0.0076
run no.4		t_a=25°C			Δp_{pitot}=222.8N/m^2, v_{hi}=19.46m/s		
1	415.9	1293.7	10.82	1.7979	177.4	0.9865	0.5326
3	472.5	1182.9	10.88	1.7879	155.9	0.6404	0.2037
5	463.3	1155.9	10.85	1.7930	162.2	0.7353	0.2898
7	498.5	1172.6	10.87	1.7902	149.6	0.5614	0.1134
9	433.9	1227.5	10.90	1.7859	138.7	0.3975	-0.0343
run no.5		t_a=25°C			Δp_{pitot}=343.9N/m^2, v_{hi}=24.18m/s		
1	417.2	1304.8	10.84	2.2301	188.5	1.1383	0.6843
3	472.7	1181.8	10.89	2.2208	154.8	0.6230	0.1863
5	463.7	1158.8	10.86	2.2270	165.1	0.7754	0.3300
7	497.4	1171.4	10.86	2.2270	148.4	0.5488	0.1008
9	433.8	1224.3	10.89	2.2194	135.5	0.3521	-0.0797

Table D.11: Upstream backward facing step, open 2D configuration, a=10mm, b=15mm, p_{atm}=100525N/m^2 (fig.4.20).

Lat. no.	Δp_p [N/m^2]	$p_{atm}-p_{pl}$ [N/m^2]	v_l [m/s]	v_{hi}/v_l	p_h-p_l [N/m^2]	$K_i-\alpha_{eh}(v_h/v_l)^2$	K_{ivr}
run no.1		t_a=25°C			Δp_{pitot}=15.6N/m^2, v_{hi}=5.16m/s		
1	407.5	1244.3	10.71	0.4820	128.0	0.3126	-0.1413
2	457.3	1182.2	10.66	0.4839	147.0	0.6015	0.1338
3	457.0	1171.3	10.69	0.4825	144.2	0.5486	0.1119
4	461.0	1199.5	10.71	0.4819	147.3	0.5900	0.1051
5	450.6	1137.3	10.70	0.4823	143.6	0.5282	0.0828
6	474.3	1134.8	10.71	0.4820	138.6	0.4582	0.0513
7	480.8	1160.2	10.67	0.4837	137.2	0.4587	0.0108
8	412.4	1213.8	10.67	0.4838	136.3	0.4472	0.0114
9	415.2	1222.1	10.63	0.4853	133.4	0.4163	-0.0155
10	392.8	1221.0	10.67	0.4837	133.8	0.4125	-0.0596
run no.2		t_a=25°C			Δp_{pitot}=50.8N/m^2, v_{hi}=9.30m/s		
1	407.7	1225.6	10.71	0.8685	109.3	0.0327	-0.4212
2	459.6	1189.6	10.69	0.8699	154.4	0.7001	0.2324
3	453.7	1176.8	10.65	0.8734	149.8	0.6484	0.2116
4	456.9	1205.1	10.65	0.8731	152.8	0.6949	0.2100
5	447.7	1142.3	10.66	0.8726	148.5	0.6172	0.1718
6	469.4	1140.5	10.64	0.8739	144.3	0.5669	0.1600
7	480.0	1164.6	10.66	0.8728	141.6	0.5286	0.0806
8	412.3	1217.6	10.67	0.8722	140.0	0.5044	0.0685
9	418.9	1223.1	10.69	0.8705	134.4	0.4120	-0.0197
10	393.4	1215.9	10.68	0.8711	128.6	0.3315	-0.1406
run no.3		t_a=25°C			Δp_{pitot}=126.0N/m^2, v_{hi}=14.65m/s		
1	408.0	1232.4	10.72	1.3674	116.1	0.1321	-0.3218
2	458.9	1188.0	10.68	1.3713	152.8	0.6804	0.2127
3	456.0	1179.2	10.68	1.3717	152.1	0.6716	0.2348
4	458.3	1210.5	10.67	1.3730	158.2	0.7683	0.2834
5	448.1	1149.7	10.67	1.3738	155.9	0.7260	0.2806
6	473.0	1145.3	10.69	1.3707	149.2	0.6210	0.2141
7	480.5	1168.8	10.66	1.3739	145.9	0.5896	0.1416
8	412.9	1220.3	10.67	1.3727	142.7	0.5417	0.1059
9	420.3	1224.5	10.71	1.3684	135.8	0.4250	-0.0068
10	396.0	1212.8	10.72	1.3668	125.6	0.2729	-0.1993

Table D.11 continued:

Lat. no.	Δp_p [N/m^2]	$p_{atm}-p_{p1}$ [N/m^2]	v_l [m/s]	v_{hi}/v_l	p_h-p_l [N/m^2]	$K_i-\alpha_{eh}(v_h/v_l)^2$	K_{ivr}
run no.4		t_a=25°C			Δp_{pitot}=237.N/m^2, v_{hi}=20.1m/s		
1	405.4	1265.9	10.67	1.8841	149.6	0.6470	0.1930
2	461.5	1172.2	10.72	1.8761	137.0	0.4327	-0.0350
3	453.7	1173.6	10.65	1.8880	146.6	0.6003	0.1636
4	456.5	1211.8	10.65	1.8885	159.6	0.7983	0.3134
5	443.5	1153.6	10.60	1.8963	159.8	0.8111	0.3656
6	470.6	1143.4	10.66	1.8865	147.2	0.6045	0.1976
7	484.2	1170.9	10.71	1.8777	148.0	0.6032	0.1552
8	411.9	1219.3	10.66	1.8867	141.8	0.5327	0.0968
9	418.8	1220.9	10.69	1.8818	132.1	0.3779	-0.0539
10	395.6	1204.1	10.71	1.8770	116.8	0.1447	-0.3274
run no.5		t_a=25°C			Δp_{pitot}=354.7N/m^2, v_{hi}=24.58m/s		
1	403.1	1315.4	10.63	2.3112	199.1	1.4083	0.9544
2	456.9	1155.0	10.66	2.3055	119.8	0.1961	-0.2717
3	455.5	1163.5	10.68	2.3021	136.5	0.4395	0.0027
4	457.9	1209.0	10.67	2.3040	156.8	0.7483	0.2634
5	444.4	1153.3	10.62	2.3151	159.5	0.8017	0.3563
6	469.4	1141.5	10.65	2.3088	145.3	0.5811	0.1742
7	480.6	1166.9	10.67	2.3045	143.9	0.5603	0.1123
8	413.0	1216.6	10.68	2.3023	139.1	0.4870	0.0511
9	418.9	1215.9	10.69	2.2997	127.2	0.3042	-0.1276
10	389.4	1191.5	10.62	2.3151	104.3	-0.0144	-0.4865

Table D.12: Upstream backward facing step, open 2D configuration, a=10mm, b=55mm, p_{atm}=100477N/m^2 (fig.4.21).

Lat. no.	Δp_p [N/m^2]	$p_{atm}-p_{p1}$ [N/m^2]	v_1 [m/s]	v_{hi}/v_1	p_h-p_1 [N/m^2]	$K_i-\alpha_{eh}(v_h/v_1)^2$	K_{ivr}
run no.1		t_a=25°C			Δp_{pitot}=14.0N/m^2, v_{hi}=4.88m/s		
2	492.1	1229.2	11.11	0.4398	163.9	0.6716	0.2038
3	484.1	1208.5	11.04	0.4424	156.2	0.5892	0.1525
4	487.5	1229.6	11.05	0.4421	154.9	0.5705	0.0857
5	478.1	1172.4	11.05	0.4419	153.6	0.5399	0.0944
6	503.3	1164.2	11.06	0.4418	147.5	0.4587	0.0518
7	511.3	1188.7	11.03	0.4427	147.9	0.4803	0.0323
8	437.9	1245.3	11.04	0.4422	146.4	0.4586	0.0228
9	444.2	1235.9	11.05	0.4419	142.9	0.4063	-0.0255
10	418.3	1263.7	11.07	0.4414	143.0	0.4052	-0.0669
run no.2		t_a=25°C			Δp_{pitot}=54.0N/m^2, v_{hi}=9.59m/s		
2	486.9	1248.5	11.04	0.8689	169.6	0.7770	0.3093
3	479.5	1230.9	10.98	0.8734	163.3	0.7113	0.2746
4	482.3	1253.0	10.98	0.8737	163.5	0.7173	0.2324
5	471.1	1193.4	10.96	0.8750	159.8	0.6624	0.2170
6	497.9	1180.5	10.99	0.8727	154.0	0.5748	0.1679
7	514.7	1233.5	11.07	0.8665	153.7	0.5485	0.1005
8	434.8	1267.5	11.00	0.8722	148.8	0.5087	0.0729
9	437.6	1256.6	10.96	0.8753	142.8	0.4379	0.0062
10	414.0	1277.1	11.00	0.8722	138.1	0.3604	-0.1117
run no.3		t_a=25°C			Δp_{pitot}=126.0N/m^2, v_{hi}=14.65m/s		
2	493.7	1282.2	11.12	1.3174	176.5	0.8385	0.3708
3	483.0	1262.1	11.02	1.3291	166.9	0.7460	0.3092
4	488.5	1276.2	11.06	1.3251	170.0	0.7767	0.2918
5	475.3	1225.7	11.01	1.3303	168.0	0.7558	0.3103
6	502.0	1212.1	11.04	1.3274	160.4	0.6467	0.2398
7	514.1	1246.4	11.06	1.3244	157.5	0.6041	0.1561
8	437.8	1294.4	11.04	1.3272	152.2	0.5400	0.1042
9	443.9	1284.7	11.05	1.3265	146.4	0.4575	0.0257
10	419.1	1303.0	11.07	1.3231	134.8	0.2894	-0.1827

Table D.12 continued:

Lat. no.	Δp_p [N/m^2]	$p_{atm}-p_{pl}$ [N/m^2]	v_l [m/s]	v_{hi}/v_l	p_h-p_l [N/m^2]	$K_i-\alpha_{eh}(v_h/v_l)^2$	K_{ivr}
run no.4	t_a=25°C				Δp_{pitot}=222.0N/m^2, v_{hi}=19.45m/s		
2	487.8	1294.0	11.05	1.7605	176.8	0.8743	0.4066
3	481.0	1271.8	11.00	1.7686	163.5	0.7092	0.2724
4	484.5	1292.0	11.01	1.7673	173.0	0.8411	0.3563
5	472.2	1240.1	10.97	1.7724	169.6	0.7966	0.3511
6	499.7	1234.6	11.01	1.7668	160.7	0.6624	0.2555
7	511.6	1268.2	11.03	1.7631	156.3	0.5998	0.1518
8	437.2	1309.5	11.03	1.7633	151.8	0.5382	0.1024
9	442.8	1297.2	11.03	1.7633	142.7	0.4119	-0.0198
10	418.1	1320.9	11.06	1.7588	128.6	0.2081	-0.2640
run no.5	t_a=25°C				Δp_{pitot}=334.0N/m^2, v_{hi}=23.86m/s		
2	488.5	1235.5	11.06	2.1571	176.0	0.8581	0.3904
3	484.1	1215.1	11.04	2.1606	157.3	0.6042	0.1674
4	487.0	1242.9	11.04	2.1608	172.2	0.8139	0.3290
5	482.3	1209.5	11.10	2.1484	176.2	0.8326	0.3872
6	502.8	1181.4	11.05	2.1591	158.2	0.6114	0.2045
7	511.3	1211.3	11.03	2.1624	155.4	0.5869	0.1389
8	438.4	1252.2	11.05	2.1587	151.6	0.5287	0.0928
9	443.5	1245.1	11.04	2.1602	138.8	0.3517	-0.0801
10	418.3	1250.5	11.07	2.1559	120.9	0.0986	-0.3735

Table D.13: Upstream backward facing step, open 2D configuration, a=10mm, b=100mm, p_{atm}=100068 N/m^2 (fig.4.22).

Lat. no.	Δp_p [N/m^2]	p_{atm}-p_{p1} [N/m^2]	v_l [m/s]	v_{hi}/v_l	p_h-p_l [N/m^2]	K_i-$\alpha_{eh}(v_h/v_l)^2$	K_{ivr}
run no.1		t_a=26°C			Δp_{pitot}=15.0N/m^2, v_{hi}=5.07m/s		
3	482.4	1215.1	11.05	0.4591	159.6	0.6473	0.2106
4	492.3	1243.2	11.14	0.4555	159.7	0.6155	0.1306
5	475.6	1175.9	11.05	0.4590	153.7	0.5547	0.1092
6	500.1	1168.1	11.05	0.4591	147.4	0.4726	0.0657
7	503.4	1193.4	10.97	0.4624	145.2	0.4788	0.0308
8	432.2	1251.2	10.99	0.4618	142.3	0.4339	-0.0020
9	441.5	1235.3	11.05	0.4594	141.2	0.3984	-0.0334
10	410.5	1241.2	10.97	0.4624	138.2	0.3834	-0.0887
run no.2		t_a=26°C			Δp_{pitot}=58.0N/m^2, v_{hi}=9.98m/s		
3	476.3	1238.2	10.97	0.9092	173.1	0.8699	0.4331
4	483.0	1250.1	11.02	0.9054	169.0	0.7934	0.3085
5	473.9	1212.5	11.03	0.9046	164.4	0.7148	0.2694
6	498.9	1194.1	11.04	0.9041	157.0	0.6140	0.2071
7	505.2	1209.4	10.99	0.9077	152.3	0.5714	0.1234
8	432.1	1279.5	10.99	0.9082	148.7	0.5250	0.0891
9	438.4	1259.5	11.00	0.9071	143.0	0.4401	0.0083
10	409.8	1272.4	10.96	0.9102	135.6	0.3495	-0.1226
run no.3		t_a=26°C			Δp_{pitot}=128.0N/m^2, v_{hi}=14.82m/s		
3	476.4	1266.6	10.97	1.3509	183.0	1.0114	0.5747
4	480.8	1278.3	10.99	1.3486	174.3	0.8815	0.3966
5	473.2	1227.1	11.02	1.3451	171.2	0.8153	0.3699
6	497.9	1226.0	11.02	1.3447	160.6	0.6693	0.2624
7	504.6	1234.2	10.99	1.3494	156.0	0.6271	0.1791
8	430.4	1297.4	10.96	1.3525	151.4	0.5738	0.1380
9	439.1	1284.4	11.01	1.3466	146.3	0.4834	0.0517
10	411.7	1286.4	10.99	1.3488	134.2	0.3205	-0.1516

Table D.13 continued:

Lat. no.	Δp_p [N/m^2]	p_{atm}-p_{p1} [N/m^2]	v_l [m/s]	v_{hi}/v_l	p_h-p_l [N/m^2]	K_i-$\alpha_{eh}(v_h/v_l)^2$	K_{ivr}
run no.4		t_a =28°C			Δp_{pitot} =225.0N/m^2, v_{hi} =19.72m/s		
3	484.3	1323.6	11.10	1.7771	193.5	1.1191	0.6824
4	481.0	1298.9	11.02	1.7895	178.3	0.9404	0.4556
5	470.5	1255.1	11.01	1.7906	174.8	0.8847	0.4393
6	496.8	1240.9	11.04	1.7866	161.2	0.6855	0.2786
7	503.5	1264.5	11.00	1.7929	157.6	0.6580	0.2100
8	432.7	1316.6	11.01	1.7903	152.1	0.5761	0.1403
9	439.4	1301.6	11.03	1.7870	143.3	0.4428	0.0111
10	411.8	1305.9	11.01	1.7906	127.1	0.2229	-0.2493
run no.5		t_a =28°C			Δp_{pitot} =334.0N/m^2, v_{hi} =24.02m/s		
3	475.1	1309.9	10.98	2.1878	195.3	1.1997	0.7630
4	480.3	1307.6	11.01	2.1822	179.3	0.9597	0.4748
5	472.3	1258.2	11.04	2.1771	175.9	0.8896	0.4442
6	497.8	1247.0	11.05	2.1745	159.8	0.6623	0.2554
7	499.7	1263.4	10.95	2.1934	154.2	0.6276	0.1796
8	432.8	1320.8	11.02	2.1808	150.8	0.5563	0.1205
9	439.0	1305.8	11.03	2.1785	139.6	0.3928	-0.0389
10	412.3	1309.9	11.02	2.1799	120.0	0.1190	-0.3531

Table D.14: Upstream backward facing step, open 2D configuration, a=20mm, b=15mm, p_{atm}=100525N/m^2 (fig.4.23).

Lat. no.	Δp_p [N/m^2]	p_{atm}-p_{p1} [N/m^2]	v_l [m/s]	v_{hi}/v_l	p_h-p_p [N/m^2]	K_i-$\alpha_{eh}(v_h/v_l)^2$	K_{ivr}
run no.1		t_a=24.5°C			Δp_{pitot}=15.6N/m^2, v_{hi}=5.16m/s		
1	408.9	1254.1	10.72	0.4808	137.8	0.4484	-0.0056
2	465.7	1180.3	10.77	0.4789	145.1	0.5318	0.0641
3	461.3	1169.9	10.74	0.4799	142.9	0.5070	0.0703
4	466.0	1198.1	10.77	0.4789	145.8	0.5422	0.0574
5	455.0	1135.2	10.75	0.4796	141.4	0.4747	0.0292
6	479.3	1134.7	10.76	0.4792	138.5	0.4338	0.0269
7	488.0	1162.1	10.75	0.4797	139.2	0.4553	0.0073
8	419.7	1212.9	10.77	0.4787	135.4	0.3937	-0.0422
9	424.6	1221.6	10.76	0.4790	132.8	0.3584	-0.0734
10	398.0	1219.9	10.75	0.4798	132.7	0.3657	-0.1064
run no.2		t_a=24.5°C			Δp_{pitot}=52.8N/m^2, v_{hi}=9.47m/s		
1	412.0	1279.0	10.77	0.8796	162.7	0.7978	0.3439
2	466.9	1177.5	10.78	0.8785	142.3	0.4836	0.0159
3	459.3	1171.7	10.72	0.8838	144.7	0.5436	0.1068
4	463.0	1202.4	10.73	0.8829	150.2	0.6219	0.1371
5	452.0	1140.0	10.71	0.8843	146.3	0.5610	0.1155
6	473.9	1138.1	10.69	0.8857	142.0	0.5091	0.1022
7	487.9	1164.8	10.75	0.8814	141.8	0.4952	0.0472
8	418.4	1215.0	10.75	0.8811	137.5	0.4325	-0.0033
9	423.2	1222.3	10.74	0.8816	133.5	0.3764	-0.0553
10	399.1	1214.9	10.76	0.8801	127.6	0.2855	-0.1866
run no.3		t_a=24.5			Δp_{pitot}=127.0N/m^2, v_{hi}=14.70m/s		
1	429.9	1370.5	11.03	1.3321	254.2	1.9672	1.5132
2	459.8	1156.8	10.69	1.3746	121.6	0.2098	-0.2579
3	458.5	1166.7	10.71	1.3725	139.7	0.4736	0.0368
4	462.4	1204.3	10.72	1.3711	152.0	0.6534	0.1685
5	451.1	1145.2	10.70	1.3738	151.5	0.6436	0.1982
6	475.5	1141.5	10.71	1.3719	145.3	0.5519	0.1450
7	489.0	1167.0	10.76	1.3658	144.1	0.5233	0.0753
8	416.3	1216.3	10.72	1.3710	138.8	0.4623	0.0265
9	423.0	1221.4	10.74	1.3682	132.6	0.3637	-0.0680
10	399.9	1210.1	10.77	1.3640	122.9	0.2121	-0.2600

Table D.15: Upstream backward facing step, open 2D configuration, a=20mm, b=55mm, p_{atm}=100525N/m^2 (fig.4.24).

Lat. no.	Δp_p [N/m^2]	p_{atm}-p_{pl} [N/m^2]	v_l [m/s]	v_{hi}/v_l	p_h-p_l [N/m^2]	K_i-$\alpha_{eh}(v_h/v_l)^2$	K_{ivr}
run no.1		t_a =24.4°C			Δp_{pitot} =40.1N/m^2, v_{hi} =8.25m/s		
2	520.6	1185.4	11.45	0.7208	150.2	0.3599	-0.1078
3	511.7	1190.8	11.38	0.7254	163.8	0.5623	0.1255
4	517.7	1222.4	11.41	0.7230	170.1	0.6325	0.1476
5	505.9	1156.9	11.39	0.7244	163.1	0.5394	0.0940
6	537.1	1157.4	11.44	0.7212	161.3	0.5029	0.0960
7	545.0	1180.4	11.41	0.7230	157.4	0.4708	0.0228
8	465.9	1232.6	11.44	0.7213	155.1	0.4331	-0.0028
9	470.6	1238.4	11.42	0.7229	149.6	0.3703	-0.0614
10	435.1	1228.9	11.31	0.7293	141.6	0.3007	-0.1714
run no.2		t_a =24.4°C			Δp_{pitot} =122.1N/m^2, v_{hi} =14.41m/s		
2	519.6	1153.5	11.44	1.2596	118.3	-0.0511	-0.5188
3	514.5	1186.5	11.41	1.2627	159.5	0.4940	0.0572
4	517.7	1225.2	11.41	1.2625	172.9	0.6694	0.1845
5	505.8	1164.9	11.39	1.2651	171.1	0.6453	0.1999
6	532.1	1160.7	11.38	1.2656	164.5	0.5661	0.1592
7	545.4	1185.5	11.42	1.2620	162.5	0.5362	0.0882
8	464.0	1235.4	11.41	1.2625	157.9	0.4799	0.0441
9	473.8	1240.3	11.46	1.2572	151.5	0.3805	-0.0513
10	441.3	1227.1	11.41	1.2630	139.9	0.2478	-0.2244
run no.3		t_a =25°C			Δp_{pitot} =218.9N/m^2, v_{hi} =19.31m/s		
2	518.6	1143.7	11.44	1.6884	108.5	-0.1748	-0.6425
3	517.5	1168.9	11.46	1.6853	141.8	0.2522	-0.1845
4	518.8	1220.0	11.44	1.6884	167.8	0.5978	0.1129
5	506.2	1165.7	11.40	1.6931	172.0	0.6546	0.2092
6	535.0	1159.7	11.43	1.6895	163.6	0.5421	0.1352
7	548.5	1185.0	11.46	1.6844	162.1	0.5177	0.0697
8	465.5	1235.7	11.44	1.6875	158.2	0.4770	0.0411
9	474.9	1236.3	11.48	1.6815	147.6	0.3255	-0.1062
10	443.3	1219.5	11.45	1.6869	132.3	0.1413	-0.3308

Table D.16: Upstream backward facing step, open 2D configuration, a-20mm, b=100mm, p_{atm}=99982 N/m^2 (fig.4.25).

Lat. no.	Δp_p [N/m^2]	p_{atm}-p_{p1} [N/m^2]	v_1 [m/s]	v_{hi}/v_1	p_h-p_1 [N/m^2]	K_i-$\alpha_{eh}(v_h/v_1)^2$	K_{ivr}
run no.1		t_a=26.5°C			Δp_{pitot}=17.5N/m^2, v_{hi}=5.49m/s		
3	481.0	1208.5	11.05	0.4969	157.0	0.6186	0.1818
4	486.6	1225.1	11.08	0.4953	157.4	0.6121	0.1272
5	472.7	1159.9	11.03	0.4976	150.0	0.5171	0.0716
6	502.7	1156.9	11.10	0.4946	147.1	0.4576	0.0507
7	511.7	1187.1	11.08	0.4952	146.1	0.4555	0.0075
8	439.1	1249.3	11.10	0.4944	143.9	0.4212	-0.0146
9	443.1	1234.7	11.08	0.4954	141.2	0.3908	-0.0409
10	410.8	1250.0	10.99	0.4994	139.6	0.4031	-0.0691
run no.2		t_a=26.5°C			Δp_{pitot}=55.5N/m^2, v_{hi}=9.77m/s		
3	481.4	1204.0	11.05	0.8843	156.2	0.6042	0.1674
4	484.0	1221.9	11.05	0.8847	161.2	0.6794	0.1945
5	478.1	1186.6	11.10	0.8807	160.4	0.6378	0.1923
6	497.5	1167.9	11.03	0.8858	151.3	0.5391	0.1322
7	508.1	1187.5	11.04	0.8851	149.8	0.5227	0.0747
8	436.8	1246.4	11.07	0.8831	146.7	0.4719	0.0360
9	442.0	1238.2	11.06	0.8835	142.8	0.4197	-0.0121
10	414.7	1245.9	11.05	0.8845	134.8	0.3138	-0.1583
run no.3		t_a=26.5°C			Δp_{pitot}=116.0N/m^2, v_{hi}=14.13m/s		
3	478.2	1207.1	11.01	1.2832	151.9	0.5594	0.1226
4	481.9	1225.2	11.02	1.2822	159.6	0.6668	0.1819
5	478.0	1193.0	11.10	1.2733	161.8	0.6577	0.2123
6	497.8	1166.4	11.04	1.2803	153.3	0.5664	0.1595
7	507.1	1200.3	11.03	1.2811	150.9	0.5437	0.0957
8	435.4	1255.0	11.05	1.2791	147.3	0.4885	0.0526
9	442.0	1246.9	11.06	1.2774	142.3	0.4127	-0.0191
10	412.2	1255.7	11.01	1.2834	130.5	0.2660	-0.2061

Table D.16 continued:

Lat. no.	Δp_p [N/m^2]	$p_{atm}-p_{p1}$ [N/m^2]	v_l [m/s]	v_{hi}/v_l	p_h-p_l [N/m^2]	$K_i-\alpha_{eh}(v_h/v_l)^2$	K_{ivr}
run no.4		t_a=26.5°C			Δp_{pitot}=222.0N/m^2, v_{hi}=19.55m/s		
3	483.4	1194.3	11.05	1.7697	141.0	0.3929	-0.0439
4	484.2	1218.3	11.05	1.7693	149.4	0.5122	0.0273
5	474.8	1176.6	11.06	1.7679	159.1	0.6352	0.1898
6	494.8	1156.0	11.00	1.7767	149.4	0.5242	0.1173
7	504.9	1191.0	11.01	1.7751	148.8	0.5208	0.0728
8	436.7	1250.6	11.07	1.7665	144.4	0.4401	0.0043
9	437.9	1235.3	11.00	1.7764	137.3	0.3617	-0.0701
10	414.7	1238.4	11.05	1.7690	117.4	0.0678	-0.4043
run no.5		t_a=26.5°C			Δp_{pitot}=326.0N/m^2, v_{hi}=23.69m/s		
3	482.6	1184.0	11.07	2.1398	132.3	0.2620	-0.1748
4	485.5	1207.0	11.07	2.1404	135.2	0.3055	-0.1794
5	474.4	1177.2	11.05	2.1435	152.9	0.5502	0.1048
6	496.0	1153.9	11.02	2.1501	142.5	0.4208	0.0139
7	504.1	1183.9	10.99	2.1544	143.0	0.4433	-0.0047
8	435.1	1238.0	11.04	2.1451	140.4	0.3929	-0.0429
9	437.6	1227.7	11.00	2.1532	130.4	0.2653	-0.1665
10	413.4	1233.2	11.03	2.1474	111.3	-0.0121	-0.4842

Table D.17: Upstream triangular ramp, open 2D configuration, b=40mm, p_{atm}=101005N/m^2 (fig.4.27).

Lat. no.	Δp_p [N/m^2]	p_{atm}-p_{p1} [N/m^2]	v_1 [m/s]	v_{hi}/v_1	p_h-p_1 [N/m^2]	K_i-$\alpha_{eh}(v_h/v_1)^2$	K_{ivr}
run no.1		t_a=28°C			Δp_{pitot}=17.1N/m^2, v_{hi}=5.41m/s		
1	406.8	1215.3	10.71	0.5053	137.3	0.4582	0.0043
2	463.3	1149.3	10.76	0.5028	150.6	0.6266	0.1588
3	456.9	1139.0	10.72	0.5049	144.7	0.5569	0.1201
4	462.7	1155.2	10.75	0.5034	146.3	0.5693	0.0844
5	448.8	1096.6	10.70	0.5059	141.0	0.5008	0.0553
6	470.6	1087.4	10.68	0.5066	135.7	0.4313	0.0244
7	485.7	1127.7	10.75	0.5034	136.4	0.4260	-0.0220
8	415.9	1175.9	10.73	0.5041	134.6	0.4075	-0.0283
9	419.9	1159.4	10.72	0.5048	130.5	0.3513	-0.0805
10	393.4	1163.2	10.69	0.5059	128.3	0.3287	-0.1434
run no.2		t_a=29.5°C			Δp_{pitot}=54.7N/m^2, v_{hi}=9.70m/s		
1	407.1	1207.4	10.73	0.9044	126.2	0.2935	-0.1604
2	460.3	1145.7	10.74	0.9033	157.2	0.7420	0.2743
3	454.3	1134.1	10.70	0.9067	151.5	0.6732	0.2365
4	460.3	1156.1	10.74	0.9037	154.1	0.6991	0.2143
5	446.5	1094.4	10.69	0.9081	148.2	0.6210	0.1755
6	468.0	1086.0	10.67	0.9093	140.6	0.5189	0.1120
7	481.1	1127.1	10.71	0.9058	141.8	0.5293	0.0813
8	413.7	1174.5	10.72	0.9055	137.8	0.4705	0.0347
9	420.2	1155.5	10.74	0.9035	132.2	0.3777	-0.0541
10	391.3	1159.3	10.68	0.9087	124.1	0.2800	-0.1922
run no.3		t_a=31°C			Δp_{pitot}=147.5N/m^2, v_{hi}=15.72m/s		
1	404.9	1204.6	10.71	1.4679	134.7	0.3777	-0.0763
2	458.9	1141.8	10.74	1.4634	154.8	0.6493	0.1816
3	452.8	1134.7	10.70	1.4690	153.0	0.6384	0.2016
4	456.5	1156.3	10.71	1.4684	159.8	0.7384	0.2535
5	443.1	1096.6	10.66	1.4748	155.8	0.6879	0.2425
6	471.9	1096.4	10.74	1.4638	147.3	0.5377	0.1308
7	480.1	1130.7	10.72	1.4662	143.5	0.4979	0.0499
8	407.6	1153.6	10.64	1.4774	137.0	0.4349	-0.0009
9	416.8	1144.3	10.71	1.4682	128.7	0.2883	-0.1434
10	397.1	1167.0	10.70	1.4694	115.9	0.1068	-0.3653

Table D.17 continued:

Lat. no.	Δp_p [N/m^2]	$p_{atm}-p_{p1}$ [N/m^2]	v_l [m/s]	v_{hi}/v_l	p_h-p_l [N/m^2]	$K_i-\alpha_{eh}(v_h/v_l)^2$	K_{ivr}
run no.4	t_a =32°C				Δp_{pitot}=241.3N/m^2, v_{hi}=20.46m/s		
1	406.0	1257.1	10.77	1.9005	179.7	1.0956	0.6416
2	459.4	1130.8	10.76	1.9012	141.0	0.5081	0.0403
3	450.2	1123.3	10.68	1.9153	148.4	0.6500	0.2133
4	457.5	1155.0	10.66	1.9200	158.6	0.8187	0.3338
5	450.9	1121.7	10.63	1.9249	153.8	0.7459	0.3005
6	469.4	1091.2	10.67	1.9180	146.6	0.6260	0.2191
7	475.7	1110.5	10.69	1.9144	144.6	0.5960	0.1480
8	411.0	1162.2	10.63	1.9254	136.4	0.4970	0.0612
9	415.8	1138.3	10.73	1.9075	130.1	0.3635	-0.0683
10	391.8	1140.6	10.70	1.9126	115.9	0.1614	-0.3107

Table D.18: Upstream triangular ramp, open 2D configuration, b=80mm, p_{atm}=100725N/m^2 (fig.4.28).

Lat. no.	Δp_p [N/m^2]	$p_{atm}-p_{pl}$ [N/m^2]	v_l [m/s]	v_{hi}/v_l	p_h-p_l [N/m^2]	$K_i-\alpha_{eh}(v_h/v_l)^2$	K_{ivr}
run no.1			t_a=29°C		Δp_{pitot}=15.6N/m^2, v_{hi}=5.19m/s		
1	409.2	1230.5	10.77	0.4820	150.6	0.6462	0.1923
2	465.0	1156.6	10.81	0.4802	152.4	0.6469	0.1791
3	457.6	1140.8	10.75	0.4827	144.3	0.5481	0.1114
4	463.3	1163.6	10.70	0.4850	144.0	0.5660	0.0811
5	456.2	1112.5	10.74	0.4830	141.1	0.4945	0.0491
6	477.9	1104.2	10.75	0.4829	136.4	0.4300	0.0231
7	483.2	1130.6	10.76	0.4823	135.8	0.4235	-0.0245
8	416.1	1179.2	10.65	0.4874	133.9	0.4387	0.0028
9	419.0	1158.9	10.73	0.4838	130.5	0.3590	-0.0727
10	394.1	1179.6	10.73	0.4838	130.6	0.3628	-0.1093
run no.2			t_a=29°C		Δp_{pitot}=55.7N/m^2, v_{hi}=9.79m/s		
1	406.8	1223.4	10.73	0.9128	152.3	0.6858	0.2318
2	459.1	1149.8	10.73	0.9126	158.0	0.7607	0.2930
3	451.5	1132.0	10.67	0.9179	151.0	0.6815	0.2448
4	460.7	1158.2	10.75	0.9114	153.1	0.6830	0.1981
5	450.9	1110.5	10.75	0.9113	148.0	0.5957	0.1502
6	472.5	1097.1	10.73	0.9126	142.3	0.5228	0.1159
7	481.2	1117.6	10.72	0.9136	140.3	0.5055	0.0575
8	412.0	1169.0	10.70	0.9156	135.6	0.4464	0.0106
9	417.5	1150.6	10.71	0.9148	130.6	0.3670	-0.0647
10	394.3	1171.1	10.73	0.9128	125.1	0.2788	-0.1934
run no.3			t_a=31°C		Δp_{pitot}=138.7N/m^2, v_{hi}=15.51m/s		
1	404.3	1215.0	10.71	1.4481	148.9	0.6552	0.2012
2	458.5	1143.4	10.75	1.4427	157.6	0.7605	0.2928
3	451.4	1125.8	10.70	1.4501	152.8	0.7114	0.2746
4	456.9	1154.3	10.72	1.4464	158.8	0.7926	0.3077
5	446.7	1107.1	10.72	1.4468	155.9	0.7384	0.2930
6	472.1	1097.2	10.76	1.4421	147.1	0.5988	0.1919
7	479.3	1117.5	10.73	1.4462	142.3	0.5460	0.0980
8	414.5	1168.2	10.76	1.4420	138.2	0.4741	0.0383
9	417.0	1144.6	10.72	1.4466	130.6	0.3727	-0.0590
10	394.3	1159.1	10.75	1.4425	118.6	0.1847	-0.2874

Table D.18 continued:

Lat. no.	Δp_p [N/m^2]	p_{atm}-p_{p1} [N/m^2]	v_l [m/s]	v_{hi}/v_l	p_h-p_l [N/m^2]	K_i-$\alpha_{eh}(v_h/v_l)^2$	K_{ivr}
run no.4	t_a=31°C				Δp_{pitot}=247.2 N/m^2, v_{hi}=20.70 m/s		
1	403.8	1209.4	10.71	1.9323	149.2	0.6580	0.2041
2	458.1	1136.2	10.76	1.9242	146.9	0.5965	0.1288
3	453.8	1121.6	10.74	1.9275	150.0	0.6497	0.2130
4	455.8	1150.4	10.72	1.9311	160.0	0.8104	0.3255
5	446.8	1108.1	10.73	1.9287	158.7	0.7753	0.3298
6	470.7	1092.8	10.75	1.9257	145.9	0.5824	0.1755
7	477.8	1115.2	10.72	1.9313	142.2	0.5460	0.0980
8	411.1	1165.2	10.72	1.9320	136.3	0.4603	0.0245
9	417.0	1144.4	10.73	1.9289	125.4	0.2907	-0.1410
10	394.5	1150.4	10.77	1.9230	109.0	0.0366	-0.4356
run no.5	t_a=31°C				Δp_{pitot}=312.7 N/m^2, v_{hi}=23.28 m/s		
1	409.8	1243.5	10.71	2.1732	149.2	0.6580	0.2041
2	461.2	1129.2	10.76	2.1641	146.9	0.5965	0.1288
3	452.7	1119.3	10.74	2.1677	150.0	0.6497	0.2130
4	454.8	1148.9	10.72	2.1718	160.0	0.8104	0.3255
5	445.2	1104.4	10.73	2.1691	158.7	0.7753	0.3298
6	466.6	1083.3	10.75	2.1657	145.9	0.5824	0.1755
7	476.1	1115.6	10.72	2.1720	142.2	0.5460	0.0980
8	411.4	1155.9	10.72	2.1728	136.3	0.4603	0.0245
9	416.0	1133.7	10.73	2.1693	125.4	0.2907	-0.1410
10	396.2	1143.2	10.77	2.1627	109.0	0.0366	-0.4356

Table D.19: Upstream wall like strip,open 2D configuration, b=40mm, p_{atm}=100232 N/m^2 (fig.4.29).

Lat. no.	Δp_p [N/m^2]	$p_{atm}-p_{pl}$ [N/m^2]	v_l [m/s]	v_{hi}/v_l	p_h-p_l [N/m^2]	$K_i-\alpha_{eh}(v_h/v_l)^2$	K_{ivr}
run no.1		t_a=26°C			Δp_{pitot}=11.7N/m^2, v_{hi}=4.48m/s		
1	420.4	1274.9	10.93	0.4103	143.5	0.4718	0.0179
2	479.3	1181.6	10.97	0.4085	153.4	0.5866	0.1189
3	471.0	1178.3	10.90	0.4112	149.0	0.5510	0.1142
4	479.4	1197.8	10.97	0.4086	148.5	0.5202	0.0353
5	468.7	1149.5	10.96	0.4090	147.5	0.4987	0.0533
6	492.1	1141.1	10.95	0.4094	142.6	0.4381	0.0312
7	503.8	1176.9	10.97	0.4085	141.6	0.4236	-0.0244
8	430.9	1233.2	10.97	0.4088	141.3	0.4247	-0.0112
9	435.8	1228.3	10.96	0.4091	138.2	0.3830	-0.0488
10	408.6	1245.3	10.94	0.4099	139.0	0.4043	-0.0679
run no.2		t_a=26°C			Δp_{pitot}=54.7N/m^2, v_{hi}=9.68m/s		
1	420.9	1274.4	10.93	0.8859	133.9	0.3325	-0.1214
2	475.9	1197.2	10.93	0.8861	157.7	0.6653	0.1976
3	478.1	1203.4	10.99	0.8810	157.3	0.6347	0.1980
4	477.4	1210.4	10.94	0.8848	158.0	0.6649	0.1800
5	464.1	1161.3	10.90	0.8884	153.1	0.6021	0.1567
6	488.8	1155.6	10.91	0.8877	147.0	0.5168	0.1099
7	503.0	1186.7	10.96	0.8835	146.3	0.4956	0.0476
8	428.0	1246.4	10.92	0.8868	143.1	0.4662	0.0304
9	437.0	1232.3	10.97	0.8824	137.6	0.3683	-0.0635
10	412.3	1249.2	10.99	0.8808	132.3	0.2901	-0.1821
run no.3		t_a=26°C			Δp_{pitot}=123.1N/m^2, v_{hi}=14.53m/s		
1	418.8	1315.5	10.90	1.3330	164.0	0.7790	0.3251
2	475.9	1207.3	10.93	1.3293	153.6	0.6074	0.1397
3	473.1	1226.6	10.93	1.3294	158.9	0.6831	0.2463
4	474.9	1229.7	10.91	1.3313	162.6	0.7442	0.2593
5	462.3	1174.6	10.88	1.3357	160.8	0.7232	0.2777
6	488.9	1167.4	10.91	1.3314	150.5	0.5665	0.1596
7	502.2	1202.0	10.95	1.3265	149.2	0.5403	0.0923
8	431.1	1256.2	10.97	1.3246	145.0	0.4769	0.0411
9	433.6	1241.5	10.92	1.3297	138.5	0.3996	-0.0322
10	411.7	1261.6	10.99	1.3223	128.3	0.2358	-0.2364

Table D.19 continued:

Lat. no.	Δp_p [N/m^2]	$p_{atm}-p_{p1}$ [N/m^2]	v_1 [m/s]	v_{hi}/v_1	p_h-p_1 [N/m^2]	$K_i-\alpha_{eh}(v_h/v_1)^2$	K_{ivr}
run no.4		t_a =26°C			Δp_{pitot}=218.9N/m^2, v_{hi}=19.37m/s		
1	423.8	1427.3	10.97	1.7663	256.3	2.0661	1.6121
2	475.9	1196.4	10.93	1.7722	133.7	0.3212	-0.1466
3	471.9	1220.6	10.91	1.7752	153.5	0.6127	0.1759
4	473.8	1237.7	10.90	1.7773	163.8	0.7682	0.2833
5	459.3	1175.1	10.84	1.7871	161.2	0.7445	0.2991
6	492.2	1183.7	10.95	1.7688	152.0	0.5733	0.1664
7	497.9	1198.0	10.90	1.7770	148.2	0.5459	0.0979
8	427.3	1249.6	10.91	1.7752	144.3	0.4876	0.0517
9	432.6	1239.3	10.91	1.7752	133.1	0.3262	-0.1056
10	409.9	1248.0	10.96	1.7674	120.3	0.1305	-0.3416

Table D.20: Upstream wall like strip, open 2D configuration, b=80mm, p_{atm}=100232 N/m^2 (fig.4.30).

Lat. no.	Δp_p [N/m^2]	p_{atm}-p_{p1} [N/m^2]	v_l [m/s]	v_{hi}/v_l	p_h-p_l [N/m^2]	K_i-$\alpha_{eh}(v_h/v_l)^2$	K_{ivr}
run no.1		t_a=27°C			Δp_{pitot}=17.6N/m^2, v_{hi}=5.50m/s		
1	418.1	1309.5	10.92	0.5038	152.9	0.6171	0.1632
2	474.4	1213.3	10.92	0.5035	153.7	0.6183	0.1506
3	474.5	1221.1	10.96	0.5019	150.1	0.5524	0.1157
4	478.2	1238.3	10.97	0.5015	152.7	0.5873	0.1024
5	464.6	1172.8	10.92	0.5036	147.0	0.5134	0.0680
6	490.0	1164.0	10.94	0.5028	142.0	0.4401	0.0332
7	500.4	1195.4	10.94	0.5025	142.5	0.4527	0.0047
8	429.7	1255.3	10.96	0.5019	139.3	0.4049	-0.0310
9	433.1	1243.4	10.93	0.5032	134.9	0.3512	-0.0806
10	409.4	1263.4	10.96	0.5018	136.3	0.3630	-0.1091
run no.2		t_a=27°C			Δp_{pitot}=62.5N/m^2, v_{hi}=10.37m/s		
1	417.8	1302.7	10.89	0.9519	153.1	0.6289	0.1749
2	473.5	1208.9	10.91	0.9504	158.2	0.6875	0.2198
3	474.4	1219.7	10.96	0.9465	158.1	0.6670	0.2302
4	478.6	1232.7	10.97	0.9452	159.0	0.6749	0.1901
5	465.1	1168.0	10.93	0.9491	155.4	0.6309	0.1855
6	489.2	1162.9	10.93	0.9489	148.2	0.5328	0.1259
7	501.4	1201.8	10.96	0.9465	147.9	0.5263	0.0783
8	430.9	1257.2	10.97	0.9449	142.2	0.4403	0.0044
9	434.5	1238.5	10.95	0.9472	138.4	0.3952	-0.0366
10	412.4	1263.5	11.01	0.9422	132.7	0.2969	-0.1753
run no.3		t_a=27°C			Δp_{pitot}=128.0N/m^2, v_{hi}=14.84m/s		
1	420.5	1320.2	10.93	1.3569	159.8	0.7094	0.2554
2	473.1	1203.4	10.91	1.3604	153.5	0.6208	0.1531
3	474.2	1217.3	10.95	1.3543	157.6	0.6603	0.2235
4	478.2	1237.3	10.97	1.3529	161.7	0.7160	0.2311
5	467.0	1180.5	10.95	1.3548	160.7	0.6978	0.2523
6	487.6	1162.4	10.91	1.3600	150.9	0.5801	0.1732
7	499.3	1195.1	10.93	1.3573	148.5	0.5443	0.0963
8	429.4	1255.0	10.95	1.3546	145.8	0.4994	0.0636
9	435.1	1237.6	10.96	1.3540	137.2	0.3743	-0.0575
10	406.4	1247.4	10.91	1.3593	126.0	0.2297	-0.2424

Table D.20 continued:

Lat. no.	Δp_p [N/m^2]	p_{atm}-p_{p1} [N/m^2]	v_l [m/s]	v_{hi}/v_l	p_h-p_l [N/m^2]	K_i-$\alpha_{eh}(v_h/v_l)^2$	K_{ivr}
run no.4		t_a =27°C			Δp_{pitot} =230.6N/m^2, v_{hi} =19.91m/s		
1	415.8	1332.8	10.86	1.8334	183.7	1.0886	0.6346
2	478.4	1193.5	10.97	1.8147	139.6	0.3956	-0.0721
3	473.3	1215.7	10.94	1.8198	150.2	0.5585	0.1218
4	475.2	1232.4	10.93	1.8221	160.9	0.7204	0.2356
5	464.7	1177.6	10.92	1.8235	160.5	0.7078	0.2624
6	484.9	1164.2	10.88	1.8310	149.0	0.5639	0.1570
7	497.3	1201.4	10.91	1.8258	148.0	0.5460	0.0980
8	429.0	1258.5	10.95	1.8193	143.6	0.4703	0.0345
9	433.4	1237.9	10.93	1.8213	135.2	0.3544	-0.0774
10	409.7	1250.3	10.97	1.8160	118.0	0.0994	-0.3727
run no.5		t_a =27°C			Δp_{pitot} =338.1N/m^2, v_{hi} =24.11m/s		
1	421.0	1383.8	10.94	2.2047	228.3	1.6939	1.2399
2	478.8	1190.0	10.98	2.1960	119.3	0.1048	-0.3629
3	477.5	1209.1	11.00	2.1926	139.3	0.3842	-0.0526
4	475.6	1227.0	10.93	2.2055	157.0	0.6620	0.1771
5	463.9	1178.5	10.91	2.2099	159.7	0.7001	0.2547
6	488.8	1168.6	10.92	2.2075	146.9	0.5163	0.1094
7	497.8	1185.9	10.91	2.2093	143.9	0.4847	0.0367
8	429.2	1246.9	10.95	2.2021	140.0	0.4175	-0.0183
9	435.0	1235.1	10.96	2.2006	128.1	0.2450	-0.1868
10	410.3	1237.9	10.98	2.1968	108.5	-0.0391	-0.5112

Table D.21: Grid configuration without upstream ramp, open 2D configuration, p_{atm}=100096 N/m^2 (fig.4.32).

Lat. no.	Δp_p [N/m^2]	p_{atm}-p_{p1} [N/m^2]	v_1 [m/s]	v_{hi}/v_1	p_h-p_1 [N/m^2]	K_i-$\alpha_{eh}(v_h/v_1)^2$	K_{ivr}
run no.1		t_a=32°C			Δp_{pitot}=13.0N/m^2, v_h=4.77m/s		
1	411.4	1197.1	10.86	0.4392	115.4	0.1172	-0.3368
2	463.8	1127.9	10.86	0.4391	143.9	0.5306	0.0629
3	460.5	1131.0	10.85	0.4395	137.8	0.4439	0.0071
4	464.6	1144.5	10.87	0.4390	138.7	0.4539	-0.0310
5	446.5	1083.1	10.76	0.4433	135.9	0.4401	-0.0054
6	475.6	1089.4	10.84	0.4399	134.4	0.3936	-0.0133
7	484.6	1116.3	10.83	0.4403	135.3	0.4178	-0.0302
8	415.2	1166.1	10.81	0.4415	135.3	0.4317	-0.0041
9	418.5	1157.4	10.78	0.4424	134.8	0.4312	-0.0005
10	395.6	1179.1	10.81	0.4414	138.4	0.4792	0.0071
run no.2		t_a=32°C			Δp_{pitot}=56.0N/m^2, v_{hi}=9.90m/s		
1	413.2	1175.6	10.89	0.9093	93.5	-0.2136	-0.6676
2	462.0	1129.6	10.84	0.9134	152.5	0.6680	0.2002
3	462.0	1109.7	10.88	0.9104	122.0	0.2020	-0.2348
4	463.2	1131.1	10.85	0.9126	131.2	0.3492	-0.1357
5	450.5	1061.3	10.82	0.9155	112.6	0.0716	-0.3738
6	480.3	1068.6	10.90	0.9082	109.5	0.0059	-0.4010
7	485.8	1092.5	10.85	0.9126	110.0	0.0372	-0.4108
8	419.5	1143.7	10.87	0.9108	108.8	0.0156	-0.4202
9	423.5	1134.4	10.86	0.9119	104.2	-0.0504	-0.4821
10	400.7	1156.4	10.89	0.9092	106.9	-0.0160	-0.4881
run no.3		t_a=32°C			Δp_{pitot}=120.0N/m^2, v_{hi}=14.49m/s		
1	414.2	1244.1	10.90	1.3295	76.1	-0.4734	-0.9274
2	466.1	1245.7	10.89	1.3314	168.6	0.8863	0.4186
3	459.9	1196.5	10.84	1.3367	111.1	0.0494	-0.3873
4	469.1	1237.8	10.92	1.3272	141.4	0.4747	-0.0102
5	452.1	1128.9	10.83	1.3379	93.6	-0.2178	-0.6633
6	480.2	1147.4	10.90	1.3302	95.5	-0.1980	-0.6049
7	488.2	1171.7	10.88	1.3327	99.3	-0.1289	-0.5769
8	420.5	1218.2	10.88	1.3319	89.0	-0.2803	-0.7162
9	427.7	1205.9	10.92	1.3278	76.3	-0.4750	-0.9067
10	400.6	1234.5	10.88	1.3317	86.8	-0.3110	-0.7831

Table D.21 continued:

Lat. no.	Δp_p [N/m^2]	p_{atm}-p_{p1} [N/m^2]	v_l [m/s]	v_{hi}/v_l	p_h-p_l [N/m^2]	K_i- $\alpha_{eh}(v_h/v_l)^2$	K_{ivr}
run no.4		t_a=32°C			Δp_{pitot}=225.0N/m^2, v_{hi}=19.85m/s		
1	413.0	1216.0	10.88	1.8234	48.9	-0.8718	-1.3257
2	466.9	1266.1	10.89	1.8217	194.6	1.2673	0.7996
3	465.6	1180.7	10.92	1.8177	93.8	-0.2264	-0.6632
4	464.5	1243.7	10.86	1.8276	156.7	0.7236	0.2387
5	454.5	1114.0	10.87	1.8266	67.6	-0.6106	-1.0561
6	481.7	1137.0	10.92	1.8181	89.8	-0.2864	-0.6933
7	490.8	1158.3	10.91	1.8197	73.6	-0.5154	-0.9634
8	421.1	1202.2	10.89	1.8221	77.4	-0.4542	-0.8900
9	431.6	1181.5	10.98	1.8083	40.3	-1.0089	-1.4407
10	398.4	1195.2	10.85	1.8288	60.5	-0.6950	-1.1672

Table D.22: Grid configuration with upstream ramp, open 2D configuration, a=40mm, p_{atm}=100096 N/m^2 (fig.4.33).

Lat. no.	Δp_p [N/m^2]	$p_{atm}-p_{p1}$ [N/m^2]	v_l [m/s]	v_{hi}	p_h-p_l [N/m^2]	$K_i-\alpha_{eh}(v_h/v_l)^2$	K_{ivr}
run no.1		t_a=28°C			Δp_{pitot}=15.0N/m^2, v_{hi}=5.09m/s		
1	415.8	1215.2	10.89	0.4677	123.8	0.2143	-0.2397
2	470.2	1141.2	10.89	0.4674	142.7	0.4786	0.0108
3	467.8	1146.8	10.90	0.4672	140.9	0.4498	0.0130
4	467.6	1149.6	10.85	0.4690	140.3	0.4591	-0.0258
5	460.3	1103.1	10.89	0.4675	140.0	0.4317	-0.0137
6	483.2	1094.9	10.88	0.4679	137.9	0.4101	0.0032
7	491.6	1124.8	10.86	0.4687	137.5	0.4176	-0.0304
8	426.1	1191.9	10.92	0.4660	139.7	0.4307	-0.0052
9	427.2	1179.7	10.86	0.4686	138.3	0.4315	-0.0003
10	400.7	1195.9	10.85	0.4694	139.6	0.4603	-0.0118
run no.2		t_a=28°C			Δp_{pitot}=56.0N/m^2, v_{hi}=9.84m/s		
1	409.5	1218.1	10.79	0.9117	113.6	0.0939	-0.3601
2	461.7	1145.3	10.78	0.9122	130.7	0.3413	-0.1264
3	463.4	1142.5	10.84	0.9074	124.6	0.2316	-0.2051
4	465.2	1165.6	10.82	0.9089	132.0	0.3479	-0.1369
5	459.3	1103.4	10.88	0.9044	115.9	0.0845	-0.3609
6	483.4	1098.0	10.88	0.9039	112.0	0.0312	-0.3758
7	490.1	1122.3	10.85	0.9069	111.5	0.0424	-0.4056
8	423.9	1190.5	10.89	0.9031	111.5	0.0307	-0.4052
9	430.1	1181.8	10.91	0.9019	108.0	-0.0243	-0.4560
10	399.8	1184.3	10.83	0.9081	106.9	-0.0173	-0.4894
run no.3		t_a=28°C			Δp_{pitot}=124.0N/m^2, v_{hi}=14.64m/s		
1	412.2	1274.2	10.83	1.3519	143.6	0.5253	0.0713
2	467.6	1138.7	10.86	1.3478	87.4	-0.3193	-0.7870
3	461.9	1156.0	10.82	1.3528	111.5	0.0446	-0.3922
4	466.8	1183.4	10.84	1.3501	133.0	0.3552	-0.1296
5	458.2	1105.4	10.86	1.3477	93.9	-0.2342	-0.6796
6	477.3	1096.9	10.81	1.3543	91.7	-0.2469	-0.6538
7	485.3	1137.6	10.79	1.3570	97.5	-0.1483	-0.5963
8	418.5	1180.8	10.81	1.3538	88.8	-0.2809	-0.7167
9	427.7	1171.2	10.87	1.3462	73.7	-0.5154	-0.9471
10	398.4	1196.6	10.81	1.3541	84.4	-0.3437	-0.8159

Table D.22 continued:

Lat. no.	Δp_p [N/m^2]	$p_{atm}-p_{pl}$ [N/m^2]	v_l [m/s]	v_{hi}/v_l	p_h-p_l [N/m^2]	$K_i-\alpha_{eh}(v_h/v_l)^2$	K_{ivr}
run no.4		t_a =28°C			Δp_{pitot} =232.0N/m^2, v_{hi} =20.02m/s		
1	409.4	1349.9	10.78	1.8575	206.5	1.4781	1.0242
2	468.1	1105.8	10.87	1.8423	38.7	-1.0335	-1.5012
3	463.2	1158.5	10.84	1.8477	89.9	-0.2784	-0.7152
4	465.2	1212.2	10.82	1.8504	143.5	0.5189	0.0340
5	456.2	1099.3	10.84	1.8477	70.6	-0.5708	-1.0162
6	478.1	1119.5	10.82	1.8509	90.3	-0.2698	-0.6767
7	486.1	1129.8	10.80	1.8544	72.0	-0.5292	-0.9772
8	415.5	1174.2	10.77	1.8595	74.8	-0.4801	-0.9160
9	429.3	1158.4	10.90	1.8372	38.6	-1.0309	-1.4627
10	393.2	1168.6	10.73	1.8659	58.1	-0.7205	-1.1926

Table D.23: Grid configuration with upstream ramp, open 2D configuration, a = 80mm, p_{atm}=99837 N/m^2 (fig.4.34).

Lat. no.	Δp_p [N/m^2]	p_{atm}-p_{p1} [N/m^2]	v_1 [m/s]	v_{hi}/v_1	p_h-p_1 [N/m^2]	K_i-$\alpha_{eh}(v_h/v_1)^2$	K_{ivr}
run no.1		t_a=30°C			Δp_{pitot}=15.0N/m^2, v_{hi}=5.11m/s		
1	415.6	1231.4	10.91	0.4686	123.9	0.2214	-0.2326
2	472.5	1160.0	10.96	0.4666	144.6	0.4981	0.0303
3	466.5	1143.1	10.92	0.4684	141.0	0.4605	0.0238
4	473.3	1169.4	10.97	0.4664	140.5	0.4386	-0.0463
5	459.5	1109.2	10.92	0.4685	140.0	0.4383	-0.0072
6	485.5	1106.1	10.95	0.4671	137.2	0.3910	-0.0159
7	494.7	1144.9	10.94	0.4675	139.5	0.4366	-0.0114
8	424.9	1192.1	10.94	0.4675	139.2	0.4334	-0.0025
9	427.1	1185.5	10.90	0.4693	137.6	0.4261	-0.0057
10	403.9	1212.8	10.93	0.4680	141.5	0.4742	0.0021
run no.2		t_a=30°C			Δp_{pitot}=56.0N/m^2, v_{hi}=9.88m/s		
1	413.2	1220.2	10.88	0.9084	116.5	0.1243	-0.3297
2	468.6	1143.8	10.91	0.9056	137.1	0.4067	-0.0610
3	464.2	1136.8	10.89	0.9074	122.7	0.2020	-0.2348
4	467.5	1158.0	10.89	0.9073	133.8	0.3663	-0.1185
5	460.4	1092.9	10.93	0.9041	114.7	0.0641	-0.3813
6	484.5	1089.1	10.94	0.9035	111.7	0.0233	-0.3836
7	495.0	1127.2	10.94	0.9029	113.5	0.0556	-0.3924
8	425.7	1173.5	10.95	0.9022	110.8	0.0167	-0.4192
9	428.2	1165.2	10.92	0.9053	106.8	-0.0322	-0.4640
10	403.7	1189.9	10.93	0.9045	108.9	-0.0015	-0.4736
run no.3		t_a=30°C			Δp_{pitot}=135.0N/m^2, v_{hi}=15.34m/s		
1	419.3	1250.0	10.97	1.3987	127.7	0.2588	-0.1952
2	467.8	1115.1	10.90	1.4073	101.3	-0.1161	-0.5838
3	467.0	1143.1	10.92	1.4044	119.2	0.1398	-0.2969
4	473.0	1170.0	10.96	1.3997	135.8	0.3718	-0.1131
5	459.5	1072.8	10.92	1.4051	90.9	-0.2810	-0.7264
6	481.6	1070.5	10.90	1.4071	94.1	-0.2249	-0.6318
7	496.9	1104.6	10.97	1.3987	97.3	-0.1866	-0.6346
8	423.7	1152.1	10.92	1.4044	89.6	-0.2847	-0.7205
9	430.2	1140.3	10.95	1.4016	70.7	-0.5652	-0.9970
10	405.7	1174.0	10.96	1.4001	85.1	-0.3561	-0.8282

Table D.23 continued:

Lat. no.	Δp_p [N/m^2]	p_{atm}-p_{p1} [N/m^2]	v_1 [m/s]	v_{hi}/v_1	p_h-p_1 [N/m^2]	K_i-$\alpha_{eh}(v_h/v_1)^2$	K_{ivr}
run no.4		t_a =30°C			Δp_{pitot} =241.0N/m^2, v_{hi} =20.50m/s		
1	418.6	1278.4	10.96	1.8710	156.9	0.6868	0.2329
2	470.8	1105.9	10.94	1.8736	85.3	-0.3583	-0.8260
3	471.5	1126.3	10.98	1.8664	81.5	-0.4230	-0.8598
4	470.7	1162.8	10.93	1.8753	126.6	0.2471	-0.2378
5	461.7	1062.3	10.95	1.8724	66.7	-0.6405	-1.0859
6	481.3	1062.6	10.90	1.8806	80.2	-0.4286	-0.8355
7	499.5	1084.2	11.00	1.8635	60.2	-0.7276	-1.1756
8	424.8	1138.0	10.94	1.8736	67.5	-0.6105	-1.0463
9	428.2	1091.2	10.92	1.8772	25.4	-1.2232	-1.6549
10	406.6	1135.7	10.98	1.8677	41.1	-0.9967	-1.4689
run no.5		t_a =30°C			Δp_{pitot} =324.0N/m^2, v_{hi} =23.77m/s		
1	417.2	1290.0	10.94	2.1735	168.8	0.8688	0.4149
2	471.3	1096.8	10.95	2.1710	74.2	-0.5221	-0.9898
3	472.9	1103.7	11.00	2.1601	66.6	-0.6420	-1.0788
4	476.1	1177.6	11.00	2.1607	125.1	0.2034	-0.2815
5	464.6	1058.1	10.99	2.1633	57.2	-0.7834	-1.2288
6	488.6	1058.5	10.99	2.1629	63.0	-0.6934	-1.1003
7	494.7	1070.9	10.94	2.1718	48.5	-0.8902	-1.3382
8	422.8	1119.6	10.91	2.1781	45.7	-0.9258	-1.3616
9	430.4	1075.9	10.95	2.1702	4.1	-1.5351	-1.9668
10	408.5	1109.5	11.01	2.1597	17.8	-1.3338	-1.8059

Table D.24: Normal inlet loss coefficients for rounded laterals, with 3mm radius (fig.4.36).

p_{atm}=100420N/m^2			t_a=16.5°C			
Lat no.	Δp_p [N/m^2]	Δp_p [N/m^2]	v_l [m/s]	Δp_p [N/m^2]	K_0	K_0 avg.
1	436.1	1392.9	11.04	120.1	0.0541	0.04634
1	435.8	1389.5	11.04	119.6	0.0490	
1	437.8	1392.1	11.07	119.2	0.0360	
2	493.3	1285.5	11.00	122.8	0.0940	0.09440
2	494.3	1281.4	11.02	122.5	0.0862	
2	494.8	1278.2	11.02	123.9	0.1030	
3	492.4	1263.8	11.03	120.5	0.0543	0.05911
3	492.0	1256.3	11.02	121.3	0.0662	
3	493.7	1254.0	11.04	121.0	0.0567	
4	498.5	1302.7	11.07	126.9	0.1311	0.13298
4	497.3	1303.6	11.05	126.9	0.1358	
4	498.8	1303.6	11.07	127.0	0.1321	
5	483.4	1213.4	11.00	120.8	0.0587	0.05835
5	482.0	1208.7	10.98	120.8	0.0629	
5	482.5	1210.0	10.99	120.2	0.0535	
6	511.4	1233.0	11.03	121.8	0.0701	0.06539
6	511.6	1235.2	11.03	121.2	0.0618	
6	511.5	1238.5	11.03	121.4	0.0643	
7	525.6	1268.2	11.07	125.3	0.1109	0.11804
7	525.5	1266.9	11.07	125.9	0.1193	
7	525.3	1273.0	11.07	126.1	0.1238	
8	443.2	1313.0	11.02	122.9	0.0951	0.07978
8	447.0	1306.6	11.08	121.6	0.0630	
8	444.4	1311.0	11.04	122.2	0.0812	
9	455.3	1271.0	11.11	126.1	0.1145	0.11771
9	453.6	1279.2	11.08	126.2	0.1222	
9	455.4	1282.4	11.11	126.3	0.1164	
10	424.0	1278.0	11.06	125.3	0.1203	0.12334
10	425.5	1280.2	11.08	125.4	0.1154	
10	422.9	1286.2	11.04	125.9	0.1343	

Table D.25: 10 laterals with 40mm pitch with 3mm inlet rounding in passing flow, open 2D configuration, p_{atm}= 100420N/m^2 (fig.4.37).

Lat. no.	Δp_p [N/m^2]	p_{atm}-p_{pl} [N/m^2]	v_l [m/s]	v_{hi}/v_l	p_h-p_l [N/m^2]	K_i-$\alpha_{eh}(v_h/v_l)^2$	K_{ivr}
run no.1		t_a=16.5°C			Δp_{pitot}=19.5N/m^2, v_{hi}=5.69m/s		
1	425.2	1360.8	10.88	0.5229	133.9	0.2934	-0.1606
2	482.4	1255.7	10.87	0.5234	126.9	0.1899	-0.2778
3	486.6	1254.4	10.95	0.5194	128.3	0.1826	-0.2541
4	483.7	1262.6	10.89	0.5226	125.8	0.1713	-0.3135
5	473.4	1189.7	10.88	0.5231	119.3	0.0728	-0.3726
6	499.3	1204.3	10.88	0.5227	117.9	0.0575	-0.3494
7	504.4	1210.1	10.83	0.5253	114.4	0.0307	-0.4172
8	430.8	1250.9	10.85	0.5245	111.8	-0.0079	-0.4437
9	433.1	1202.9	10.80	0.5269	108.6	-0.0403	-0.4720
10	407.3	1212.3	10.81	0.5265	107.0	-0.0617	-0.5338
run no.2		t_a=16.5°C			Δp_{pitot}=58.6N/m^2, v_{hi}=9.85m/s		
1	423.8	1369.1	10.86	0.9075	141.5	0.4084	-0.0455
2	482.4	1257.3	10.87	0.9066	131.5	0.2545	-0.2132
3	482.8	1250.6	10.91	0.9033	131.6	0.2435	-0.1932
4	485.2	1254.6	10.91	0.9036	125.9	0.1670	-0.3178
5	471.3	1190.5	10.85	0.9083	119.2	0.0795	-0.3660
6	495.6	1201.2	10.84	0.9090	118.5	0.0782	-0.3287
7	505.0	1200.4	10.84	0.9091	109.2	-0.0451	-0.4931
8	430.7	1241.7	10.85	0.9084	106.6	-0.0812	-0.5170
9	435.1	1198.7	10.83	0.9100	101.5	-0.1480	-0.5797
10	408.1	1202.6	10.82	0.9107	99.3	-0.1753	-0.6475
run no.3		t_a=16.5°C			Δp_{pitot}=132.9N/m^2, v_h=14.84m/s		
1	420.6	1366.2	10.81	1.3722	150.0	0.5449	0.0910
2	479.5	1246.1	10.83	1.3694	128.9	0.2302	-0.2376
3	480.3	1249.1	10.88	1.3639	131.7	0.2554	-0.1814
4	484.9	1253.5	10.90	1.3609	125.1	0.1574	-0.3275
5	471.6	1178.8	10.85	1.3668	115.6	0.0271	-0.4183
6	496.6	1194.9	10.85	1.3669	116.0	0.0390	-0.3679
7	506.7	1191.8	10.86	1.3662	99.0	-0.1935	-0.6415
8	430.7	1235.8	10.85	1.3678	96.2	-0.2282	-0.6641
9	436.7	1185.4	10.85	1.3672	89.0	-0.3302	-0.7620
10	410.0	1193.4	10.85	1.3673	83.4	-0.4054	-0.8775

Table D.25 continued:

Lat. no.	Δp_p [N/m^2]	p_{atm}-p_{p1} [N/m^2]	v_1 [m/s]	v_{hi}/v_1	p_h-p_1 [N/m^2]	K_i-$\alpha_{eh}(v_h/v_1)^2$	K_{ivr}
run no.4		t_a=16.5°C			Δp_{pitot}=223.8N/m^2, v_{hi}=19.25m/s		
1	419.5	1367.6	10.79	1.7834	161.5	0.7144	0.2605
2	479.7	1240.7	10.84	1.7767	126.0	0.1890	-0.2787
3	477.4	1241.5	10.84	1.7757	129.1	0.2301	-0.2067
4	482.7	1252.3	10.87	1.7703	124.3	0.1534	-0.3315
5	471.9	1175.0	10.86	1.7731	110.7	-0.0417	-0.4872
6	497.8	1187.5	10.87	1.7715	108.9	-0.0642	-0.4711
7	509.7	1185.9	10.90	1.7669	88.9	-0.3423	-0.7903
8	433.5	1223.8	10.89	1.7680	85.9	-0.3808	-0.8167
9	437.8	1179.6	10.87	1.7715	77.2	-0.4993	-0.9311
10	411.1	1182.4	10.87	1.7713	67.1	-0.6383	-1.1104
run no.5		t_a=16.5°C			Δp_{pitot}=355.7N/m^2, v_{hi}=24.27m/s		
1	421.0	1388.0	10.82	2.2439	173.7	0.8790	0.4251
2	481.3	1238.3	10.86	2.2357	121.0	0.1115	-0.3562
3	481.7	1237.1	10.90	2.2277	124.3	0.1456	-0.2912
4	482.6	1245.9	10.87	2.2322	117.3	0.0566	-0.4283
5	469.1	1169.8	10.82	2.2427	104.9	-0.1152	-0.5606
6	496.4	1184.6	10.85	2.2367	102.1	-0.1559	-0.5628
7	510.7	1185.2	10.91	2.2254	77.4	-0.5059	-0.9539
8	432.6	1214.8	10.88	2.2315	73.0	-0.5588	-0.9947
9	440.7	1170.7	10.91	2.2246	61.6	-0.7244	-1.1562
10	414.1	1172.0	10.91	2.2240	46.4	-0.9332	-1.4054

Table D.26: 10 laterals with rounded inlets, open 3D configuration, $p_{atm}=101519 N/m^2$ (fig.4.38).

Lat. no.	Δp_p [N/m^2]	$p_{atm}-p_{p1}$ [N/m^2]	v_l [m/s]	v_{hi}/v_l	p_h-p_l [N/m^2]	$K_i-\alpha_{eh}(v_h/v_l)^2$	K_{ivr}
run no.1		$t_a=13°C$			$\Delta p_{pitot}=15.6 N/m^2$, $v_{hi}=5.03$ m/s		
1	432.6	1405.8	10.90	0.4614	129.8	0.1938	0.1474
2	496.2	1303.4	10.94	0.4600	124.9	0.1074	0.0130
3	488.8	1273.6	10.88	0.4623	126.2	0.1421	0.0830
4	496.8	1300.1	10.95	0.4595	126.5	0.1277	-0.0053
5	484.8	1232.1	10.91	0.4610	121.5	0.0593	0.0010
6	513.3	1251.2	10.94	0.4598	121.5	0.0574	-0.0080
7	522.4	1270.5	10.93	0.4601	121.2	0.0629	-0.0551
8	441.4	1306.3	10.91	0.4611	118.4	0.0345	-0.0453
9	449.8	1267.6	10.94	0.4598	115.7	-0.0113	-0.1290
10	417.5	1269.6	10.87	0.4627	112.4	-0.0351	-0.1584
run no.2		$t_a=13°C$			$\Delta p_{pitot}=53.7 N/m^2$, $v_{hi}=9.33$ m/s		
1	436.1	1415.2	10.95	0.8515	132.7	0.2175	0.1711
2	491.3	1294.0	10.88	0.8575	126.7	0.1496	0.0552
3	489.9	1278.4	10.89	0.8561	128.0	0.1620	0.1029
4	492.3	1302.0	10.89	0.8562	125.8	0.1337	0.0007
5	482.8	1225.8	10.89	0.8566	119.8	0.0437	-0.0146
6	509.4	1239.9	10.89	0.8561	122.1	0.0790	0.0136
7	516.8	1253.0	10.87	0.8580	116.1	0.0112	-0.1068
8	439.6	1299.1	10.88	0.8570	113.6	-0.0239	-0.1037
9	448.5	1252.5	10.92	0.8539	110.2	-0.0810	-0.1987
10	414.7	1259.0	10.83	0.8611	106.8	-0.1013	-0.2246
run no.3		$t_a=13°C$			$\Delta p_{pitot}=124.1N/m^2$, $v_{hi}=14.17$ m/s		
1	432.3	1408.5	10.90	1.3005	132.6	0.2328	0.1864
2	490.2	1290.9	10.86	1.3047	119.1	0.0501	-0.0443
3	487.4	1265.0	10.87	1.3043	123.6	0.1104	0.0513
4	489.7	1287.6	10.86	1.3048	121.5	0.0853	-0.0477
5	481.2	1218.0	10.87	1.3039	114.2	-0.0278	-0.0862
6	508.4	1235.3	10.88	1.3021	117.1	0.0133	-0.0521
7	519.6	1243.3	10.90	1.2999	103.4	-0.1700	-0.2880
8	438.5	1287.1	10.87	1.3041	103.9	-0.1525	-0.2323
9	449.5	1243.9	10.94	1.2958	97.1	-0.2617	-0.3794
10	418.7	1244.0	10.89	1.3012	91.3	-0.3277	-0.4510

Table D.26 continued:

Lat. no.	Δp_p [N/m^2]	$p_{atm}-p_{p1}$ [N/m^2]	v_1 [m/s]	v_{hi}/v_1	p_h-p_1 [N/m^2]	$K_i-\alpha_{eh}(v_h/v_1)^2$	K_{ivr}
run no.4		t_a=13°C			Δp_{pitot}=203.2N/m^2, v_{hi}=18.14 m/s		
1	432.3	1402.9	10.90	1.6644	134.3	0.2559	0.2096
2	494.8	1270.6	10.92	1.6608	112.0	-0.0631	-0.1575
3	486.7	1260.8	10.86	1.6706	117.1	0.0239	-0.0352
4	489.0	1276.5	10.85	1.6711	116.4	0.0169	-0.1161
5	481.5	1205.8	10.87	1.6680	108.3	-0.1090	-0.1674
6	508.5	1231.0	10.89	1.6662	110.7	-0.0741	-0.1395
7	519.4	1233.4	10.90	1.6639	96.0	-0.2709	-0.3889
8	440.9	1275.9	10.90	1.6634	95.8	-0.2719	-0.3517
9	447.2	1232.8	10.91	1.6631	87.1	-0.3908	-0.5085
10	419.0	1235.4	10.90	1.6645	76.0	-0.5376	-0.6609
run no.5		t_a=13°C			Δp_{pitot}=331.2N/m^2, v_{hi}=23.15 m/s		
1	431.1	1405.1	10.88	2.1283	139.5	0.3330	0.2867
2	492.4	1258.7	10.89	2.1260	101.6	-0.1968	-0.2912
3	486.4	1236.4	10.85	2.1332	107.4	-0.1082	-0.1673
4	492.6	1273.0	10.90	2.1246	108.5	-0.1026	-0.2356
5	481,0	1188.2	10.87	2.1304	100.2	-0.2198	-0.2781
6	503.5	1204.4	10.83	2.1383	101.5	-0.1859	-0.2512
7	518.3	1210.0	10.89	2.1263	84.5	-0.4251	-0.5431
8	441.3	1259.2	10.91	2.1224	82.2	-0.4583	-0.5380
9	450.3	1208.8	10.95	2.1143	69.0	-0.6441	-0.7618
10	423.2	1204.2	10.96	2.1124	36.2	-1.0858	-1.2091

Table D.27: Rounded lateral inlets upstream backward facing step, open 2D configuration, a=20mm, b=100mm, p_{atm}=100544 N/m^2 (fig.4.39).

Lat. no.	Δp_p [N/m^2]	p_{atm}-p_{p1} [N/m^2]	v_l [m/s]	v_{hi}/v_l	p_h-p_l [N/m^2]	K_i-$\alpha_{eh}(v_h/v_l)^2$	K_{ivr}
run no.1	t_a=17°C				Δp_{pitot}=17.6N/m^2, v_{hi}=5.40m/s		
3	487.2	1258.5	10.96	0.4924	128.5	0.1829	0.1238
4	493.4	1287.0	11.01	0.4905	127.9	0.1641	0.0311
5	480.7	1210.0	10.97	0.4922	122.2	0.0879	0.0295
6	504.3	1223.6	10.94	0.4933	119.6	0.0636	-0.0018
7	514.2	1236.4	10.95	0.4932	116.2	0.0247	-0.0933
8	435.6	1282.1	10.92	0.4946	114.1	0.0059	-0.0739
9	440.8	1223.3	10.91	0.4949	110.7	-0.0392	-0.1569
10	394.2	1177.7	10.61	0.5090	103.9	-0.0524	-0.1758
run no.2	t_a=17°C				Δp_{pitot}=55.7N/m^2, v_{hi}=9.61m/s		
3	484.6	1242.0	10.93	0.8788	120.7	0.0851	0.0260
4	490.2	1275.6	10.97	0.8760	121.5	0.0871	-0.0458
5	474.7	1199.1	10.89	0.8820	117.2	0.0391	-0.0193
6	502.0	1206.6	10.92	0.8800	117.2	0.0380	-0.0274
7	508.8	1213.7	10.88	0.8826	109.2	-0.0563	-0.1743
8	436.3	1264.2	10.93	0.8792	106.5	-0.1035	-0.1832
9	437.7	1210.6	10.86	0.8843	102.5	-0.1433	-0.2610
10	392.4	1161.8	10.58	0.9082	95.1	-0.1749	-0.2982
run no.3	t_a=17°C				Δp_{pitot}=135.8N/m^2, v_{hi}=15.00m/s		
3	481.8	1231.8	10.90	1.3765	104.7	-0.1285	-0.1876
4	491.5	1255.5	10.99	1.3656	101.4	-0.1934	-0.3264
5	473.6	1178.4	10.88	1.3790	100.9	-0.1849	-0.2432
6	497.3	1194.5	10.86	1.3810	105.6	-0.1086	-0.1740
7	511.0	1199.0	10.91	1.3749	94.1	-0.2739	-0.3919
8	435.0	1246.7	10.91	1.3753	92.3	-0.2963	-0.3761
9	436.4	1195.5	10.85	1.3830	85.2	-0.3826	-0.5003
10	394.7	1148.0	10.62	1.4132	77.7	-0.4406	-0.5640

Table D.27 continued:

Lat. no.	Δp_p [N/m^2]	p_{atm}-p_{p1} [N/m^2]	v_l [m/s]	v_{hi}/v_l	p_h-p_l [N/m^2]	K_i-$\alpha_{eh}(v_h/v_l)^2$	K_{ivr}
run no.4		t_a =17°C			Δp_{pitot} =233.5N/m^2, v_{hi} =19.67m/s		
3	485.3	1216.9	10.94	1.7978	97.5	-0.2393	-0.2985
4	487.6	1220.9	10.94	1.7983	76.2	-0.5307	-0.6637
5	477.9	1169.1	10.94	1.7989	84.5	-0.4259	-0.4842
6	501.6	1187.3	10.91	1.8024	91.2	-0.3221	-0.3875
7	513.9	1195.1	10.95	1.7973	77.1	-0.5171	-0.6351
8	435.9	1237.7	10.92	1.8009	78.5	-0.4914	-0.5712
9	441.7	1184.3	10.92	1.8009	70.1	-0.6070	-0.7247
10	397.9	1135.5	10.67	1.8441	60.0	-0.7089	-0.8322
run no.5		t_a =17°C			Δp_{pitot} =332.2N/m^2, v_{hi} =23.46m/s		
3	481.3	1213.5	10.89	2.1539	91.2	-0.3153	-0.3744
4	491.3	1196.5	10.99	2.1357	46.2	-0.9522	-1.0852
5	480.7	1155.6	10.97	2.1388	62.4	-0.7371	-0.7955
6	503.1	1174.9	10.93	2.1462	75.0	-0.5515	-0.6169
7	509.9	1175.1	10.90	2.1527	59.8	-0.7494	-0.8674
8	438.1	1214.6	10.96	2.1415	62.0	-0.7252	-0.8049
9	439.6	1168.8	10.90	2.1535	53.2	-0.8387	-0.9564
10	395.9	1119.1	10.64	2.2059	42.5	-0.9603	-1.0836

Table D.28: Rounded lateral inlets with triangular ramp, open 2D configuration, b=80mm, p_{atm}=100818 N/m^2 (fig.4.40).

Lat. no.	Δp_p [N/m^2]	p_{atm}-p_{p1} [N/m^2]	v_1 [m/s]	v_{hi}/v_1	p_h-p_1 [N/m^2]	K_i-$\alpha_{eh}(v_h/v_1)^2$	K_{ivr}
run no.1		t_a=16°C			Δp_{pitot}=16.6N/m^2, v_{hi}=5.23m/s		
1	431.6	1388.6	10.95	0.4776	131.7	0.2315	0.1852
2	489.0	1279.2	10.92	0.4788	127.5	0.1731	0.0787
3	488.8	1265.4	10.96	0.4774	128.9	0.1824	0.1233
4	497.0	1299.1	11.02	0.4745	126.8	0.1350	0.0020
5	484.4	1221.0	10.99	0.4761	122.5	0.0769	0.0186
6	508.9	1230.8	10.97	0.4769	118.6	0.0352	-0.0302
7	516.8	1249.0	10.95	0.4778	117.0	0.0268	-0.0912
8	439.1	1287.9	10.94	0.4780	113.2	-0.0216	-0.1014
9	442.0	1240.9	10.90	0.4798	109.2	-0.0659	-0.1836
10	411.1	1237.3	10.84	0.4825	108.6	-0.0560	-0.1794
run no.2		t_a=16°C			Δp_{pitot}=60.6N/m^2, v_{hi}=9.99m/s		
1	429.1	1373.8	10.92	0.9151	131.0	0.2332	0.1868
2	486.1	1272.9	10.89	0.9174	126.5	0.1697	0.0753
3	480.5	1259.9	10.85	0.9203	129.4	0.2209	0.1618
4	490.4	1289.2	10.94	0.9127	125.9	0.1461	0.0131
5	477.9	1211.0	10.91	0.9159	117.3	0.0294	-0.0290
6	501.7	1224.8	10.88	0.9177	118.9	0.0624	-0.0030
7	513.2	1241.8	10.91	0.9158	109.9	-0.0608	-0.1789
8	436.5	1277.8	10.91	0.9159	105.7	-0.1164	-0.1961
9	441.7	1224.3	10.90	0.9167	101.7	-0.1698	-0.2875
10	410.3	1223.6	10.83	0.9224	99.4	-0.1833	-0.3066
run no.3		t_a=16°C			Δp_{pitot}=111.4N/m^2, v_{hi}=13.54m/s		
1	425.7	1373.0	10.87	1.2466	129.9	0.2342	0.1879
2	485.7	1267.4	10.88	1.2445	121.3	0.0991	0.0047
3	478.9	1252.1	10.83	1.2501	126.2	0.1820	0.1229
4	488.3	1283.4	10.92	1.2407	124.2	0.1316	-0.0013
5	474.5	1201.3	10.86	1.2468	115.6	0.0168	-0.0416
6	500.0	1215.3	10.87	1.2466	115.2	0.0168	-0.0486
7	512.5	1225.9	10.90	1.2428	102.5	-0.1612	-0.2792
8	439.5	1265.6	10.95	1.2371	98.3	-0.2284	-0.3081
9	440.3	1217.2	10.88	1.2453	92.0	-0.3000	-0.4177
10	410.4	1218.8	10.83	1.2506	87.1	-0.3558	-0.4791

Table D.28 continued:

Lat. no.	Δp_p [N/m^2]	$p_{atm}-p_{p1}$ [N/m^2]	v_1 [m/s]	v_{hi}/v_1	p_h-p_1 [N/m^2]	$K_i-\alpha_{eh}(v_h/v_1)^2$	K_{ivr}
run no.4		t_a=16°C			Δp_{pitot}=233.5N/m^2, v_{hi}=19.61m/s		
1	430.6	1391.7	10.94	1.7930	139.1	0.3372	0.2908
2	488.9	1252.2	10.92	1.7952	101.7	-0.1834	-0.2778
3	479.2	1241.0	10.84	1.8093	115.0	0.0241	-0.0350
4	489.0	1273.7	10.93	1.7948	116.1	0.0166	-0.1164
5	474.4	1196.7	10.86	1.8054	106.6	-0.1086	-0.1669
6	499.2	1209.6	10.86	1.8064	105.5	-0.1162	-0.1816
7	510.9	1213.5	10.88	1.8024	88.2	-0.3557	-0.4737
8	436.4	1256.7	10.90	1.7985	82.4	-0.4387	-0.5185
9	440.5	1205.9	10.88	1.8024	73.0	-0.5646	-0.6823
10	411.3	1199.1	10.85	1.8081	64.2	-0.6795	-0.8028
run no.5		t_a=16°C			Δp_{pitot}=342.0N/m^2, v_{hi}=23.73m/s		
1	427.6	1393.5	10.89	2.1790	151.7	0.5275	0.4812
2	486.2	1239.4	10.89	2.1790	83.1	-0.4336	-0.5280
3	476.6	1230.2	10.81	2.1961	104.6	-0.1132	-0.1723
4	486.1	1260.9	10.89	2.1790	108.9	-0.0735	-0.2065
5	473.0	1185.7	10.85	2.1882	98.4	-0.2194	-0.2777
6	498.4	1200.0	10.85	2.1880	97.6	-0.2238	-0.2892
7	512.6	1206.2	10.90	2.1770	75.8	-0.5315	-0.6495
8	438.6	1251.9	10.94	2.1698	74.1	-0.5592	-0.6390
9	441.3	1189.8	10.89	2.1786	61.4	-0.7279	-0.8456
10	412.8	1185.2	10.87	2.1832	46.9	-0.9246	-1.0480

Table D.29: Manifold configuration, sharp lateral inlets (fig.4.42).

p_{atm}=99847N/m^2				t_a=26.5°C			
Lat no.	Δp_p [N/m^2]	$p_{atm}-p_{pl}$ [N/m^2]	v_l [m/s]	p_h-p_l [N/m^2]	f_D	$K_0-\alpha_{eh}(v_h/v_l)^2$	K_{ivr}
1	417.2	1344.5	10.90	158.9	0.0324	0.7166	0.2627
2	472.4	1238.2	10.91	153.7	0.0325	0.6267	0.1590
3	467.6	1226.3	10.89	148.1	0.0325	0.5563	0.1196
4	468.5	1240.4	10.86	150.0	0.0325	0.5952	0.1103
5	461.0	1177.7	10.89	145.6	0.0326	0.5094	0.0640
6	483.4	1175.9	10.87	146.7	0.0325	0.5376	0.1307
7	490.7	1195.9	10.84	143.6	0.0325	0.5103	0.0623
8	423.2	1261.9	10.88	143.3	0.0324	0.4960	0.0602
9	432.2	1263.5	10.93	147.7	0.0324	0.5409	0.1091
10	403.9	1275.1	10.89	131.1	0.0324	0.3170	-0.1551
1	412.3	1328.2	10.82	157.0	0.0324	0.7201	0.2661
2	466.5	1226.5	10.84	152.2	0.0325	0.6347	0.1670
3	467.1	1220.9	10.88	147.5	0.0325	0.5488	0.1121
4	461.6	1226.8	10.77	148.4	0.0326	0.6068	0.1220
5	452.5	1170.8	10.78	147.2	0.0327	0.5742	0.1287
6	470.8	1154.4	10.72	142.7	0.0326	0.5366	0.1297
7	488.0	1196.4	10.81	145.6	0.0325	0.5527	0.1047
8	415.3	1237.5	10.76	145.6	0.0325	0.5747	0.1388
9	423.5	1237.8	10.81	142.5	0.0325	0.5106	0.0788
10	403.9	1275.1	10.89	131.1	0.0324	0.3170	-0.1551
1	411.5	1323.5	10.81	156.0	0.0324	0.7103	0.2563
2	465.4	1225.0	10.82	151.8	0.0325	0.6352	0.1675
3	464.6	1220.2	10.85	146.6	0.0325	0.5489	0.1121
4	464.1	1219.8	10.80	146.6	0.0325	0.5678	0.0829
5	452.4	1168.5	10.78	143.6	0.0327	0.5223	0.0769
6	480.5	1171.4	10.84	143.5	0.0326	0.5031	0.0962
7	488.6	1202.4	10.82	143.1	0.0325	0.5137	0.0657
8	412.7	1227.3	10.72	142.3	0.0325	0.5400	0.1042
9	419.8	1245.8	10.75	147.4	0.0325	0.6056	0.1738
10	394.8	1252.3	10.75	127.8	0.0325	0.3156	-0.1565

Table D.30: Manifold configuration, rounded lateral inlets (fig.4.42).

p_{atm}=100292N/m^2				t_a=17°C			
Lat no.	Δp_p [N/m^2]	p_{atm}-p_{p1} [N/m^2]	v_l [m/s]	p_h-p_l [N/m^2]	f_D	K_0-$\alpha_{eh}(v_h/v_l)^2$	K_{ivr}
1	428.5	1420.9	10.89	122.9	0.0318	0.1406	0.0942
2	482.2	1294.8	10.83	114.7	0.0320	0.0328	-0.0616
3	476.4	1280.5	10.80	121.3	0.0320	0.1377	0.0785
4	477.8	1293.0	10.78	120.5	0.0320	0.1326	-0.0003
5	472.7	1244.0	10.83	117.1	0.0321	0.0591	0.0008
6	499.5	1240.6	10.86	117.0	0.0320	0.0575	-0.0079
7	509.7	1259.7	10.86	119.3	0.0319	0.0950	-0.0230
8	430.3	1294.4	10.81	121.0	0.0319	0.1379	0.0581
9	437.0	1263.3	10.82	114.5	0.0319	0.0420	-0.0757
10	408.9	1257.6	10.80	113.8	0.0319	0.0408	-0.0825
1	425.2	1418.6	10.85	122.1	0.0319	0.1442	0.0978
2	480.1	1292.5	10.81	115.0	0.0320	0.0458	-0.0486
3	475.9	1281.1	10.79	119.7	0.0320	0.1174	0.0583
4	477.7	1279.6	10.78	118.9	0.0320	0.1103	-0.0226
5	471.2	1222.2	10.82	117.3	0.0321	0.0664	0.0080
6	499.6	1233.4	10.86	122.4	0.0320	0.1328	0.0674
7	508.7	1253.7	10.85	113.3	0.0319	0.0143	-0.1037
8	431.7	1291.1	10.83	116.2	0.0319	0.0640	-0.0158
9	438.6	1257.6	10.84	120.7	0.0319	0.1231	0.0053
10	407.8	1262.9	10.78	112.5	0.0319	0.0262	-0.0971
1	426.4	1417.0	10.86	123.1	0.0319	0.1516	0.1053
2	480.4	1291.5	10.81	113.9	0.0320	0.0283	-0.0661
3	476.2	1272.5	10.80	118.6	0.0320	0.0994	0.0403
4	479.7	1281.5	10.81	118.6	0.0320	0.0990	-0.0340
5	471.1	1220.1	10.82	117.0	0.0321	0.0622	0.0039
6	490.6	1225.3	10.75	116.7	0.0321	0.0828	0.0174
7	509.2	1262.1	10.86	122.9	0.0319	0.1479	0.0299
8	425.5	1279.2	10.74	115.9	0.0320	0.0859	0.0061
9	438.1	1253.5	10.84	112.6	0.0319	0.0103	-0.1074
10	418.1	1297.3	10.94	114.9	0.0318	0.0171	-0.1062

Table D.31: Five laterals sucking from combining-dividing header (fig.4.44).

p_{atm}=100162 N/m^2				t_a=25°C			
Lat no.	Δp_p [N/m^2]	p_{atm}-p_{pl} [N/m^2]	v_l [m/s]	p_h-p_l [N/m^2]	f_D	K_0-$\alpha_{eh}(v_h/v_l)^2$	K_{ivr}
1	444.4	2964.6	11.35	149.4	0.0319	0.4022	-0.0517
2	499.2	2901.7	11.29	153.9	0.0321	0.4739	0.0062
3	498.3	2917.7	11.31	157.4	0.0320	0.5137	0.0769
4	504.6	2953.0	11.35	165.3	0.0320	0.6050	0.1202
5	492.0	2889.1	11.32	209.5	0.0321	1.1968	0.7514

Table D.32: First of seven laterals in suction mode, totally closed header (fig.4.45).

p_{atm}=100199N/m^2				t_a=27°C			
Lat no.	Δp_p [N/m^2]	p_{atm}-p_{p1} [N/m^2]	v_l [m/s]	p_h-p_l [N/m^2]	Re	K_0-$\alpha_{eh}(v_h/v_l)^2$	K_{ivr}
1	706.9	2369.4	14.73	253.9	17819	0.0299	0.4680
1	703.9	2368.7	14.70	253.7	17775	0.0299	0.4759
1	705.4	2376.5	14.72	253.7	17797	0.0299	0.4712
1	706.3	2373.9	14.73	252.8	17810	0.0299	0.4607
1	705.4	2370.2	14.72	252.7	17797	0.0299	0.4631
1	707.9	2373.1	14.75	252.9	17834	0.0299	0.4562
1	441.1	1405.1	11.25	152.0	13602	0.0321	0.4831
1	442.5	1402.3	11.27	152.0	13628	0.0321	0.4746
1	439.8	1400.3	11.23	151.5	13579	0.0321	0.4829
1	441.6	1402.3	11.26	152.0	13612	0.0321	0.4787
1	441.7	1398.8	11.26	151.9	13614	0.0321	0.4778
1	441.0	1398.8	11.25	151.8	13602	0.0321	0.4797
1	274.7	809.7	8.55	89.7	10340	0.0346	0.4810
1	275.9	809.7	8.57	89.8	10369	0.0346	0.4707
1	274.6	810.6	8.55	89.8	10339	0.0346	0.4839
1	274.5	808.4	8.55	89.6	10338	0.0346	0.4796
1	274.3	808.9	8.54	89.7	10333	0.0346	0.4841
1	275.0	807.6	8.56	90.0	10348	0.0346	0.4855

Table D.33: Fourth of seven laterals in suction mode, totally closed header (fig.4.45).

p_{atm}=100123N/m^2				t_a=28°C			
Lat no.	Δp_p [N/m^2]	p_{atm}-p_{p1} [N/m^2]	v_l [m/s]	p_h-p_l [N/m^2]	Re	K_0-$\alpha_{eh}(v_h/v_l)^2$	K_{ivr}
1	706.9	2369.4	14.73	253.9	17819	0.0299	0.4680
1	703.9	2368.7	14.70	253.7	17775	0.0299	0.4759
1	705.4	2376.5	14.72	253.7	17797	0.0299	0.4712
1	706.3	2373.9	14.73	252.8	17810	0.0299	0.4607
1	705.4	2370.2	14.72	252.7	17797	0.0299	0.4631
1	707.9	2373.1	14.75	252.9	17834	0.0299	0.4562
1	441.1	1405.1	11.25	152.0	13602	0.0321	0.4831
1	442.5	1402.3	11.27	152.0	13628	0.0321	0.4746
1	439.8	1400.3	11.23	151.5	13579	0.0321	0.4829
1	441.6	1402.3	11.26	152.0	13612	0.0321	0.4787
1	441.7	1398.8	11.26	151.9	13614	0.0321	0.4778
1	441.0	1398.8	11.25	151.8	13602	0.0321	0.4797
1	274.7	809.7	8.55	89.7	10340	0.0346	0.4810
1	275.9	809.7	8.57	89.8	10369	0.0346	0.4707
1	274.6	810.6	8.55	89.8	10339	0.0346	0.4839
1	274.5	808.4	8.55	89.6	10338	0.0346	0.4796
1	274.3	808.9	8.54	89.7	10333	0.0346	0.4841
1	275.0	807.6	8.56	90.0	10348	0.0346	0.4855

Table D.34: 90° inlet section mounted (fig.4.47).

p_{atm}=99917N/m^2				t_a=28.5°C		
Lat no.	Δp_p [N/m^2]	p_{atm}-p_{pl} [N/m^2]	v_l [m/s]	p_h-p_l [N/m^2]	f_D	K_i
1	424.9	1265.4	11.03	142.5	0.0323	0.4398
2	482.9	1181.7	11.07	146.3	0.0324	0.4733
3	473.6	1173.8	10.98	141.1	0.0325	0.4286
4	478.4	1187.5	11.01	144.9	0.0325	0.4762
5	470.8	1139.8	11.04	144.2	0.0325	0.4449
6	495.7	1134.3	11.05	141.1	0.0325	0.4039
7	499.5	1158.2	10.97	140.4	0.0324	0.4273
8	433.9	1228.0	11.05	140.9	0.0324	0.4092
9	432.2	1203.0	10.95	140.6	0.0324	0.4404
10	409.6	1228.1	11.00	143.1	0.0324	0.4631
1	425.6	1257.2	11.05	141.0	0.0323	0.4153
2	481.0	1178.7	11.04	145.0	0.0324	0.4626
3	472.0	1161.2	10.96	140.7	0.0325	0.4288
4	475.6	1179.2	10.97	144.2	0.0325	0.4793
5	469.2	1137.5	11.02	142.9	0.0326	0.4334
6	493.2	1132.3	11.02	140.4	0.0325	0.4042
7	496.8	1149.2	10.94	140.4	0.0325	0.4392
8	431.7	1229.9	11.02	141.1	0.0324	0.4241
9	430.4	1203.1	10.92	139.5	0.0325	0.4344
10	409.8	1225.1	11.00	142.5	0.0324	0.4526
1	421.6	1264.8	10.98	142.4	0.0324	0.4566
2	482.5	1186.7	11.06	145.9	0.0324	0.4696
3	472.4	1168.5	10.97	142.2	0.0325	0.4495
4	478.5	1191.0	11.01	144.1	0.0325	0.4642
5	466.9	1139.2	10.99	143.3	0.0326	0.4500
6	493.6	1135.3	11.02	140.2	0.0325	0.4000
7	497.7	1147.2	10.95	140.0	0.0325	0.4295
8	431.7	1223.9	11.02	141.9	0.0324	0.4352
9	431.0	1193.6	10.93	139.0	0.0324	0.4235
10	405.2	1225.1	10.93	141.7	0.0324	0.4677

Table D.35: 60° inlet section mounted (fig.4.47).

p_{atm}=99917N/m^2				t_a=28.5°C		
Lat no.	Δp_p [N/m^2]	p_{atm}-p_{p1} [N/m^2]	v_1 [m/s]	p_h-p_1 [N/m^2]	f_D	K_i
1	420.3	1252.5	10.97	143.0	0.0324	0.4711
2	482.2	1174.6	11.06	147.1	0.0324	0.4875
3	471.6	1159.9	10.96	142.9	0.0325	0.4633
4	473.5	1184.8	10.94	145.9	0.0325	0.5139
5	466.1	1135.6	10.98	145.0	0.0326	0.4776
6	492.9	1133.3	11.01	141.6	0.0325	0.4224
7	501.3	1163.3	10.99	143.2	0.0324	0.4596
8	433.9	1235.0	11.05	143.4	0.0324	0.4449
9	433.2	1199.5	10.96	141.0	0.0324	0.4421
10	401.3	1204.5	10.87	139.6	0.0325	0.4582
1	422.7	1263.7	11.00	145.2	0.0324	0.4905
2	471.1	1161.8	10.92	145.6	0.0325	0.5172
3	470.5	1166.9	10.94	142.4	0.0325	0.4618
4	476.7	1184.1	10.98	145.4	0.0325	0.4919
5	468.2	1136.9	11.00	145.6	0.0326	0.4771
6	493.6	1132.6	11.02	142.1	0.0325	0.4273
7	501.4	1165.0	10.99	143.7	0.0324	0.4674
8	435.3	1226.2	11.07	143.1	0.0323	0.4333
9	435.7	1207.8	11.00	141.5	0.0324	0.4362
10	402.6	1211.8	10.89	139.6	0.0325	0.4509
1	423.9	1268.0	11.02	145.0	0.0324	0.4806
2	476.1	1163.3	10.98	145.7	0.0325	0.4962
3	472.4	1167.4	10.97	143.9	0.0325	0.4742
4	476.8	1188.0	10.99	146.3	0.0325	0.5042
5	466.4	1136.5	10.98	144.9	0.0326	0.4761
6	491.1	1133.8	10.99	142.2	0.0325	0.4386
7	500.7	1165.3	10.99	143.3	0.0324	0.4643
8	430.2	1226.1	11.00	142.6	0.0324	0.4525
9	433.6	1202.8	10.97	141.1	0.0324	0.4404
10	403.1	1205.1	10.90	139.5	0.0324	0.4474

Table D.36: 30° inlet section mounted (fig.4.47).

p_{atm}=99917N/m^2				t_a=28.5°C		
Lat no.	Δp_p [N/m^2]	p_{atm}-p_{p1} [N/m^2]	v_1 [m/s]	p_h-p_1 [N/m^2]	f_D	K_i
1	421.1	1288.5	10.97	170.3	0.0324	0.8621
2	468.6	1174.6	10.89	162.6	0.0326	0.7791
3	468.9	1178.9	10.92	158.7	0.0325	0.7065
4	475.7	1200.5	10.97	161.3	0.0325	0.7265
5	465.4	1152.0	10.97	159.1	0.0326	0.6847
6	490.6	1151.4	10.98	156.2	0.0325	0.6429
7	492.5	1170.1	10.89	156.3	0.0325	0.6910
8	428.4	1241.4	10.97	155.8	0.0324	0.6529
9	433.3	1225.3	10.96	155.4	0.0324	0.6494
10	405.0	1237.5	10.92	153.9	0.0324	0.6459
1	419.1	1286.7	10.94	168.9	0.0324	0.8541
2	470.4	1178.6	10.91	162.0	0.0326	0.7602
3	468.4	1184.6	10.92	160.5	0.0326	0.7356
4	473.9	1201.3	10.95	161.7	0.0325	0.7418
5	468.6	1152.6	11.01	160.1	0.0326	0.6829
6	491.2	1148.5	10.99	156.1	0.0325	0.6393
7	494.2	1166.9	10.91	155.5	0.0325	0.6704
8	431.6	1237.5	11.02	155.5	0.0324	0.6300
9	433.5	1219.2	10.97	155.6	0.0324	0.6501
10	405.3	1236.7	10.93	153.7	0.0324	0.6410
1	420.5	1287.4	10.97	169.9	0.0324	0.8597
2	466.6	1162.0	10.86	160.6	0.0326	0.7607
3	472.5	1189.1	10.97	159.5	0.0325	0.6983
4	472.9	1194.8	10.93	160.5	0.0325	0.7297
5	463.1	1147.8	10.94	160.2	0.0326	0.7128
6	486.2	1134.1	10.93	154.9	0.0326	0.6454
7	497.9	1169.8	10.95	155.5	0.0325	0.6536
8	425.7	1218.9	10.93	153.9	0.0325	0.6416
9	430.8	1210.0	10.93	153.8	0.0325	0.6399
10	407.7	1251.8	10.97	156.0	0.0324	0.6596

APPENDIX E

DISCUSSION OF THE DESIGN EQUATION FOR AIR-COOLED CONDENSER PROPOSED BY SCHREY [95SC1]

E.1 DESIGN EQUATION OF SCHREY

Schrey proposes the following equation to calculate the maximum allowable mass flow rate through a single tube row air-cooled condenser in combined Z-U-configuration to avoid the formation of dead zones:

$$m_{tot} = A_{hd} \sqrt{\frac{12\, z\, \rho\, \Delta p_1 (1 - \Gamma)}{B_1 \theta_d \left(1 + 2(1 - \Gamma) + 3(1 - \Gamma)^2\right)(3 + \alpha_Z B_3)}} \qquad \text{(E.1)}$$

where

z : steam compressibility;

Δp_1: static pressure change over condenser section bundle;

Γ : condensation ratio of the total mass flow through condenser;

α_Z: ratio of heat transfer of Z-section to heat transfer of entire condenser/dephlegmator system and

α_U: ratio of heat transfer of U-section to heat transfer of entire condenser/dephlegmator system,

with $\alpha_Z + \alpha_U = \Gamma$;

$$B_1 = \frac{\alpha_Z}{\alpha_Z + \alpha_U}$$

and

$$B_3 = \frac{\theta_c (1 - \Gamma)}{\theta_d} \left(\frac{\sigma_c}{\sigma_d} \right)^2 - 1$$

where

$$\sigma_c = \frac{N A_l}{A_{hc}}$$

$$\sigma_d = \frac{2 N A_l}{A_{hd}}$$

Note that from the dividing header two rows of laterals branch off. The equation does not provide for an air-cooled condenser in entire in U-configuration, a part of the system must be in Z-configuration in order to apply the formula. Although a change of dividing header area from the Z- to the U-configuration is indicated in a figure in his publication, Schrey's method does not make allowance for this change. Therefore only a constant dividing header area dividing header can be investigated with the above equation. Furthermore an average value has to be used for the static pressure change over the bundles, Δp_B; Schrey does however not specify how this value should be determined. We will use the pressure change over a typical single lateral calculated by equation (2.30). The mass flow rate through that lateral is calculated by assuming a uniform mass flow distribution through all the laterals.

E.2 SAMPLE CALCULATION

E.2.1 DIMENSIONS OF THE CONDENSER

The air-cooled condenser is configured in combined Z-U-configuration as shown in figure E.1. The part in Z-configuration has two fans providing the air flow while that in U-configuration is supplied by three fans. The bundle areas above every fan and their heat transfer rates are assumed to be identical.

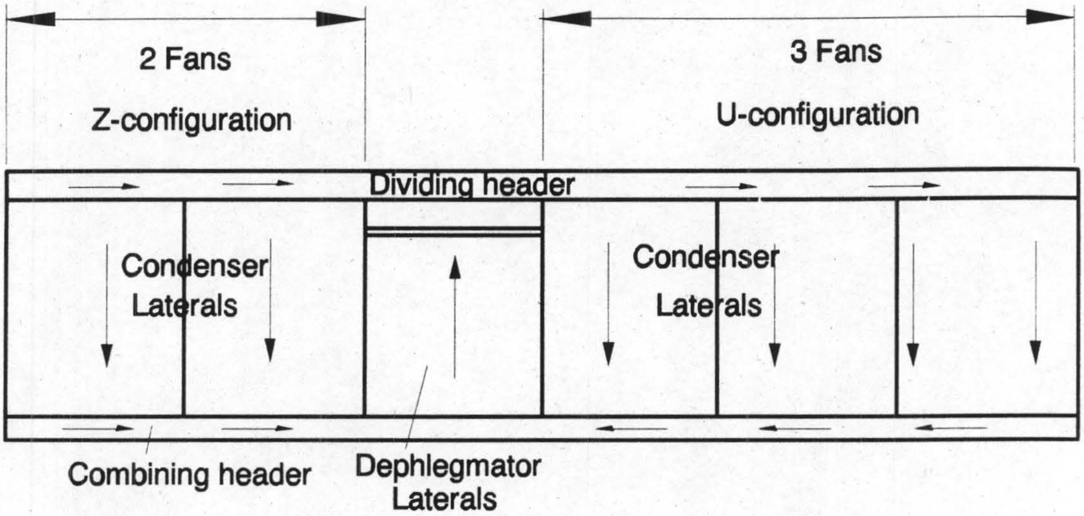

Figure E.1: Air-cooled condenser configuration.

Specifications:

Steam temperature, T = 60°C

Number of laterals per row per fan, N_f = 250

Number of laterals per row N = 5×250

Condensation rate per fan, m_{fc} = 11.4117kg/s

Laterals:

Lateral pitch, Δz = 0.04m

Lateral height, h = 0.19m

Lateral width, w = 0.01m

lateral length, L_l = 9m

Dividing header:

Dividing header diameter: d_{hd} = 2.3m

Combining header:

Combining header area: d_{hc} = 0.70711m

E.2.2 CALCULATION

The thermo-physical properties of saturated steam at 60°C can be calculated in the same way as shown in section 5.6 as:

$\rho = 0.13023 \text{kg/m}^3$

$\mu = 1.1083 \times 10^{-5} \text{Ns/m}^2$

The steam compressibility, $z = 1$. The solution for the condensation ratio of the condenser, Γ, cannot be obtained by an explicit formulation of the expression. We will therefore use the correct value for this calculation:

$\Gamma = 0.872278$.

From $\alpha_Z + \alpha_U = \Gamma$ and the specified heat transfer ratios it follows that

$$\alpha_Z = \frac{2}{5}\Gamma = \frac{2}{5} \times 0.872278 = 0.348911$$

$$\alpha_U = \frac{3}{5}\Gamma = \frac{3}{5} \times 0.872278 = 0.523367$$

Calculate

$$B_1 = \frac{\alpha_Z}{\alpha_Z + \alpha_U} = \frac{0.348911}{0.348911 + 0.523367} = 0.4$$

The area ratio for the combining header is:

$$\sigma_c = \frac{N A_1}{A_{hc}} = \frac{5 \times 250 \times (0.01 \times 0.19)}{\frac{\pi}{4} \times (0.7071)^2} = 6.04789$$

and of the dividing header:

$$\sigma_d = \frac{2 N A_1}{A_{hc}} = \frac{2 \times 5 \times 250 \times (0.01 \times 0.19)}{\frac{\pi}{4} \times (2.3)^2} = 1.14327$$

Calculate

$$B_3 = \frac{\theta_c(1-\Gamma)}{\theta_d}\left(\frac{\sigma_c}{\sigma_d}\right)^2 - 1 = 2.24 \times \frac{(1-0.872278)}{0.99}\left(\frac{6.04789}{1.14327}\right)^2 - 1$$

$$= 7.086991$$

The average pressure change over the bundle is calculated as follows. Firstly calculate the total mass flow through the condenser:

$$m_{tot} = \frac{5\,m_{fc}}{\Gamma} = \frac{5 \times 11.41172}{0.872278} = 65.41327\text{kg/s}$$

The above value is the left hand side of equation (E.1).

The mass flow rate through a single lateral is:

$$m_l = \frac{m_{tot}}{2\,N} = \frac{65.41327}{2 \times 5 \times 250} = 0.026165\text{kg/s}$$

The condensation rate in a lateral is:

$$m_{lc} = \frac{m_{fc}}{2\,N_f} = \frac{11.41172}{2 \times 250} = 0.022823\text{kg/s}$$

The lateral steam inlet velocity is:

$$v_{li} = \frac{m_l}{\rho\,A_l} = \frac{0.026165}{0.13023 \times (0.01 \times 0.19)} = 105.745\text{m/s}$$

and the lateral steam outlet velocity is:

$$v_{lo} = \frac{m_l - m_{lc}}{\rho\,A_l} = \frac{0.026165 - 0.022823}{0.13023 \times (0.01 \times 0.19)} = 13.506\text{m/s}$$

The Reynolds numbers at the lateral inlet and outlet are:

$$Re_{li} = \frac{\rho\,v_{li}\,d_{el}}{\mu} = \frac{0.13023 \times 105.745 \times 0.019}{1.1083 \times 10^{-5}} = 23609.54$$

and

$$\mathrm{Re}_{lo} = \frac{\rho\, v_{lo}\, d_{el}}{\mu} = \frac{0.13023 \times 13.506 \times 0.019}{1.1083 \times 10^{-5}} = 3015.438$$

The condensation loss coefficient is calculated as follows

$$K_{con} = \frac{\Delta p_{fr}}{\frac{1}{2}\rho\, v_{li}^2} - \left(1 - x_o^2\right)$$

The first term of the right hand side of the above equation will be calculated firstly. Again the Groenewald condensation loss coefficient is used. Because the lateral condensation rate is identical to that in section 5.6, the same wall Reynolds number is valid for this case:

$\mathrm{Re}_w = 11.44117$

The wall Reynolds number yields the following values for the factors of equation (2.30b)

$A = 1.07651$

$B = 992.739$

$C = 1.08587$

The outlet steam quality is

$$x_o = \frac{\mathrm{Re}_{lo}}{\mathrm{Re}_{li}} = \frac{3015.438}{23609.54} = 0.127721$$

Calculate

$$\frac{\Delta p_1}{\frac{1}{2}\rho\, v_{li}^2} = \frac{L_1}{d_{el}}\, \frac{1}{x_o - 1} \times \frac{0.3164}{\mathrm{Re}_i^{0.25}} \times \left(\frac{A}{2.75}\left(x_o^{2.75} - 1\right) + \frac{B}{1.75\, \mathrm{Re}_i}\left(x_o^{1.75} - 1\right) \right)$$

The condensation loss coefficient is

$$= \frac{9}{0.019} \times \frac{1}{(0.127721) - 1} \times \frac{0.3164}{(23609.54)^{0.25}}$$

$$\times \left(\frac{1.07651}{2.75}\left((0.127721)^{2.75} - 1\right) + \frac{992.739}{1.75 \times 23609.54}\left((0.127721)^{1.75} - 1\right)\right)$$

$$= 5.73110$$

$$K_{con} = \frac{\Delta p_{fr}}{\frac{1}{2}\rho v_{li}^2} - \left(1 - x_o^2\right) = 5.73110 - \left(1 - (0.127721)^2\right) = 4.747404$$

As we consider a typical lateral, the average value of the reduced inlet loss coefficient of the rounded lateral inlet configuration is used. The value is

$$K_i - \alpha_{ed}\frac{v_{hd}^2}{v_{li}^2} = 0.089$$

As in section 5.6 the reduced outlet loss coefficient will be taken as:

$$K_o + \alpha_{ec}\frac{v_{hc}^2}{v_{lo}^2} = 0.5625$$

according to equation (2.54).

The static pressure change over the lateral is calculated by equation (3.10)

$$\Delta p_{dc} = \left[\left(K_i - \alpha_{ed}\frac{v_{hd}^2}{v_{li}^2}\right) + K_{lat}\right]\frac{1}{2}\rho v_{li}^2 + \left(K_o + \alpha_{ec}\frac{v_{hc}^2}{v_{lo}^2}\right)\frac{1}{2}\rho v_{lo}^2$$

$$= \left((0.089) + 4.747404\right) \times \frac{1}{2} \times 0.13023 \times (105.7447)^2$$

$$+ 1 \times \frac{1}{2} \times 0.13023 \times (13.506)^2$$

$$= 3528.15 \text{N/m}^2 = \Delta p_B$$

The right hand side of equation (E.1) is determined

$$\text{RHS} = \frac{\pi}{4}(2.3)^2$$

$$\times \sqrt{\frac{12 \times 0.99504 \times 0.13023 \times 3528.15 \times (1 - 0.872278)}{0.4 \times 0.99 \times (3 + 0.348911 \times 7.086991) \times (1 + 2 \times (1 - 0.872278) + 3 \times (1 - 0.872278)^2)}}$$

$$= 65.4133\text{kg/s} = \text{LHS}$$

This shows that the choice of Γ has been correct.

APPENDIX F

NUMERICAL SOLUTION OF STEAM FLOW DISTRIBUTION THROUGH AIR-COOLED CONDENSER

F.1 INTRODUCTION

In order to investigate the accuracy of the design approach presented in chapter 5 and the actual flow distribution, a computer program was written in the *FORTRAN* code to calculate the flow distribution through a section of an air-cooled condenser numerically. The finite difference scheme and the algorithm used in the program is presented in section 3.7.

The same condenser configuration and mass flow rate, as used to demonstrate the proposed design approach, will be used in order to compare the results of the numerical solution to those of the proposed design approach. A diagram of the condenser sections in the U and the Z-configuration is shown in figure F.1.

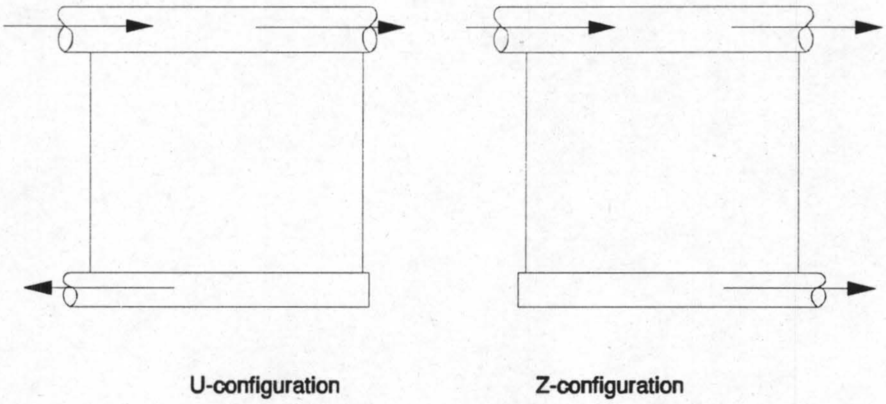

Figure F.1: Diagram of numerically investigated condenser sections.

The individual lateral mass flow rates (m_l) will be compared in dimensionless form, based on the constant lateral condensation rate (m_{lc}). This means that if the dimensionless mass flow rate is smaller than unity, dead zones can be expected at the outlet section in the specific lateral. Furthermore the influence of the header area ratio (σ) and the condensation ratio (Γ) will be investigated numerically. It has been shown in chapter 5 that the difference of the solutions of the cases where the lateral inlets were sharp or rounded is very small. Therefore only the case of lateral inlets with rounded edges with a 3mm radius was investigated here.

F.2 U-CONFIGURATION

The situation of the entire flow that enters the dividing header enters the laterals is investigated. Figure F.2 shows the dimensionless mass flow distributions for different condensation ratios at a constant header area ratio of 16.

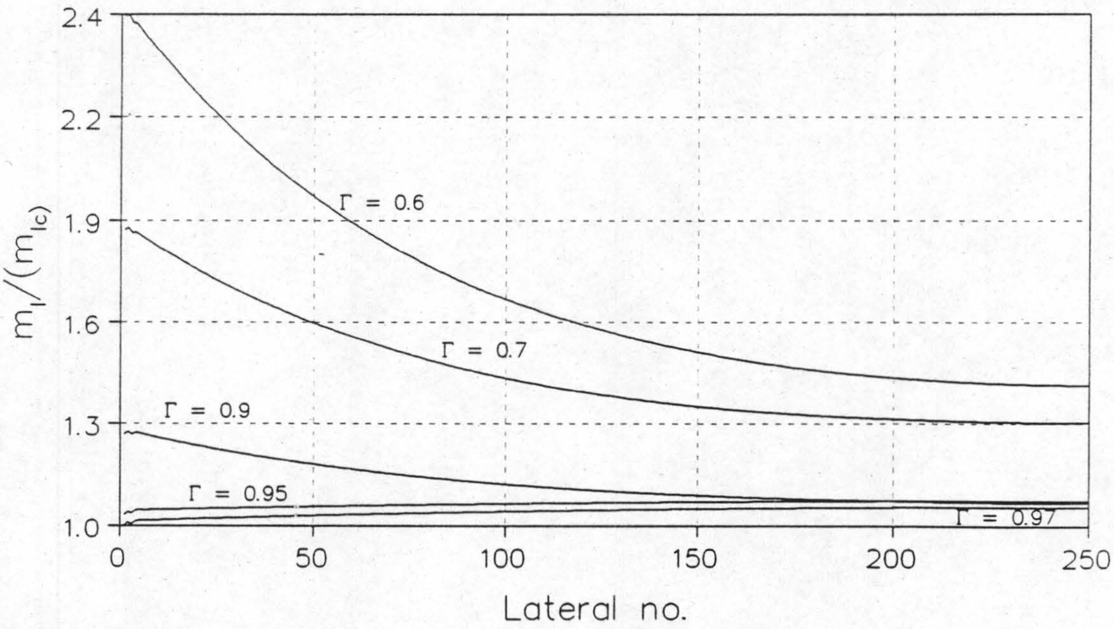

Figure F.2: Dimensionless mass flow distributions as function of Γ for σ =16.

At Γ = 0.97 the mass flow rate through the first lateral is equal to the lateral condensation rate. For decreasing values of Γ the flow distribution becomes increasingly non-uniform. with the mass flow rate through the first laterals being the maximum. The mass flow rate through the last lateral always remains larger than the condensation rate. The "wiggles" indicated in figure F.2 are a result of the varying inlet loss coefficients used in this investigation. Figure F.3 shows the dimensionless mass flow distribution for different header area ratios at a constant condensation ratio of 0.8.

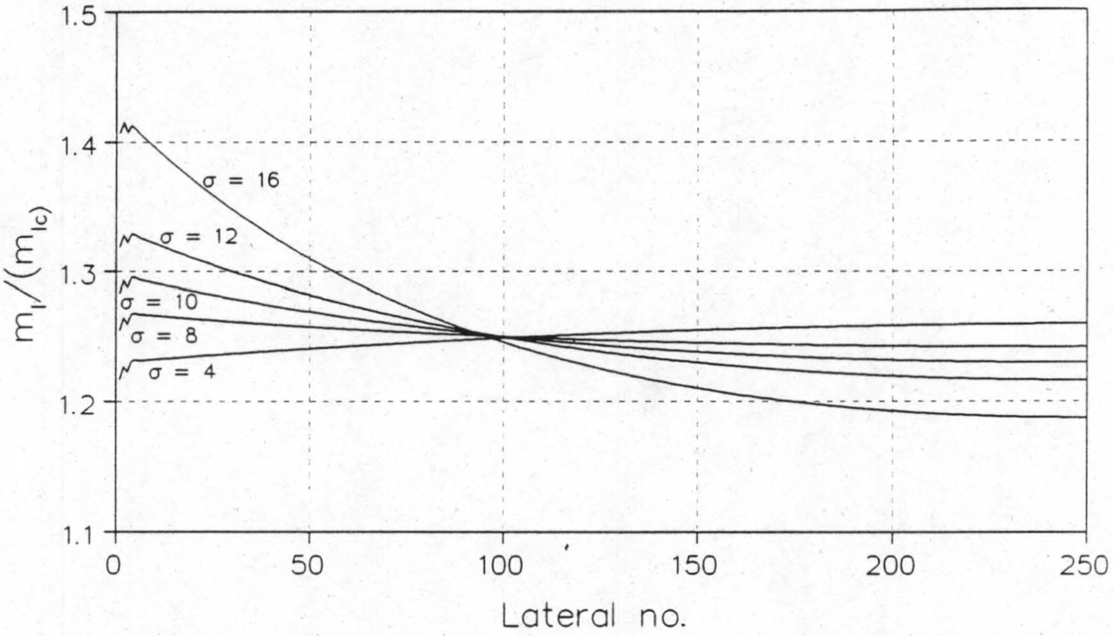

Figure F.3: Dimensionless mass flow distributions as function of σ for Γ = 0.8.

It can be seen that with increasing header area ratio the flow distribution becomes increasingly non-uniform. The mass flow rate through the last laterals decreases while that of the first laterals increases.

F.3 Z-CONFIGURATION

The situation of the entire flow that enters the dividing header enters the laterals is investigated. Figure F.4 shows the dimensionless mass flow distributions for different condensation ratios at a constant header area ratio of 16.

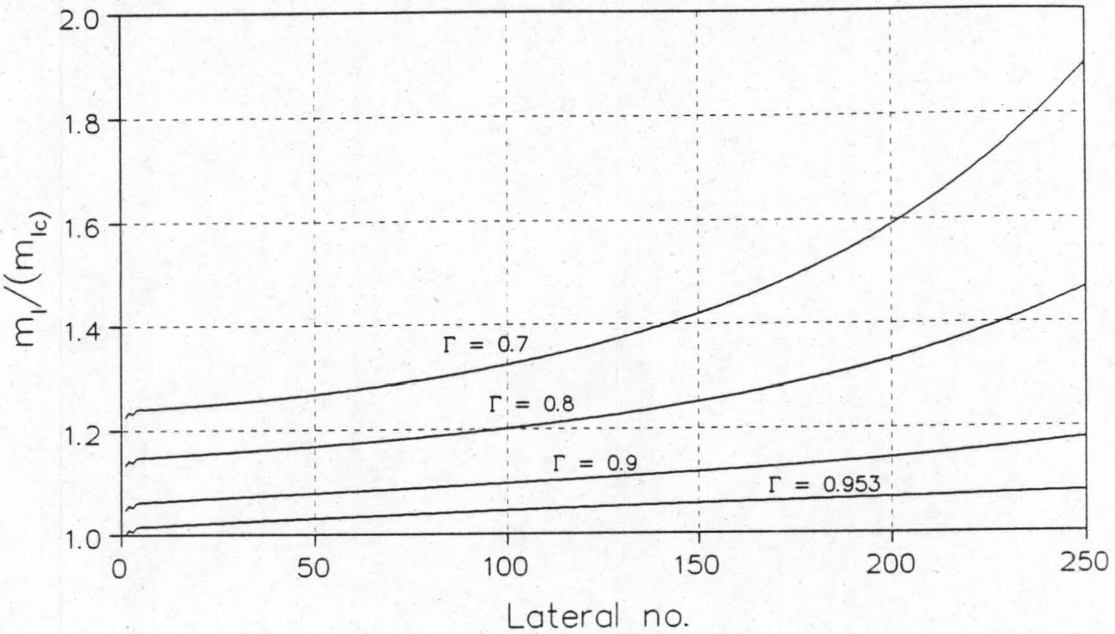

Figure F.4: Dimensionless mass flow distributions as function of Γ for σ =16.

The flow distribution becomes increasingly non-uniform with decreasing condensation ratio. No back flow is expected for condensation ratios smaller than 0.953 for this case. Figure F.5 shows the dimensionless mass flow distribution for different header area ratios at a constant condensation ratio of 0.8.

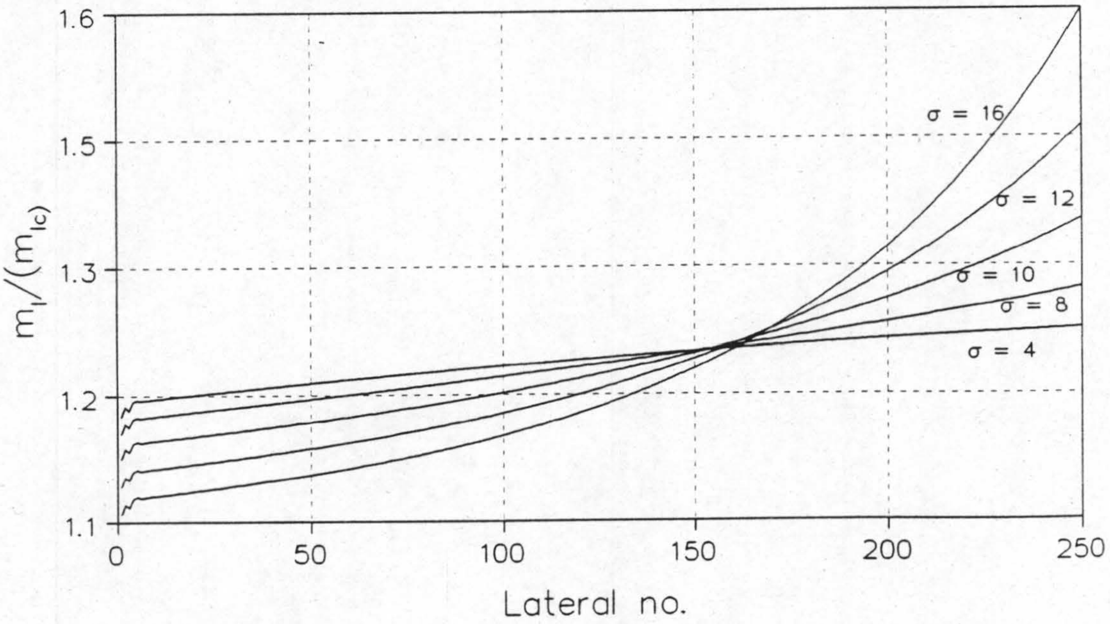

Figure F.5: Dimensionless mass flow distributions as function of σ for Γ = 0.8.

The non-uniformity of the flow distribution increases with increasing area ratio. For a maximum area ratio the first lateral will experience back flow.

If the flow distributions of the U and the Z-configuration are compared, the non-uniformity of the distribution is similar in magnitude and almost symmetrical for both configurations. The reason for the similarity is found in the nearly constant low pressure change along the dividing header, which for high header to header area ratios or low condensation ratios, or both, is relatively small compared to that over combining header for this particular condenser configuration. An increase in the area ratio and a decrease in the condensation ratio give an increase in the combining header velocities therefore the absolute value of the pressure change over the combining header increases. Thereby the influence of the dividing header pressure distribution on the pressure difference over the laterals becomes smaller, and the header to header pressure difference becomes a function of only the pressure distribution in the combining header.